Final state interactions in strong two-body baryon decays

Dissertation

zur

Erlangung des Doktorgrades (Dr. rer. nat.)

der

Mathematisch-Naturwissenschaftlichen Fakultät

der

Rheinischen Friedrich-Wilhelms-Universität Bonn

vorgelegt von

Daniela Morales Tolentino Zang

aus

São Paulo, Brasilien

Bonn 2014

Angefertigt mit der Genehmigung der Mathmatisch-Naturwissenschaftlichen Fakultät
der Rheinischen Friedrich-Wilhelms-Universität Bonn.

1. Gutachter: PD. Dr. Bernard Ch. Metsch
2. Gutachter: Prof. Dr. Ulf-G. Meißner
Tag der Promotion: 15.07.2014
Erscheinungsjahr: 2014

Aos meus pais, Pedro e Iracy.

Abstract

In the first part of this thesis, masses and strong decay widths of non-strange baryon resonances are described in the framework of a covariant quark model. The model is based on the solutions of the Bethe-Salpeter equation, considered in instantaneous approximation and with effective free-quark propagators. Here, the underlying quark interactions are parameterized by a confinement potential with an appropriate spin structure, supplemented by a residual spin- and flavor-dependent potential motivated by instanton effects. In such an approach the strong decays of baryon resonances can be described in a parameter-free calculation, by applying the Mandelstam formalism in lowest-order of perturbation theory.

Whereas the resulting mass spectrum accounts for most of the features observed experimentally, the theoretical decay widths are generally to small when compared to the data. In this context, the aim of this work is to investigate corrections from final state rescattering to these lowest-order results for strong decays. For this purpose we limit the scope of our investigation to the decays of low-lying N and Δ resonances into the πN, $\pi\Delta$ and ηN channels. Accordingly, in the second part of the thesis we implement a model for coupled-channel interactions involving these two-body states, and then employ the resulting amplitudes to dress the strong decay vertices from the quark model and re-evaluate the corresponding decay widths.

It was found, that this method does not improve the quark-model results for strong baryon decays. After inclusion of final state interactions, the decay widths into πN and ηN are roughly the same while those into $\pi\Delta$ are even smaller than before. Such results indicate that the problem lies in the assumptions introduced in the quark model. Accordingly, we suggest a possible modification of the framework: We conjecture that by employing full quark propagators – also taken in instantaneous approximation – instead of the effective free-quark propagators utilized before, one would obtain different results for strong baryon decays as depicted in the present approach.

Contents

Chapter 1

Introduction

With the discovery of the first nucleon excitation in the early 1950s, the $\Delta(1232)$ [1], the physics of baryon resonances has become an important topic of research. Nowadays, the spectrum of light-flavored baryons, *i.e.* those containing up, down and strange valence quarks, is still under intensive experimental investigation at several electron- and photon-beam facilities, *e.g.* ELSA at Bonn, CEBAF at the Jefferson Lab or MAMI at Mainz. In spite of the rich amount of data available – the last Review of Particle Physics [2] lists more than 80 light-flavored resonances, see Figs. 1.1 and 1.2 – the underlying mechanism leading to the observed spectra is still not completely understood. Whereas some regularities such as Regge trajectories or alternating parity shells indicate that the gross features of the baryon spectra predominantly emerge from the underlying quark dynamics, the striking low position of some states, such as *e.g.* the Roper $N(1440)$ or the lowest negative-parity hyperon excitation $\Lambda(1405)$, indicates that the molecular nature of resonances, *i.e.* the contribution of meson-baryon components, can also become very important.

In principle, the properties of baryon excitations should come out directly from Quantum Chromodynamics (QCD), which is presently accepted as the underlying quantum field theory of strong interactions. By construction it is a non-Abelian gauge theory with a gauge $SU(3)$ color group and has quarks and gluons as fundamental fields. In particular, QCD falls into the class of those non-Abelian theories that feature asymptotic freedom [3, 4], which means that for processes at sufficiently large momentum transfer ($\gtrsim$ 10 GeV) quarks and gluons behave as free particles and QCD is amenable to perturbative methods. At low and intermediate energies on the other hand, the strong coupling constant becomes larger as the momentum transfer decreases and QCD is then dominated by the phenomenon of quark confinement, giving rise to the rich spectrum of hadrons. In this region, theoretical investigations can only be carried out with the use of non-perturbative methods.

Up to this day the only *ab initio* calculations of light-baryon properties has been provided by numerical simulation of the non-Abelian QCD gauge theory into a space-time lattice [5]. Few years ago complete agreement with experimental masses has been achieved for ground states [6] and work on higher excitations up to spin 7/2 is currently in progress, see *e.g.* Ref. [7]. The first results from simulating single-baryon states on the lattice are very promising, but there are still some problems to overcome. Apart from technical difficulties, such as reducing pion masses to the physical value and the

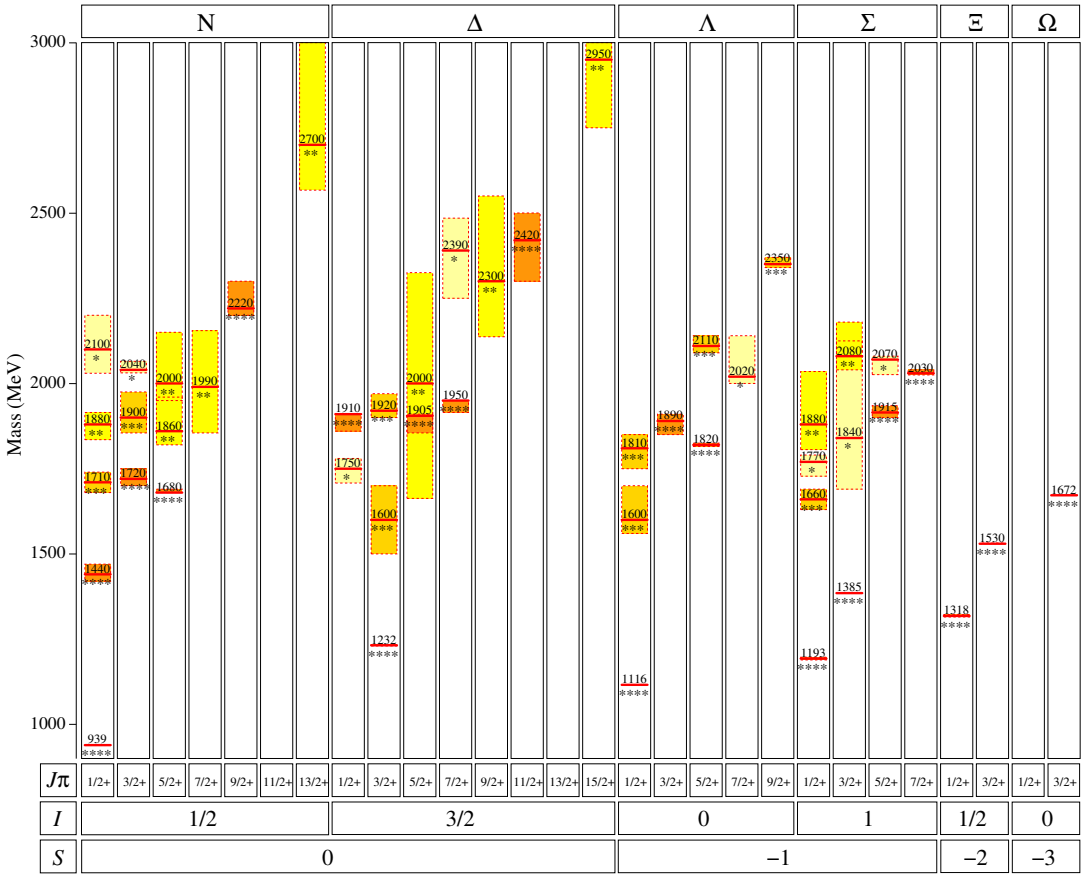

Figure 1.1. Experimental status of positive parity ($\pi = +$) light-flavored baryon resonances, according to the Particle Data Group [2]. The states are classified by spin J, isospin I and strangeness S. The excitation masses are indicated by a bar and their uncertainties by a shaded box, which is darker for better established states. The status of each resonance is additionally indicated by stars.

proper treatment of finite volume effects [8–10], a major task now is the inclusion of operators designed to couple to scattering states directly, in order to account for the unstable nature of resonances [11]. For higher mass excitations, this issue becomes increasingly important due to the opening of inelastic channels. In view of this situation, it is still worthwhile to formulate phenomenological models that incorporate the relevant degrees of freedom for baryon spectroscopy and at the same time attempt to cover as many aspects of QCD as possible.

Unitary coupled-channel methods

Since light baryons are mostly identified in experiments of meson scattering or production off the proton, a common approach is to consider hadrons themselves as the relevant degrees of freedom. In this case resonance parameters such as masses, decay widths and pole-positions are derived from hadronic scattering amplitudes, which are calculated in a coupled-channel framework and respect basic principles such as unitarity and analyticity. The connection to the underlying theory is reflected by the use of interaction kernels based on chiral symmetry breaking of QCD.

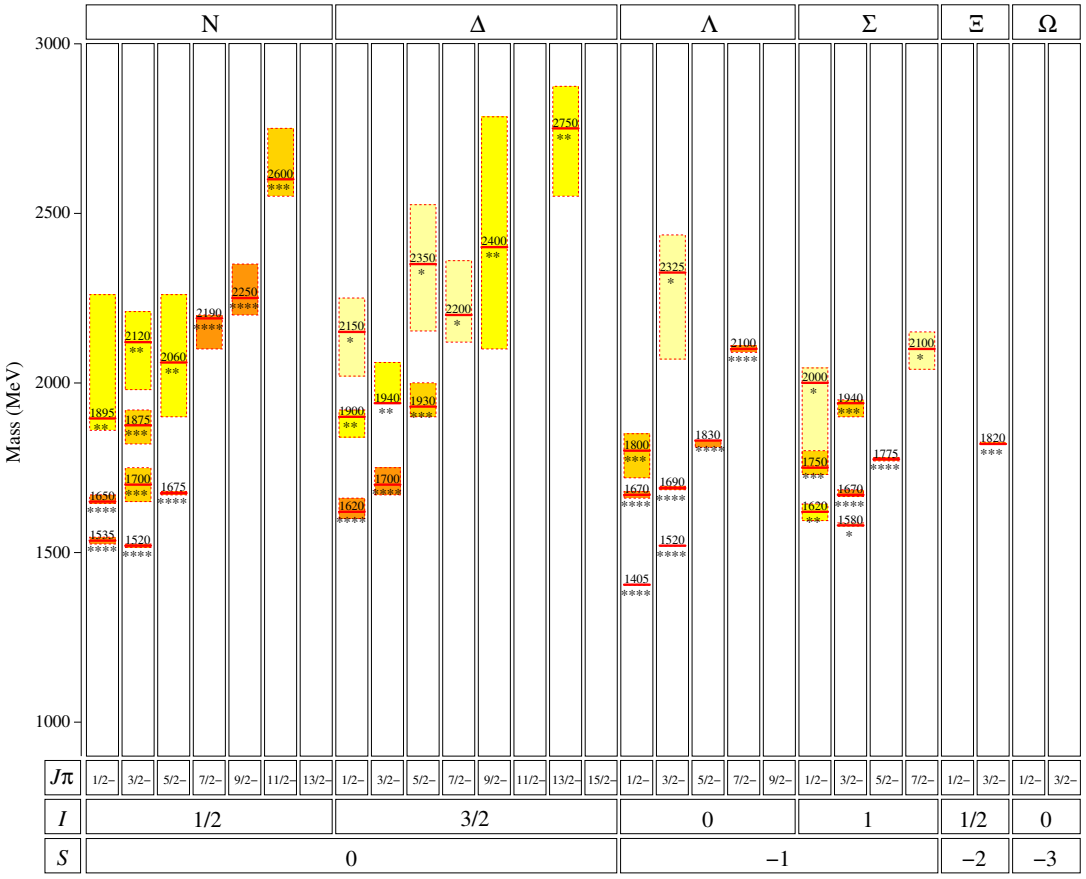

Figure 1.2. Experimental status of negative parity ($\pi = -$) light-flavored baryon resonances, according to the Particle Data Group [2]. The notation is the same as in Fig. 1.1.

As pointed out in Ref. [12], such unitarized coupled-channel methods can be roughly categorized in three major groups, namely K-matrix approaches, unitary extensions of Chiral Perturbation Theory (UχPT) and dynamical coupled-channel models (DCC). The first group includes those models based on the K-matrix approximation, which consists of reducing the full-scattering to an algebraic equation by neglecting the contribution of off-shell intermediate states. In this approximation, the scattering amplitudes fulfill unitarity but analyticity is violated because the real and imaginary parts of the amplitudes are no longer related by dispersion relations. Moreover, all resonances must be included explicitly, since the truncation of the basis states into on-shell components alone does not provide sufficient strength for the dynamical generation of resonances. Due to its simplicity, this method is widely used in partial-wave analyses of meson production data, for instance in the analyses of the Bonn/Gatchina [13], GWU/SAID [14], MAID [15] and Gießen [16] groups, with the purpose of extracting single resonance parameters from the complex structures observed in cross sections and polarization measurements [17].

If one wants to go deeper into the nature of baryon excitations, whose positions may be strongly affected or even purely described by non-resonant interactions, the contribution of off-shell states has to be taken into consideration. In the framework of

UχPT this is done through different methods, which extend from on-shell dispersive methods [18, 19] to the solution of the full off-shell Bethe-Salpeter equation [20]. The kernel in the scattering equation is rigorously matched order-by-order to χPT and resonances are dynamically generated by chiral interactions. Excited baryon fields might be explicitly included [18], but in this case the kernel has to be modified in order to achieve a consistent power counting. Among the unitary methods, this one is certainly as close as possible to an effective theory of QCD. However, exactly for this reason, its scope of applicability has been tested for a few partial-waves only.

In contrast to UχPT, in DCC models resonant fields are included in the Lagrangian phenomenologically, covering this way several partial-waves at the same time. The background interactions are given by t- and u-channel exchange potentials iterated in the full scattering equation – hence dynamical generation of resonances is possible – while those resonant structures present in the data that cannot be depicted by the background alone are explicitly included as s-channel pole contributions. A drawback of such a procedure is the large set of free parameters: Each resonant field introduced in the Lagrangian brings its own bare mass and bare coupling constants, which have no direct physical meaning and must be fitted to data. Nevertheless, these approaches represent a powerful tool to systematically extract resonance parameters from a large amount of data and, very importantly, to provide realistic background interactions for other applications, for instance the inclusion of final state interactions in strong baryon decays, which is the goal of the present thesis.

The unitary coupled-channel methods have provided many insights into the structure of baryon states, especially those which cannot be easily understood in the simple three-quark picture, such as for instance the already mentioned Roper $N(1440)$, which is dynamically generated in the framework of the Jülich model [21], or the hyperon excitation $\Lambda(1405)$, whose double pole structure naturally emerges in the framework of UχPT [19]. Besides, these methods enable the extraction of resonance parameters from raw experimental data, which is obviously fundamental. But despite all this, they cannot help with a better understanding of how those resonance parameters emerge from quark dynamics and ultimately, which interquark interactions primarily lead to the observed baryon spectrum. To this end, quarks themselves must be considered as degrees of freedom.

Constituent Quark Models

In the picture of constituent quark models, light mesons ($q\bar{q}$) and baryons (qqq) are built of spin 1/2 quark fields, which occur in the flavors u, d and s, combined in the 3-dimensional fundamental representation q of the $SU(3)$ flavor group. The gluonic degrees of freedom are replaced by an effective potential between quarks, while quark self-interaction effects generated by QCD are assumed to be absorbed in an effective quark mass contribution called constituent mass. In the most conventional versions, quarks interact through a non-relativistic potential, consisting of a confinement part and an additional QCD-based hyperfine interaction, such as one-gluon exchange or instanton induced forces. For a review of several phenomenological models applied to baryon spectroscopy, see Ref. [22].

Since light quarks, even when adopting constituent, effective quark masses, move in hadrons with velocities which are a significant fraction of the velocity of light, the quark model description should actually be based on the usual concepts of relativistic quantum field theories. In this thesis we thus employ a covariant version of the quark model, developed in Refs. [23–27] for mesons and [28–30] for baryons, where hadronic excitations are described by the solutions of the quark-antiquark and three-quark Bethe-Salpeter equations, respectively. Here, the quark dynamics is given by an instantaneous confinement potential, which includes an appropriate spin-structure and rises linearly with interquark distances, and a residual spin-flavor dependent interaction based on instanton effects. The resulting light-flavored baryon spectrum accounts for many of the gross features observed experimentally, such as linear Regge trajectories, mass splittings and parity doublets [31]. In contrast to the DCC models mentioned before, the description of the complete spectrum is here achieved with seven parameters only, which are adjusted to the ground-state masses and Regge trajectories. The positions of all other excitations in the spectrum are then determined by the same parameter set.

Another advantage of this covariant version over non-relativistic quark models is to provide a natural framework for the calculation of non-static observables, which might involve large momentum transfers and require a full relativistic treatment. In fact, the scope of applicability of this approach has been tested through the evaluation of several baryon observables, such as electroweak form factors and helicity amplitudes [32–35], observables related to semileptonic decays [36] and also the structure of two-body strong decays [37–39]. All these quantities can be calculated in lowest order without any additional parameter and as such are genuine predictions of the model.

Among these applications the calculation of two-body strong decays of baryons is particularly interesting, while being closely related to the problem of missing resonances [17, 22]. All constituent quark models, including the present approach, predict a large number of excited states in the region above 1800 MeV, whose experimental counterparts have not been detected in meson-induced scattering experiments. This question was addressed in a systematic theoretical study of roughly 1700 strong two-body decays of baryon resonances into a pseudoscalar octet meson and a (possibly excited) baryon final state [39]. It was found that these missing excited states in general decouple from πN or KN, *i.e.* the channels through which most baryon resonances have been observed, offering a natural solution to the missing resonance problem this way.

Despite the success in clarifying why missing states have not been observed so far, it is important to emphasize that up to now strong decay widths were merely calculated in lowest order of perturbation theory. Possibly due to the neglect of rescattering effects in this approximation, the theoretical widths are in general quantitatively too small when compared to the experiment – not only for states in the high-energy region where missing resonances occur, but also for low-lying well-established resonances. In this regard, it is still an open issue whether the discrepancy between predictions and experiment results from neglecting final state interactions or it is a consequence of the various phenomenological approximations employed in the model.

Goals and outline of this thesis

Among the phenomenological methods discussed above both DCC approaches and the relativistic constituent quark model (referred as RCQM below) seem to be the most suitable for a systematic investigation of light-baryon spectra and their strong decays. Interestingly these methods depict baryons in a complementary way: On the one hand, DCC models account for the interplay between resonance properties and non-resonant background interactions, however at the expense of a large parameter set consisting of bare masses and bare coupling constants. On the other hand, in the framework of the RCQM baryon masses and decay widths can be predictions on the basis of few parameters, but non-resonant contributions to these quantities are completely disregarded.

In view of this, the goal of the present thesis is to investigate whether the non-resonant interactions of a DCC model, when employed as parameterization of meson-baryon rescattering in strong two-body decays, provide enough strength to correct the decay widths predicted by the RCQM. If so, the discrepancy between predicted and experimental decay widths results from the neglect of final state interactions.

For a first investigation on this issue we limit the scope of this work to low-lying N and Δ resonances with masses $M_R \lesssim 1700$ MeV and consider their strong decays into some of the lightest two-body channels with vanishing strangeness, namely πN, $\pi\Delta$ and ηN. We have chosen this approach mainly because only decays involving pseudoscalar mesons have been calculated in the quark model so far. Note however, that even only three rescattering channels form a large enough basis to illustrate coupled-channel effects. The strangeness production channels $K\Lambda$ and $K\Sigma$ could be considered as well, but here we neglect them since the theoretical states from the RQCM in general decouple from these, see Ref. [39].

Among several DCC approaches found in the literature – see Ref. [40] for a bibliographical survey – one particularly suitable for the applications we have in mind is the Jülich model [21, 40–46], basically for two reasons: Firstly, its non-resonant background is realistic and well-constrained, due to the use of correlated $\pi\pi$ exchange in the scalar and vector channels instead of the usual σ- and ρ-meson exchanges in πN scattering. Secondly, in its current version of Ref. [40] this model includes effective Lagrangians for resonances up to spin 3/2 plus phenomenological couplings for states up to 9/2, covering the spectrum of non-strange baryons almost completely. This way, our investigations might be extended to higher spins in the future.

As it stands, however, the Jülich model cannot be directly connected to the quantities we calculate in the RCQM. As we shall see already in the next chapter, in constituent quark models hadrons are considered to be quark bound-states in a strictly physical sense, *i.e.* they are associated to on-shell, asymptotic momentum eigenstates. Consequently, meson-baryon rescattering amplitudes for strong decays calculated in the RCQM have to be necessarily evaluated on the mass shell. Since this is not the case with the amplitudes from the Jülich model, in this thesis we elaborate an on-shell reduction of their approach.

Accordingly, the present thesis is organized as follows:

In **Chapter 2** we review the formalism of the relativistic constituent quark model, explaining which approximations and phenomenological interactions are used in the framework. Although mesons are not our subject of study, they participate in strong decays of baryons and therefore should be discussed as well. After this review, we end the chapter with model predictions for non-strange hadron spectra, focusing on the ingredients we need in this thesis, *i.e.* the spectrum of low-lying N and Δ baryons as well as the masses of ground-state hadrons present in the strong-decay πN, $\pi\Delta$ and ηN channels.

In **Chapter 3** we then describe how strong two-body decays of baryon resonances are depicted in the framework of the RCQM. Specifically, we calculate the corresponding widths by applying the Mandelstam formalism [47] in lowest order of perturbation theory. We show that within such a method the resulting decay widths are fully determined by the same parameter set fitted to hadronic spectra, and in this sense are parameter-free predictions. Finally, we close the chapter with model results for strong decays of non-strange baryon resonances, with special attention to the low-lying states.

After explaining how baryon spectra and strong decays are depicted in the quark model, the purpose of **Chapter 4** is to present the theoretical basis to relate such properties to meson-baryon transition amplitudes, and thereby establish a procedure to account for rescattering effects in baryon decays. This will be done by applying the general concepts of scattering theory to meson-baryon systems. As we shall see in this chapter, such a formalism not only allows for the inclusion of final state interactions in strong decays, but also leads to the physical interpretation of the baryon masses as evaluated in the relativistic quark model.

At this point, the only ingredient left before the calculation of rescattering effects is an on-shell description of coupled-channel meson-baryon interactions. Such a model will be implemented in **Chapter 5** based on an on-shell reduction of the Jülich model. We shall demonstrate in this chapter that, despite the on-shell approximation, we achieve a very good description for non-resonant contributions in most of the partial waves in $\pi N \to \pi N$ scattering, considering the energy range from πN threshold up to 1700 MeV and total angular momentum up to $J = \frac{5}{2}$; this provides a suitable parameterization for the rescattering matrix in the strong decays of low-lying baryons. One exception is the P_{11} partial-wave, which due to the contribution of the Roper resonance $N(1440)$ cannot be described in the framework. For this reason, N states coupling to the πN system in the P_{11} wave will be excluded from our analysis.

As we shall demonstrate in **Chapter 6**, the inclusion of final state interactions does not improve the quark-model description of strong decay widths at all: Whereas the decay widths into πN and ηN remain roughly the same after including rescattering effects, those into $\pi\Delta$ turn out to be much smaller than before. These results show that final state interactions as treated here do lead to sizable corrections in strong baryon decays, at least concerning decays into $\pi\Delta$, but the effect is the opposite of what we initially expected. As these results indicate that the couplings of baryon resonances to the considered decay channels are too small in the RCQM, we finish the chapter with a suggestion of how the framework may be improved in the future.

Finally, we close this thesis in **Chapter 7** with a concise summary and outlook.

Chapter 2

The relativistic constituent quark model

2.1 Introduction

The aim of this chapter is to review the formalism of the relativistic constituent quark model and its predictions for hadron spectra, focusing on the ingredients we need in this thesis, *i.e.* the spectra of the low-lying N and Δ resonances, as well as the results for ground-state π and η mesons, as these are present in the strong decay channels πN, $\pi\Delta$ and ηN considered in the next chapter. The equations will be simply stated for further reference, since their derivation can be found in greater detail in previous works, see Refs. [23, 24, 26, 27] for meson and [28–30] for baryon spectra.

The formalism is based on the Bethe-Salpeter equation [48], which is a covariant integral equation and provides a suitable framework for the description of hadrons as relativistic bound states of quarks. In the case of strong interactions, however, this equation cannot be directly applied since its basic ingredients, *i.e.* the full quark propagators and interaction kernels, are still unknown functions in QCD. Moreover, even if these functions were known, their dependence on relative energy variables as it occurs in a relativistic treatment leads to a complicated pole structure, which prevents the solution of the full integral equation. Therefore, to obtain a solvable bound-state equation which can be used in explicit calculations, one has to introduce phenomenological approximations for the propagators and the interaction kernels.

In the present model we employ two approximations: Firstly, we parametrize the full quark propagators by the usual free propagators with poles at effective constituent quark masses, which enter as free parameters in the model and should account for a part of the effects related to quark self-interactions. Secondly, we adopt instantaneous interaction kernels in the hadron rest frame, simplifying the energy dependence of the Bethe-Salpeter equation this way. As we shall see in this chapter, these assumptions allow for the reduction of the Bethe-Salpeter equation to a three-dimensional Salpeter equation [49], which can be formulated as an eigenvalue problem and solved by standard methods once the underlying potential is specified.

As already mentioned, is it still not possible to derive the interquark potential from QCD in the confinement regime, where hadron resonances occur ($\lesssim$ 3 GeV). Hence, we rely on the structure of the experimental hadron spectra in order to construct an

appropriate phenomenological parameterization. On the one hand, the global features of the mass spectra such as the occurrence of Regge trajectories suggest that quarks interact through a flavor-independent confinement potential, which rises linearly with interquark distances. On the other hand, the existence of mass-splittings in the baryon ($N-\Delta$, $\Lambda-\Sigma-\Sigma^*$, $\Xi-\Xi^*$) or likewise in the meson spectrum ($\pi-\eta-\eta'$, $K-K^*$) indicate the presence of an additional spin-flavor-dependent interaction. Based on these observations, we parametrize the underlying quark interactions by a linear confinement potential, which includes a suitable spin structure in a fully relativistic framework, as well as a residual interaction motivated by instanton effects.

The Bethe-Salpeter formalism applied to the case of mesons as quark-antiquark ($q\bar{q}$) and baryons as three-quark (qqq) bound states is recapitulated in Sections 2.2 and 2.3, respectively. The phenomenological potentials employed in the model are discussed in more detail in the subsequent Section 2.4. Although mesons are not the subject of this thesis, they are of course present in strong decay of baryons and therefore were also taken into consideration. Moreover, the reduction to the Salpeter equation is simpler in the case of treating $q\bar{q}$ bound states and provides an instructive example before the treatment of the more complicated qqq systems. Finally, we conclude this chapter in Section 2.5 with an overview of the predictions of the model for non-strange hadrons, focusing on those which are relevant for this thesis.

2.2 Mesons as quark-antiquark bound states

In constituent quark models mesons are considered to be strongly bound states of a quark-antiquark $q\bar{q}$ pair. In a relativistic treatment, this description should be based on the principles of quantum field theory, according to which two-fermion bound states emerge as poles in the four-point Green's function. In the Heisenberg picture, this function is defined via quark field operators Ψ^i and their adjoints $\bar{\Psi}=\Psi^\dagger\gamma^0$ by

$$G^{(4)}_{\alpha_1'\alpha_2'\alpha_1\alpha_2}(x_1',x_2',x_1,x_2) := -\langle\Omega|T\Psi^1_{\alpha_1'}(x_1')\bar{\Psi}^2_{\alpha_2'}(x_2')\Psi^2_{\alpha_2}(x_2)\bar{\Psi}^1_{\alpha_1}(x_1)|\Omega\rangle, \tag{2.1}$$

where $|\Omega\rangle$ denotes the physical vacuum state, T denotes the time-ordering operator and α_i are multi-indices combining spin, flavor and color degrees of freedom. The superscripts 1 and 2 label the quark and the antiquark fields, respectively.

Using standard techniques of time-dependent perturbation theory (see for instance the textbook [50]) the four-point Green's function can also be expressed in the interaction picture in the form of an infinite power series

$$\begin{aligned} G^{(4)}(x_1',x_2',x_1,x_2) = {} & \frac{-1}{\langle 0|T\exp\left(-i\int_\infty^\infty \mathrm{d}\,t\hat{H}_I(t)\right)|0\rangle}\sum_{k=1}^{\infty}\frac{(-i)^k}{k!}\int \mathrm{d}^{\,4}y_1\cdots\mathrm{d}^{\,4}y_k \\ & \times\langle 0|T\Psi^1_I(x_1')\bar{\Psi}^2_I(x_2')\Psi^2_I(x_2)\bar{\Psi}^1_I(x_1)\hat{\mathcal{H}}_I(y_1)\cdots\hat{\mathcal{H}}_I(y_k)|0\rangle, \end{aligned} \tag{2.2}$$

suppressing the multi-indices α_i. Now, the vector $|0\rangle$ denotes the unperturbed vacuum state, $\hat{H}$ and $\hat{\mathcal{H}}$ are the Hamiltonian and the Hamiltonian density operators and the subscript I indicates that the corresponding operators are defined in the interaction picture.

2.2.1 The integral equation for the four-point Green's function

In the absence of bound states the infinite sum in (2.2) might be evaluated through perturbative calculations in $\hat{\mathcal{H}}_I$ up to some finite order k. For the investigation of bound states however, where poles in the Green's function are present, an infinite set of perturbative contributions must be taken into account. It was shown by Bethe and Salpeter [48] and later rigorously proven by Gell-Mann and Low [51] that the sum of all perturbative contributions to the four-point Green's function can be rearranged in the form of an inhomogeneous integral equation

$$\begin{aligned} &G^{(4)}{}_{\alpha_1'\alpha_2'\alpha_1\alpha_2}(x_1', x_2', x_1, x_2) \\ &\qquad = G_0^{(4)}{}_{\alpha_1'\alpha_2'\alpha_1\alpha_2}(x_1', x_2', x_1, x_2) - i \int \mathrm{d}^4 x_1'' \, \mathrm{d}^4 x_2'' \, \mathrm{d}^4 x_1''' \, \mathrm{d}^4 x_2''' \\ &\qquad \times G_0^{(4)}{}_{\alpha_1'\alpha_2'\alpha_1''\alpha_2''}(x_1', x_2', x_1'', x_2'') K^{(2)}{}_{\alpha_1''\alpha_2''\alpha_1'''\alpha_2'''}(x_1'', x_2'', x_1''', x_2''') \\ &\qquad \times G^{(4)}{}_{\alpha_1'''\alpha_2''',\alpha_1\alpha_2}(x_1''', x_2''', x_1, x_2) \end{aligned} \tag{2.3}$$

by introducing the concept of irreducibility. Here, we use the convention of summing over repeated multi-indices α_i, the four-point function $G_0^{(4)}$ denotes the tensor product

$$G_0^{(4)}(x_1', x_2', x_1, x_2) = S_F^1(x_1', x_1) \otimes S_F^2(x_2, x_2') \tag{2.4}$$

of full fermion propagators

$$S_{F\alpha\beta}^i(x, y) := \langle \Omega | T \Psi_\alpha^i(x) \bar{\Psi}_\beta^i(y) | \Omega \rangle \tag{2.5}$$

and $K^{(2)}$ represents the irreducible two-body interaction kernel, which is defined as the sum of all irreducible Feynman diagrams included in the perturbative series of $G^{(4)}$. A two-fermion diagram is called irreducible when it cannot be split into simpler graphs by cutting two fermion lines, as the examples depicted in Fig. 2.1.

Now, as bound-state poles appear in the total four-momentum of the $q\bar{q}$ system, for our purposes it is more convenient to formulate the integral equation for $G^{(4)}$ in momentum space. For this we first introduce Jacobi coordinates, *i.e.* a set of variables consisting of an external center-of-mass coordinate X and an internal relative coordinate x, as well as their conjugate momenta P and p, in terms of which the translational invariance of the four-point functions $G^{(4)}$, $G_0^{(4)}$ and $K^{(2)}$ can be formulated explicitly. These coordinates are defined by the linear transformations

$$\begin{pmatrix} X \\ x \end{pmatrix} = \begin{pmatrix} \frac{1}{2} & \frac{1}{2} \\ 1 & -1 \end{pmatrix} \begin{pmatrix} x_1 \\ x_2 \end{pmatrix} \tag{2.6}$$

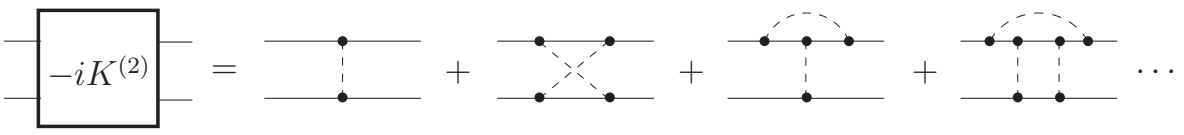

Figure 2.1. Perturbative contributions to the two-body irreducible kernel $K^{(2)}$.

and

$$\begin{pmatrix} P \\ p \end{pmatrix} = \begin{pmatrix} 1 & 1 \\ \frac{1}{2} & -\frac{1}{2} \end{pmatrix} \begin{pmatrix} p_1 \\ p_2 \end{pmatrix}, \tag{2.7}$$

where the variables p_1 and p_2 denote the four-momentum carried by q and $\bar{q}$. In terms of these new variables, the Fourier-transform for any four-point function $A = G^{(4)}$, $G_0^{(4)}$ and $K^{(2)}$ is defined by

$$\begin{aligned} A(x_1', x_2', x_1, x_2) &\equiv A(X' - X, x', x) \\ &=: \int \frac{\mathrm{d}^4 P}{(2\pi)^4} e^{-iP\cdot(X'-X)} \int \frac{\mathrm{d}^4 p'}{(2\pi)^4} e^{-ip'\cdot x'} \int \frac{\mathrm{d}^4 p}{(2\pi)^4} e^{+ip\cdot x} A_P(p', p), \end{aligned} \tag{2.8}$$

where the subscript in A_P indicates that its dependence on the total four-momentum is only parametric, in agreement with translational invariance. According to Eq. (2.8), the integral equation for $G^{(4)}$ in momentum space then reads

$$G_P^{(4)}(p', p) = G_{0P}^{(4)}(p', p) - i \int \frac{\mathrm{d}^4 p''}{(2\pi)^4} \frac{\mathrm{d}^4 p'''}{(2\pi)^4} G_{0P}^{(4)}(p', p'') K_P^{(2)}(p'', p''') G_P^{(4)}(p''', p), \tag{2.9}$$

where $G_{0P}^{(4)}$ denotes the product

$$G_{0P}^{(4)}(p', p) = (2\pi)^4 \delta^{(4)}(p' - p) S_F^1\left(\tfrac{P}{2} + p\right) \otimes S_F^2\left(-\tfrac{P}{2} + p\right) \tag{2.10}$$

of full fermion propagators in momentum space, defined by their Fourier-transform

$$S_F^i(x, y) =: \int \frac{\mathrm{d}^4 p}{(2\pi)^4} e^{-ip\cdot(x-y)} S_F^i(p). \tag{2.11}$$

2.2.2 Quark-antiquark bound state contributions

Depending on the time-ordering dictated by the operator T in Eq. (2.1) the four-point Green's function accounts for all kinds of processes involving four quark fields, as well as related bound states such as mesons, diquarks and their antiparticles. Here we shall consider the meson contributions only, which in quark models correspond to $q\bar{q}$ bound states with positive energy propagating forward in time. Accordingly, we focus on those terms in $G^{(4)}$ corresponding to the particular time-ordering $\min\{x_1'^0, x_2'^0\} > \max\{x_1^0, x_2^0\}$, *i.e.*

$$\begin{aligned} G^{(4)}(x_1', x_2', x_1, x_2) = &-\langle\Omega| \left[T\Psi^1(x_1')\bar{\Psi}^2(x_2')\right] \left[T\Psi^2(x_2)\bar{\Psi}^1(x_1)\right] |\Omega\rangle \\ &\times\theta\big(\min\{x_1'^0, x_2'^0\} - \max\{x_1^0, x_2^0\}\big) + \text{other time-orderings}, \end{aligned} \tag{2.12}$$

and then investigate the contribution of bound states with total mass M and positive energy

$$\omega_{\bar{P}} = \sqrt{\mathbf{P}^2 + M^2} \tag{2.13}$$

by inserting a complete set of momentum eigenstates $|\bar{P}\rangle$ between the time-ordered products in Eq. (2.12). These states are normalized covariantly according to

$$\langle\bar{P}'|\bar{P}\rangle = (2\pi)^3 2\omega_{\bar{P}} \delta^{(3)}(\mathbf{P} - \mathbf{P}'), \tag{2.14}$$

where we introduced a specific notation for the on-shell momentum $\bar{P}$ to emphasize the difference with the generally off-shell momentum P (*cf.* Eq. (2.7)). Following this procedure, we arrive at

$$\begin{aligned} G^{(4)}(x_1', x_2', x_1, x_2) = -\int \frac{\mathrm{d}^3\,\bar{P}}{(2\pi)^3 2\omega_{\bar{P}}} \left[\chi_{\bar{P}}(x_1', x_2') \otimes \bar{\chi}_{\bar{P}}(x_1, x_2)\right] \\ \times\theta\left(\min\{x_1'^0, x_2'^0\} - \max\{x_1^0, x_2^0\}\right) + \text{other terms}, \end{aligned} \tag{2.15}$$

where only the contribution of meson states $|\bar{P}\rangle$ is written explicitly, whereas terms arising from different time-orderings and intermediate states are collected in "other terms". Here, the amplitudes $\chi_{\bar{P}}$ and $\bar{\chi}_{\bar{P}}$ denote the **Bethe-Salpeter amplitude** and its adjoint, respectively, defined as the matrix elements

$$\chi_{\bar{P}\alpha_1\alpha_2}(x_1, x_2) := \langle\Omega|T\Psi^1_{\alpha_1}(x_1)\bar{\Psi}^2_{\alpha_2}(x_2)|\bar{P}\rangle \tag{2.16}$$

and

$$\bar{\chi}_{\bar{P}\alpha_2\alpha_1}(x_1, x_2) := \langle\bar{P}|T\Psi^2_{\alpha_2}(x_2)\bar{\Psi}^1_{\alpha_1}(x_1)|\Omega\rangle \tag{2.17}$$

between the physical vacuum $|\Omega\rangle$ and the bound state $|\bar{P}\rangle$. In terms of Jacobi coordinates, the Bethe-Salpeter amplitudes can be written as

$$\chi_{\bar{P}}(x_1, x_2) = e^{-i\bar{P}\cdot X}\chi_{\bar{P}}(x) =: e^{-i\bar{P}\cdot X}\int \frac{\mathrm{d}^4\,p}{(2\pi)^4} e^{-ip\cdot x}\chi_{\bar{P}}(p) \tag{2.18}$$

and

$$\bar{\chi}_{\bar{P}}(x_1, x_2) = e^{+i\bar{P}\cdot X}\bar{\chi}_{\bar{P}}(x) =: e^{+i\bar{P}\cdot X}\int \frac{\mathrm{d}^4\,p}{(2\pi)^4} e^{+ip\cdot x}\bar{\chi}_{\bar{P}}(p), \tag{2.19}$$

where the dependence on the center-of-mass variable factorizes.

The Heaviside function $\theta(\min\{x_1'^0, x_2'^0\} - \max\{x_1^0, x_2^0\})$ in Eq. (2.15), which specifies the time-ordering corresponding to mesons, gives rise to a pole in the total energy variable at $P^0 = \omega_{\bar{P}}$ or, equivalently, at $P^2 = M^2$. Indeed, as shown in detail in Ref. [52], by replacing the Heaviside function by its integral representation and applying inverse Fourier-transforms on both sides of Eq. (2.15), one obtains the following expression for the four-point Green's function in momentum space:

$$G^{(4)}_P(p', p) = \frac{-i}{2\omega_{\bar{P}}} \frac{\zeta_{\bar{P}}(p', P^0 - \omega_{\bar{P}}) \otimes \bar{\zeta}_{\bar{P}}(p, P^0 - \omega_{\bar{P}})}{P^0 - \omega_{\bar{P}} + i\epsilon} + \text{ other terms}, \tag{2.20}$$

which contains an explicit pole at $\omega_{\bar{P}}$. The amplitudes $\zeta_{\bar{P}}$ and $\bar{\zeta}_{\bar{P}}$ are defined by

$$\zeta_{\bar{P}}(x, \omega) := \chi_{\bar{P}}(x)e^{i\omega\frac{|x^0|}{2}} =: \int \frac{\mathrm{d}^4\,p}{(2\pi)^4} e^{-ip\cdot x}\zeta_{\bar{P}}(p, \omega) \tag{2.21}$$

and

$$\bar{\zeta}_{\bar{P}}(x, \omega) := \bar{\chi}_{\bar{P}}(x)e^{i\omega\frac{|x^0|}{2}} =: \int \frac{\mathrm{d}^4\,p}{(2\pi)^4} e^{+ip\cdot x}\bar{\zeta}_{\bar{P}}(p, \omega) \tag{2.22}$$

as off-shell generalizations of the Bethe-Salpeter amplitude and its adjoint, respectively, and respect the conditions $\zeta_{\bar{P}}(p, 0) = \chi_{\bar{P}}(p)$ and $\bar{\zeta}_{\bar{P}}(p, 0) = \bar{\chi}_{\bar{P}}(p)$.

2.2.3 The two-body Bethe-Salpeter equation

A set of bound-state equations, namely the **Bethe-Salpeter equation** and its adjoint for the amplitudes $\chi_{\bar{P}}$ and $\bar{\chi}_{\bar{P}}$, as well as their normalization condition can be derived in a simple and uniform way based on the analytical behavior of $G^{(4)}$ in the vicinity of the pole $P^0 = \omega_{\bar{P}}$. In the following we shall merely sketch the main steps of this derivation and refer to [52] for further details. The starting point is the integral equation (2.9) for $G^{(4)}$ in momentum space, which can be more concisely written as an operator equation

$$G_P = G_{0P} - iG_{0P}K_PG_P \tag{2.23}$$

by defining the product

$$[A_PB_P](p',p) = \int \frac{\mathrm{d}^4 p''}{(2\pi)^4} A_P(p',p'')B_P(p'',p) \tag{2.24}$$

of two four-point functions A_P and B_P in momentum space. For the sake of clarity, we suppress the superscripts on the four-point functions for now. It is straightforward to show that the operator equation above is equivalent to

$$\left[G_{0P}^{-1} + iK_P\right] G_P = G_P \left[G_{0P}^{-1} + iK_P\right] = I, \tag{2.25}$$

where the identity operator I is defined with respect to the product (2.24) and the inverse operator G_{0P}^{-1} fulfills $G_{0P}^{-1}G_{0P} = G_{0P}G_{0P}^{-1} = I$. Moreover, from Eq. (2.25) one also obtains the inverse operator of G_P, *i.e.*

$$G_P^{-1} = G_{0P}^{-1} + iK_P, \tag{2.26}$$

such that $G_P^{-1}G_P = G_PG_P^{-1} = I$. Now, to investigate the analytical behavior of the four-point Green's function in the vicinity of the pole, we replace the operators G_P and G_P^{-1} by their expansions

$$G_P \approx \frac{-i}{2\omega_{\bar{P}}} \frac{\chi_{\bar{P}} \otimes \bar{\chi}_{\bar{P}}}{P^0 - \omega_{\bar{P}} + i\epsilon} + \left[\frac{\partial}{\partial P^0}\left(\left(P^0 - \omega_{\bar{P}}\right) G_P\right)\right]_{P^0=\omega_{\bar{P}}} \tag{2.27}$$

(*cf.* Eq. (2.20)) and

$$G_P^{-1} \approx G_{\bar{P}}^{-1} + \left(P^0 - \omega_{\bar{P}}\right)\left[\frac{\partial}{\partial P^0} G_P^{-1}\right]_{P^0=\omega_{\bar{P}}} \tag{2.28}$$

for $P^0 \approx \omega_{\bar{P}}$ into Eq. (2.25), and then compare the resulting Laurent expansions to the identity operator on the right-hand side of this equation, order-by-order in powers of $(P^0 - \omega_{\bar{P}})$. From the comparison between terms of order $\mathcal{O}(-1)$ we arrive at the Bethe-Salpeter equation

$$\chi_{\bar{P}} = -iG_{0\bar{P}}K_{\bar{P}}\chi_{\bar{P}} \tag{2.29}$$

and its adjoint

$$\bar{\chi}_{\bar{P}} = -i\bar{\chi}_{\bar{P}}K_{\bar{P}}G_{0\bar{P}}. \tag{2.30}$$

The normalization condition

$$-i\bar{\chi}_{\bar{P}}\left[\frac{\partial}{\partial P^0}G_P^{-1}\right]_{P^0=\omega_{\bar{P}}}\chi_{\bar{P}} = 2\omega_{\bar{P}}, \tag{2.31}$$

in turn, follows from the comparison between terms of $\mathcal{O}(0)$. Although not explicitly covariant, Eq. (2.31) might also be relativistically formulated as [53]

$$-i\bar{\chi}_{\bar{P}}\left[\frac{\partial}{\partial P_\mu}G_P^{-1}\right]_{P=\bar{P}}\chi_{\bar{P}} = 2\bar{P}^\mu. \tag{2.32}$$

Finally, with its full momentum dependence, the Bethe-Salpeter equation (2.29) is given by

$$\chi_{\bar{P}}(p) = -i\left[S_F^1\left(\tfrac{\bar{P}}{2}+p\right)\otimes S_F^2\left(-\tfrac{\bar{P}}{2}+p\right)\right]\int\frac{\mathrm{d}^4p'}{(2\pi)^4}K_{\bar{P}}^{(2)}(p,p')\chi_{\bar{P}}(p'), \tag{2.33}$$

where we used the definition (2.10) of $G_{0P}^{(4)}$ and the product defined in (2.24).

2.2.4 Reduction to the two-body Salpeter equation

In principle, the Bethe-Salpeter equation (2.33) provides the theoretical basis for any covariant quark model of mesons. In the case of strongly interacting systems however, several difficulties prevent the exact solution of this equation. Firstly, as usually happens in any relativistic framework, each one of its basic ingredients depend on relative energy variables, leading to an intricate pole structure in the complex plane. Moreover, specifically in the case of strong interactions, neither the full quark propagators S_F^i nor the interaction kernel $K^{(2)}$ are presently known. In fact, these quantities are only defined perturbatively as infinite series of diagrams, which in the confinement region of QCD cannot be truncated in a meaningful way.

Therefore, in order to obtain an integral equation which can be directly applied for practical calculations, some simplifying approximations and assumptions have to be introduced. In the present model we employ two approximations: firstly, we assume that full quark propagators S_F^i can be parametrized by the usual free fermion propagator, *i. e.*

$$S_F^i(p_i) \stackrel{!}{=} \frac{i}{\not{p}_i - m_i + i\epsilon}, \tag{2.34}$$

with poles at effective *constituent quark masses* m_i. These are in turn considered to be a reasonable parameterization for effects related to quark self-interactions. The constituent masses m_i enter as free parameters in the model, thus for the light-flavored hadron spectrum in the isospin-conserving limit one has two free parameters: The non-strange quark mass $m_n := m_u \equiv m_d$ and the strange quark mass m_s, where u, d and s denote the up, down and strange quark flavors.

As a second approximation, the irreducible kernel $K^{(2)}$ is assumed to be instantaneous in the meson rest frame. This is equivalent to neglecting retardation effects in the center-of-mass of the $q\bar{q}$ system and is explicitly formulated as

$$K_M^{(2)}(p',p) \stackrel{!}{=} V^{(2)}(\mathbf{p}',\mathbf{p}), \tag{2.35}$$

where the subscript M indicates that the corresponding quantity is evaluated at the center-of-mass where $\bar{P} = (M, \mathbf{0})$. Although Eq. (2.35) is not explicitly covariant, the instantaneous approximation can be covariantly written as well. For simplicity here we work in the center-of-mass and refer to [52] for details on the relativistic formulation.

These two approximations together enable the reduction of the full four-dimensional Bethe-Salpeter equation to an equivalent three-dimensional problem. To show this, we evaluate Eq. (2.33) in instantaneous approximation and integrate both its sides over the relative energy variable p^0, leading to

$$\Phi(\mathbf{p}) = -i \left[\int \frac{\mathrm{d}\, p^0}{2\pi} S_F^1 \left(\tfrac{M}{2} + p \right) \otimes S_F^2 \left(-\tfrac{M}{2} + p \right) \right] \left[\int \frac{\mathrm{d}^3 p'}{(2\pi)^3} V^{(2)}(\mathbf{p}', \mathbf{p}) \Phi(\mathbf{p}') \right], \quad (2.36)$$

where we defined the **Salpeter amplitude**

$$\Phi(\mathbf{p}) := \int \frac{\mathrm{d}\, p^0}{2\pi} \chi_M(p^0, \mathbf{p}). \quad (2.37)$$

Now, we note that due to the instantaneous approximation the relative energy dependence of the integrand in (2.36) is a factor inside the full quark propagators S_F^i only. As these are unknown functions in the confinement regime of QCD, we employ the effective free quark parameterization (2.34) to perform the remaining integral over p^0 analytically. To this end, it is more convenient to use the following decomposition of the free quark propagators (see *e.g.* the textbook [54]):

$$S_F^i(p_i) = i \left[\frac{\Lambda_i^+(\mathbf{p}_i)}{p_i^0 - \omega_i(\mathbf{p}_i) + i\epsilon} + \frac{\Lambda_i^-(\mathbf{p}_i)}{p_i^0 + \omega_i(\mathbf{p}_i) - i\epsilon} \right] \gamma^0, \quad (2.38)$$

which separates the two poles $p_i^0 = \pm\omega_i$, located at the on-shell quark energy

$$\omega_i(\mathbf{p}_i) := \sqrt{|\mathbf{p}_i|^2 + m_i^2}. \quad (2.39)$$

The operators $\Lambda_i^\pm$ in Eq. (2.38) denote the projectors

$$\Lambda_i^\pm(\mathbf{p}_i) := \frac{\omega_i(\mathbf{p}_i) I \pm H_i(\mathbf{p}_i)}{2\omega_i(\mathbf{p}_i)} \quad (2.40)$$

onto positive and negative energy solutions of the Dirac equation, and are defined in terms of the on-shell energies w_i and the usual Dirac Hamiltonian

$$H_i(\mathbf{p}_i) := \gamma^0 \left(\gamma \cdot \mathbf{p}_i + m_i \right). \quad (2.41)$$

After integrating the effective propagators over p^0, Eq. (2.36) finally reduces to

$$\begin{aligned} \Phi(\mathbf{p}) = &- \frac{1}{M - \omega_1 - \omega_2} \Lambda_1^+(\mathbf{p}) \gamma^0 \left[\int \frac{\mathrm{d}^3 p'}{(2\pi)^3} V^{(2)}(\mathbf{p}, \mathbf{p}') \Phi(\mathbf{p}') \right] \gamma^0 \Lambda_2^-(-\mathbf{p}) \\ &+ \frac{1}{M + \omega_1 + \omega_2} \Lambda_1^-(\mathbf{p}) \gamma^0 \left[\int \frac{\mathrm{d}^3 p'}{(2\pi)^3} V^{(2)}(\mathbf{p}, \mathbf{p}') \Phi(\mathbf{p}') \right] \gamma^0 \Lambda_2^+(-\mathbf{p}), \end{aligned} \quad (2.42)$$

which is the so-called **Salpeter equation** [49] for the Salpeter amplitude Φ.

Thus we have shown that the four-dimensional Bethe-Salpeter equation (2.33) when considered with the approximations given in Eqs. (2.35) and (2.34) can be reduced to an equivalent three-dimensional Salpeter equation (2.42). Furthermore, note in the latter expression that the use of effective quark propagators leads to some projection properties which constrain the Salpeter amplitudes, implying that Φ respects the relation

$$\Lambda_1^+(\mathbf{p})\Phi(\mathbf{p})\Lambda_2^+(-\mathbf{p}) = \Lambda_1^-(\mathbf{p})\Phi(\mathbf{p})\Lambda_2^-(-\mathbf{p}) = 0, \tag{2.43}$$

as can be easily verified by applying the operators $\Lambda^{\pm}(\mathbf{p})$ from the left and $\Lambda^{\pm}(-\mathbf{p})$ from the right side on Eq. (2.42). This is an important remark since, as discussed in Ref. [55], the Salpeter equation can be conveniently reformulated in the Hamiltonian form of an eigenvalue equation

$$\mathcal{H}^{(2)}\Phi := M\Phi \tag{2.44}$$

with the Hamiltonian operator

$$\begin{aligned}\left[\mathcal{H}^{(2)}\Phi\right](\mathbf{p}) := {} & H_1(\mathbf{p})\Phi(\mathbf{p}) - \Phi(\mathbf{p})H_2(-\mathbf{p}) \\ & - \Lambda_1^+(\mathbf{p})\gamma^0\left[\int\frac{\mathrm{d}^3p'}{(2\pi)^3}V^{(2)}(\mathbf{p},\mathbf{p}')\Phi(\mathbf{p}')\right]\gamma^0\Lambda_2^-(-\mathbf{p}) \\ & + \Lambda_1^-(\mathbf{p})\gamma^0\left[\int\frac{\mathrm{d}^3p'}{(2\pi)^3}V^{(2)}(\mathbf{p},\mathbf{p}')\Phi(\mathbf{p}')\right]\gamma^0\Lambda_2^+(-\mathbf{p}),\end{aligned} \tag{2.45}$$

provided that Φ fulfills the constraint (2.43).

For the sake of completeness, we also give here the normalization condition for the Salpeter amplitudes, which is written as [52]

$$\int\frac{\mathrm{d}^3p}{(2\pi)^3}\,\mathrm{Tr}\left[\Phi^\dagger(\mathbf{p})\Lambda_1^+(\mathbf{p})\Phi(\mathbf{p})\Lambda_2^-(-\mathbf{p}) - \Phi^\dagger(\mathbf{p})\Lambda_1^-(\mathbf{p})\Phi(\mathbf{p})\Lambda_2^+(-\mathbf{p})\right] = 2M \tag{2.46}$$

and is derived from the normalization condition (2.32) for the Bethe-Salpeter amplitudes evaluated with the same approximations.

The Salpeter equation in the Hamiltonian form of Eq. (2.44) and the normalization condition (2.46) constitute the basis of our relativistic quark model of mesons. Once the underlying potential $V^{(2)}$ is specified, this equation can be numerically solved by standard techniques, resulting in a spectrum of eigenvalues M which is associated to the possible masses in the meson spectrum. The phenomenological potentials employed in our model are discussed later in Section 2.4. For details on the numerical implementation, see Ref. [56]. Before proceeding further, we would like to point out that, although an important ingredient for the derivation presented here, the use of free quark propagators seems to be inconsistent with the picture of interacting quark fields confined in a hadronic state. Moreover, it has been already demonstrated by Lucha and Schöberl [55] that the reduction to the two-body Salpeter equation is in fact possible with full quark propagators, as long as they are also considered to be instantaneous in the meson rest frame. This result, as well as its generalization to the case of baryons, has not been implemented in our model yet and should be discussed in a future project.

2.3 Baryons as three-quark bound states

In the previous section the description of mesons as relativistic $q\bar{q}$ bound states has been discussed in some detail. Let us now generalize to the case of baryons, following basically the same lines, but pointing out the difficulties arising from the treatment of these more complicated systems. In our framework, baryon excitations are considered to be relativistic bound states of three quarks qqq and as such, are related to the poles of the six-point Green's function

$$\begin{aligned} G^{(6)}_{\alpha_1'\alpha_2'\alpha_3',\alpha_1\alpha_2\alpha_3}(x_1',x_2',x_3',x_1,x_2,x_3) \\ := -\langle\Omega|T\Psi^1_{\alpha_1'}(x_1')\Psi^2_{\alpha_2'}(x_2')\Psi^3_{\alpha_3'}(x_3')\bar{\Psi}^1_{\alpha_1}(x_1)\bar{\Psi}^2_{\alpha_2}(x_2)\bar{\Psi}^3_{\alpha_3}(x_3)|\Omega\rangle, \end{aligned} \tag{2.47}$$

as it is defined in the Heisenberg picture, or

$$\begin{aligned} &G^{(6)}(x_1',x_2',x_3',x_1,x_2,x_3) \\ &\quad = \frac{-1}{\langle 0|T\exp\left(-i\int_\infty^\infty \mathrm{d}\,t\hat{H}_I(t)\right)|0\rangle}\sum_{k=1}^{\infty}\frac{(-i)^k}{k!}\int \mathrm{d}^{\,4}y_1\cdots\mathrm{d}^{\,4}y_k \\ &\quad \times\langle 0|T\Psi^1_I(x_1')\Psi^2_I(x_2')\Psi^3_I(x_3')\bar{\Psi}^1_I(x_1)\bar{\Psi}^2_I(x_2)\bar{\Psi}^3_I(x_3)\hat{\mathcal{H}}_I(y_1)\cdots\hat{\mathcal{H}}_I(y_k)|0\rangle, \end{aligned} \tag{2.48}$$

given in the interaction picture. In these equations, the superscripts $i=1,2,3$ label the three constituent quark fields q^i.

2.3.1 The integral equation for the six-point Green's function

Similarly to the case of $G^{(4)}$, the infinite sum of perturbative contributions to $G^{(6)}$ may also be expressed in the form of an inhomogeneous integral equation by introducing the concept of irreducibility. However, in contrast to (2.2) the perturbative series in (2.48) comprises two different classes of irreducible contributions, which should be properly summed into distinct interaction kernels. On the one hand, it contains fully connected diagrams in which all the three constituent quarks interact; these are collected into the kernel

$$K^{(3)}_{\alpha_1'\alpha_2'\alpha_3',\alpha_1\alpha_2\alpha_3}(x_1',x_2',x_3',x_1,x_2,x_3), \tag{2.49}$$

where we call a connected three-quark diagram irreducible when it cannot be split into simpler graphs by cutting three fermion lines, as the examples depicted in Fig. 2.2. On the other hand, the perturbative series of $G^{(6)}$ also contains two-body irreducible interactions which occur for each possible qq pair within the qqq system in conjunction

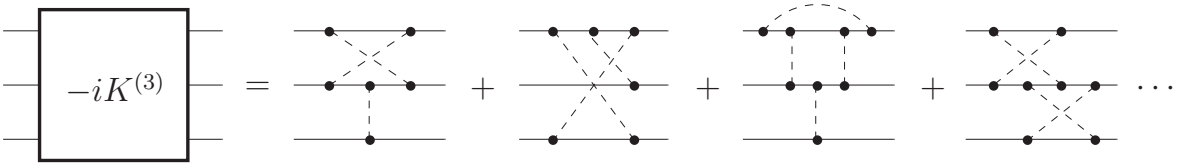

Figure 2.2. Perturbative contributions to the three-body irreducible kernel $K^{(3)}$.

with a third unconnected, non-interacting quark. Such contributions are collected into three distinct kernels

$$K^{(2)}_{\alpha_i'\alpha_j',\alpha_i\alpha_j}(x_i', x_j', x_i, x_j), \tag{2.50}$$

with $i, j = 1, 2$ or 3, where irreducibility is defined in the same manner as in the case of mesons (*cf.* Fig. 2.1). In addition, to concisely formulate an integral equation for $G^{(6)}$ we define an integral kernel

$$\bar{K}^{(2)}(x_1', x_2', x_3', x_1, x_2, x_3) := \sum_{\substack{\text{cycl.perm.}\\ \{i,j,k\}}} K^{(2)}(x_i', x_j', x_i, x_j) S_F^{k\,-1}(x_k', x_k) \tag{2.51}$$

which includes all the two-body irreducible kernels in the form of a six-point function. Here, the inverse of fermion propagators are defined according to

$$\int \mathrm{d}^4\, x_k'' S^k_{F\,\alpha_k'\alpha_k''}(x_k', x_k'') S^{k\,-1}_{F\,\alpha_k''\alpha_k}(x_k'', x_k) = \delta_{\alpha_k'\alpha_k}\delta^{(4)}(x_k' - x_k). \tag{2.52}$$

Hence, in terms of the kernels $\bar{K}^{(2)}$ and $K^{(3)}$, the integral equation for $G^{(6)}$ reads:

$$\begin{aligned} &G^{(6)}(x_1', x_2', x_3', x_1, x_2, x_3) \\ &\quad = G_0^{(6)}(x_1', x_2', x_3', x_1, x_2, x_3) - i \int \mathrm{d}^4 x_1'' \,\mathrm{d}^4 x_2'' \,\mathrm{d}^4 x_3'' \,\mathrm{d}^4 x_1''' \,\mathrm{d}^4 x_2''' \,\mathrm{d}^4 x_3''' \\ &\quad \times G_0^{(6)}(x_1', x_2', x_3', x_1'', x_2'', x_3'') \left[\bar{K}^{(2)} + K^{(3)}\right](x_1'', x_2'', x_3'', x_1''', x_2''', x_3''') \\ &\quad \times G^{(6)}(x_1''', x_2''', x_3''', x_1, x_2, x_3), \end{aligned} \tag{2.53}$$

where $G_0^{(6)}$ denotes the tensor product

$$G_0^{(6)}(x_1', x_2', x_3', x_1, x_2, x_3) = S_F^1(x_1', x_1) \otimes S_F^2(x_2', x_2) \otimes S_F^3(x_3', x_3) \tag{2.54}$$

of full fermion propagators.

Now, to formulate the integral equation for $G^{(6)}$ in momentum space, we introduce a set of three-body Jacobi coordinates consisting of a center-of-mass variable X and relative coordinates x_ξ and x_η, as well as their conjugate momenta P, p_ξ and p_η, by means of the linear transformations

$$\begin{pmatrix} X \\ x_\xi \\ x_\eta \end{pmatrix} = \begin{pmatrix} \frac{1}{3} & \frac{1}{3} & \frac{1}{3} \\ 1 & -1 & 0 \\ \frac{1}{2} & \frac{1}{2} & -1 \end{pmatrix} \begin{pmatrix} x_1 \\ x_2 \\ x_3 \end{pmatrix} \tag{2.55}$$

and

$$\begin{pmatrix} P \\ p_\xi \\ p_\eta \end{pmatrix} = \begin{pmatrix} 1 & 1 & 1 \\ \frac{1}{2} & -\frac{1}{2} & 0 \\ \frac{1}{3} & \frac{1}{3} & -\frac{2}{3} \end{pmatrix} \begin{pmatrix} p_1 \\ p_2 \\ p_3 \end{pmatrix} \tag{2.56}$$

where p_i denotes the four-momentum carried by the constituent quark q^i. Moreover,

due to the contribution of unconnected two-quark interactions a set of two-body Jacobi coordinates has to be considered here as well. In analogy to the linear transformations in Eqs. (2.6) and (2.7) we thus define for each possible $q^i q^j$ pair in the qqq system the coordinates

$$\begin{pmatrix} X_k \\ x_{\xi_k} \end{pmatrix} = \begin{pmatrix} \frac{1}{2} & \frac{1}{2} \\ 1 & -1 \end{pmatrix} \begin{pmatrix} x_i \\ x_j \end{pmatrix} \tag{2.57}$$

and respective momenta

$$\begin{pmatrix} P_k \\ p_{\xi_k} \end{pmatrix} = \begin{pmatrix} 1 & 1 \\ \frac{1}{2} & -\frac{1}{2} \end{pmatrix} \begin{pmatrix} p_i \\ p_j \end{pmatrix}, \tag{2.58}$$

such that three different sets of coordinates are generated by cyclical permutations of $\{i,j,k\} = \{1,2,3\}$. Finally, in order to relate the two- and three-body momenta variables we define

$$p_{\eta_k} := \tfrac{1}{3}\left(p_i + p_j - 2p_k\right), \tag{2.59}$$

so that the total two-body momenta P_k is related to P according to

$$P_k = \tfrac{2}{3}P + p_{\eta_k}, \tag{2.60}$$

while the two-body relative momenta p_{ξ_k} and p_{η_k} are obtained by the transformations

$$\begin{pmatrix} p_\xi \\ p_\eta \end{pmatrix} = \begin{pmatrix} p_{\xi_3} \\ p_{\eta_3} \end{pmatrix} = \begin{pmatrix} -\frac{1}{2} & -\frac{3}{4} \\ 1 & -\frac{1}{2} \end{pmatrix} \begin{pmatrix} p_{\xi_1} \\ p_{\eta_1} \end{pmatrix} = \begin{pmatrix} -\frac{1}{2} & \frac{3}{4} \\ -1 & -\frac{1}{2} \end{pmatrix} \begin{pmatrix} p_{\xi_2} \\ p_{\eta_2} \end{pmatrix}. \tag{2.61}$$

In terms of the Jacobi coordinates (2.55) and (2.56), the Fourier-transform for any six-point function $A = G^{(6)}$, $G_0^{(6)}$, $\bar{K}^{(2)}$ and $K^{(3)}$ is defined by

$$\begin{aligned} A(x_1', x_2', x_3', x_1, x_2, x_3) &\equiv A(X' - X, x_\xi', x_\eta', x_\xi, x_\eta) \\ &=: \int \frac{\mathrm{d}^4 P}{(2\pi)^4} e^{-iP\cdot(X'-X)} \int \frac{\mathrm{d}^4 p_\xi'}{(2\pi)^4} \frac{\mathrm{d}^4 p_\eta'}{(2\pi)^4} e^{-ip_\xi'\cdot x_\xi' - ip_\eta'\cdot x_\eta'} \\ &\times \int \frac{\mathrm{d}^4 p_\xi}{(2\pi)^4} \frac{\mathrm{d}^4 p_\eta}{(2\pi)^4} e^{+ip_\xi\cdot x_\xi + ip_\eta\cdot x_\eta} A_P(p_\xi', p_\eta', p_\xi, p_\eta) \end{aligned} \tag{2.62}$$

where, as before, the subscript in A_P indicates that its dependence on the total four-momentum is purely parametric. On the other hand, using definitions (2.57) to (2.61) and exploiting translational invariance, we write the following Fourier-transforms

$$\begin{aligned} K^{(2)}(x_i', x_j', x_i, x_j) &\equiv K^{(2)}(X_k' - X_k, x_{\xi_k}', x_{\xi_k}) \\ &=: \int \frac{\mathrm{d}^4 P_k}{(2\pi)^4} e^{-iP_k\cdot(X_k'-X_k)} \int \frac{\mathrm{d}^4 p_{\xi_k}'}{(2\pi)^4} e^{-ip_{\xi_k}'\cdot x_{\xi_k}'} \\ &\times \int \frac{\mathrm{d}^4 p_{\xi_k}}{(2\pi)^4} e^{+ip_{\xi_k}\cdot x_{\xi_k}} K_{P_k}^{(2)}(p_{\xi_k}', p_{\xi_k}) \end{aligned} \tag{2.63}$$

for the two-body irreducible kernels. In the equation above, one should note that the

kernels $K^{(2)}$ do not depend on P in the same way as $K^{(3)}$ does. In fact, the two-body kernels in momentum space depend parametrically on P_k, which according to Eq. (2.60) is a combination of P and the relative momentum p_{η_k}. This leads to retardation effects between the two- and three-body interactions and, consequently, the reduction to the Salpeter equation in the case of baryons is not as straightforward as it is for mesons. We return to this matter below.

Finally, according to the definitions (2.62) and (2.63), the integral equation for $G^{(6)}$ in momentum space takes the form

$$\begin{aligned} G_P^{(6)}(p'_\xi, p'_\eta, p_\xi, p_\eta) &= G_{0P}^{(6)}(p'_\xi, p'_\eta, p_\xi, p_\eta) - i \int \frac{\mathrm{d}^4 p''_\xi}{(2\pi)^4} \frac{\mathrm{d}^4 p''_\eta}{(2\pi)^4} \frac{\mathrm{d}^4 p'''_\xi}{(2\pi)^4} \frac{\mathrm{d}^4 p'''_\eta}{(2\pi)^4} \\ &\times G_{0P}^{(6)}(p'_\xi, p'_\eta, p''_\xi, p''_\eta) \left[\bar{K}_P^{(2)} + K_P^{(3)}\right] (p''_\xi, p''_\eta, p'''_\xi, p'''_\eta) G_P^{(6)}(p'''_\xi, p'''_\eta, p_\xi, p_\eta), \end{aligned} \tag{2.64}$$

where $G_{0P}^{(6)}$ denotes the tensor product

$$\begin{aligned} &G_{0P}^{(6)}(p'_\xi, p'_\eta, p_\xi, p_\eta) \\ &\qquad = S_F^1\left(\tfrac{1}{3}P + p_\xi + \tfrac{1}{2}p_\eta\right) \otimes S_F^2\left(\tfrac{1}{3}P - p_\xi + \tfrac{1}{2}p_\eta\right) \otimes S_F^3\left(\tfrac{1}{3}P - p_\eta\right) \\ &\qquad \times (2\pi)^4 \delta^{(4)}(p'_\xi - p_\xi)(2\pi)^4 \delta^{(4)}(p'_\eta - p_\eta) \end{aligned} \tag{2.65}$$

and the integral kernel $\bar{K}_P^{(2)}$ is explicitly given by

$$\begin{aligned} \bar{K}^{(2)}_{P\alpha'_1\alpha'_2\alpha'_3,\alpha_1\alpha_2\alpha_3}(p'_\xi, p'_\eta, p_\xi, p_\eta) := \sum_{\substack{\text{cycl.perm.} \\ \{i,j,k\}}} & K^{(2)}_{\left(\frac{2}{3}P + p_{\eta_k}\right)\alpha'_i\alpha'_j,\alpha_i\alpha_j}(p'_{\xi_k}, p_{\xi_k}) \\ & \times S_{F\alpha'_k\alpha_k}^{k\,-1}\left(\tfrac{1}{3}P - p_{\eta_k}\right)(2\pi)^4 \delta^{(4)}(p'_{\eta_k} - p_{\eta_k}), \end{aligned} \tag{2.66}$$

where the inverse of full quark propagators fulfill the relation

$$S^k_{F\alpha'_k\alpha''_k}(p_k) S_{F\alpha''_k\alpha_k}^{k\,-1}(p_k) = \delta_{\alpha'_k\alpha_k}. \tag{2.67}$$

2.3.2 Three-quark bound state contributions

To isolate the baryon contributions from $G^{(6)}$ we proceed in a similar way as before, *i.e.* we choose only terms with the specific time-ordering $\min\{x_1'^0, x_2'^0, x_3'^0\} > \max\{x_1^0, x_2^0, x_3^0\}$ and insert a complete set of intermediate states $|\bar{P}\rangle$. In this way,

$$\begin{aligned} &G^{(6)}(x'_1, x'_2, x'_3, x_1, x_2, x_3) \\ &\qquad = -\int \frac{\mathrm{d}^3\,\bar{P}}{(2\pi)^3 2\omega_{\bar{P}}} \left[\chi_{\bar{P}}(x'_1, x'_2, x'_3) \otimes \bar{\chi}_{\bar{P}}(x_1, x_2, x_3)\right] \\ &\qquad \times \theta\left(\min\{x_1'^0, x_2'^0, x_3'^0\} - \max\{x_1^0, x_2^0, x_3^0\}\right) + \text{ other terms}, \end{aligned} \tag{2.68}$$

where the on-shell energy $\omega_{\bar{P}}$ and the normalization of $|\bar{P}\rangle$ were previously defined in Eqs. (2.13) and (2.14). In analogy to Eqs. (2.16) and (2.17), here we also introduced the three-quark Bethe-Salpeter amplitudes

$$\chi_{\bar{P}\alpha_1\alpha_2\alpha_3}(x_1, x_2, x_3) := \langle\Omega|T\Psi^1_{\alpha_1}(x_1)\Psi^2_{\alpha_2}(x_2)\Psi^3_{\alpha_3}(x_3)|\bar{P}\rangle \tag{2.69}$$

and

$$\bar{\chi}_{\bar{P}\alpha_1\alpha_2\alpha_3}(x_1,x_2,x_3) := \langle \bar{P}|T\bar{\Psi}_{\alpha_1}(x_1)\bar{\Psi}_{\alpha_2}(x_2)\bar{\Psi}_{\alpha_3}(x_3)|\Omega\rangle, \tag{2.70}$$

which can be expressed in terms of Jacobi coordinates as

$$\begin{aligned}\chi_{\bar{P}}(x_1,x_2,x_3) &= e^{-i\bar{P}\cdot X}\chi_{\bar{P}}(x_\xi,x_\eta)\\ &=: e^{-i\bar{P}\cdot X}\int\frac{\mathrm{d}^4p_\xi}{(2\pi)^4}\frac{\mathrm{d}^4p_\eta}{(2\pi)^4}e^{-ip_\xi\cdot x_\xi}e^{-ip_\eta\cdot x_\eta}\chi_{\bar{P}}(p_\xi,p_\eta)\end{aligned} \tag{2.71}$$

and

$$\begin{aligned}\bar{\chi}_{\bar{P}}(x_1,x_2,x_3) &= e^{+i\bar{P}\cdot X}\bar{\chi}_{\bar{P}}(x_\xi,x_\eta)\\ &=: e^{+i\bar{P}\cdot X}\int\frac{\mathrm{d}^4p_\xi}{(2\pi)^4}\frac{\mathrm{d}^4p_\eta}{(2\pi)^4}e^{+ip_\xi\cdot x_\xi}e^{+ip_\eta\cdot x_\eta}\bar{\chi}_{\bar{P}}(p_\xi,p_\eta).\end{aligned} \tag{2.72}$$

As shown in Ref. [57], the Heaviside function in Eq. (2.68) produces a pole on the total energy variable of the qqq system, such that one obtains the following expression

$$\begin{aligned}G_P^{(6)}(p'_\xi,p'_\eta,p_\xi,p_\eta) = \frac{-i}{2\omega_{\bar{P}}}&\frac{\zeta_{\bar{P}}(p'_\xi,p'_\eta,P^0-\omega_{\bar{P}})\otimes\bar{\zeta}_{\bar{P}}(p_\xi,p_\eta,P^0-\omega_{\bar{P}})}{P^0-\omega_{\bar{P}}+i\epsilon}\\ &+\text{other terms}\end{aligned} \tag{2.73}$$

for the six-point Green's function in momentum space. Here, the amplitudes $\zeta_{\bar{P}}$ and $\bar{\zeta}_{\bar{P}}$ are defined by

$$\begin{aligned}\zeta_{\bar{P}}(x_\xi,x_\eta,\omega) &:= \chi_{\bar{P}}(x_\xi,x_\eta)e^{-i\omega f(x_\xi^0,x_\eta^0)}\\ &=: \int\frac{\mathrm{d}^4p_\xi}{(2\pi)^4}\frac{\mathrm{d}^4p_\eta}{(2\pi)^4}e^{-ip_\xi\cdot x_\xi-ip_\eta\cdot x_\eta}\zeta_{\bar{P}}(p_\xi,p_\eta,\omega)\end{aligned} \tag{2.74}$$

and

$$\begin{aligned}\bar{\zeta}_{\bar{P}}(x_\xi,x_\eta,\omega) &:= \bar{\chi}_{\bar{P}}(x_\xi,x_\eta)e^{+i\omega g(x_\xi^0,x_\eta^0)}\\ &=: \int\frac{\mathrm{d}^4p_\xi}{(2\pi)^4}\frac{\mathrm{d}^4p_\eta}{(2\pi)^4}e^{+ip_\xi\cdot x_\xi+ip_\eta\cdot x_\eta}\bar{\zeta}_{\bar{P}}(p_\xi,p_\eta,\omega),\end{aligned} \tag{2.75}$$

with

$$f(x_\xi^0,x_\eta^0) := \min\left\{\tfrac{x_\xi^0}{2}+\tfrac{x_\eta^0}{3},-\tfrac{x_\xi^0}{2}+\tfrac{x_\eta^0}{3},-\tfrac{2x_\eta^0}{3}\right\} \tag{2.76}$$

and

$$g(x_\xi^0,x_\eta^0) := \max\left\{\tfrac{x_\xi^0}{2}+\tfrac{x_\eta^0}{3},-\tfrac{x_\xi^0}{2}+\tfrac{x_\eta^0}{3},-\tfrac{2x_\eta^0}{3}\right\}, \tag{2.77}$$

and fulfill the conditions $\zeta_{\bar{P}}(p_\xi,p_\eta,0)=\chi_{\bar{P}}(p_\xi,p_\eta)$ and $\bar{\zeta}_{\bar{P}}(p_\xi,p_\eta,0)=\bar{\chi}_{\bar{P}}(p_\xi,p_\eta)$.

2.3.3 The three-body Bethe-Salpeter equation

The integral equation for $G^{(6)}$ in momentum space can be formulated in a concise operator form

$$G_P^{(6)} = G_{0P}^{(6)} - iG_{0P}^{(6)} \left[\bar{K}_P^{(2)} + K_P^{(3)}\right] G_P^{(6)} \tag{2.78}$$

by defining the product

$$[A_P B_P](p'_\xi, p'_\eta, p_\xi, p_\eta) = \int \frac{\mathrm{d}^4 p''_\xi}{(2\pi)^4} \frac{\mathrm{d}^4 p''_\eta}{(2\pi)^4} A_P(p'_\xi, p'_\eta, p''_\xi, p''_\eta) B_P(p''_\xi, p''_\eta, p_\xi, p_\eta) \tag{2.79}$$

of two six-point functions A_P and B_P. A comparison between Eqs. (2.23) and (2.78) shows that the derivation of the three-body Bethe-Salpeter equation and its adjoint, together with the normalization condition, proceeds exactly in the same way as for mesons. Therefore we simply state the results of this procedure below and refer to [58] for further details. It leads to the Bethe-Salpeter equation

$$\chi_{\bar{P}} = -iG_{0\bar{P}}^{(6)} \left[\bar{K}_{\bar{P}}^{(2)} + K_{\bar{P}}^{(3)}\right] \chi_{\bar{P}} \tag{2.80}$$

and its adjoint

$$\bar{\chi}_{\bar{P}} = -i\bar{\chi}_{\bar{P}} \left[\bar{K}_{\bar{P}}^{(2)} + K_{\bar{P}}^{(3)}\right] G_{0\bar{P}}^{(6)}, \tag{2.81}$$

as well as to the normalization condition

$$-i\bar{\chi}_{\bar{P}} \left[\frac{\partial}{\partial P_\mu} G_P^{-1}\right]_{P=\bar{P}} \chi_{\bar{P}} = 2\bar{P}^\mu \tag{2.82}$$

as given in a covariant form. With its full momentum dependence the Bethe-Salpeter equation (2.80) reads:

$$\begin{aligned} \chi_{\bar{P}}(p_\xi, p_\eta) = {} & S_F^1\left(\tfrac{1}{3}\bar{P} + p_\xi + \tfrac{1}{2}p_\xi\right) \otimes S_F^2\left(\tfrac{1}{3}\bar{P} - p_\xi + \tfrac{1}{2}p_\xi\right) \otimes S_F^3\left(\tfrac{1}{3}\bar{P} - p_\xi\right) \\ & \times \int \frac{\mathrm{d}^4 p'_\xi}{(2\pi)^4} \frac{\mathrm{d}^4 p'_\eta}{(2\pi)^4} (-i) \left[\bar{K}_P^{(2)} + K_P^{(3)}\right] (p_\xi, p_\eta, p'_\xi, p'_\eta) \chi_{\bar{P}}(p'_\xi, p'_\eta). \end{aligned} \tag{2.83}$$

2.3.4 Reduction to the three-body Salpeter Equation

Due to the lack of knowledge about full propagators and interaction kernels, as it stands the three-body Bethe-Salpeter equation (2.83) cannot be directly applied to the description of strong-interacting bound states either. We thus consider this equation with the same approximations employed for the two-body case, *i.e.* we replace full quark propagators S_F^i by effective free-quark parameterizations

$$S_F^i(p_i) \stackrel{!}{=} \frac{i}{\not{p}_i - m_i + i\epsilon} = i\left[\frac{\Lambda_i^+(\mathbf{p}_i)}{p_i^0 - \omega_i(\mathbf{p}_i) + i\epsilon} + \frac{\Lambda_i^-(\mathbf{p}_i)}{p_i^0 + \omega_i(\mathbf{p}_i) - i\epsilon}\right]\gamma^0 \tag{2.84}$$

and assume instantaneous two- and three-body interactions in the baryon rest frame, *i.e.*

$$K_M^{(3)}\left(p_\xi,\, p_\eta,\, p'_\xi,\, p'_\eta\right) \stackrel{!}{=} V^{(3)}(\mathbf{p}_\xi, \mathbf{p}_\eta, \mathbf{p}'_\xi, \mathbf{p}'_\eta) \tag{2.85}$$

and

$$K^{(2)}_{\left(\frac{2}{3}M+p_{\eta_k}\right)}(p_{\xi_k},p'_{\xi_k}) \stackrel{!}{=} V^{(2)}(\mathbf{p}_{\xi_k},\mathbf{p}'_{\xi_k}). \tag{2.86}$$

Recall that the projectors $\Lambda_i^{\pm}$ and the on-shell energies ω_i appearing in Eq. (2.84) were previously defined in Eqs. (2.38) and (2.39), respectively.

In the absence of two-body interactions ($K^{(2)}=0$) the two approximations above are sufficient to enable the reduction of the full Bethe-Salpeter equation to the Salpeter equation. In this specific case we proceed as before and thereby obtain

$$\begin{aligned}\Phi(\mathbf{p}_\xi,\mathbf{p}_\eta) = -i\int\frac{\mathrm{d}^3p'_\xi}{(2\pi)^3}\frac{\mathrm{d}^3p'_\eta}{(2\pi)^3}\frac{\mathrm{d}^3p''_\xi}{(2\pi)^3}\frac{\mathrm{d}^3p''_\eta}{(2\pi)^3}\langle G^{(6)}_{0M}\rangle(\mathbf{p}_\xi,\mathbf{p}_\eta,\mathbf{p}'_\xi,\mathbf{p}'_\eta)\\ \times V^{(3)}(\mathbf{p}'_\xi,\mathbf{p}'_\eta,\mathbf{p}''_\xi,\mathbf{p}''_\eta)\Phi(\mathbf{p}''_\xi,\mathbf{p}''_\eta)\end{aligned} \tag{2.87}$$

for the Salpeter amplitudes

$$\Phi(\mathbf{p}_\xi,\mathbf{p}_\eta) := \int\frac{\mathrm{d}\,p^0_\xi}{2\pi}\frac{\mathrm{d}\,p^0_\eta}{2\pi}\chi_M(p_\xi,p_\eta), \tag{2.88}$$

where we introduced the short-hand notation

$$\langle A_P\rangle(\mathbf{p}'_\xi,\mathbf{p}'_\eta,\mathbf{p}_\xi,\mathbf{p}_\eta) := \int\frac{\mathrm{d}\,p^0_\xi}{2\pi}\frac{\mathrm{d}\,p^0_\eta}{2\pi}\int\frac{\mathrm{d}\,p'^0_\xi}{2\pi}\frac{\mathrm{d}\,p'^0_\eta}{2\pi}A_P(p'_\xi,p'_\eta,p_\xi,p_\eta) \tag{2.89}$$

for the three-dimensional reduction of a six-point function A_P. Thus, $\langle G^{(6)}_{0M}\rangle$ denotes the reduction of the product (2.65) of three fermion propagators, which considered in the free-quark approximation can be evaluated analytically and expressed as

$$\begin{aligned}\langle G^{(6)}_{0M}\rangle(\mathbf{p}'_\xi,&\mathbf{p}'_\eta,\mathbf{p}_\xi,\mathbf{p}_\eta) = i\,(2\pi)^3\delta^{(3)}(\mathbf{p}'_\xi-\mathbf{p}_\xi)(2\pi)^3\delta^{(3)}(\mathbf{p}'_\eta-\mathbf{p}_\eta)\\ &\times\left[\frac{\Lambda_1^+(\mathbf{p}_1)\otimes\Lambda_2^+(\mathbf{p}_2)\otimes\Lambda_3^+(\mathbf{p}_3)}{M-\omega_1-\omega_2-\omega_3+i\epsilon}+\frac{\Lambda_1^-(\mathbf{p}_1)\otimes\Lambda_2^-(\mathbf{p}_2)\otimes\Lambda_3^-(\mathbf{p}_3)}{M+\omega_1+\omega_2+\omega_3+i\epsilon}\right]\\ &\times\left(\gamma^0\otimes\gamma^0\otimes\gamma^0\right).\end{aligned} \tag{2.90}$$

According to these results, when the two-body kernels are set to zero the Salpeter equation again exhibits projection properties which constrain the Salpeter amplitudes. In particular, due to the projector structure observed in Eq. (2.90), the solutions Φ of Eq. (2.87) consist of purely positive and purely negative energy components, *i.e.*

$$\Phi = \left[\Lambda_1^+\otimes\Lambda_2^+\otimes\Lambda_3^+\right]\Phi + \left[\Lambda_1^-\otimes\Lambda_2^-\otimes\Lambda_3^-\right]\Phi, \tag{2.91}$$

while all mixed energy components vanish. Consequently, only the projected part

$$V^{(3)}_\Lambda(\mathbf{p}'_\xi,\mathbf{p}'_\eta,\mathbf{p}_\xi,\mathbf{p}_\eta) := \bar\Lambda(\mathbf{p}'_\xi,\mathbf{p}'_\eta)V^{(3)}(\mathbf{p}'_\xi,\mathbf{p}'_\eta,\mathbf{p}_\xi,\mathbf{p}_\eta)\Lambda(\mathbf{p}_\xi,\mathbf{p}_\eta) \tag{2.92}$$

of the three-body potential $V^{(3)}$, defined by the projection operators

$$\Lambda(\mathbf{p}_\xi,\mathbf{p}_\eta) := \Lambda_1^+(\mathbf{p}_1)\otimes\Lambda_2^+(\mathbf{p}_2)\otimes\Lambda_3^+(\mathbf{p}_3)+\Lambda_1^-(\mathbf{p}_1)\otimes\Lambda_2^-(\mathbf{p}_2)\otimes\Lambda_3^-(\mathbf{p}_3) \tag{2.93}$$

and

$$\bar\Lambda(\mathbf{p}_\xi,\mathbf{p}_\eta) := \left[\gamma^0\otimes\gamma^0\otimes\gamma^0\right]\Lambda(\mathbf{p}_\xi,\mathbf{p}_\eta)\left[\gamma^0\otimes\gamma^0\otimes\gamma^0\right], \tag{2.94}$$

is relevant for the dynamics of qqq bound states, whereas the residual part

$$V_R^{(3)} := V^{(3)} - V_\Lambda^{(3)} \quad \Leftrightarrow \quad \bar{\Lambda} V_R^{(3)} \Lambda = 0 \tag{2.95}$$

does not couple to the amplitudes Φ as these fulfill the constraint (2.91).

However, if also two-body irreducible kernels are taken into account, the projection properties discussed above do not hold anymore. In this case, despite the instantaneous approximation the dependence on the relative energies p_ξ^0 and p_η^0 remains in the two-body kernel

$$\begin{aligned} \bar{K}_M^{(2)}(p'_\xi, p'_\eta, p_\xi, p_\eta) \stackrel{!}{=} & \sum_{\substack{\text{cycl.perm.} \\ \{i,j,k\}}} V^{(2)}_{\left(\frac{2}{3}M + p_{\eta_k}\right)}(\mathbf{p}'_{\xi_k}, \mathbf{p}_{\xi_k}) \\ & \otimes S_F^{k-1}\left(M - p_{\eta_k}\right)(2\pi)^4 \delta^{(4)}(p'_{\eta_k} - p_{\eta_k}) \end{aligned} \tag{2.96}$$

inside the relative momenta variables p_{η_k} and p'_{η_k}, defined in Eq. (2.61). This leads to retardation effects between the two- and three-body potentials and, consequently, induces the contribution of mixed energy components to the Salpeter amplitudes. In other words, the amplitudes Φ no longer fulfill the constraint (2.91) and, therefore, the residual part $V_R^{(3)}$ also contributes.

Nevertheless, it was shown in Ref. [58] that the reduction of the Bethe-Salpeter equation to an equivalent three-dimensional problem can still be achieved. The method is based on the fact that the decomposition

$$V^{(3)} = V_\Lambda^{(3)} + V_R^{(3)} \tag{2.97}$$

is still valid and, very importantly, that the residual part $V_R^{(3)}$ only becomes relevant when two-body potentials are also present. For this reason, it is more appropriate to recast the instantaneous Bethe-Salpeter equation into the equivalent expression

$$\chi_M = -i \mathcal{G}_M V_\Lambda^{(3)} \chi_M, \tag{2.98}$$

where the difficult relative energy dependencies were isolated inside a new Green's function

$$\mathcal{G}_M := \left[I + i G_{0M}^{(6)} \left(V_R^{(3)} + \bar{K}_M^{(2)} \right) \right] G_{0M}^{(6)}. \tag{2.99}$$

Now, the Bethe-Salpeter equation in the form (2.98) can be reduced in the same way as before, since its integral kernel $V_\Lambda^{(3)}$ is instantaneous, *i.e.* it does not affect mixed-energy components. Indeed, by integrating both sides of Eq. (2.98) over the relative energy variables p_ξ^0 and p_η^0 one already obtains the Salpeter equation

$$\begin{aligned} \Phi(\mathbf{p}_\xi, \mathbf{p}_\eta) = -i \int \frac{\mathrm{d}^3 p'_\xi}{(2\pi)^3} \frac{\mathrm{d}^3 p'_\eta}{(2\pi)^3} \frac{\mathrm{d}^3 p''_\xi}{(2\pi)^3} \frac{\mathrm{d}^3 p''_\eta}{(2\pi)^3} \langle \mathcal{G}_M \rangle (\mathbf{p}_\xi, \mathbf{p}_\eta, \mathbf{p}'_\xi, \mathbf{p}'_\eta) \\ \times V_\Lambda^{(3)}(\mathbf{p}'_\xi, \mathbf{p}'_\eta, \mathbf{p}''_\xi, \mathbf{p}''_\eta) \Phi(\mathbf{p}''_\xi, \mathbf{p}''_\eta) \end{aligned} \tag{2.100}$$

for the three-body Salpeter amplitudes Φ, where we introduced the notation

$$\langle A_P \rangle_\Lambda := \Lambda \langle A_P \rangle \bar{\Lambda} \tag{2.101}$$

for the projection of the reduced function $\langle A_P \rangle$. Moreover, it is interesting to write the Salpeter equation above as an integral equation

$$\begin{aligned}\Phi_\Lambda(\mathbf{p}_\xi, \mathbf{p}_\eta) = -i \int \frac{\mathrm{d}^3 p'_\xi}{(2\pi)^3} \frac{\mathrm{d}^3 p'_\eta}{(2\pi)^3} \frac{\mathrm{d}^3 p''_\xi}{(2\pi)^3} \frac{\mathrm{d}^3 p''_\eta}{(2\pi)^3} \langle \mathcal{G}_M \rangle_\Lambda(\mathbf{p}_\xi, \mathbf{p}_\eta, \mathbf{p}'_\xi, \mathbf{p}'_\eta) \\ \times V^{(3)}(\mathbf{p}'_\xi, \mathbf{p}'_\eta, \mathbf{p}''_\xi, \mathbf{p}''_\eta) \Phi_\Lambda(\mathbf{p}''_\xi, \mathbf{p}''_\eta)\end{aligned} \tag{2.102}$$

for the **projected Salpeter amplitudes** given by

$$\Phi_\Lambda(\mathbf{p}_\xi, \mathbf{p}_\eta) := \Lambda(\mathbf{p}_\xi, \mathbf{p}_\eta) \Phi(\mathbf{p}_\xi, \mathbf{p}_\eta) \tag{2.103}$$

by exploiting the projection properties of $V_\Lambda^{(3)}$. Note that this last step represents a great advantage numerically, by reducing the number of energy components necessary to describe the amplitudes Φ.

Hence, the problem of reducing the Bethe-Salpeter equation (2.83) has now been simplified to the problem of finding an explicit expression for $\langle \mathcal{G}_M \rangle_\Lambda$, which according to its definition (2.99) is solution of

$$\langle \mathcal{G}_M \rangle_\Lambda = \langle G_{0M}^{(6)} \rangle - i \langle G_{0M}^{(6)} \left(V_R^{(3)} + \bar{K}_M^{(2)} \right) \mathcal{G}_M \rangle_\Lambda. \tag{2.104}$$

For our purposes, only the projected part of $\langle \mathcal{G}_M \rangle$ is actually needed. Therefore, it is not necessary to solve Eq. (2.104) completely, but only to determine an effective potential V_M^{eff} which fulfills the relation

$$\langle \mathcal{G}_M \rangle_\Lambda \stackrel{!}{=} \langle G_{0M}^{(6)} \rangle - i \langle G_{0M}^{(6)} \rangle V_M^{\mathrm{eff}} \langle \mathcal{G}_M \rangle_\Lambda \tag{2.105}$$

and has the projection properties

$$V_M^{\mathrm{eff}} = \bar{\Lambda} V_M^{\mathrm{eff}} = V_M^{\mathrm{eff}} \Lambda. \tag{2.106}$$

In Ref. [58] it was demonstrated in detail that such potential indeed exists and is given by the perturbative series

$$V_M^{\mathrm{eff}} = \sum_{k=1}^{\infty} V_M^{\mathrm{eff}(k)}. \tag{2.107}$$

Finally, by substituting the formal solution of Eq. (2.105) into Eq. (2.102), together with Eq. (2.107) for the effective potential, we can write the following Salpeter equation

$$\begin{aligned}\Phi_\Lambda(\mathbf{p}_\xi, \mathbf{p}_\eta) = -i \int \frac{\mathrm{d}^3 p'_\xi}{(2\pi)^3} \frac{\mathrm{d}^3 p'_\eta}{(2\pi)^3} \frac{\mathrm{d}^3 p''_\xi}{(2\pi)^3} \frac{\mathrm{d}^3 p''_\eta}{(2\pi)^3} \langle G_{0M}^{(6)} \rangle(\mathbf{p}_\xi, \mathbf{p}_\eta, \mathbf{p}'_\xi, \mathbf{p}'_\eta) \\ \times \left[V^{(3)} + \sum_{k=0}^{\infty} V_M^{\mathrm{eff}(k)} \right] (\mathbf{p}'_\xi, \mathbf{p}'_\eta, \mathbf{p}''_\xi, \mathbf{p}''_\eta) \Phi_\Lambda(\mathbf{p}''_\xi, \mathbf{p}''_\eta)\end{aligned} \tag{2.108}$$

for the projected Salpeter amplitudes, which has the same structure of Eq. (2.87) except for the contribution of V_M^{eff}. In summary, the procedure presented here thus corresponds to consider only purely positive and purely negative energy components of the Salpeter amplitudes and treat the difficult mixed components by means of an effective potential which features projection properties as well.

For practical calculations, the perturbative series of Eq. (2.107) must be truncated at some finite order in k. In our model, this is done with the aim of expressing the Salpeter equation (2.108) in the form of a simple eigenvalue problem. As discussed in Ref. [58], this can be achieved just in Born approximation (*i.e.* up to $k = 1$), since higher order terms lead to generalized Hamiltonian equations whose numerical solution is much more involved. For this reason, we consider the effective potential V_M^{eff} up to the Born term only, such that the Salpeter equation (2.108) is equivalent to the eigenvalue problem

$$\mathcal{H}^{(3)}\Phi_\Lambda := M\Phi_\Lambda \tag{2.109}$$

with the Hamiltonian operator

$$\begin{aligned}\Big[\mathcal{H}^{(3)}\Phi_\Lambda\Big](\mathbf{p}_\xi,\mathbf{p}_\eta) &:= \mathcal{H}_0^{(3)}(\mathbf{p}_\xi,\mathbf{p}_\eta)\Phi_\Lambda(\mathbf{p}_\xi,\mathbf{p}_\eta)\\ &+\big[\Lambda_1^+(\mathbf{p}_1)\otimes\Lambda_2^+(\mathbf{p}_2)\otimes\Lambda_3^+(\mathbf{p}_3)+\Lambda_1^-(\mathbf{p}_1)\otimes\Lambda_2^-(\mathbf{p}_2)\otimes\Lambda_3^-(\mathbf{p}_3)\big]\\ &\times\big[\gamma^0\otimes\gamma^0\otimes\gamma^0\big]\int\frac{\mathrm{d}^3p'_\xi}{(2\pi)^3}\frac{\mathrm{d}^3p'_\eta}{(2\pi)^3}V^{(3)}(\mathbf{p}_\xi,\mathbf{p}_\eta,\mathbf{p}'_\xi,\mathbf{p}'_\eta)\Phi_\Lambda(\mathbf{p}'_\xi,\mathbf{p}'_\eta)\\ &+\big[\Lambda_1^+(\mathbf{p}_1)\otimes\Lambda_2^+(\mathbf{p}_2)\otimes\Lambda_3^+(\mathbf{p}_3)-\Lambda_1^-(\mathbf{p}_1)\otimes\Lambda_2^-(\mathbf{p}_2)\otimes\Lambda_3^-(\mathbf{p}_3)\big]\\ &\times\big[\gamma^0\otimes\gamma^0\otimes I\big]\int\frac{\mathrm{d}^3p'_\xi}{(2\pi)^3}V^{(2)}(\mathbf{p}_\xi,\mathbf{p}'_\xi)\otimes I\Phi_\Lambda(\mathbf{p}'_\xi,\mathbf{p}_\eta)\\ &+\text{corresponding terms for the quark pairs (23) and (31),}\end{aligned} \tag{2.110}$$

where the free Hamiltonian operator $\mathcal{H}_0^{(3)}$ is defined as

$$\mathcal{H}_0^{(3)}(\mathbf{p}_\xi,\mathbf{p}_\eta) := H_1(\mathbf{p}_1)\otimes I\otimes I + I\otimes H_2(\mathbf{p}_2)\otimes I + I\otimes I\otimes H_3(\mathbf{p}_3). \tag{2.111}$$

For completeness, we finally give the normalization condition for the projected Salpeter amplitudes, which reads:

$$\int\frac{\mathrm{d}^3p_\xi}{(2\pi)^3}\frac{\mathrm{d}^3p_\eta}{(2\pi)^3}\Phi_\Lambda^\dagger(\mathbf{p}_\xi,\mathbf{p}_\eta)\Phi_\Lambda(\mathbf{p}_\xi,\mathbf{p}_\eta) = 2M \tag{2.112}$$

and together with the Salpeter equation (2.109) for the amplitudes Φ_Λ, constitutes the basis of our quark model for baryons. The phenomenological parameterizations for the potentials shall be discussed in the next section. For the numerical treatment in the case of baryons, see Ref. [57].

2.4 Model Interactions

Since quark dynamics in the confinement regime cannot be directly derived from QCD, in order to solve the Salpeter equations obtained in the previous Sections 2.2 and 2.3 one has to find suitable parameterizations for the instantaneous potentials. This is done on the basis of some structures observed in the experimental light-flavored hadron spectrum which, as we shall see below, lead to the picture of quarks interacting through a linearly rising, flavor-independent confinement potential, supplemented by a residual flavor-dependent force which acts only on specific sectors of the spectrum.

2.4.1 Quark confinement

Let us start our discussion with the meson spectrum. Considering at first only mesons with spin $J \neq 0$, one observes some general features which apply for all flavor states. Among them, one of the most prominent is the occurrence of Regge trajectories for the ground states, whose masses M are related to the corresponding spin J according to $M^2 \propto J$. Another example is the existence of nearly degenerate partners between the isovector and the isoscalar sectors, for instance the pair $\rho(770) - \omega(782)$. Such general properties suggest that quark-antiquark confinement is realized through a linear, flavor-independent potential, which can be parametrized according to

$$V^{(2)}_{\text{conf}}(\mathbf{x}_1, \mathbf{x}_2) = a^{(2)} \mathcal{W}_{\text{off}} + b^{(2)} \left|\mathbf{x}_1 - \mathbf{x}_2\right| \mathcal{W}_{\text{str}}, \tag{2.113}$$

where the offset $a^{(2)}$ and the slope $b^{(2)}$ are treated as free parameters.

As indicated in Eq. (2.113), in a full relativistic treatment the confinement potential must be provided with appropriate spin structures $\mathcal{W}_{\text{off}}$ and $\mathcal{W}_{\text{str}}$. Possible choices must satisfy some basic constraints (*e.g.* Lorentz invariance) and show the correct non-relativistic limit, where the potential is assumed to be spin-independent. Moreover, the spin structure should be such that it does not induce too large spin-orbit effects, as these are not observed in the spectrum. According to the findings of Refs. [26, 27], the spin structure

$$\mathcal{W}_{\text{off}} = \mathcal{W}_{\text{str}} = \frac{1}{2}\left[I \otimes I - \gamma^0 \otimes \gamma^0\right] \tag{2.114}$$

fulfills the requirements above and, when chosen for both offset and slope components, provides a good description of the experimental data.

Turning to the baryon sector, one also observes some general features which support the hypothesis of a linearly rising confinement. An analysis of the experimental baryon spectrum up to the highest spin shows that the ground states for each total angular momentum also lie on Regge trajectories. To account for this feature, an appropriate parameterization for the three-quark confinement potential is

$$V^{(3)}_{\text{conf}}(\mathbf{x}_1, \mathbf{x}_2, \mathbf{x}_3) = a^{(3)} \mathcal{W}_{\text{off}} + b^{(3)} \sum_{i<j} \left|\mathbf{x}_i - \mathbf{x}_j\right| \mathcal{W}_{\text{str}}, \tag{2.115}$$

where $a^{(3)}$ and $b^{(3)}$ enter as free parameters. According to the results of Refs. [29, 30], some of which we briefly discuss in the following Section 2.5, the spin structures

$$\mathcal{W}_{\text{off}} = \frac{3}{4}\left[\;\; I \otimes I \otimes I + \gamma^0 \otimes \gamma^0 \otimes I + \gamma^0 \otimes I \otimes \gamma^0 + I \otimes \gamma^0 \otimes \gamma^0\right], \tag{2.116}$$

$$\mathcal{W}_{\text{str}} = \frac{1}{2}\left[-I \otimes I \otimes I + \gamma^0 \otimes \gamma^0 \otimes I + \gamma^0 \otimes I \otimes \gamma^0 + I \otimes \gamma^0 \otimes \gamma^0\right], \tag{2.117}$$

lead to a satisfactory overall description of the light-flavored baryon spectrum.

2.4.2 Instanton-induced interactions

The situation for scalar and pseudoscalar mesons is quite different from the case $J \neq 0$ discussed before. In the $J = 0$ sector of the meson spectrum larger mass-splittings occur, for instance the splitting $\pi - \eta - \eta'$, revealing the influence of a residual flavor-dependent interaction acting on $J = 0$ states only. A QCD-based candidate with the appropriate flavor- and spin-dependence to describe this effect is the instanton-induced interaction. As firstly shown by 't Hooft [59], instantons lead to an effective interquark potential which acts only on very specific $q\bar{q}$ states. The instanton effective Lagrangian in the two-fermion channel is given by [58]

$$\Delta\mathcal{L}^{(2)}_{\text{eff}}(y) = \bar{\Psi}_{\alpha_1'}(y)\bar{\Psi}_{\alpha_2'}(y)\mathcal{W}^{(2)}_{\alpha_1'\alpha_2'\alpha_1\alpha_2}\Psi_{\alpha_1}(y)\Psi_{\alpha_2}(y), \tag{2.118}$$

with the interaction vertex

$$\begin{aligned}\mathcal{W}^{(2)}_{\alpha_1'\alpha_2'\alpha_1\alpha_2} = -\frac{1}{2}G_{f_1'f_2'f_1f_2}\Bigg\{&\frac{2}{3}\left[I\otimes I+\gamma^5\otimes\gamma^5\right]_{s_1's_2's_1s_2}\left[I\otimes I\right]_{c_1'c_2'c_1c_2}\\ +\frac{1}{16}&\left[I\otimes I+\gamma^5\otimes\gamma^5-\frac{3}{2}\sigma_{\mu\nu}\otimes\sigma^{\mu\nu}\right]_{s_1's_2's_1s_2}\left[\sum_{a=1}^{8}\lambda^a\otimes\lambda^a\right]_{c_1'c_2'c_1c_2}\Bigg\},\end{aligned} \tag{2.119}$$

where the matrices λ^a are the usual Gell-Mann matrices, the multi-indices α_i combine the quantum numbers s_i, f_i and c_i in spin, flavor and color space, respectively, and the flavor matrix

$$G_{f_1'f_2'f_1f_2} = \frac{3}{8}\sum_{f=u,d,s} g_{\text{eff}}(f)\epsilon_{ff_1'f_2'}\epsilon_{ff_1f_2} \tag{2.120}$$

includes the flavor-dependent effective couplings $g_{\text{eff}}(f)$. In the case of exact isospin symmetry, it is more convenient to define new coupling constants

$$g_{nn} := \frac{3}{8}g_{\text{eff}}(s), \qquad g_{ns} := \frac{3}{8}g_{\text{eff}}(u) = \frac{3}{8}g_{\text{eff}}(d), \tag{2.121}$$

such that

$$G_{f_1'f_2'f_1f_2} \equiv G(g_{nn}, g_{ns}) = \begin{cases} g_{f_1f_2}, & \text{if } f_1 = f_1' \neq f_2 = f_2' \\ -g_{f_1'f_2}, & \text{if } f_1 = f_2' \neq f_2 = f_1' \\ 0, & \text{otherwise.}\end{cases} \tag{2.122}$$

From the interaction vertex $\mathcal{W}^{(2)}$ and the flavor matrix G above, one easily reads off which meson states are affected by instanton interactions: Firstly, as mesons are necessarily color-singlets, only the first term on the right-hand side of Eq. (2.119) is relevant for meson spectroscopy in terms of $q\bar{q}$-configurations, and the spin structure of this term shows that it acts on $J = 0$ states exclusively. Moreover, due to the Levi-Civita tensors in Eq. (2.120), the interaction leads to $u\bar{u} \leftrightarrow d\bar{d}$, $u\bar{u} \leftrightarrow s\bar{s}$ and $d\bar{d} \leftrightarrow s\bar{s}$ transition matrix elements which then explain the mass-splittings in the $J = 0$ sector.

Due to these desirable properties, in the present model we employ as residual interaction a spin-dependent potential based on instanton effects, which for $q\bar{q}$ states can be directly calculated from the two-fermion Lagrangian in Eq. (2.118). In lowest order of perturbation theory, this potential reads:

$$\int \frac{\mathrm{d}^3 p'}{(2\pi)^3} V^{(q\bar{q})}_{\text{'t Hooft}}(\mathbf{p},\mathbf{p}')\Phi(\mathbf{p}') = 4G(g_{nn},g_{ns}) \int \frac{\mathrm{d}^3 p'}{(2\pi)^3} v_{\text{reg}}(\mathbf{p},\mathbf{p}') \times \left(I \,\mathrm{Tr}\left[\Phi(\mathbf{p}')\right] + \gamma^5 \,\mathrm{Tr}\left[\Phi(\mathbf{p}')\gamma^5\right]\right). \tag{2.123}$$

As it stands, see the Lagrangian of Eq. (2.118), the instanton force is a point-like interaction and has to be regularized. In Eq. (2.123) this is done by means of a regularizing Gaussian function v_{reg}, which in configuration space is given by

$$v_{\text{reg}}(\mathbf{x}) = \frac{1}{(\lambda\sqrt{\pi})^3} e^{-\frac{|\mathbf{x}|^2}{\lambda^2}}, \tag{2.124}$$

introducing an effective range λ to the interaction. As the constituent quark masses and confinement parameters, the couplings g_{nn} and g_{ns} and the effective range λ enter the model as free parameters, leading to a total of seven free parameters to be adjusted to experimental data.

In the case of baryons, the description of the mass splittings $N-\Delta$, $\Lambda-\Sigma-\Sigma^*$ and $\Xi-\Xi^*$ between the octet and decuplet ground-states also requires the contribution of a residual spin-dependent force. Because of its antisymmetric flavor-dependence, the two-body 't Hooft's interaction can be used to explain this effect too, since it acts exclusively on octet ground-states, leaving the flavor-symmetric decuplet states unaffected. For the analysis of instanton effects in the two-quark channel, it is more convenient to write the vertex $\mathcal{W}^{(2)}$ in terms of projection operators in flavor, spin and color spaces according to [58]

$$\begin{aligned}\mathcal{W}^{(2)} = &-2\left[\left(I\otimes I+\gamma^5\otimes\gamma^5\right)\mathcal{P}^s_{S=0}\otimes\left(g_{nn}\mathcal{P}^f_A(nn)+g_{ns}\mathcal{P}^f_A(ns)\right)\otimes\mathcal{P}^c_{\bar{3}}\right] \\ &-\left[\left(I\otimes I+\gamma^5\otimes\gamma^5\right)\mathcal{P}^s_{S=1}\otimes\left(g_{nn}\mathcal{P}^f_A(nn)+g_{ns}\mathcal{P}^f_A(ns)\right)\otimes\mathcal{P}^c_{6}\right],\end{aligned} \tag{2.125}$$

where the operators $\mathcal{P}^c_{\bar{3}}$ and $\mathcal{P}^c_6$ are projectors on color-antitriplets and sextets, $\mathcal{P}^s_{S=0}$ and $\mathcal{P}^s_{S=1}$ on spin-singlets and triplets and, finally, $\mathcal{P}^f_A(nn)$ and $\mathcal{P}^f_A(ns)$ on flavor-antisymmetric nn and ns quark pairs. Again, only the first term on the right-hand side of Eq. (2.125) contributes spectroscopically, since the qq pairs inside a color-singlet qqq state are necessarily color-antitriplets. From the projector structure of this first term, we conclude that the 't Hooft's interaction acts just on those scalar and pseudoscalar qq pairs which are antisymmetric in flavor space, with different strengths for non-strange and non-strange-strange pairs.

The instanton interaction leads to an effective potential between the quark fields within qq pairs, which in lowest order is given by

$$\begin{aligned}V^{qq}_{\text{'t Hooft}}(\mathbf{x}) = &-4v_{\text{reg}}(\mathbf{x})\left(I\otimes I+\gamma^5\otimes\gamma^5\right)\mathcal{P}^s_{S=0} \\ &\otimes\left(g_{nn}\mathcal{P}^f_A(nn)+g_{ns}\mathcal{P}^f_A(ns)\right)\otimes\mathcal{P}^c_{\bar{3}},\end{aligned} \tag{2.126}$$

and which we use as a phenomenological parameterization for the unconnected two-body potentials in our model for baryons.

Instantons also induce an effective three-quark potential, derived from the three-fermion effective Lagrangian

$$\begin{aligned}\Delta\mathcal{L}_{\text{eff}}^{(3)} = &\frac{27}{80} g_{\text{eff}}^{(3)} \bar{\Psi}\otimes\bar{\Psi}\otimes\bar{\Psi} \\ &\times \left[I\otimes I\otimes I + \gamma^5\otimes\gamma^5\otimes I + \gamma^5\otimes I\otimes\gamma^5 + I\otimes\gamma^5\otimes\gamma^5\right] \\ &\otimes \mathcal{P}_A^f \otimes \left[2\mathcal{P}_{10}^c + 5\mathcal{P}_8^c\right] \Psi\otimes\Psi\otimes\Psi,\end{aligned} \tag{2.127}$$

where $\mathcal{P}_8^c$ and $\mathcal{P}_{10}^c$ are projectors on color-octets and decuplets and $\mathcal{P}_A^f$ a projector on the completely flavor-antisymmetric three-quark state uds. The three-body instanton force does not act on color-singlets and, therefore, is irrelevant for spectroscopic calculations. Nevertheless, it leads to a highly selective contribution to strong two-body decays of mesons (see Ref. [60]) and of baryons as well, as we shall discuss in Chapter 3.

2.5 Mass spectra of non-strange hadrons

In this section we compare the calculated mass spectra of non-strange hadrons to the experimental data from the Review of Particle Physics published by the Particle Data Group (PDG) in 2012 [2]. More specifically, we compare bound-state mass parameters corresponding to poles of Green's functions (*cf.* Eqs. (2.20) and (2.73)) to experimental estimates for Breit-Wigner masses as provided by the PDG. It should be mentioned, however, that both mass parameters are only equivalent in the absence of higher-order contributions to baryon properties. We shall return to this issue later in Chapter 4.

The notation for the baryon resonances is given as follows: The experimental states are in general denoted by $B[J^\pi](M)$, where B is either a N (isospin $I = 1/2$) or a Δ resonance ($I = 3/2$). Moreover, J denotes the spin, π the parity and M the mass of the state. If necessary, the status of the resonance is explicitly given by one to four stars, according to the classification of the PDG. The theoretical states, in turn, are denoted by $B[J^\pi]_n(M)$, where the additional label n represents the principal quantum number or radial excitation of the state, with $n = 0$ for ground-state baryons. We start our discussion with the free parameters of the model and how these are adjusted to the experimental data and then present the resulting hadron spectra, focusing on those states which are the subject of investigation in this thesis.

2.5.1 Parameters of the model

Both quark models for mesons and baryons contain seven free parameters each, namely the offset $a^{(2,3)}$ and the slope $b^{(2,3)}$ stemming from the two- or three-body confinement potentials, the constituent quark masses m_n and m_s from the effective free-quark propagators and, finally, the couplings g_{nn} and g_{ns} and the effective range λ from the residual instanton interactions. Although the parameters related to strange quarks are not necessary for the calculation non-strange baryon spectra, the ground-state η-meson is present in the strong decays into ηN considered in the next chapter. Therefore, also the constituent quark mass m_s and the coupling g_{ns} are considered here.

Table 2.1. Parameters of the model for baryons, taken from Ref. [29]. The last column indicates to which states or mass-splittings the parameters were adjusted.

Parameter			Value	Adjusted to
Confinement potential	offset	$a^{(3)}$	-744 MeV	well-established Δ baryons
	slope	$b^{(3)}$	470 MeV fm^{-1}	
Constituent quark masses	non-strange	m_n	330 MeV	
	strange	m_s	670 MeV	$\Delta - \Sigma^* - \Xi^* - \Omega$
't Hooft's Lagrangian	nn-coupling	g_{nn}	136 MeV fm^3	$N - \Delta$ $\Lambda - \Sigma - \Sigma^*$ $\Xi - \Xi^*$
	ns-coupling	g_{ns}	94 MeV fm^3	
	effective range	λ	0.4 fm	

Let us start by explaining how these parameters were fitted to the light-flavored baryon spectrum, according to Ref. [29]. The procedure was based on the fact that instantons act only on flavor octet states, leaving the totally symmetric decuplet states unaffected. Consequently, the whole spectrum of decuplet baryons should be determined by the parameters from the confinement potential and the constituent quark masses alone, while the parameters from the 't Hooft's interaction have to account for the mass-splittings between the decuplet and octet states. In this way, the first step was to adjust $a^{(3)}$, $b^{(3)}$ and m_n to well-established Δ resonances, choosing those which have small experimental uncertainties on the excitation mass: These are the four-star $\Delta[\frac{3}{2}^+](1232)$, $\Delta[\frac{5}{2}^+](1950)$ and $\Delta[\frac{7}{2}^+](2420)$ resonances from the positive-parity Regge-trajectory, as well as the two negative-parity resonances $\Delta[\frac{1}{2}^-](1600)$ and $\Delta[\frac{3}{2}^-](1720)$, which were included in the fit so that the energy difference between the ground-state $\Delta(1232)$ and the lowest negative-parity states is correctly described. Subsequently, the strange quark mass m_s was adjusted to the mass-splittings $\Delta - \Sigma^* - \Xi^* - \Omega$ between the decuplet ground-states, since they are unaffected by instantons. Finally, the remaining three parameters g_{nn}, g_{ns} and λ were fitted to the mass-splittings $N - \Delta$, $\Sigma - \Sigma^*$ and $\Xi - \Xi^*$ between octet and decuplet ground-states, as well as to the splitting $\Lambda - \Sigma$ between the isoscalar and isovector hyperons. The fitting procedure and the numerical values of the parameters, taken from Ref. [29], are collected in Table 2.1.

In the case of mesons, the fit is usually performed in a similar way, considering that instanton effects are relevant only for scalar and pseudoscalar states, while all other mesons with $J > 0$ should be well described by the parameters of the confinement potential and the constituent quark masses alone. For details on the procedure and numerical values for the complete meson spectrum, see Refs. [26, 27]. Here, we are only interested in π and η ground states because they are present in the decay channels considered in this thesis and, in this case, the fit has to be done in a slightly different way.

Table 2.2. Parameters of the model for mesons, according to Ref. [39]. The constituent quark masses were not included in the fit, but kept fixed to the values of Table 2.1.

Parameter			Value
Confinement potential	offset	$a^{(2)}$	-1810 MeV
	slope	$b^{(2)}$	2118 MeV fm^{-1}
't Hooft's Lagrangian	nn-coupling	g_{nn}	12.7 MeV fm^3
	ns-coupling	g_{ns}	13.4 MeV fm^3
	effective range	λ	0.3 fm

As we shall see in the next chapter, the matrix elements corresponding to strong decays of baryons involve quark loop contributions in which baryon and meson amplitudes are connected through quark propagators. Consequently, in such calculations at least the constituent quark masses m_n and m_s should be the same in both models. According to the findings of Refs. [26, 27], however, this is unfortunately not the case: The best fit found in their analysis of the meson spectrum was for constituent masses $m_n = 306$ MeV and $m_s = 503$ MeV, below the values presented in Table 2.1. Therefore, in former investigations of strong decays of baryons [37–39] the parameters of the model for mesons were readjusted, keeping the constituent quark masses fixed to the values of Table 2.1 and paying special attention to the correct description of the ground-state pseudoscalar mesons. In Table 2.2 we present the results of this procedure, taken from Ref. [39].

2.5.2 N and Δ baryons

The results for the spectra of N and Δ resonances, calculated within the framework discussed here and with the parameters listed in Table 2.1, are shown in Figs. 2.3 and 2.4, respectively. These results were originally published in Ref. [29]; the theoretical masses shown in the figures slightly differ from those of this reference, due to a different dimension of the finite basis used to solve the Bethe-Salpeter equation as an eigenvalue problem. In the figures, the baryon states are placed in different columns according to their spin J, parity π and corresponding partial-wave $L_{2I\,2J}$ in πN scattering, where I denotes the isospin and L the orbital angular momentum. The theoretical predictions for the position of the resonances in the spectrum are on the left side of each column and the experimental masses and uncertainties, on the right side. In the cases where the PDG does not give estimates to the experimental masses and uncertainties, we use our own estimates based on the data available in their Review [2]. The position of the states is indicated by a bar, while the experimental uncertainties are denoted by a shaded box, which is darker for better established resonances. Additionally, the status of each experimental state is given by stars, according to the notation and classification of the PDG.

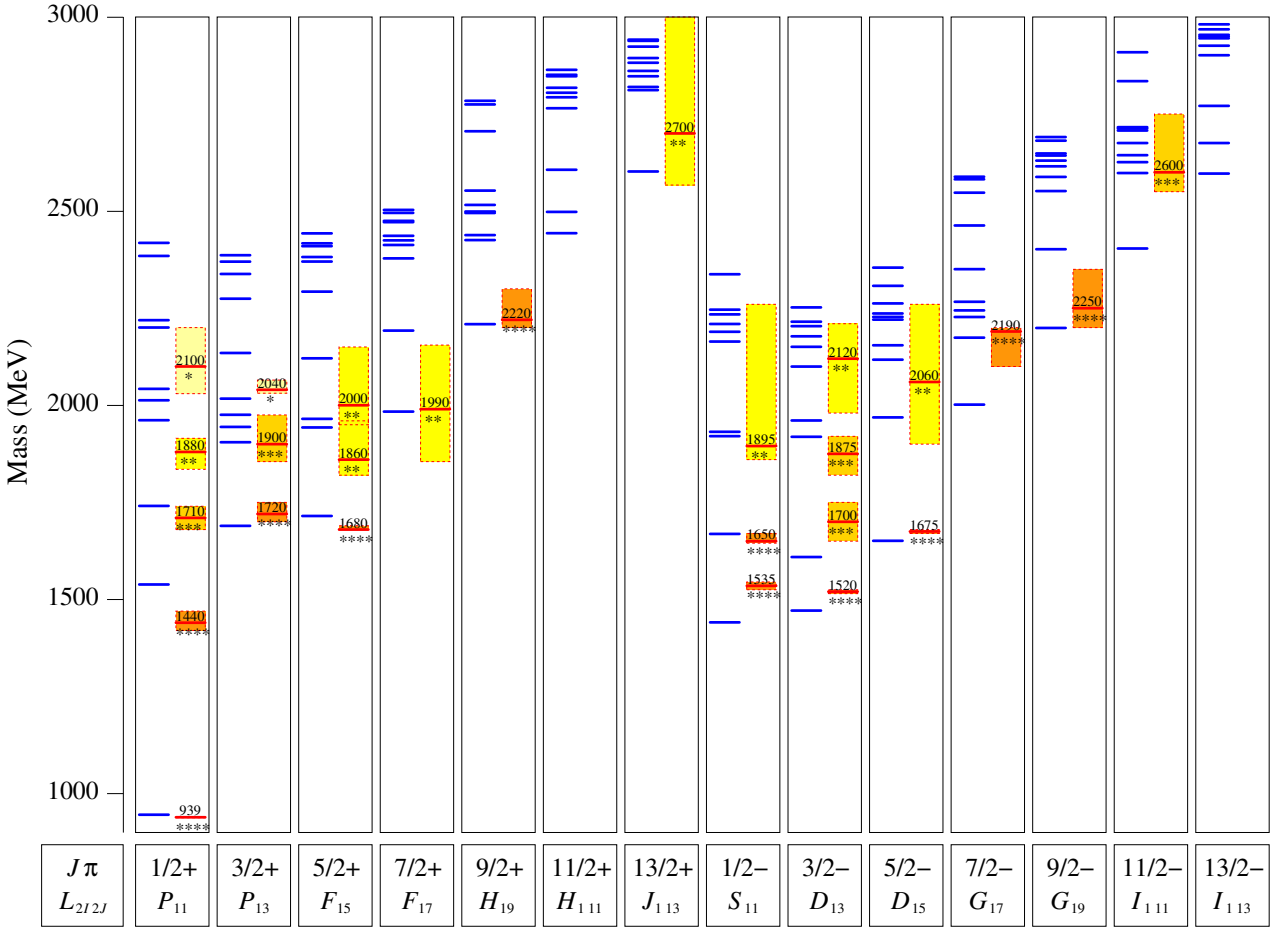

Figure 2.3. The calculated N spectrum (on the left of each column) in comparison to the experimental data from the Particle Data Group [2] (on the right). The states are classified by spin J, parity π and the corresponding partial-wave in πN scattering. The excitation masses are indicated by a bar and the experimental uncertainties by a shaded box, which is darker for better established states. The status of each resonance is additionally indicated by stars. The theoretical masses were calculated with the parameters taken from Ref. [29] (*cf.* Table 2.1); the results presented above slightly differ from those of this reference due to a different dimension of the basis used to solve the Bethe-Salpeter equation.

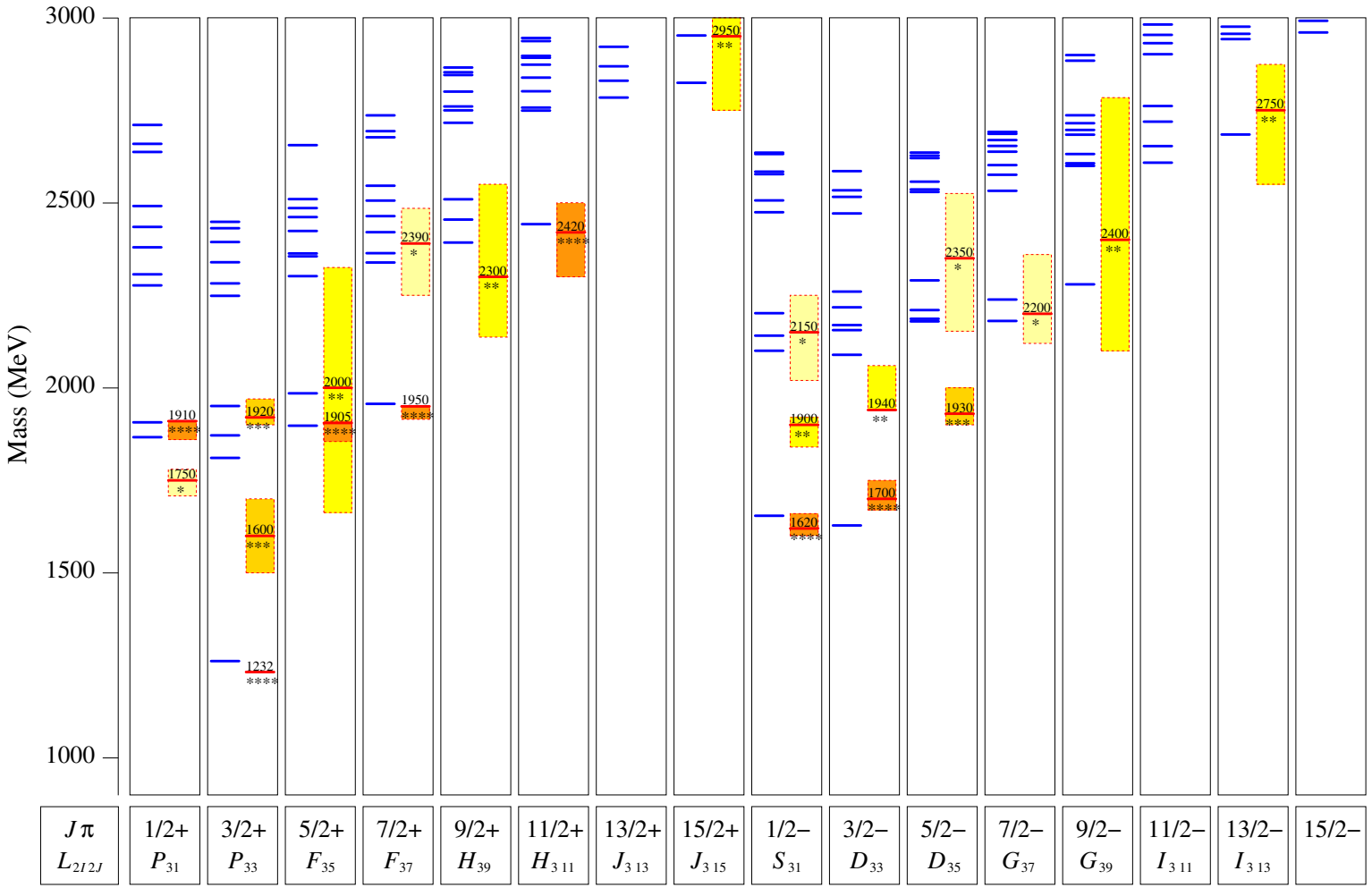

Figure 2.4. The calculated Δ spectrum (on the left of each column) in comparison to the experimental data from the Particle Data Group [2] (on the right). The notation is the same as in Fig. 2.3.

Concerning the results for N resonances, the spectrum of Fig. 2.3 shows that the present framework provides a very good description of the gross features observed in the experimental spectrum. In the lower energy region for instance, there is a remarkable agreement with the experimental mass-splittings between the negative-parity states with masses from 1500 to 1700 MeV. In the positive-parity sector, in turn, the model also accounts for the almost degenerate states around 1700 MeV, and even the low position of the Roper $N[\frac{1}{2}^+](1440)$ is at least qualitatively well described. Recalling that from the N spectrum only the ground-state $N(939)$ was included in the fit, this should be considered a success of the model.

In the high energy region of the N spectrum ($M \gtrsim 1800$ MeV), one still finds a reasonable agreement with the data: The model predicts at least one theoretical state for each one of the three- and four-star resonances, and in some cases the correspondence between model and experiment is even one-to-one. However, the multiplicity of theoretical states with higher masses becomes very large and leads to the problem of missing resonances. As mentioned before, this is a feature common to all constituent quark models in which the degrees of freedom are quark fields q occurring in the flavors $f = u, d, s$ and with spin $s = +\frac{1}{2}, -\frac{1}{2}$. In this way, such models predict all the states allowed by the symmetry $SU(6) = SU_f(3) \otimes SU_s(2)$.

The same analysis for Δ resonances, represented in the spectrum of Fig. 2.4, shows that this sector of the spectrum is also quite well described. Noticeably, for each one of the seven four-stars resonances the model predicts a corresponding theoretical state and, except for the $\Delta[\frac{1}{2}^+](1910, ****)$, all the assignments are clearly one-to-one. Moreover, the several even- and odd-parity bands are in general in good agreement with the position of the experimental states, considering the experimental uncertainty. Exceptions to this rule are however the negative-parity states from 1900 to 1940 MeV and the positive-parity $\Delta[\frac{3}{2}^+](1600)$, to which there are no obvious theoretical counterparts. The same happens to the resonance $\Delta[\frac{1}{2}^+](1750, *)$, although the existence of this state is only poorly established. Finally, in the high energy region ($M \gtrsim 2000$ MeV) of the Δ spectrum, one again finds a large multiplicity of theoretical states as usually expected from constituent quark models.

After this short overview on the complete theoretical spectrum of N and Δ baryons, we turn to the results for low-lying resonances specifically. All these states are either three- or four-stars resonances and for those there is always an one-to-one assignment between theoretical predictions and experiment. As already mentioned, one exception is the $\Delta[\frac{3}{2}^+](1600)$ state, to which – together with the negative-parity $\Delta[\frac{1}{2}^-](1900)$, $\Delta[\frac{3}{2}^-](1940)$ and $\Delta[\frac{5}{2}^-](1930)$ as well as the positive-parity $\Delta[\frac{1}{2}^+](1750)$ – apparently there is no theoretical state assignable.

In a recent study [61], Ronniger and Metsch addressed the problematic Δ states listed above. They pointed out that the poor description of these resonances in the present framework can be improved by phenomenologically introducing a flavor-dependent interaction which acts on the Δ sector of the spectrum as well. In this study, they showed that this additional residual interaction systematically improves the description of the excited negative-parity Δ resonances and, at the same time, gives a much better description of the first radial excitations of the ground-states in each sector. Based on their results, we thus associate the $\Delta[\frac{3}{2}^+](1600)$ resonance to the first theoretical radial excitation $\Delta[\frac{3}{2}^+]_1(1811)$.

Table 2.3. Calculated positions of low-lying N and Δ baryons (given in the last column) in comparison to the experimental data from the Particle Data Group [2] (PDG). The states are classified by their spin J, parity π and the corresponding partial-wave in πN scattering. The theoretical masses were calculated with the parameters taken from Ref. [29] (*cf.* Table 2.1); the results below slightly differ from those of this reference due to a different dimension of the basis used to solve the Bethe-Salpeter equation.

$L_{2I\,2J}$	J^π	PDG			Quark Model
		Label	Status	Mass range (MeV)	
S_{11}	$\frac{1}{2}^-$	$N(1535)$	****	1525 - 1545	$[N\frac{1}{2}^-]_0(1441)$
		$N(1650)$	****	1645 - 1670	$[N\frac{1}{2}^-]_1(1669)$
P_{11}	$\frac{1}{2}^+$	$N(939)$	****	939 - 939	$[N\frac{1}{2}^+]_0(946)$
		$N(1440)$	****	1420 - 1470	$[N\frac{1}{2}^+]_1(1539)$
		$N(1710)$	***	1680 - 1740	$[N\frac{1}{2}^+]_2(1741)$
P_{13}	$\frac{3}{2}^+$	$N(1720)$	****	1700 - 1750	$[N\frac{3}{2}^+]_0(1689)$
D_{13}	$\frac{3}{2}^-$	$N(1520)$	****	1515 - 1525	$[N\frac{3}{2}^-]_0(1471)$
		$N(1700)$	***	1650 - 1750	$[N\frac{3}{2}^-]_1(1609)$
D_{15}	$\frac{5}{2}^-$	$N(1675)$	****	1670 - 1680	$[N\frac{5}{2}^-]_0(1651)$
F_{15}	$\frac{5}{2}^+$	$N(1680)$	****	1680 - 1690	$[N\frac{5}{2}^+]_0(1715)$
S_{31}	$\frac{1}{2}^-$	$\Delta(1620)$	****	1600 - 1660	$[\Delta\frac{1}{2}^-]_0(1654)$
P_{33}	$\frac{3}{2}^+$	$\Delta(1232)$	****	1230 - 1234	$[\Delta\frac{3}{2}^+]_0(1262)$
		$\Delta(1600)$	***	1500 - 1700	$[\Delta\frac{1}{2}^+]_1(1811)$
D_{33}	$\frac{3}{2}^-$	$\Delta(1700)$	****	1670 - 1750	$[\Delta\frac{3}{2}^-]_0(1628)$

The calculated positions of low-lying N and Δ baryons in the spectrum and the corresponding experimental assignments are collected in Table 2.3, as well as the mass uncertainties (or range) and the status of the experimental resonances. In addition, the theoretical mass of the $N(939)$ ground-state is also given there, as it participates in the strong decay channels considered in the next chapter. According to the results shown in the table, the calculated masses are in reasonable agreement with the data, considering experimental uncertainties. For the majority of the states the deviation is in general below 85 MeV, which is a good result in view of the typical values for the widths of baryon resonances. The only exception is the aforementioned $\Delta[\frac{3}{2}^+]_1(1811)$, whose position deviates from the experimental range by around 110 MeV.

2.5.3 π and η mesons

For the sake of completeness, we compare in Fig. 2.5 the experimental spectra of π and η mesons to the predicted spectra calculated with the parameters of Table 2.2. The theoretical values shown in the figure were taken from Ref. [39]. The spin J, parity π and charge conjugation quantum number c of the states are given in each column according to the notation $J^{\pi c}$. The representation of both theoretical and experimental positions, as well as of experimental uncertainties, is the same as we used for baryon resonances. In the resulting spectra, one observes that the calculated masses are in general larger than the experimental values. This effect is due to reasons already explained in the text: Here, the constituent quark masses m_n and specially m_s are higher than the values leading to the best fit of the meson spectrum. Nonetheless, a good description of the ground states, necessary for the calculation of strong decays of baryons into πN, $\pi\Delta$ and ηN, could still be achieved. As shown in the picture, the calculated values are

$$\begin{aligned} m_{\pi}^{\mathrm{RCQM}} &= 139 \text{ MeV}, \\ m_{\eta}^{\mathrm{RCQM}} &= 503 \text{ MeV}. \end{aligned} \tag{2.128}$$

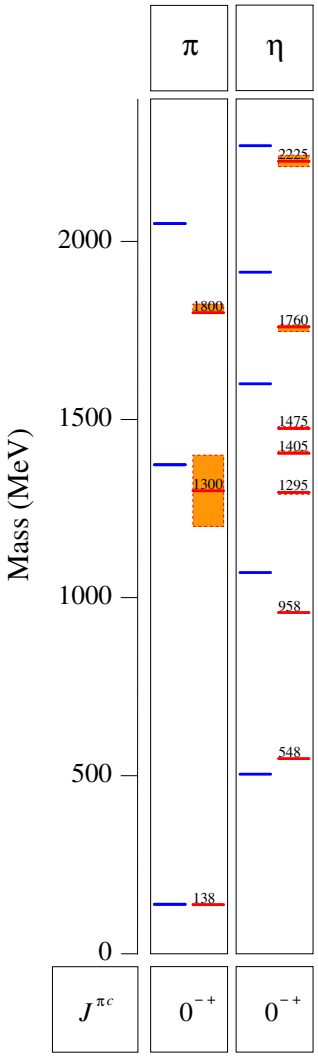

Figure 2.5. The calculated π and η spectra (on the left side of each column) in comparison to the experimental values from the Particle Data Group [2] (on the right). The theoretical masses were taken from Ref. [39]. The spin J, parity π and charge conjugation quantum number c of the states are given in each column according to the notation $J^{\pi c}$. The positions and experimental uncertainties are denoted as in Fig. 2.3.

Chapter 3

Strong two-body decays of baryons

3.1 Introduction

In the baryon spectrum at higher energies ($M \gtrsim 1800$ MeV), the relativistic quark model reviewed in Chapter 2 predicts many excitations for which no experimental counterpart has been detected. These are the so-called missing resonances, common to all constituent quark models on the basis of three quarks as degrees of freedom. As pointed out *e.g.* by Capstick and Roberts [22], a possible explanation to the problem of the missing states might be that these simply decouple from the strong decay channels measured in π- or K-induced reactions.

To investigate this possibility, an extensive study of strong baryon decays has been done in the framework of the quark model [39], and the results indeed show that missing states in general decouple from πN and KN, thus offering a natural solution to the problem. However, despite the success in clarifying the matter, there are some important issues demanding further investigation. Up to now, the strong decay widths have been calculated only in lowest order of perturbation theory, and possibly due to the neglect of important final state interactions in this approximation, the calculated widths are in general too small in comparison to experimental data. Concerning this matter, one still has to verify whether the inclusion of rescattering effects provides sufficient strength to correct the calculated widths. On the other hand, the results indicate that the contribution of coupled-channel effects might be very important too: as we shall see in this chapter, some low-lying N and Δ states with sizable experimental partial decay widths into πN almost decouple from this channel theoretically, but at the same time show substantial theoretical partial decay widths into $\pi\Delta$.

The main goal of this thesis is to provide a framework in which final state interactions and coupled-channel effects can be taken into account. In a first study, however, we shall not investigate missing resonances directly: as they occur at higher energies in the spectrum, this would require the complete treatment of meson-baryon scattering up to the highest inelastic channels. Instead, here we only consider strong decays of low-lying N and Δ resonances into πN, $\pi\Delta$ and ηN and investigate in how far the inclusion of rescattering effects improves the description of the corresponding widths. Accordingly, we dedicate this chapter to explain how strong baryon decays have been investigated so far and give an overview of the results for strong decays of non-strange resonances, focusing on the low-energy sector of the spectrum.

In the following Section 3.2 we show a detailed derivation of decay matrix elements in the framework of the relativistic quark model. For this purpose, we apply the Mandelstam formalism [47] in lowest order of perturbation theory, which introduces no further parameters in the model and therefore leads to parameter-free predictions. Next, in Section 3.3 we recall the basic formulae for two-body decay widths, calculated from the matrix elements considered before, and then summarize the results for strong decays of N- and Δ-baryons with special attention to low-energy states.

3.2 Strong decay matrix elements

In this section we consider the strong two-body decay

$$M_R(\bar{Q},\mu_{\bar{Q}}) \to M(\bar{P},\mu_{\bar{P}}) + m(\bar{K},\mu_{\bar{K}}) \tag{3.1}$$

of a initial baryon resonance with mass M_R into a final baryon and a meson with masses M and m, respectively. In the center-of-mass frame, the corresponding four-momenta variables $\bar{Q}$, $\bar{P}$ and $\bar{K}$ are given by

$$\bar{Q} = \begin{pmatrix} M_R \\ 0 \\ 0 \\ 0 \end{pmatrix}, \qquad \bar{P} = \begin{pmatrix} \omega_{\bar{P}} \\ 0 \\ 0 \\ |\mathbf{P}| \end{pmatrix} \qquad \text{and} \qquad \bar{K} = \begin{pmatrix} \omega_{\bar{K}} \\ 0 \\ 0 \\ -|\mathbf{P}| \end{pmatrix}, \tag{3.2}$$

where the $\mathbf{P}$ denotes the relative three-momentum and

$$\omega_{\bar{P}} = \sqrt{\mathbf{P}^2 + M^2} \quad \text{and} \quad \omega_{\bar{K}} = \sqrt{\mathbf{P}^2 + m^2} \tag{3.3}$$

are the on-shell energies of the outgoing states. The variables $\mu_{\bar{Q}}$, $\mu_{\bar{P}}$ and $\mu_{\bar{K}}$ represent additional quantum numbers necessary to label the states, such as helicities and isospin projections, and are explicitly written only when needed. In the following we apply the Mandelstam formalism [47] in lowest order of perturbation theory in order to extract the corresponding decay matrix element

$$\langle \bar{P}\bar{K}|\bar{Q}\rangle \tag{3.4}$$

from the eight-point Green's function

$$\begin{aligned} G^{(8)}(x_1,&x_2,x_3,y_1,y_2,z_1,z_2,z_3) := \\ &- \langle\Omega|T\Psi^1(x_1)\Psi^2(x_2)\Psi^3(x_3)\Psi^q(y_1)\bar{\Psi}^{\bar{q}}(y_2)\bar{\Psi}^{1'}(z_1)\bar{\Psi}^{2'}(z_2)\bar{\Psi}^{3'}(z_3)|\Omega\rangle, \end{aligned} \tag{3.5}$$

both defined in the Heisenberg picture. Here, the superscripts $i = 1,2,3$ ($i' = 1',2',3'$) label the constituent quarks in the final (initial) baryon state and the superscripts $\bar{q}$ and q label the quark-antiquark pair in the meson.

To proceed, we recall that the momentum eigenstates $|\bar{Q}\rangle$ and $|\bar{P}\bar{K}\rangle \equiv |\bar{P}\rangle \otimes |\bar{K}\rangle$ correspond to on-shell, asymptotic states. Therefore, it is meaningful to consider in particular

$$x_1^0, x_2^0, x_3^0, y_1^0, y_2^0 \to +\infty \quad \text{and} \quad z_1^0, z_2^0, z_3^0 \to -\infty \tag{3.6}$$

for the time-ordering in the Green's function $G^{(8)}$ since we want to isolate the $\langle \bar{P}\bar{K}|\bar{Q}\rangle$ contribution. Moreover, we here neglect rescattering effects completely, by assuming that after the meson creation the quarks confined in the final baryon do not interact with those confined in the meson. Based on these arguments, we obtain

$$\begin{aligned} G^{(8)}(x_1,x_2,x_3,y_1,y_2,z_1,z_2,z_3) &= \\ &- \langle\Omega|\Big[T\Psi^1(x_1)\Psi^2(x_2)\Psi^3(x_3)\Big]\Big[T\Psi^q(y_1)\bar{\Psi}^{\bar{q}}(y_2)\Big]\Big[T\bar{\Psi}^{1'}(z_1)\bar{\Psi}^{2'}(z_2)\bar{\Psi}^{3'}(z_3)\Big]|\Omega\rangle \\ &+ \text{other time-orderings.} \end{aligned} \tag{3.7}$$

Finally, the contribution of $\langle \bar{P}\bar{K}|\bar{Q}\rangle$ can then be isolated by inserting complete sets of momentum eigenstates between the time-ordered products in Eq. (3.7). In this way,

$$\begin{aligned} G^{(8)}(x_1,x_2,x_3,y_1,&y_2,z_1,z_2,z_3) = \\ &- \int \frac{\mathrm{d}^3\,\bar{P}}{(2\pi)^3}\frac{\mathrm{d}^3\,\bar{K}}{(2\pi)^3}\frac{\mathrm{d}^3\,\bar{Q}}{(2\pi)^3}\frac{1}{8\omega_{\bar{Q}}\omega_{\bar{P}}\omega_{\bar{K}}} \\ &\quad\times\left[\chi_{\bar{P}}(x_1,x_2,x_3)\otimes\chi_{\bar{K}}(y_1,y_2)\right]\langle\bar{P}\bar{K}|\bar{Q}\rangle\bar{\chi}_{\bar{Q}}(z_1,z_2,z_3) \\ &+ \text{ other decay processes,} \end{aligned} \tag{3.8}$$

where we employed the definitions of the Bethe-Salpeter amplitudes and their adjoints, given by Eqs. (2.16) and (2.17) for mesons and Eqs. (2.69) and (2.70) for baryons.

3.2.1 The current interaction kernel

To describe the interactions leading to strong decays in our framework we define a current interaction kernel $K^{(4)}$ according to the integral equation

$$\begin{aligned} G^{(8)}(x_1,x_2,x_3,y_1,&y_2,z_1,z_2,z_3) = \\ &\int \mathrm{d}^4\,x_1'\,\mathrm{d}^4\,x_2'\,\mathrm{d}^4\,x_3'\,\mathrm{d}^4\,y_1'\,\mathrm{d}^4\,y_2'\,\mathrm{d}^4\,z_1'\,\mathrm{d}^4\,z_2'\,\mathrm{d}^4\,z_3' \\ &\quad\times G^{(10)}(x_1,x_2,x_3,y_1,y_2,x_1',x_2',x_3',y_1',y_2') \\ &\quad\times K^{(4)}(x_1',x_2',x_3',y_1',y_2',z_1',z_2',z_3') \\ &\quad\times G^{(6)}(z_1',z_2',z_3',z_1,z_2,z_3), \end{aligned} \tag{3.9}$$

where we introduced the ten-point Green's function

$$\begin{aligned} G^{(10)}(x_1,x_2,x_3,y_1,y_2,x_1',x_2',&x_3',y_1',y_2') := \\ &-\langle\Omega|T\,\Psi^1(x_1)\Psi^2(x_2)\Psi^3(x_3)\Psi^q(y_1)\bar{\Psi}^{\bar{q}}(y_2) \\ &\quad\times\bar{\Psi}^1(x_1')\bar{\Psi}^2(x_2')\bar{\Psi}^3(x_3')\Psi^{\bar{q}}(y_2')\bar{\Psi}^q(y_1')|\Omega\rangle. \end{aligned} \tag{3.10}$$

Since final state interactions are completely neglected here, the ten-point function $G^{(10)}$ separates into the tensor product $G^{(6)} \otimes G^{(4)}$, such that

$$\begin{aligned} G^{(8)}(x_1, x_2, x_3, y_1, &y_2, z_1, z_2, z_3) \approx \\ &\int \mathrm{d}^4\, x_1' \, \mathrm{d}^4\, x_2' \, \mathrm{d}^4\, x_3' \, \mathrm{d}^4\, y_1' \, \mathrm{d}^4\, y_2' \, \mathrm{d}^4\, z_1' \, \mathrm{d}^4\, z_2' \, \mathrm{d}^4\, z_3' \\ &\times G^{(6)}(x_1, x_2, x_3, x_1', x_2', x_3') \otimes G^{(4)}(y_1, y_2, y_1', y_2') \\ &\times K^{(4)}(x_1', x_2', x_3', y_1', y_2', z_1', z_2', z_3') \\ &\times G^{(6)}(z_1', z_2', z_3', z_1, z_2, z_3). \end{aligned} \tag{3.11}$$

To find a relation between the matrix element $\langle \bar{P}\bar{K}|\bar{Q}\rangle$ and the kernel $K^{(4)}$, we now assume the same time-dependence of Eq. (3.6) for all Green's functions in Eq. (3.11) and then introduce complete sets of momentum eigenstates. In this way, we obtain

$$\begin{aligned} G^{(8)}(x_1, x_2, x_3, y_1, y_2, z_1, z_2, z_3) &\approx \\ -\int \frac{\mathrm{d}^3\, \bar{P}}{(2\pi)^3} \frac{\mathrm{d}^3\, \bar{K}}{(2\pi)^3} \frac{\mathrm{d}^3\, \bar{Q}}{(2\pi)^3} &\frac{1}{8\omega_{\bar{Q}}\omega_{\bar{P}}\omega_{\bar{K}}} \left[\chi_{\bar{P}}(x_1, x_2, x_3) \otimes \chi_{\bar{K}}(y_1, y_2)\right] \\ \times \int \mathrm{d}^4\, x_1' \, \mathrm{d}^4\, x_2' \, \mathrm{d}^4\, x_3' \, \mathrm{d}^4\, y_1' \, \mathrm{d}^4\, y_2' \, \mathrm{d}^4\, z_1' \, \mathrm{d}^4\, z_2' \, \mathrm{d}^4\, z_3' & \\ \times \left[\bar{\chi}_{\bar{P}}(x_1', x_2', x_3') \otimes \bar{\chi}_{\bar{K}}(y_1', y_2')\right] & \\ \times K^{(4)}(x_1', x_2', x_3', y_1', y_2', z_1', z_2', z_3') & \\ \times \left[\bar{\chi}_{\bar{Q}}(z_1', z_2', z_3') \chi_{\bar{Q}}(z_1, z_2, z_3)\right] & \\ + \text{ other decay processes,} & \end{aligned} \tag{3.12}$$

where we again use the definitions of the Bethe-Salpeter amplitudes, as well as the definitions of the four- and six-point Green's functions, given by Eqs. (2.1) and (2.47) respectively. Finally, from the comparison between Eqs. (3.8) and (3.12), it follows that the decay matrix element is given in terms of the current kernel according to

$$\begin{aligned} \langle \bar{P}\bar{K}|\bar{Q}\rangle \approx \int &\mathrm{d}^4\, x_1 \, \mathrm{d}^4\, x_2 \, \mathrm{d}^4\, x_3 \, \mathrm{d}^4\, y_1 \, \mathrm{d}^4\, y_2 \, \mathrm{d}^4\, z_1 \, \mathrm{d}^4\, z_2 \, \mathrm{d}^4\, z_3 \\ &\times \bar{\chi}_{\bar{P}}(x_1, x_2, x_3) \otimes \bar{\chi}_{\bar{K}}(y_1, y_2) \\ &\times K^{(4)}(x_1, x_2, x_3, y_1, y_2, z_1, z_2, z_3) \\ &\times \chi_{\bar{Q}}(z_1, z_2, z_3). \end{aligned} \tag{3.13}$$

3.2.2 Model interactions

For the sake of consistency, both baryon spectra and strong decays should be described by the same interactions in the same order of perturbation theory. Assuming that the confinement potential plays no role in decays, this means that in our framework the kernel $K^{(4)}$ has to be parametrized by effective instanton interactions up to first order in the couplings $g_{\mathrm{eff}}^{(2)} \equiv g_{nn}, g_{ns}$ and $g_{\mathrm{eff}}^{(3)}$ of the 't Hooft's Lagrangian (*cf.* Section 2.4). Thus, expanding both sides of Eq. (3.11) in the 't Hooft's couplings, applying Wick's

theorem and finally collecting terms up $\mathcal{O}(g_{\text{eff}}^{(2,3)})$, we obtain two contributions. Firstly, zeroth order quark loops, given explicitly by

$$\begin{aligned} K_0^{(4)}&(x_1,x_2,x_3,y_1,y_2,z_1,z_2,z_3) \\ &= {S_F^1}^{-1}(x_1,z_1)\otimes {S_F^2}^{-1}(x_2,z_2)\otimes {S_F^{\bar{q}}}^{-1}(x_3,y_2)\otimes {S_F^q}^{-1}(y_1,z_3) \\ &+ {S_F^2}^{-1}(x_2,z_2)\otimes {S_F^3}^{-1}(x_3,z_3)\otimes {S_F^{\bar{q}}}^{-1}(x_1,y_2)\otimes {S_F^q}^{-1}(y_1,z_1) \\ &+ {S_F^3}^{-1}(x_3,z_3)\otimes {S_F^1}^{-1}(x_1,z_1)\otimes {S_F^{\bar{q}}}^{-1}(x_2,y_2)\otimes {S_F^q}^{-1}(y_1,z_2), \end{aligned} \tag{3.14}$$

and represented by the diagram of Fig. 3.1a, as well as three-body forces induced by instantons, as depicted in Fig. 3.1b. Up to first order no further terms contribute, since all other possible two- and three-particle instanton diagrams can be reabsorbed into the integral equation for the Bethe-Salpeter amplitudes appearing in Eq. (3.13).

Unfortunately, as shown in Ref. [39] the numerical implementation of instanton three-body forces in strong baryon decays turns out to be much involved and not feasible with a reasonable effort. In this respect however, we note that instantons would effectively contribute to very few decays only, due to the occurrence of the totally anti-symmetric flavor-projector $\mathcal{P}_A^f$ in the Lagrangian of Eq. (2.127). Among decays into πN, $\pi\Delta$ and ηN, *i.e.* the channels considered in this thesis, only the latter would be affected. For this reason, the current kernel is here approximated by quark loops only, such that the strong decay matrix element is given by

$$\begin{aligned} \langle \bar{P}\bar{K}|\bar{Q}\rangle \approx \int \mathrm{d}^4x_1\,\mathrm{d}^4x_2\,\mathrm{d}^4x_3\,\mathrm{d}^4y_1\,\mathrm{d}^4y_2\,\mathrm{d}^4z_1\,\mathrm{d}^4z_2\,\mathrm{d}^4z_3 \\ \times \bar{\chi}_{\bar{P}}(x_1,x_2,x_3)\left[{S_F^1}^{-1}(x_1,z_1)\otimes {S_F^2}^{-1}(x_2,z_2)\right] \\ \otimes \left[{S_F^{\bar{q}}}^{-1}(x_3,y_2)\bar{\chi}_{\bar{K}}(y_1,y_2){S_F^q}^{-1}(y_1,z_3)\right] \\ \times \chi_{\bar{Q}}(z_1,z_2,z_3) \\ + \text{ meson couplings to quarks 1 and 2.} \end{aligned} \tag{3.15}$$

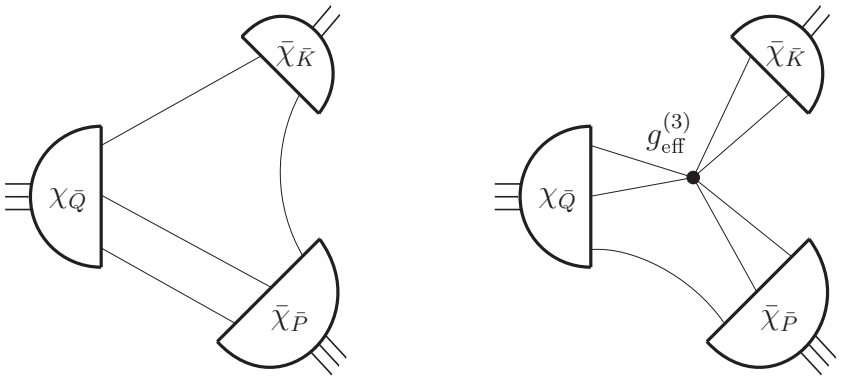

(a) Quark-Loops. **(b)** Instanton induced decay.

Figure 3.1. Perturbative contributions to the decay matrix element $\langle \bar{P}\bar{K}|\bar{Q}\rangle$.

3.2.3 Approximations and reduction

Having defined the phenomenological interactions contributing to strong baryon decays, we now evaluate Eq. (3.15) in the same instantaneous approximation and free-quark parametrization as discussed in Section 2.3.4. Therefore, it is clear that the full propagators in Eq. (3.15) will be replaced by free effective propagators; we shortly comment on this subject later in this section. Concerning the interaction kernels, recall from Section 2.3.4 that in our framework we evaluate the Salpeter amplitudes only, whereas Eq. (3.15) is written in terms of the full Bethe-Salpeter amplitudes. Accordingly, we now need a relation between both.

In the case of mesons it is straightforward to derive such a relation directly from the two-body Bethe-Salpeter equation. To see this, note that the quantity

$$\Gamma_{\bar{K}}(k) := \left[S_F^{q\,-1}\left(\tfrac{\bar{K}}{2}+k\right)\otimes S_F^{\bar{q}\,-1}\left(-\tfrac{\bar{K}}{2}+k\right)\right]\chi_{\bar{K}}(k), \tag{3.16}$$

called **vertex function** or **amputated Bethe-Salpeter amplitude**, is calculated from the Salpeter amplitude in the rest frame of the meson. Indeed, from the Bethe-Salpeter equation (2.33) evaluated in instantaneous approximation and the definition (2.37) of the two-body Salpeter amplitudes, one easily shows that

$$\Gamma_m(k) = -i\int\frac{\mathrm{d}^3\,k'}{(2\pi)^3}V^{(2)}(\mathbf{k},\mathbf{k}')\Phi(\mathbf{k}') \equiv \Gamma_m(\mathbf{k}) \tag{3.17}$$

in the rest frame. Moreover, vertex functions are relativistically covariant by definition (*cf.* Eq. (3.16)) and therefore can be evaluated in any reference system by an appropriate Lorentz transformation. This is of course crucial for calculations of observables involving multiple hadron states, such as strong decay widths.

Turning to the case of baryons, the connection between Bethe-Salpeter and Salpeter amplitudes is not that obvious. Due to the retardation effects in three-quark systems as discussed in Section 2.3.4, only the projected part of the Salpeter amplitudes in Born approximation is evaluated in our framework. Therefore, an explicit relation between the three-body vertex function

$$\begin{aligned}\Gamma_{\bar{P}}(p_\xi,p_\eta) := {}& S_F^{1\,-1}\left(\tfrac{1}{3}\bar{P}+p_\xi+\tfrac{1}{2}p_\eta\right)\otimes S_F^{2\,-1}\left(\tfrac{1}{3}\bar{P}-p_\xi+\tfrac{1}{2}p_\eta\right)\\ &\otimes S_F^{3\,-1}\left(\tfrac{1}{3}\bar{P}-p_\eta\right)\chi_{\bar{P}}(p_\xi,p_\eta)\end{aligned} \tag{3.18}$$

and three-body Salpeter amplitudes requires a lengthy and careful derivation. This has been carried out in Ref. [32], leading to the result

$$\begin{aligned}\Gamma_M(p_\xi,p_\eta) &\approx -i\int\frac{\mathrm{d}^3\,p'_\xi}{(2\pi)^3}\frac{\mathrm{d}^3\,p'_\eta}{(2\pi)^3}\left[V_\Lambda^{(3)}+V_M^{\mathrm{eff}\,(1)}\right](\mathbf{p}_\xi,\mathbf{p}_\eta,\mathbf{p}'_\xi,\mathbf{p}'_\eta)\Phi_\Lambda^{(1)}(\mathbf{p}'_\xi,\mathbf{p}'_\eta)\\ &\equiv \Gamma_M(\mathbf{p}_\xi,\mathbf{p}_\eta),\end{aligned} \tag{3.19}$$

where the superscripts in V_M^{eff} and Φ_Λ indicate that these quantities are evaluated by including up to the leading Born term only.

From the discussion above, it follows that vertex functions are the appropriate quantities to express $\langle \bar{P}\bar{K}|\bar{Q}\rangle$, since they can be evaluated from Salpeter amplitudes in the rest frame of the corresponding meson or baryon state and then boosted to the rest frame of the decaying resonance. We thus write Eq. (3.15) in terms of the vertex functions defined in (3.16) and (3.18) and the corresponding adjoints, arriving at

$$\begin{aligned}\langle \bar{P}\bar{K}|\bar{Q}\rangle \approx 3\int &\frac{\mathrm{d}^4 p_\xi}{(2\pi)^4}\frac{\mathrm{d}^4 p_\eta}{(2\pi)^4} \\ &\times (2\pi)^4\delta^{(4)}(\bar{P}+\bar{K}-\bar{Q})\bar{\Gamma}_{\bar{P}}\left(p_\xi, p_\eta+\tfrac{2}{3}\bar{K}\right) \\ &\times S_F^1\left(\tfrac{1}{3}M_R+p_\xi+\tfrac{1}{2}p_\eta\right)\otimes S_F^2\left(\tfrac{1}{3}M_R-p_\xi+\tfrac{1}{2}p_\eta\right) \\ &\otimes S_F^{\bar{q}}\left(\tfrac{1}{3}M_R+p_\eta-\bar{K}\right)\bar{\Gamma}_{\bar{K}}\left(\tfrac{1}{3}M_R-p_\eta-\tfrac{1}{2}\bar{K}\right) \\ &\otimes S_F^{q}\left(\tfrac{1}{3}M_R-p_\eta\right)\Gamma_{M_R}(p_\xi,p_\eta),\end{aligned} \tag{3.20}$$

where we employed the Fourier-transforms and Jacobi coordinates defined in Sections 2.2 and 2.3. The result above is our final expression for strong decay matrix elements, and the only step left is to substitute the full propagators by their effective free-quark parameterizations and then solve the integral numerically. Details on this procedure can be found in Refs. [39, 62]. As we see from Eq. (3.20), the formalism applied here leads to no further parameters other than those listed in Tables 2.1 and 2.2, allowing for the calculation of strong decay matrix elements from the same parameters adjusted to hadronic spectra this way. In this sense, the resulting decay widths are predictions of the model.

Before proceeding further, an important remark concerning the matrix elements in (3.20) and the use of these quantities in the next chapters is in order. As a matter of fact, Eq. (3.20) allows for the determination of the *magnitude* of $\langle \bar{P}\bar{K}|\bar{Q}\rangle$ but not of its absolute sign. This results from the fact that the eigenvalue Salpeter equations (2.45) and (2.109) determine Salpeter amplitudes up to a phase only, and it also holds for vertex functions as these are obtained from the former according to Eqs. (3.17) and (3.19). Although irrelevant for the calculation of lowest-order decay widths (see the formulae in Section 3.3), the relative sign of matrix elements corresponding to decays into different channels plays an important role in the investigation of final state interactions. This point shall be further clarified later in Section 4.4.

3.3 Strong decay widths of non-strange baryons

Below we summarize the main findings of Ref. [39] concerning strong two-body decays of non-strange baryons into πN, $\pi\Delta$ and ηN. Before presenting the results, we shortly review the basic formulae for the calculation of two-body decay widths.

3.3.1 Two-body decay widths

The differential decay width related to two-body decays is calculated according to the standard formula:

$$\mathrm{d}\,\Gamma_{\bar{P}\bar{K}\leftarrow\bar{Q}} = (2\pi)^4\delta^{(4)}(\bar{P}+\bar{K}-\bar{Q})\frac{1}{2M_R}\frac{\mathrm{d}^3\,\bar{P}}{(2\pi)^3 2\omega_{\bar{P}}}\frac{\mathrm{d}^3\,\bar{K}}{(2\pi)^3 2\omega_{\bar{K}}}|\gamma_{\bar{P}\bar{K}\leftarrow\bar{Q}}|^2, \tag{3.21}$$

see *e.g.* the textbook [63], where the decay amplitude $\gamma_{\bar{P}\bar{K}\leftarrow\bar{Q}}$ is related to the matrix element $\langle\bar{P}\bar{K}|\bar{Q}\rangle$ by

$$\langle\bar{P}\bar{K}|\bar{Q}\rangle =: (2\pi)^4\delta^{(4)}(\bar{P}+\bar{K}-\bar{Q})\gamma_{\bar{P}\bar{K}\leftarrow\bar{Q}}. \tag{3.22}$$

The total decay width in turn is easily obtained from these expressions by considering the kinematics of the center-of-mass frame (*cf.* Eq. (3.2)) and integrating both sides of Eq. (3.21). In this way,

$$\Gamma_{\bar{P}\bar{K}\leftarrow\bar{Q}} = \frac{|\mathbf{P}|}{8\pi M_R^2}|\gamma_{\bar{P}\bar{K}\leftarrow\bar{Q}}|^2. \tag{3.23}$$

In the calculations of Ref. [39] only unpolarized widths have been considered, and therefore we now have to carry out sums and averages over the possible initial and final helicity states. The same applies for isospin projections, since isospin symmetry is considered to be exact in the relativistic quark model. Hence, following the notation of Eq. (3.1) we obtain

$$\Gamma_{\bar{P}\bar{K}\leftarrow\bar{Q}} = \frac{|\mathbf{P}|}{8\pi M_R^2}\frac{1}{2J+1}\frac{1}{2I+1}\sum_{\mu_{\bar{Q}},\mu_{\bar{P}},\mu_{\bar{K}}}|\gamma_{\bar{P}\bar{K}\leftarrow\bar{Q}}(\mu_{\bar{Q}},\mu_{\bar{P}},\mu_{\bar{K}})|^2, \tag{3.24}$$

where J denotes the spin of the decaying resonance and I represents its isospin.

3.3.2 N and Δ baryons

Concerning the calculation of strong decays of non-strange baryons in general, the findings of Ref. [39] can be summarized as follows:

- Firstly, the theoretical πN-decay widths fall into three categories: Those which represent a substantial fraction of the experimental value, those which are too small but still clearly finite, and finally those which vanish numerically (*i.e.* are by several orders of magnitude smaller than 1 MeV). All resonances with decay widths belonging to the first and second categories have indeed been observed experimentally.

- Moreover, clear selection rules for decays into ground-state baryons under emission of a pseudoscalar meson have been observed: N resonances preferably decay into πN and $\pi\Delta$ and rarely decay into ηN (but recall that the latter would be affected by instantons); Δ resonances in turn mostly decay into $\pi\Delta$ and $\eta\Delta$ and occasionally into πN. In both cases, strangeness production channels are in general suppressed.

- Despite the qualitative description of experimental data, even the non-vanishing decay widths are generally too small when compared to experimental data. However, decay widths for the missing resonances are usually smaller by several orders of magnitude.

According to these results, the framework does offer a solution to the problem of the missing resonances, as such states simply decouple from πN. To illustrate this fact, we again present the spectra of N and Δ baryons in Figs. 3.2 and 3.3 with a slightly different emphasis. Based on the results and the notation of Ref. [39], we denote by dashed lines those resonances which decouple from πN and by full lines the states whose πN-decay widths are at least in qualitative agreement with the experimental values. In these figures, we clearly see that the results provide an explanation to the missing resonances, and in addition allow for many unique assignments between theoretical and experimental states which would not have been possible based on the mass spectra alone.

Nevertheless, we still have to understand why the calculated decay widths tend to be smaller than the experimental value. Larger discrepancies are mostly found for high-energy states, but even for low-lying states a quantitative description of decay widths could not be achieved. To further investigate this topic, from now on we focus on strong decays of low-lying N and Δ baryons (whose masses were listed in Table 2.3) into πN, $\pi\Delta$ and ηN. Decays into $K\Lambda$ and $K\Sigma$ will not be considered here, as strangeness production was found to be negligible [39].

The calculated decay widths into the channels of interest in comparison to the experimental data are given in Table 3.1. The theoretical values shown in the table slightly differ from those of Ref. [39], due to a different dimension of the basis used to solve the Bethe-Salpeter equation for the initial and final baryon states. Concerning the empirical data, it should be mentioned that the values quoted as experimental are estimates of the Particle Data Group for total (Breit-Wigner) widths multiplied by branching ratios, considering experimental uncertainties.

The values presented in the table show a reasonable description of πN and $\pi\Delta$ decays for most low-lying states, albeit with calculated widths in general below or at best very close to the lower experimental limit. An exception is the $N[\frac{3}{2}^-](1700)$, which theoretically decouples from πN. Interestingly, the calculated $\pi\Delta$-decay width for this resonance is relatively large, indicating that coupled-channel rescattering effects might provide a finite value for the πN width. The calculated ηN widths, on the other hand, do not describe the data and most resonances simply decouple from this channel. For most of the states this might be a consequence of neglecting instanton three-body contributions to strong decays, which could contribute to the ηN channel specifically. In this respect, however, we note that the theoretical $N[\frac{1}{2}^-]_0(1441)$ state, which corresponds to the experimental $N[\frac{1}{2}^-](1535)$, lies below the theoretical ηN threshold ($\omega_{\rm thr}^{\eta N} = 1448$ MeV, *c.f.* Table 2.3 and Eq. (2.128)) and in any case would not couple to this channel in the present framework.

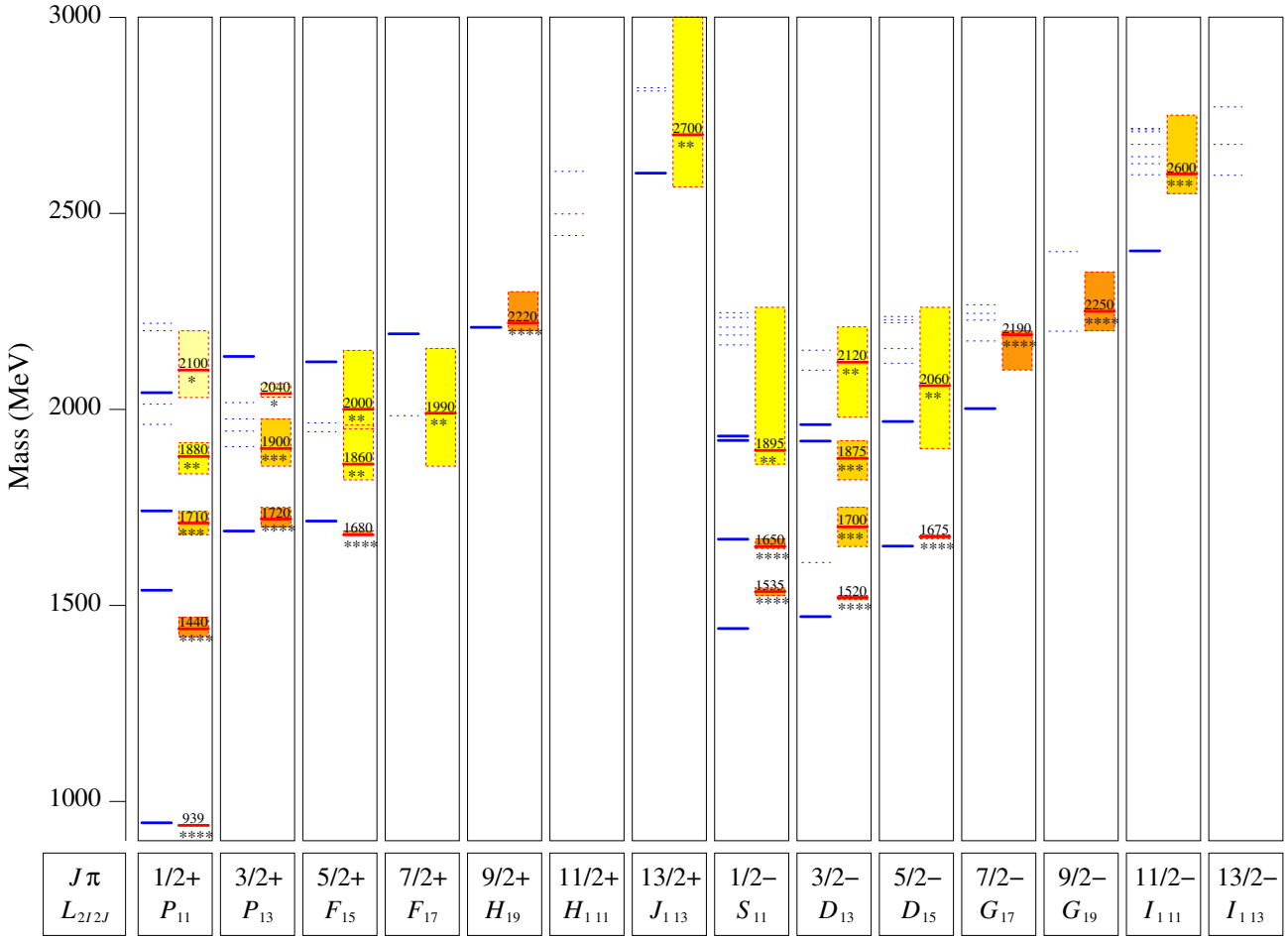

Figure 3.2. The calculated N spectrum (on the left of each column) in comparison to the experimental data from the Particle Data Group [2] (on the right). Dotted lines indicate that the calculated πN-decay width of the resonance vanishes, whereas solid lines represent those states for which the calculated width is finite and for most states at least in qualitative agreement with the experimental value. The classification scheme of the theoretical states according to their πN-decay widths is based on the results and notation of Ref. [39].

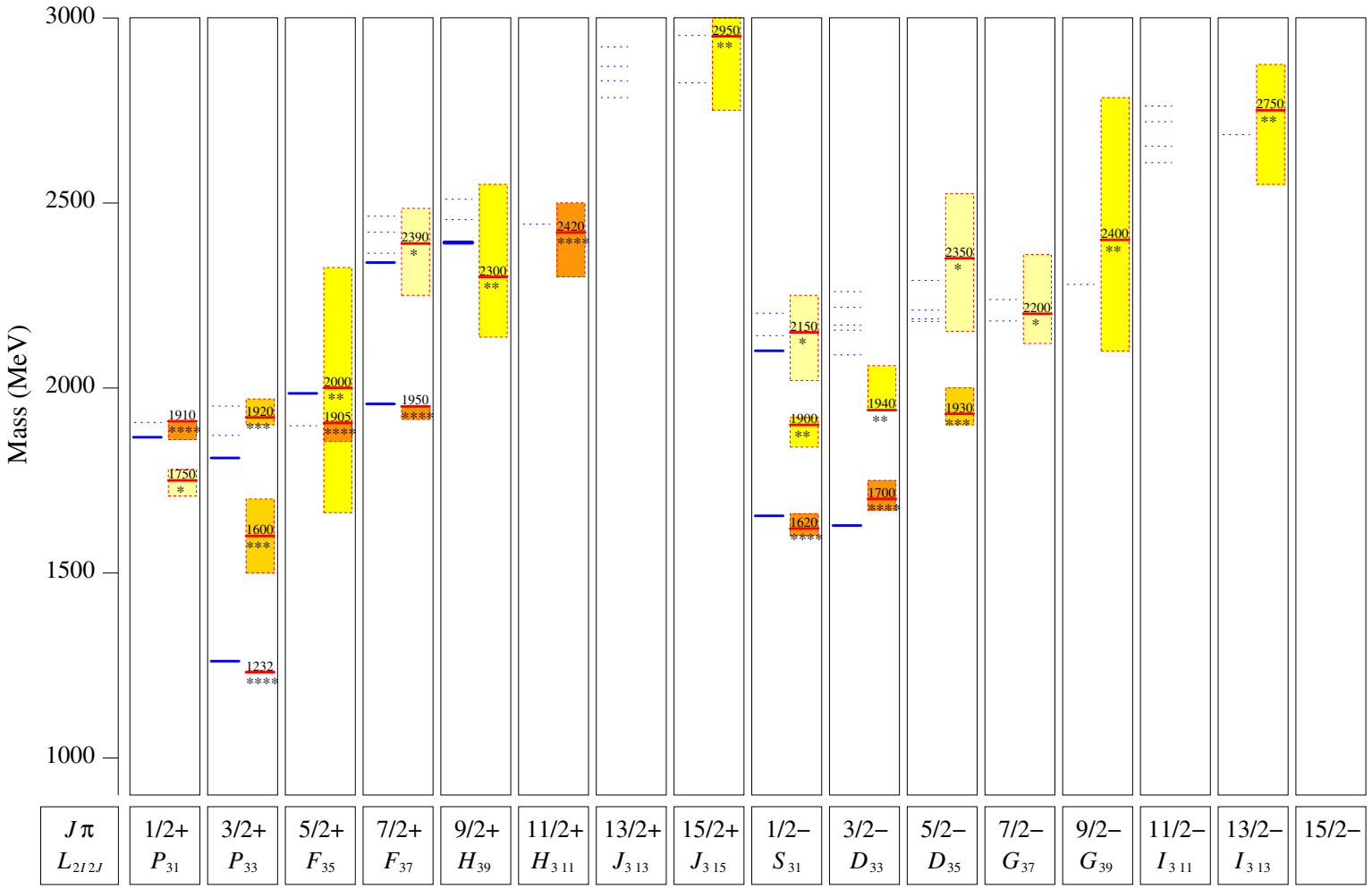

Figure 3.3. The calculated Δ spectrum (on the left part of each column) in comparison to the experimental data from the Particle Data Group [2] (on the right). The notation is the same as in Fig. 3.2.

Table 3.1. Strong decay widths of low-lying N and Δ baryons into πN, $\pi\Delta$ and ηN. The quark-model predictions (Q.M.) are compared to the estimates from the Particle Data Group [2] (PDG). A long dash (—) indicates that the decay is kinematically forbidden. The theoretical values below slightly differ from those of Ref. [39] due to a different dimension of the basis used to solve the Bethe-Salpeter equation for the initial and final baryon states.

$L_{2I\,2J}$	J^π	Label	$\Gamma_{\pi N}$ (MeV)		$\Gamma_{\pi\Delta}$ (MeV)		$\Gamma_{\eta N}$ (MeV)	
			Q.M.	PDG	Q.M.	PDG	Q.M.	PDG
S_{11}	$\frac{1}{2}^-$	$N(1535)$	32	44 – 97	0	0 – 2	—	40 – 91
		$N(1650)$	3	60 – 162	5	0 – 45	0	6 – 27
P_{11}	$\frac{1}{2}^+$	$N(1440)$	38	110 – 338	33	40 – 135	0	0 – 5
		$N(1710)$	5	3 – 50	44	8 – 100	4	5 – 75
P_{13}	$\frac{3}{2}^+$	$N(1720)$	14	12 – 56	2	90 – 360	0	5 – 20
D_{13}	$\frac{3}{2}^-$	$N(1520)$	35	55 – 81	58	15 – 31	0	0
		$N(1700)$	0	7 – 43	104	10 – 225, S-wave < 50, D-wave	1	0 – 3
D_{15}	$\frac{5}{2}^-$	$N(1675)$	3	46 – 74	35	65 – 99	6	0 – 2
F_{15}	$\frac{5}{2}^+$	$N(1680)$	35	78 – 98	5	6 – 21	3	0 – 1
S_{31}	$\frac{1}{2}^-$	$\Delta(1620)$	4	26 – 45	73	39 – 90	isospin violation	
P_{33}	$\frac{3}{2}^+$	$\Delta(1232)$	63	114 – 120	—	—		
		$\Delta(1600)$	15	22 – 105	3	88 – 294		
D_{33}	$\frac{3}{2}^-$	$\Delta(1700)$	2	20 – 80	53	60 – 240		

Chapter 4

Baryon resonances in scattering theory

4.1 Introduction

In the model of Chapter 2 baryon resonances were described as relativistic bound states of three constituent quarks, whose masses correspond to simple poles of the six-point Green's function in the total energy variable of the three-fermion system. Theoretical masses defined this way were compared to experimental estimates for Breit-Wigner masses, providing a good description of the light-baryon spectrum. So far, however, we have not discussed the relation between poles of the six-point Green's function and Breit-Wigner masses at all: As we shall eventually see in this chapter, both mass parameters are only equivalent if non-resonant contributions to baryon properties are completely neglected, which is the case in our constituent quark model.

Subsequently, in Chapter 3 the same framework was used in the description of strong two-body decays of baryons. The corresponding decay widths were evaluated in lowest order of perturbation theory, thus disregarding (non-resonant) rescattering effects as well, with the same parameter set fitted to hadronic spectra. Unfortunately, in contrast to the good results for baryon masses, the theoretical strong decay widths turn out to be too small in comparison to data, suggesting that non-resonant contributions possibly lead to sizable corrections in strong decays. In view of this situation, the question arises how to include final state rescattering in strong decays and, at the same time, still have a meaningful interpretation of the baryon masses calculated in the approach.

Ultimately the properties of baryon resonances such as masses and strong decay widths should be inferred from a genuine description based on the fundamental principles of scattering theory. According to this latter, unstable hadrons are related to simple poles appearing in unphysical Riemann sheets of analytic hadronic amplitudes, which respect at least two-body unitarity and, while describing strong interacting systems in processes with an appreciable momentum transfer, full Poincaré invariance as well. Breit-Wigner masses and widths in turn are only defined from the analytic behavior of the amplitudes in the vicinity of these poles. That said, it is clear that a study of scattering at the hadronic level provides both a framework to include final

state interactions consistently and, in the presence of these, the correct interpretation of the baryon masses as defined in the quark model.

The aim of this chapter is therefore to review some aspects of scattering theory applied to the case of meson-baryon systems, and thereby investigate how baryon properties emerge from this context. In addition, the contents below provide the basic formulae for Chapters 5 and 6, where we implement a hadronic coupled-channel model for πN, $\pi\Delta$ and ηN scattering and then account for final state interactions in the decays into these channels. To introduce the notation and the normalization, we start Section 4.2 with an overview of two-body kinematics and relativistic amplitudes. Furthermore, based on the helicity formalism of Jacob and Wick [64], we present the implications of Poincaré invariance for meson-baryon systems, which in particular leads to partial-wave expansions for the transition amplitudes. After this, we finish Section 4.2 with some additional constraints imposed by unitarity.

As discussed in Chapter 2, the investigation of resonant states always demands the use of non-perturbative methods which iteratively generate an infinite sum of Feynman diagrams. We therefore introduce in Section 4.3 the fundamental scattering equation, *i.e.* the Bethe-Salpeter equation for a meson-baryon system, and explain the method and the approximations we employ here to solve it. We specifically consider the scattering equation in on-shell approximation, since all quark-model quantities are defined on the mass-shell, include lowest-order (tree-level) diagrams in the interaction kernel only, and finally introduce a commonly used decomposition into resonant and non-resonant terms in order to relate quark-model quantities and non-resonant hadronic contributions. For further discussion on the latter method, see for instance Ref. [65]. Based on such a decomposition of the scattering equation, we close this chapter in Section 4.4 with the interpretation of baryon properties as defined in the relativistic quark model and the relation of these quantities to meson-baryon amplitudes, finally establishing the method to account for final state interactions in strong baryon decays this way.

4.2 Meson-baryon relativistic amplitudes

In the following we consider the meson-baryon scattering process

$$M(p,\mu_1) + m(k,\mu_2) \longrightarrow M'(p',\mu_1') + m'(k',\mu_2'), \tag{4.1}$$

where M and m are the masses of the initial baryon and meson states,

$$p = \begin{pmatrix} \omega_p \\ \mathbf{p} \end{pmatrix} \qquad \text{with} \qquad \omega_p = \sqrt{M^2 + |\mathbf{p}|^2} \tag{4.2}$$

and

$$k = \begin{pmatrix} \omega_k \\ \mathbf{k} \end{pmatrix} \qquad \text{with} \qquad \omega_k = \sqrt{m^2 + |\mathbf{k}|^2} \tag{4.3}$$

denote the on-shell four-momenta of these hadrons, and primed variables refer to the same quantities for particles in the final state. The variables μ_i and μ_i' represent the helicity of the states, and for shortness we also introduce the initial and final helicity labels

$$\lambda := \mu_1 - \mu_2 \qquad \text{and} \qquad \lambda' := \mu_1' - \mu_2'. \tag{4.4}$$

In the notation above, the extension to coupled-channel scattering is as follows: It is then understood that λ and λ' label the charge states (or isospin) as well. For instance for the scattering investigated in Chapter 5 we would have

$$\lambda, \lambda' \in \left\{ (\pi N)_{\pm 1/2}\,, (\pi\Delta)_{\pm 1/2}\,, (\pi\Delta)_{\pm 3/2}\,, (\eta N)_{\pm 1/2} \right\}. \tag{4.5}$$

4.2.1 Kinematics in the center-of-mass frame

A natural reference system for two-body scattering is the center-of-mass frame, where

$$\mathbf{p} + \mathbf{k} = \mathbf{p}' + \mathbf{k}' = \mathbf{0} \tag{4.6}$$

and for the total four-momentum

$$P = p + k = p' + k' \equiv \begin{pmatrix} \omega \\ \mathbf{0} \end{pmatrix} \tag{4.7}$$

holds, where we introduced the total energy (or invariant mass)

$$\omega := \omega_p + \omega_k = \omega_{p'} + \omega_{k'}. \tag{4.8}$$

From the equations above one shows that in the center-of-mass frame the four-momenta of the initial particles can be written as

$$p = \begin{pmatrix} \omega_p \\ |\mathbf{p}| R(\Omega)\hat{e}_z \end{pmatrix} \qquad \text{and} \qquad k = \begin{pmatrix} \omega_k \\ -|\mathbf{p}| R(\Omega)\hat{e}_z \end{pmatrix}, \tag{4.9}$$

the on-shell energies as

$$\omega_p = \frac{\omega^2 + M^2 - m^2}{2\omega} \qquad \text{and} \qquad \omega_k = \frac{\omega^2 - M^2 + m^2}{2\omega} = \omega - \omega_p, \tag{4.10}$$

and finally the absolute value of the three-momenta as

$$|\mathbf{p}| = |\mathbf{k}| = \frac{1}{2\omega}\sqrt{\left[\omega^2 - (M+m)^2\right]\left[\omega^2 - (M-m)^2\right]}, \tag{4.11}$$

with similar relations for the primed variables. In our notation, $\Omega = (\theta, \phi)$ denotes the direction of $\mathbf{p}$, $\hat{e}_z$ is the unit vector in the z-direction and $R(\Omega) \in SO(3)$ is the rotation matrix which takes the z-axis into the direction of $\mathbf{p}$. In the phase convention of Jacob and Wick [64] the matrix $R(\Omega)$ is explicitly given by

$$R(\Omega) = R_z(\phi) R_y(\theta) R_z(-\phi), \tag{4.12}$$

where $R_i(\alpha)$ represents a rotation through angle α about the i-axis.

Finally, for practical calculations one usually chooses the coordinate system such that the initial three-momentum $\mathbf{p}$ is parallel to the z-axis, whereas the reaction plane coincides with the $y = 0$ plane. This is equivalent to the choice

$$\phi = \phi' \stackrel{!}{=} 0, \qquad \theta \stackrel{!}{=} 0 \qquad \text{and} \qquad \theta' \equiv \bar{\theta}, \tag{4.13}$$

where $\bar{\theta}$ is the scattering angle defined by

$$\hat{p} \cdot \hat{p}' =: \cos\bar{\theta}. \tag{4.14}$$

4.2.2 Scattering and transition amplitudes

The probability amplitude for the scattering reaction of Eq. (4.1) is given by the matrix element

$$S_{fi} := \langle f|S|i\rangle \tag{4.15}$$

of the **scattering operator $\boldsymbol{S}$** between the initial and final states

$$|i\rangle = |p\,,\mu_1\rangle \otimes |k\,,\mu_2\rangle \qquad \text{and} \qquad |f\rangle = |p',\mu_1'\rangle \otimes |k',\mu_2'\rangle. \tag{4.16}$$

For coupled-channel scattering and processes involving particles with spin, S is defined by its matrix elements between all possible initial and final states and in this form is called the S-matrix. In order to separate the trivial contribution to the amplitude S_{fi} where no interaction takes place, we also introduce the **transition operator $\boldsymbol{T}$**, defined by its matrix elements

$$T_{fi} := \langle f|T|i\rangle \tag{4.17}$$

and related to S by

$$S = I + iT, \tag{4.18}$$

where I represents the identity operator.

Now, one should note that the two-body states defined in Eq. (4.16) correspond to asymptotic, non-interacting momentum eigenstates, whose normalization

$$\langle f|i\rangle = 4\omega_p\omega_k(2\pi)^6\delta^{(3)}\left(\mathbf{p}'-\mathbf{p}\right)\delta^{(3)}\left(\mathbf{k}'-\mathbf{k}\right)\delta_{\lambda'\lambda} \tag{4.19}$$

follows from the normalization of single-particle momentum eigenstates, *cf.* Eq. (2.14). In the center-of-mass frame one may employ the variable transformation

$$\omega_p\omega_k\delta^{(3)}\left(\mathbf{p}'-\mathbf{p}\right)\delta^{(3)}\left(\mathbf{k}'-\mathbf{k}\right) = \frac{\omega}{\sqrt{|\mathbf{p}||\mathbf{p}'|}}\delta^{(4)}\left(P'-P\right)\delta^{(2)}\left(\Omega'-\Omega\right), \tag{4.20}$$

see *e.g.* Eq. (3.80) of Ref. [66], to show that (4.19) is equivalent to

$$\langle f|i\rangle = \frac{16\pi^2\omega}{\sqrt{|\mathbf{p}||\mathbf{p}'|}}(2\pi)^4\delta^{(4)}\left(P'-P\right)\delta^{(2)}\left(\Omega'-\Omega\right)\delta_{\lambda'\lambda}. \tag{4.21}$$

Consequently, the initial and final two-body states can be denoted as

$$|i\rangle = 4\pi\sqrt{\frac{\omega}{|\mathbf{p}\,|}}\,|P\,\rangle \otimes |\Omega\,,\lambda\,\rangle \qquad \text{and} \qquad |f\rangle = 4\pi\sqrt{\frac{\omega}{|\mathbf{p}'|}}\,|P'\rangle \otimes |\Omega',\lambda'\rangle, \tag{4.22}$$

where $|P\rangle$ are eigenstates of total four-momenta, normalized as

$$\langle P'|P\rangle = (2\pi)^4\delta^{(4)}(P'-P), \tag{4.23}$$

and $|\Omega,\lambda\rangle$ describe the full angular dependence and total helicity of the meson-baryon states. These latter are normalized according to

$$\langle\Omega',\lambda'|\Omega,\lambda\rangle = \delta^{(2)}(\Omega'-\Omega)\delta_{\lambda'\lambda}. \tag{4.24}$$

The representations in Eq. (4.22) are in fact the most appropriate for two-body states: Firstly, because the trivial dependence on total four-momentum factorizes, reducing the number of variables in the problem. Moreover, as we shall see in the next section, states $|\Omega,\lambda\rangle$ can be expanded in terms of angular momentum eigenstates, allowing for partial-wave analyses of the transition amplitudes.

4.2.3 Invariance under Poincaré transformations

Due to the symmetries fulfilled by strong interactions the various amplitudes related to coupled-channel scattering are not mutually independent but constrained by invariance properties. Some of these properties result from the fact that probability cannot depend on the choice of reference frame and are therefore common to all interactions observed in nature. These include invariance under translations and (proper) Lorentz transformations, where the latter include both Lorentz boosts and rotations. In the particular case of strong interactions all the symmetries of the full Poincaré group are respected, *i.e.* including parity and time-reversal transformations as well. Since the application of invariance principles greatly reduces the number of amplitudes necessary to describe the full scattering matrix, in this section we investigate the implications of Poincaré invariance for meson-baryon systems.

Translational invariance

As a consequence of translational invariance the scattering and transition operators commute with the total four-momentum operator, *i.e.*

$$[S, P] = [T, P] = 0. \tag{4.25}$$

For this reason, it is customary to introduce the **invariant transition amplitudes** $\boldsymbol{T_{\lambda'\lambda}}$, which are related to T_{fi} according to

$$T_{fi} =: (2\pi)^4 \delta^{(4)}(P' - P) T_{\lambda'\lambda}\left(p', p\right). \tag{4.26}$$

In the center-of-mass frame an explicit expression for $T_{\lambda'\lambda}$ may be derived by inserting the representations (4.22) for the states $|i\rangle$ and $|f\rangle$ into the definition (4.17) for T_{fi}, and then applying the invariance property (4.25). This procedure leads to

$$T_{\lambda'\lambda}\left(p', p\right)\Big|_{P=(\omega,\mathbf{0})} \equiv T_{\lambda'\lambda}\left(\omega, \Omega', \Omega\right) = \frac{16\pi^2\omega}{\sqrt{|\mathbf{p}||\mathbf{p}'|}} \langle \Omega', \lambda' | T(\omega) | \Omega, \lambda \rangle, \tag{4.27}$$

where we employed the normalization (4.23) of the states $|P\rangle$ and the fact that $|\mathbf{p}|$ and $|\mathbf{p}'|$ are merely functions of ω, see Eq. (4.11).

Invariance under (proper) Lorentz transformations

Lorentz invariance implies that scattering and transition amplitudes depend on Lorentz scalars only. Hence, apart from tensorial products related to the internal quantum numbers of scattering particles (see *e.g.* Eqs. (5.1), (5.2) and (5.3)), all other functions describing the amplitudes should depend on scalar combinations of the four-momenta involved in the process. Due to four-momentum conservation and the mass-shell condition of scattering states, there are only two possible independent scalar combinations in two-body scattering. These are commonly chosen among the Mandelstam variables

$$s = \left(p + k\right)^2, \qquad t = \left(p - p'\right)^2 \qquad \text{and} \qquad u = \left(p - k'\right)^2 \tag{4.28}$$

which are related by

$$s + t + u = M^2 + M'^2 + m^2 + m'^2. \tag{4.29}$$

Now, due to Eqs. (4.28) and (4.29), the kinematic variables in any reference system can always be expressed in terms of Mandelstam invariants. This allows us to choose a particular reference frame to evaluate the amplitudes $T_{\lambda'\lambda}$ and further investigate their invariance properties. For the sake of simplicity we choose the center-of-mass frame, where the Mandelstam variable s is related to the total energy of the system by

$$s = \omega^2 \tag{4.30}$$

while the other two variables can be written as

$$t = M^2 + M'^2 - 2\omega_p\omega_{p'} + 2|\mathbf{p}||\mathbf{p}'|\cos\bar{\theta} \tag{4.31}$$

and

$$u = m^2 + m'^2 - s + 2\omega_p\omega_{p'} - 2|\mathbf{p}||\mathbf{p}'|\cos\bar{\theta}, \tag{4.32}$$

according to the kinematics defined in Section 4.2.1.

Rotational invariance

The spherical states $|\Omega,\lambda\rangle$ appearing in Eq. (4.27) describe the angular dependence and total helicity of meson-baryon systems. As such, these states cannot be angular momentum eigenstates, but admit any total angular momentum $\mathbf{J} = (J_x, J_y, J_z)$ in the range

$$|\mathbf{j}_1 - \mathbf{j}_2| \leq |\mathbf{J}| \leq |\mathbf{j}_1 + \mathbf{j}_2| \tag{4.33}$$

defined by the total angular momenta $\mathbf{j}_1$ and $\mathbf{j}_2$ of the single baryon and meson states. Nevertheless, due to the property (4.33) we can expand $|\Omega,\lambda\rangle$ in terms of a complete set of angular momentum eigenstates

$$|JM_J,\lambda\rangle, \tag{4.34}$$

which are defined by the properties

$$\begin{aligned} J^2|JM_J,\lambda\rangle &= J(J+1)|JM_J,\lambda\rangle \\ J_z|JM_J,\lambda\rangle &= M_J|JM_J,\lambda\rangle \end{aligned} \tag{4.35}$$

and normalized as

$$\langle J'M'_J,\lambda|JM_J,\lambda\rangle = \delta_{J'J}\delta_{M'_JM_J}. \tag{4.36}$$

Because the normalization of $|\Omega,\lambda\rangle$ and $|JM_J,\lambda\rangle$ is given by Eqs. (4.24) and (4.36) respectively, as shown in Ref. [66] this expansion reads:

$$|\Omega,\lambda\rangle = \sum_{J,M_J}\sqrt{\frac{2J+1}{4\pi}}\,D^J_{M_J\lambda}(\phi,\theta,-\phi)|JM_J,\lambda\rangle, \tag{4.37}$$

where

$$\begin{aligned} D^J_{M'_JM_J}(\alpha,\beta,\gamma) :=&\ \langle JM'_J,\lambda'|R(\alpha,\beta,\gamma)|JM_J,\lambda\rangle \\ =&\ e^{-iM'_J\alpha}\langle JM'_J,\lambda'|e^{-i\beta J_y}|JM_J,\lambda\rangle(\beta)e^{-iM_J\gamma} \\ =:&\ e^{-iM'_J\alpha}d^J_{M'_JM_J}(\beta)e^{-iM_J\gamma} \end{aligned} \tag{4.38}$$

denote the usual Wigner rotation matrices.

Using the expansion in Eq. (4.37) we are now able to investigate the consequences of rotational invariance, *i.e.*

$$[S, \mathbf{J}] = [T, \mathbf{J}] = 0, \tag{4.39}$$

for the invariant amplitudes $T_{\lambda'\lambda}$. For this we replace the states $|\Omega, \lambda\rangle$ appearing in (4.27) by the corresponding partial-wave expansions as in (4.37), which leads to

$$\begin{aligned} T_{\lambda'\lambda}\left(\omega, \Omega', \Omega\right) = \frac{16\pi^2\omega}{\sqrt{|\mathbf{p}||\mathbf{p}'|}} \sum_{J', M'_J} \sqrt{\frac{2J'+1}{4\pi}} \sum_{J, M_J} \sqrt{\frac{2J+1}{4\pi}} \\ \times D^{J'*}_{M'_J\lambda'}(\phi', \theta', -\phi') D^{J}_{M_J\lambda}(\phi, \theta, -\phi) \langle J'M'_J, \lambda'|T(\omega)|JM_J, \lambda\rangle, \end{aligned} \tag{4.40}$$

and then apply the properties (4.35), (4.36) and (4.39) to show that

$$T_{\lambda'\lambda}\left(\omega, \Omega', \Omega\right) = \sum_{J, M_J} (2J+1)\, D^{J*}_{M_J\lambda'}(\phi', \theta', -\phi') D^{J}_{M_J\lambda}(\phi, \theta, -\phi) T^J_{\lambda'\lambda}(\omega), \tag{4.41}$$

where we defined the **partial-wave amplitudes**

$$T^J_{\lambda'\lambda}(\omega) := \frac{4\pi\omega}{\sqrt{|\mathbf{p}||\mathbf{p}'|}} \langle JM_J, \lambda'|T(\omega)|JM_J, \lambda\rangle \equiv \frac{4\pi\omega}{\sqrt{|\mathbf{p}||\mathbf{p}'|}} \langle \lambda'|T^J(\omega)|\lambda\rangle. \tag{4.42}$$

Finally, to simplify the treatment of Eq. (4.41), we choose the coordinate system as in Eq. (4.13) such that

$$T_{\lambda'\lambda}\left(\omega, \bar{\theta}\right) = \sum_{J} (2J+1)\, d^J_{\lambda\lambda'}(\bar{\theta})\, T^J_{\lambda'\lambda}(\omega), \tag{4.43}$$

where we employed the definition (4.38), the fact that Wigner d-functions are real and also the property

$$d^J_{M'_J M_J}(0) = \delta_{M'_J M_J}. \tag{4.44}$$

Time-reversal and parity symmetries

As shown in Ref. [66] the angular momentum states $|JM_J, \lambda\rangle$ introduced in (4.34) transform under the time-reversal operator τ and the parity operator π as

$$\tau|JM_J, \lambda\rangle = (-1)^{J-M_J}|J - M_J, \lambda\rangle \tag{4.45}$$

and

$$\pi|JM_J, \lambda\rangle = \eta_1\eta_2(-1)^{J-j_1-j_2}|JM_J, -\lambda\rangle, \tag{4.46}$$

respectively, where η_1 and η_2 represent the intrinsic parities of the baryon and meson belonging to the state $|JM_J, \lambda\rangle$. Hence, from the invariance properties

$$\begin{aligned} S &= \tau^\dagger S^\dagger \tau, \\ T &= \tau^\dagger T^\dagger \tau \end{aligned} \tag{4.47}$$

and

$$[S, \pi] = [T, \pi] = 0, \tag{4.48}$$

where the former result from the anti-unitarity of τ, the following symmetry properties for the matrix elements appearing in Eq. (4.42) hold:

$$\begin{aligned}\langle\lambda'|T^J(\omega)|\lambda\rangle &\equiv \langle JM_J,\lambda'|\tau^\dagger T^\dagger\tau|JM_J,\lambda\rangle \\ &= \langle JM_J,\lambda|\tau^\dagger T\tau|JM_J,\lambda'\rangle \\ &= (-1)^{J-M_J}(-1)^{J-M_J}\langle J-M_J,\lambda|T|J-M_J,\lambda'\rangle \\ &\equiv \langle\lambda|T^J(\omega)|\lambda'\rangle\end{aligned} \tag{4.49}$$

and

$$\begin{aligned}\langle\lambda'|T^J(\omega)|\lambda\rangle &\equiv \langle JM_J,\lambda'|\pi^\dagger T\pi|JM_J,\lambda\rangle \\ &= \eta_1'\eta_2'\eta_1\eta_2(-1)^{j_1'+j_2'-j_1-j_2}\langle JM_J,-\lambda'|T|JM_J,-\lambda\rangle \\ &\equiv \eta_1'\eta_2'\eta_1\eta_2(-1)^{j_1'+j_2'-j_1-j_2}\langle-\lambda'|T^J(\omega)|-\lambda\rangle.\end{aligned} \tag{4.50}$$

Accordingly, we have

$$T^J_{\lambda'\lambda}(\omega) = T^J_{\lambda\lambda'}(\omega) \tag{4.51}$$

and

$$T^J_{\lambda'\lambda}(\omega) = \eta_1'\eta_2'\eta_1\eta_2(-1)^{j_1'+j_2'-j_1-j_2}T^J_{-\lambda'-\lambda}(\omega) \tag{4.52}$$

for the partial-wave amplitudes $T^J_{\lambda'\lambda}$.

The first of these equations implies that a time-reversal invariant matrix T^J should be symmetric, whereas the second shows that parity conservation reduces the number of independent amplitudes by a factor of two, since λ and λ' are necessarily half-integers in the case of meson-baryon states. A further consequence of (4.52) is however that the partial-waves defined in Eq. (4.42) do not conserve parity, and are therefore not a suitable choice to represent hadronic scattering. Following Ref. [67] we thus introduce the linear combinations

$$|JM_J,\lambda\pm\rangle := \sqrt{\frac{1}{2}}\,[\,|JM_J,\lambda\rangle \pm \eta|JM_J,-\lambda\rangle\,] \tag{4.53}$$

with

$$\eta := \eta_1\eta_2(-1)^{j_1+j_2+\frac{1}{2}}, \tag{4.54}$$

which transform as $|JM_J,\lambda\rangle$ under time-reversal operations but according to

$$\pi|JM_J,\lambda\pm\rangle = (-1)^{J\pm\frac{1}{2}}|JM_J,\lambda\pm\rangle \tag{4.55}$$

under parity. Hence, in terms of these new basis states, we define the **parity-invariant partial-wave amplitudes**

$$T^{J\pm}_{\lambda'\lambda}(\omega) := \frac{4\pi\omega}{\sqrt{|\mathbf{p}||\mathbf{p}'|}}\langle JM_J,\lambda'\pm|T(\omega)|JM_J,\lambda\pm\rangle \equiv \frac{4\pi\omega}{\sqrt{|\mathbf{p}||\mathbf{p}'|}}\langle\lambda'\pm|T^J(\omega)|\lambda\pm\rangle \tag{4.56}$$

which now have definite parity $\pi = (-1)^{J\pm\frac{1}{2}}$.

Finally, we close this section with some useful symmetry relations applicable to the amplitudes $T^{J\pm}_{\lambda'\lambda}$. Firstly from the definition (4.54), we rewrite Eq. (4.52) as

$$T^J_{\lambda'\lambda} = \eta'\eta T^J_{-\lambda'-\lambda}. \tag{4.57}$$

Furthermore, from Eqs. (4.53) and (4.57), we show that the amplitudes $T^{J}_{\lambda'\lambda}$ and $T^{J\pm}_{\lambda'\lambda}$ are related by

$$\begin{aligned} T^{J\pm}_{\lambda'\lambda} &= \frac{1}{2}\left[T^{J}_{\lambda'\lambda} \pm \eta' T^{J}_{-\lambda'\lambda} \pm \eta T^{J}_{\lambda'-\lambda} + \eta'\eta T^{J}_{-\lambda'-\lambda}\right] \\ &= \frac{1}{2}\left[T^{J}_{\lambda'\lambda} \pm \eta T^{J}_{\lambda'-\lambda} \pm \eta T^{J}_{\lambda'-\lambda} + T^{J}_{\lambda'\lambda}\right] = T^{J}_{\lambda'\lambda} \pm \eta T^{J}_{\lambda'-\lambda}. \end{aligned} \tag{4.58}$$

Then, from Eqs. (4.57) and (4.58), we derive the parity invariance condition

$$\begin{aligned} T^{J\pm}_{\lambda'\lambda} &= T^{J}_{\lambda'\lambda} \pm \eta T^{J}_{\lambda'-\lambda} \\ &= \eta'\eta T^{J}_{-\lambda'-\lambda} \pm \eta' T^{J}_{-\lambda'\lambda} \\ &= \pm\eta'\left[T^{J}_{-\lambda'\lambda} \pm \eta T^{J}_{-\lambda'-\lambda}\right] = \pm\eta' T^{J\pm}_{-\lambda'\lambda}, \end{aligned} \tag{4.59}$$

which constraints the number of independent amplitudes $T^{J\pm}_{\lambda'\lambda}$. According to (4.51), (4.57) and (4.58), we also see that

$$\begin{aligned} T^{J\pm}_{\lambda'\lambda} &= T^{J\pm}_{\lambda'\lambda} \pm \eta\, T^{J\pm}_{\lambda'-\lambda} \\ &= T^{J\pm}_{\lambda\lambda'} \pm \eta\, T^{J\pm}_{-\lambda\lambda'} \\ &= T^{J\pm}_{\lambda\lambda'} \pm \eta' T^{J\pm}_{\lambda-\lambda'} = T^{J\pm}_{\lambda\lambda'}, \end{aligned} \tag{4.60}$$

and thus the time-reversal invariance condition for the amplitudes $T^{J\pm}_{\lambda'\lambda}$ reads the same as for $T^{J}_{\lambda'\lambda}$.

Partial-wave helicity amplitudes

In hadronic models one usually employs effective Lagrangians to determine invariant amplitudes $T_{\lambda'\lambda}$, see for instance the model implemented in Chapter 5. However, since baryons have definite spin and parity, the properties of a specific baryon state should emerge from the partial-wave amplitude $T^{J\pm}_{\lambda'\lambda}$ with the same quantum numbers as the resonance. Accordingly, for partial-wave analyses it is often necessary to calculate $T^{J\pm}_{\lambda'\lambda}$ in terms of $T_{\lambda'\lambda}$. In the helicity formalism employed here this is done by first applying the orthogonality relation

$$\int_{-1}^{1} \mathrm{d}(\cos\beta)\, d^{J}_{\lambda\lambda'}(\beta)\, d^{J'}_{\lambda\lambda'}(\beta) = \frac{2}{2J+1}\delta_{JJ'} \tag{4.61}$$

of the Wigner d-functions [68] to invert Eq. (4.43), leading to

$$T^{J}_{\lambda'\lambda}(\omega) = \frac{1}{2}\int_{-1}^{1} \mathrm{d}(\cos\bar{\theta})\, d^{J}_{\lambda\lambda'}(\bar{\theta}) T_{\lambda'\lambda}(p', p), \tag{4.62}$$

and then substituting Eq. (4.62) into (4.58). In this way it immediately follows that

$$T^{J\pm}_{\lambda'\lambda}(\omega) = \frac{1}{2}\int_{-1}^{1} \mathrm{d}(\cos\bar{\theta})\left[d^{J}_{\lambda\lambda'}(\bar{\theta}) T_{\lambda'\lambda}(\omega,\bar{\theta}) \pm \eta\, d^{J}_{-\lambda\lambda'}(\bar{\theta}) T_{\lambda'-\lambda}(\omega,\bar{\theta})\right], \tag{4.63}$$

with η previously defined in Eq. (4.54).

4.2.4 Unitarity condition for partial-waves

For interactions characterized by a sufficiently small strength the transition amplitudes may be determined by a sum of Feynman diagrams. However, meson-baryon scattering in the low-energy region is characterized by residual strong forces which might even generate resonances, requiring the application of non-perturbative methods. In this sense, general scattering theory principles are of particular relevance for strong interactions.

The very first of these principles is probability conservation, which implies that the scattering operator S is unitary, *i.e.*

$$SS^\dagger = S^\dagger S = I. \tag{4.64}$$

For the transition operator T, the condition above reads

$$(T - T^\dagger) = iT^\dagger T, \tag{4.65}$$

where we used relation (4.18) between S and T. Now, since baryon properties emerge from partial-waves which conserve parity, we shall derive the unitarity condition (4.65) directly for amplitudes $T^{J\pm}_{\lambda'\lambda}$.

For this purpose we first consider a complete set of meson-baryon states normalized as in (4.21), *i.e.*

$$1 = \sum_{\lambda_n} \frac{|\mathbf{p}_n|}{16\pi^2\omega} \int \frac{\mathrm{d}^4 P_n}{(2\pi)^4} \int \mathrm{d}^2\,\Omega_n |n\rangle\langle n|, \tag{4.66}$$

between the product on the right-hand side of (4.65), and then evaluate both sides of this equation between the initial and final states $|i\rangle$ and $|f\rangle$. In this way,

$$T_{\lambda'\lambda}(p',p) - T^*_{\lambda\lambda'}(p,p') = i \sum_{\lambda_n} \frac{|\mathbf{p}_n|}{16\pi^2\omega} \int \mathrm{d}^2\,\Omega_n T^*_{\lambda_n\lambda'}(p_n,p') T_{\lambda_n\lambda}(p_n,p), \tag{4.67}$$

where we also used Eq. (4.26) to identify the invariant amplitudes $T_{\lambda'\lambda}$. The next step is to decompose Eq. (4.67) in terms of partial-wave amplitudes; however, before doing this we note that the simplified expansion (4.43) cannot be used here since the three-momenta $\mathbf{p}_n$, $\mathbf{p}$ and $\mathbf{p}'$ are not necessarily coplanar. We therefore use the most general expansion (4.41), together with the orthogonality relation

$$\int \mathrm{d}^2\,\Omega\, D^{J*}_{M_J\lambda_n}(\phi,\theta,-\phi)\, D^{J'}_{M'_J\lambda_n}(\phi,\theta,-\phi) = \frac{4\pi}{2J+1}\delta_{M_J M'_J}\delta_{JJ'} \tag{4.68}$$

of the Wigner rotation matrices [68], to rewrite (4.67) as

$$T^J_{\lambda'\lambda}(\omega) - T^{J*}_{\lambda\lambda'}(\omega) = i \sum_{\lambda_n} 2\rho_{nn}(\omega) T^{J*}_{\lambda_n\lambda'}(\omega) T^J_{\lambda_n\lambda}(\omega), \tag{4.69}$$

where we defined the phase-space matrix ρ by its elements

$$\rho_{ab}(\omega) := \frac{\sqrt{|\mathbf{p}_a||\mathbf{p}_b|}}{8\pi\omega}\delta_{ab}. \tag{4.70}$$

Finally, an analogous expression for the amplitudes $T^{J\pm}_{\lambda'\lambda}$ can now be derived from Eq. (4.69) and the properties (4.57), (4.58) and (4.59) as follows:

$$
\begin{aligned}
T^{J\pm}_{\lambda'\lambda}(\omega) - & T^{J\pm *}_{\lambda\lambda'}(\omega) \\
&\overset{(4.58)}{=} \left[T^{J}_{\lambda'\lambda} \pm \eta T^{J}_{\lambda'-\lambda}\right] - \left[T^{J*}_{\lambda\lambda'} \pm \eta' T^{J*}_{\lambda-\lambda'}\right] \\
&\overset{(4.57)}{=} \left[T^{J}_{\lambda'\lambda} - T^{J*}_{\lambda\lambda'}\right] \pm \eta \left[T^{J}_{\lambda'-\lambda} - T^{J*}_{-\lambda\lambda'}\right] \\
&\overset{(4.69)}{=} i \sum_{\lambda_n} 2\rho_{nn} \left\{T^{J*}_{\lambda_n\lambda'} T^{J}_{\lambda_n\lambda} \pm \eta T^{J*}_{\lambda_n\lambda'} T^{J}_{\lambda_n-\lambda}\right\} \\
&\overset{(4.58)}{=} i \sum_{\lambda_n} 2\rho_{nn}\, T^{J*}_{\lambda_n\lambda'} T^{J\pm}_{\lambda_n\lambda} \\
&\equiv\ i \sum_{\lambda_n>0} 2\rho_{nn} \left\{T^{J*}_{-\lambda_n\lambda'} T^{J\pm}_{-\lambda_n\lambda} + T^{J*}_{\lambda_n\lambda'} T^{J\pm}_{\lambda_n\lambda}\right\} \\
&\overset{(4.57)}{=} i \sum_{\lambda_n>0} 2\rho_{nn} \left\{\eta_n\eta' T^{J*}_{\lambda_n-\lambda'} T^{J\pm}_{-\lambda_n\lambda} + T^{J*}_{\lambda_n\lambda'} T^{J\pm}_{\lambda_n\lambda}\right\} \\
&\overset{(4.59)}{=} i \sum_{\lambda_n>0} 2\rho_{nn} \left\{\pm\eta' T^{J*}_{\lambda_n-\lambda'} T^{J\pm}_{\lambda_n\lambda} + T^{J*}_{\lambda_n\lambda'} T^{J\pm}_{\lambda_n\lambda}\right\} \\
&\overset{(4.58)}{=} i \sum_{\lambda_n>0} 2\rho_{nn}(\omega) T^{J\pm *}_{\lambda_n\lambda'}(\omega) T^{J\pm}_{\lambda_n\lambda}(\omega).
\end{aligned}
\tag{4.71}
$$

The unitarity condition in Eq. (4.71) for partial-wave transition amplitudes may be written in a suitable matrix form by exploiting parity and time-reversal invariance once more. Because parity conservation reduces the number of independent amplitudes by half, in Eq. (4.71) it is sufficient to consider positive-parity initial and final states only, thus $\lambda, \lambda' > 0$ just as $\lambda_n > 0$. In addition, we recall from Eq. (4.60) that time-reversal invariance requires the matrix $T^{J\pm}$ to be symmetric. In agreement with these two properties the unitarity condition (4.71) finally reads:

$$
\frac{1}{2i}\left[(T^{J\pm}) - (T^{J\pm})^\dagger\right] \equiv \mathrm{Im}\left[T^{J\pm}\right] = (T^{J\pm})^\dagger \rho (T^{J\pm}) \ , \tag{4.72}
$$

or, equivalently,

$$
\mathrm{Im}\left[(T^{J\pm})^{-1}\right] = -\rho. \tag{4.73}
$$

The important result in (4.73) shows that the imaginary part of $(T^{J\pm})^{-1}$ is fixed by unitarity and depends on kinematic variables only. Consequently all the dynamics involved in the process should be contained in the real part. The latter is related to the imaginary part through dispersion relations resulting from the analytical properties of the transition amplitudes and is, therefore, determined up to a subtraction constant which is model dependent. In this work we shall not discuss analytical properties of the amplitudes directly; see for instance the textbook [66] for details on the subject. Instead, in Section 4.3 we show how the unitarity condition (4.73) emerges from scattering equations.

4.3 Meson-baryon scattering equations

In the literature several methods to implement unitarity in hadronic scattering have been suggested, for instance the N/D method [18, 19], the inverse amplitude method [69], or also approaches based on the coupled-channel Lippmann-Schwinger [70] and Bethe-Salpeter equations [71]. In the following we adopt the latter, where two-body unitarity in meson-baryon scattering is implemented by means of the integral equation

$$M_{fi}(p',p) = M^{\text{irr}}_{fi}(p',p) + i\sum_n \int \frac{\mathrm{d}^4 p_n}{(2\pi)^4} M^{\text{irr}}_{fn}(p',p_n) G_n(p_n) M_{ni}(p_n,p) \tag{4.74}$$

as represented in the diagram of Fig. 4.1. The summation above includes all possible meson-baryon states with relative four-momentum p_n which couple to both initial and final scattering states. Moreover, for all the matrices M, M^{irr} and G a parametric dependence on the total four-momentum variable P should be understood. The Feynman propagator or Green's function of an intermediate state n is here denoted by G_n, while M represents an operator in spin space which evaluated on a basis of spinors gives the corresponding transition amplitudes. Omitting Lorentz indices related to possible higher-spin fields we have

$$G_n(p_n) := S_n(p_n)\Delta_n(P - p_n) \tag{4.75}$$

where S_n and Δ_n denote the *full* propagators of the intermediate baryon and meson states, respectively, and

$$T_{\lambda'\lambda}(p',p) =: \bar{u}_{\lambda'}(p') M(p',p) u_\lambda(p) \tag{4.76}$$

where u and $\bar{u}$ denote spinors for arbitrary spin. Finally, in the scattering equation (4.74) M^{irr} stands for the meson-baryon irreducible interaction kernel which, similarly to the kernels introduced in Chapter 2, is given by the sum of all contributions to M which cannot be split into two simpler diagrams by cutting a meson and a baryon line. We accordingly define the matrix elements

$$V_{\lambda'\lambda}(p',p) := \bar{u}_{\lambda'}(p') M^{\text{irr}}(p',p) u_\lambda(p), \tag{4.77}$$

now of a meson-baryon potential V, which comprise all irreducible contributions to the transition amplitudes $T_{\lambda'\lambda}$.

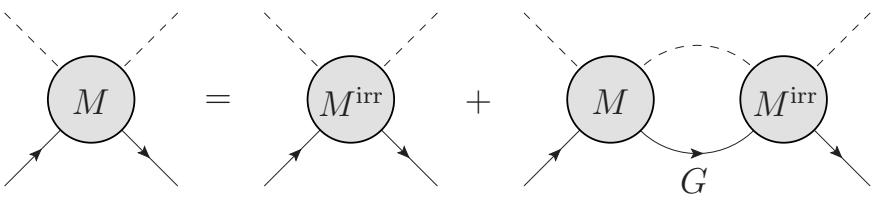

Figure 4.1. The Bethe-Salpeter equation for a meson-baryon system. Full and dashed lines represent baryon and meson fields, respectively.

Analogously to the two- and three-body Bethe-Salpeter equations investigated in Chapter 2, applying Eq. (4.74) in the description of meson-baryon scattering requires the use of some simplifying approximations. In other words, here we also have to deal with the full dependence on the relative energy p_n^0 and have to find suitable parametrizations for the interaction kernel M^{irr} and the meson-baryon propagator G. Moreover, for practical calculations the sum over intermediate states has of course to be truncated to some finite set of contributions. In the following Sections 4.3.1 and 4.3.2 we discuss the approximations employed in this work.

4.3.1 The on-shell approximation

The main purpose of investigating meson-baryon scattering in this thesis is to account for final state interactions in strong two-body decays as calculated in the quark model. However, due to the approximations introduced in that framework, the off-shell behavior of hadronic amplitudes (*e.g.* the strong decay matrix elements in (3.20)) cannot be addressed at all: in fact, in that approach all matrix elements are determined from Salpeter amplitudes (or, equivalently, amputated Bethe-Salpeter amplitudes) which are on-shell objects by definition. Hence, for our purposes it makes little sense to consider the full off-shell behavior of the integrand in the Bethe-Salpeter equation (4.74). We instead approximate this equation by

$$\begin{aligned} M_{fi}(p',p) &\stackrel{!}{=} M_{fi}^{\text{irr}}(p',p) \\ &\quad + i\sum_n \int \frac{\mathrm{d}^4 p_n}{(2\pi)^4} M_{fn}^{\text{irr}}(p',p_n^{\text{on}}) G_n^{\text{free}}(p_n) M_{ni}(p_n^{\text{on}},p), \end{aligned} \tag{4.78}$$

where the intermediate states n are assumed to be on mass-shell.

Accordingly, the matrix elements M_{fn}^{irr} and M_{ni} are here evaluated at the on-shell four-momentum

$$p_n^{\text{on}} := p_n\Big|_{p_n^2=M_n^2} = \begin{pmatrix} \omega_{p_n} \\ \mathbf{p}_n^{\text{on}} \end{pmatrix} \tag{4.79}$$

and energy

$$\omega_{p_n} = \sqrt{M_n^2 + |\mathbf{p}_n^{\text{on}}|^2} = \omega - \sqrt{m_n^2 + |\mathbf{p}_n^{\text{on}}|^2}, \tag{4.80}$$

where M_n and m_n denote the *physical* masses of the baryon and meson belonging to the intermediate state n, respectively. The full propagator in turn here reduces to its free form G_n^{free}, describing the propagation of non-interacting meson-baryon systems. For coupled-channel scattering involving pseudoscalar mesons only, *i.e.* the case of the process studied in Chapter 5, the latter is given by

$$G_n^{\text{free}}(p_n) = -\frac{\sum_{\lambda_n} u_{\lambda_n}(p_n)\bar{u}_{\lambda_n}(p_n)}{\left[p_n^2 - M_n^2 + i\epsilon\right]\left[(P-p_n)^2 - m_n^2 + i\epsilon\right]} \tag{4.81}$$

where we used the free forms of the scalar propagator

$$\Delta_n^{\text{free}}(P-p_n) = \frac{i}{(P-p_n)^2 - m_n^2 + i\epsilon} \tag{4.82}$$

and the fermion propagator

$$G_n^{\text{free}}(p_n) = i\,\frac{\not{p}_n + M_n}{p_n^2 - M_n^2 + i\epsilon}\,\bar{\Theta}_s(p_n) \tag{4.83}$$

for arbitrary (half-integer) spin s [72], and also the fact that for non-interacting spinor fields the identity

$$(\not{p}_n + M_n)\,\bar{\Theta}_s(p_n) = \sum_{\lambda_n} u_{\lambda_n}(p_n)\bar{u}_{\lambda_n}(p_n) \tag{4.84}$$

holds. Here, $\bar{\Theta}_s$ represents the projection operator on spin-s states.

Using the general expression for the free propagator we now simplify the solution of the on-shell scattering equation as follows. Firstly, we substitute the propagator appearing in Eq. (4.78) by its explicit form as given in Eq. (4.81). Next, we evaluate the former expression between spinors and utilize the definitions (4.76) and (4.77) in order to identify the T- and V-matrix elements. In this way, we write the scattering equation (4.78) as an integral equation for the transition amplitudes, *i.e.*

$$\begin{aligned} T_{\lambda'\lambda}(p',p) = V_{\lambda'\lambda}(p',p) + i\sum_{\lambda_n}\int\frac{\mathrm{d}^4\,p_n}{(2\pi)^4}\,V_{\lambda'\lambda_n}(p',p_n^{\text{on}}) \\ \times\,\tilde{G}_n(p_n^0,|\mathbf{p}_n|)T_{\lambda_n\lambda}(p_n^{\text{on}},p), \end{aligned} \tag{4.85}$$

where we introduced the scalar propagator

$$\tilde{G}_n(p_n^0,|\mathbf{p}_n|) := -\,\frac{1}{p_n^2 - M_n^2 + i\epsilon}\,\frac{1}{(P-p_n)^2 - m_n^2 + i\epsilon}. \tag{4.86}$$

At this point, one should note that in contrast to G_n^{free} the propagator $\tilde{G}_n$ depends on Lorentz invariants only, so that the on-shell equation, when written for transition amplitudes, can be easily solved by means of a partial-wave decomposition. To show this we consider Eq. (4.85) in the center-of-mass frame where

$$p_n^{\text{on}}\Big|_{P=(\omega,\mathbf{0})} \equiv p_n^{\text{on}}(\omega,\Omega_n), \tag{4.87}$$

cf. Eqs. (4.9), (4.10) and (4.11), and therefore

$$\begin{aligned} T_{\lambda'\lambda}(\omega,\Omega',\Omega) = V_{\lambda'\lambda}(\omega,\Omega',\Omega) + \frac{i}{(2\pi)^4}\sum_{\lambda_n}\int\mathrm{d}^2\,\Omega_n V_{\lambda'\lambda_n}(\omega,\Omega',\Omega_n) \\ \times\left[\int\mathrm{d}\,p_n^0\int\mathrm{d}\,|\mathbf{p}_n||\mathbf{p}_n|^2\tilde{G}_n(p_n^0,|\mathbf{p}_n|)\right]T_{\lambda_n\lambda}(\omega,\Omega_n,\Omega). \end{aligned} \tag{4.88}$$

From this result it is then clear that by expanding all V- and T-matrix elements in Eq. (4.88) according to Eq. (4.41), and also applying the orthogonality relation (4.68) of the Wigner rotation matrices, one can evaluate the remaining integral over Ω_n and obtain

$$T^J_{\lambda'\lambda}(\omega) = V^J_{\lambda'\lambda}(\omega) + \sum_{\lambda_n} V^J_{\lambda'\lambda_n}(\omega)\mathcal{G}_n(\omega)T^J_{\lambda_n\lambda}(\omega), \tag{4.89}$$

where we introduced the **meson-baryon scalar-loop integral**

$$\mathcal{G}_n(P)\Big|_{P=(\omega,\mathbf{0})} \equiv \mathcal{G}_n(\omega) := \frac{i}{(2\pi)^4}\,(4\pi)\int \mathrm{d}\,p_n^0 \int \mathrm{d}\,|\mathbf{p}_n||\mathbf{p}_n|^2 \tilde{G}_n(p_n^0,|\mathbf{p}_n|). \tag{4.90}$$

The latter may also be recast in the familiar form

$$\mathcal{G}_n(\omega) \;= -i\int \frac{\mathrm{d}^4\,p_n}{(2\pi)^4}\,\frac{1}{p_n^2-M_n^2+i\epsilon}\,\frac{1}{(P-p_n)^2-m_n^2+i\epsilon} \tag{4.91}$$

by inserting (4.86) into (4.90) and using $4\pi = \int \mathrm{d}^2\,\Omega_n$ to recover the four-dimensional notation. Later in Section 4.3.3 we discuss the solution of the integral above.

As it stands the on-shell scattering equation (4.89) is still of limited practical value for the applications we aim at in this work: recall from our former discussions that to investigate baryon properties we need to construct parity-conserving partial-wave amplitudes. We therefore proceed with the derivation of an equation for $T^{J\pm}_{\lambda'\lambda}$, and to this end we exploit the consequences of parity invariance in a calculation similar to Eq. (4.71) as below:

$$\begin{aligned}
T^{J\pm}_{\lambda'\lambda}(\omega) &\overset{(4.58)}{=} T^{J}_{\lambda'\lambda} \pm \eta T^{J}_{\lambda'-\lambda} \\
&\overset{(4.89)}{=} V^{J}_{\lambda'\lambda} + \sum_{\lambda_n} V^{J}_{\lambda'\lambda_n}\mathcal{G}_n T^{J}_{\lambda_n\lambda} \pm \eta V^{J}_{\lambda'-\lambda} \pm \eta \sum_{\lambda_n} V^{J}_{\lambda'\lambda_n}\mathcal{G}_n T^{J}_{\lambda_n-\lambda} \\
&\overset{(4.58)}{=} V^{J\pm}_{\lambda'\lambda} + \sum_{\lambda_n} V^{J}_{\lambda'\lambda_n}\mathcal{G}_n T^{J\pm}_{\lambda_n\lambda} \\
&\equiv\; V^{J\pm}_{\lambda'\lambda} + \sum_{\lambda_n>0}\left[V^{J\pm}_{\lambda'-\lambda_n}\mathcal{G}_n T^{J\pm}_{-\lambda_n\lambda} + V^{J\pm}_{\lambda'\lambda_n}\mathcal{G}_n T^{J\pm}_{\lambda_n\lambda}\right] \\
&\overset{(4.59)}{=} V^{J\pm}_{\lambda'\lambda} + \sum_{\lambda_n>0}\left[V^{J\pm}_{\lambda'-\lambda_n}\mathcal{G}_n\,(\pm\eta_n)\,T^{J\pm}_{\lambda_n\lambda} + V^{J\pm}_{\lambda'\lambda_n}\mathcal{G}_n T^{J\pm}_{\lambda_n\lambda}\right] \\
&\overset{(4.58)}{=} V^{J\pm}_{\lambda'\lambda} + \sum_{\lambda_n>0} V^{J\pm}_{\lambda'\lambda_n}\mathcal{G}_n T^{J\pm}_{\lambda_n\lambda}.
\end{aligned} \tag{4.92}$$

Then, by recalling that due to parity invariance it is sufficient to consider $\lambda,\lambda' > 0$, and also defining the matrix elements

$$\mathcal{G}_{n'n}(\omega) := \mathcal{G}_n\,(\omega)\delta_{n'n} \tag{4.93}$$

of a diagonal matrix $\mathcal{G}$, we rewrite Eq. (4.92) in the matrix form

$$T^{J\pm} = V^{J\pm} + V^{J\pm}\mathcal{G}T^{J\pm} \tag{4.94}$$

whose solutions are formally given by

$$T^{J\pm} = \left[V^{J\pm\,-1} - \mathcal{G}\right]^{-1}. \tag{4.95}$$

Hence, as we see from the results above, the advantage of the on-shell approach is that the dependence on the relative four-momentum p_n remains inside the integrand of $\mathcal{G}_n$ only (*cf.* Eq. (4.90)), so that the full scattering equation (4.74) reduces to an algebraic expression whose solution is of course much simpler. As demonstrated in Refs. [70, 73] (there specifically for S-waves only) such an approximation is equivalent to accounting for off-shell fluctuations by means of the renormalization of the coupling constants in V. In this respect it is also worth mentioning that even without a general proof the same method has been successfully applied to D-waves as well [74]. Now, to calculate the $T^{J\pm}$-matrix from Eq. (4.95) we basically need two ingredients: an expression for the potential $V^{J\pm}$ and the solution of the loop integral $\mathcal{G}_n$. The former issue is extensively investigated in Chapter 5 in the framework of an effective Lagrangian approach; in the next Section 4.3.2 we just present some general remarks concerning the construction of $V^{J\pm}$ without going into detail regarding its explicit form. For the analytical solution of $\mathcal{G}_n$ we refer the reader to Section 4.3.3.

4.3.2 Lowest-order background and resonant contributions

Even when approximating the kernel by its on-shell components only, it still contains an infinite number of two-body irreducible contributions which evidently cannot all be evaluated in an effective Lagrangian model. Therefore for practical calculations we need to truncate the summation in $M^{\rm irr}$ to some finite order in the coupling constants appearing in the Lagrangian. Following the same method as in Refs. [18, 19, 67, 75] for example, in Chapter 5 we strictly consider lowest-order (tree-level) contributions to the kernel. More specifically, as represented in Fig. 4.2 we include (I) one-particle reducible diagrams consisting of a single baryon in the intermediate state, which are called s-channel or pole graphs, as well as (II) diagrams corresponding to t- and u-channel exchanges, which in relation to the former pole terms are usually referred as non-resonant or background contributions. Accordingly, we separate the kernel as

$$M^{\rm irr} = M^{\rm P} + M^{\rm NP}, \tag{4.96}$$

where the pole ($M^{\rm P}$) and non-pole ($M^{\rm NP}$) parts include only resonant and background diagrams, respectively.

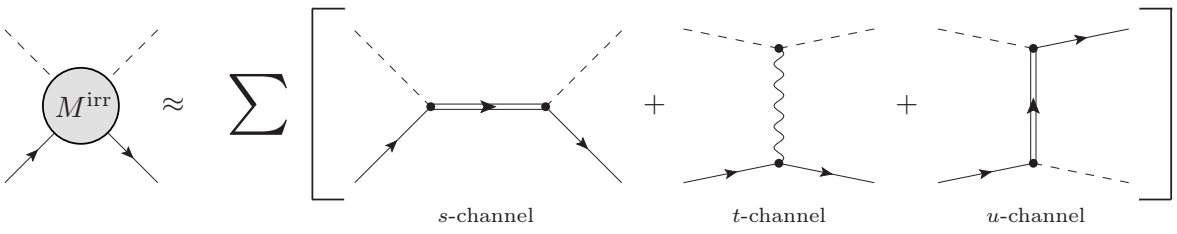

Figure 4.2. Lowest-order diagrams included in the kernel. Asymptotic baryons (mesons) are denoted by full (dashed) lines. Intermediate baryons (mesons) in turn are represented by double (wavy) lines.

Such a decomposition of the interaction kernel is often used in the literature to simplify the solution of the full (off-shell) scattering equation, see *e.g.* Refs. [45, 76, 77]. Our interest in writing the kernel this way, on the other hand, lies in the fact that it is a convenient manner to relate quark-model quantities to those derived from a hadronic Lagrangian approach. To show this we first note that baryon resonances have definite spin and parity and thus contribute to a single partial-wave. Moreover, we recall that s-channel diagrams are one-particle reducible and therefore separable in the momenta of the external particles. For these reasons we write:

$$M^{\mathrm{P}} = \sum_{J} \sum_{R(J)} v_{0R} S_{0R}(P) v_{0R}^{\dagger}, \tag{4.97}$$

where the summation includes resonances with all possible angular momenta coupling to both initial and final states, and S_{0R}, v_{0R} and $v_{0R}^{\dagger}$ represent the propagator, the annihilation and the creation operators for a *bare* resonance R, respectively. Hence, by evaluating (4.96) between spinors and employing the general form of bare fermion propagators (*i.e.* Eqs. (4.83) and (4.84) with $M_n \to M_0$), from (4.77) we obtain

$$V = V^{\mathrm{P}} + V^{\mathrm{NP}} \tag{4.98}$$

where

$$V^{\mathrm{NP}}_{\lambda'\lambda}(p',p) := \bar{u}_{\lambda'}(p') M^{\mathrm{NP}}(p',p) u_{\lambda}(p) \tag{4.99}$$

and for the pole part

$$V^{\mathrm{P}}_{\lambda'\lambda}(p',p) := \bar{u}_{\lambda'}(p') M^{\mathrm{P}}(p',p) u_{\lambda}(p) = \sum_{J} \sum_{R(J)} \sum_{\mu_R} \frac{\gamma_{\lambda'\mu_R}(p') \gamma^{\dagger}_{\mu_R\lambda}(p)}{s - M_{0R}^2 + i\epsilon} \tag{4.100}$$

holds. Here, M_{0R} is the bare mass and μ_R the helicity of an intermediate baryon R. We also defined the **bare vertex functions**

$$\gamma_{\lambda\mu_R}(p) := \bar{u}_{\lambda}(p) v_{0R}(p) u_{\mu_R}(P) \overset{\text{c.m.}}{\equiv} 4\pi \sqrt{\frac{\omega}{|\mathbf{p}|}} \langle \Omega, \lambda | \gamma | \mu_R \rangle \tag{4.101}$$

which, as should be noted, are equivalent to the strong decay amplitudes defined in (3.22) and calculated in the framework of the relativistic quark model. To check this last argument, one evaluates the left-hand side of (3.22) in the center-of-mass frame, describes meson-baryon by spherical states as those in (4.22), and then compares the final result to the right-hand side of that equation.

From the discussion above it becomes clear that the matching between our quark model and a Lagrangian description of meson-baryon scattering should be performed by comparing the matrix elements of γ as evaluated in both frameworks. This topic will be addressed later in Chapter 6, where we eventually consider the effect of final state interactions for the decay widths calculated in Chapter 3. In the present chapter we wish to focus on an interesting consequence of the decomposition (4.98) concerning the scattering equation (4.94): As we shall see in Section 4.3.4, provided that the matrix elements of γ are known, the solutions $T^{J\pm}$ of Eq. (4.94) are fully determined from background quantities. Please note that this result is very important in this context, as it gives the prescription for how to connect strong decay amplitudes, in particular those from the quark model, to non-resonant hadronic rescattering amplitudes.

Resonant amplitude in the $|JM_J, \lambda\pm\rangle$ basis

Before finishing this section a few comments about the partial-wave expansion of the potential in the form given in Eq. (4.98) are in order. Evidently, both the potential and its non-resonant part can be expanded with the formalism of Section 4.2.3. On the other hand, since resonances have definite spin and parity, the contributions to the pole part in Eq. (4.100) have by construction well-defined quantum numbers J^π and would not have to be expanded at all. To study the implications of Eq. (4.98) however, we should write the whole potential in the same basis we use for the scattering equation (4.94), *i.e.* the basis of the states $|JM_J, \lambda\pm\rangle$ introduced in Eq. (4.53). Hence, we now employ Eq. (4.37) to expand the bare vertices as

$$\gamma_{\lambda\mu_R}(p) \overset{\text{c.m.}}{=} (2J+1)^{1/2}\, D^{J*}_{\mu_R\lambda}(\phi,\theta,-\phi)\gamma^J_\lambda(\omega), \tag{4.102}$$

where we used rotational invariance and defined

$$\gamma^J_\lambda(\omega) := \sqrt{\frac{4\pi\omega}{|\mathbf{p}|}}\,\langle J\mu_R|\gamma(\omega)|J\mu_R,\lambda\rangle \equiv \sqrt{\frac{4\pi\omega}{|\mathbf{p}|}}\,\langle\mu_R|\gamma^J(\omega)|\lambda\rangle, \tag{4.103}$$

such that the resonant part of the potential can be written as

$$V^{\mathrm{P}}_{\lambda'\lambda}\left(\omega,\Omega',\Omega\right) = \sum_{J,\mu_R}(2J+1)\, D^{J*}_{\mu_R\lambda'}(\phi',\theta',-\phi')D^J_{\mu_R\lambda}(\phi,\theta,-\phi)\left[V^{\mathrm{P}}\right]^J_{\lambda'\lambda}(\omega) \tag{4.104}$$

with

$$\left[V^{\mathrm{P}}\right]^J_{\lambda'\lambda}(\omega) = \sum_{R(J)}\frac{\gamma^J_{\lambda'}(\omega)\gamma^{J\dagger}_{\lambda}(\omega)}{s-M^2_{0R}+i\epsilon}. \tag{4.105}$$

Then, we introduce new vertex functions

$$\gamma^{J\pm}_\lambda(\omega) := \sqrt{\frac{4\pi\omega}{|\mathbf{p}|}}\,\langle J\mu_R|\gamma(\omega)|J\mu_R,\lambda\pm\rangle \equiv \sqrt{\frac{4\pi\omega}{|\mathbf{p}|}}\,\langle\mu_R|\gamma^J(\omega)|\lambda\pm\rangle, \tag{4.106}$$

now in terms of states $|JM_J,\lambda\pm\rangle$, which are related to the former according to

$$\gamma^{J\pm}_\lambda \overset{(4.53)}{=} \sqrt{\frac{1}{2}}\left[\gamma^J_\lambda \pm \eta\gamma^J_{-\lambda}\right]. \tag{4.107}$$

The relation above may be simplified by exploiting parity invariance to show that

$$\begin{aligned}\langle\mu_R|\gamma^J|\lambda\rangle &\overset{(4.46)}{=} \eta_R\eta_1\eta_2(-1)^{J-j_1-j_2}\langle\mu_R|\gamma^J|-\lambda\rangle \\ &\overset{(4.54)}{=} \pm\eta_R(-1)^{J\pm\frac{1}{2}}\eta\langle\mu_R|\gamma^J|-\lambda\rangle = \pm\eta\langle\mu_R|\gamma^J|-\lambda\rangle\end{aligned} \tag{4.108}$$

and therefore

$$\gamma^{J\pm}_\lambda = \sqrt{2}\gamma^J_\lambda, \tag{4.109}$$

where η_R denotes the intrinsic parity of a resonance R and where we used

$$\langle\mu_R|\gamma^J|\lambda\pm\rangle \overset{(4.55)}{=} \eta_R(-1)^{J\pm\frac{1}{2}}\langle\mu_R|\gamma^J|\lambda\pm\rangle \quad\Leftrightarrow\quad \eta_R = (-1)^{J\pm\frac{1}{2}}. \tag{4.110}$$

Finally, by applying the equations above together with the formalism of Section 4.2.3, we write the potential in the $|JM_J, \lambda\pm\rangle$ basis, *i.e.*

$$\Big[V\Big]^{J\pm}_{\lambda'\lambda} = \Big[V^{\mathrm{P}} + V^{\mathrm{NP}}\Big]^{J\pm}_{\lambda'\lambda}, \tag{4.111}$$

whose resonant part reads:

$$\Big[V^{\mathrm{P}}\Big]^{J\pm}_{\lambda'\lambda}(\omega) \overset{(4.58)}{=} \Big[V^{\mathrm{P}}\Big]^{J}_{\lambda'\lambda} \pm \eta \Big[V^{\mathrm{P}}\Big]^{J}_{\lambda'-\lambda} = \sum_{R(J)} \frac{\gamma^{J\pm}_{\lambda'}(\omega)\gamma^{J\pm\dagger}_{\lambda}(\omega)}{s - M_{0R}^2 + i\epsilon} \tag{4.112}$$

since

$$\gamma^{J}_{\lambda'}\Big[\gamma^{J\dagger}_{\lambda} \pm \eta\gamma^{J\dagger}_{-\lambda}\Big] \overset{(4.107)}{=} \frac{1}{\sqrt{2}}\gamma^{J}_{\lambda'}\gamma^{J\pm\dagger}_{\lambda} \overset{(4.109)}{=} \gamma^{J\pm}_{\lambda'}\gamma^{J\pm\dagger}_{\lambda}. \tag{4.113}$$

As a last remark, an expression for $\gamma^{J\pm}$ in terms of γ is relevant in Chapter 5 in order to obtain the potential in the basis of the states $|JM_J, \lambda\pm\rangle$. It is given by

$$\gamma^{J\pm}_{\lambda}(\omega) = \sqrt{\frac{2J+1}{2}} \int_{-1}^{1} \mathrm{d}(\cos\bar{\theta})\, d^{J}_{\mu_R\lambda}(\bar{\theta})\, \gamma_{\lambda\mu_R}(\omega, \bar{\theta}) \tag{4.114}$$

and derived by evaluating (4.102) with $y = 0$ as the reaction plane, then using (4.61) to invert the result and finally applying (4.109) to relate γ^{J} to $\gamma^{J\pm}$.

4.3.3 The scalar-loop integral

After explaining a general formalism to construct the potential $V^{J\pm}$ we now elaborate on the analytical solution of the scalar-loop integral $\mathcal{G}_n$ defined in Eq. (4.91). For this purpose we note that for large momentum transfers and in four space-time dimensions the integral $\mathcal{G}_n$ is logarithmically divergent, and thus needs to be regularized. In the literature there are various methods to regulate this integral, *e.g.* by the introduction of a cutoff parameter, the method of Pauli-Villars [78] or dimensional regularization [79]. Among these we utilize the latter in the so-called $\overline{MS}$ scheme, where one extracts the finite part

$$\begin{aligned}\big[\mathcal{G}_{\mathrm{fin}}\big]_n(\omega, \mu_n) := \frac{1}{16\pi^2}\Bigg\{1 - \log\left(\frac{m_n^2}{\mu_n^2}\right) - \left(\frac{M_n^2 - m_n^2 + \omega^2}{2\omega^2}\right)\log\left(\frac{M_n^2}{m_n^2}\right) \\ - \frac{|\mathbf{p}_n|}{\omega}\log\left(\frac{M_n^2 + m_n^2 - s - 2\omega|\mathbf{p}_n|}{M_n^2 + m_n^2 - s + 2\omega|\mathbf{p}_n|}\right)\Bigg\}\end{aligned} \tag{4.115}$$

of the loop integral, while collecting divergent terms and further constants stemming from dimensional regularization into the subtraction constant

$$\big[\mathcal{G}_{\infty}\big]_n(\mu_n) := \lim_{\delta\to 0} \frac{\mu^{-2\delta}}{16\pi^2}\left[\frac{1}{\delta} - \gamma_E + \log(4\pi) + 1\right] \tag{4.116}$$

for

$$\mathcal{G}_n(\omega) = \big[\mathcal{G}_{\mathrm{fin}}\big]_n(\omega, \mu_n) + \big[\mathcal{G}_{\infty}\big]_n(\mu_n). \tag{4.117}$$

Here, μ_n is the regularization scale, $\gamma_E \approx 0.5772$ is the Euler-Mascheroni constant and $2\delta = 4 - d$ where d indicates the number of space-time dimensions.

Deriving the latter results is a well-known procedure in quantum field theory and details can be found in many textbooks, *e.g.* in Ref. [63]. For our purposes, it is enough to say that one starts with the generalization of the Minkowski space to a d-dimensional space, where $\mathcal{G}_n$ converges and is thus solvable in the standard way, *i.e.* by Feynman parametrization and Wick rotation. After evaluating the integral in d dimensions, the physical picture is then recovered by taking the limit $d \to 4$ and collecting remaining singularities in the subtraction constant $\mathcal{G}_\infty$ as in Eq. (4.116). However, if $p_n^2 = M_n^2$ or $(P - p_n)^2 = m_n^2$, the loop integral of Eq. (4.91) is still divergent in d dimensions and the Wick rotation can be no longer justified. In this case the finite part of the loop has an imaginary part, *i.e.*

$$[\mathcal{G}_{\text{fin}}]_n (\omega, \mu_n) = \text{Re}\, [\mathcal{G}_{\text{fin}}]_n (\omega, \mu_n) + i\, \rho_{nn}(\omega) \tag{4.118}$$

which may be deduced by applying Cutkosky rules in Eq. (4.91). Here, ρ represents the phase-space matrix previously defined in Eq. (4.70).

There are two important consequences of the resulting loop integral concerning the solutions of the Bethe-Salpeter equation (4.94): Firstly, provided the potential is Hermitian ($V^\dagger = V$) any solution of (4.94) satisfies the two-body unitarity condition (4.72). It indeed follows from Eq. (4.94) that

$$\begin{aligned} \left[T - T^\dagger\right] &= V\mathcal{G}T - T^\dagger\mathcal{G}^\dagger V = V\mathcal{G}T - T^\dagger\mathcal{G}^\dagger \left[T - V\mathcal{G}T\right] \\ &= \left[V + T^\dagger\mathcal{G}^\dagger V\right] \mathcal{G}T - T^\dagger\mathcal{G}^\dagger T = T^\dagger \left[\mathcal{G} - \mathcal{G}^\dagger\right] T, \end{aligned} \tag{4.119}$$

where we omitted spin and parity labels for clarity, and then from Eq. (4.118)

$$\text{Im}\left[T^{J\pm}\right] = (T^{J\pm})^\dagger \text{Im}\,[\mathcal{G}]\,(T^{J\pm}) \;= (T^{J\pm})^\dagger \rho (T^{J\pm}) \;, \tag{4.120}$$

which is the same result as in Eq. (4.72). As the second important point both finite and divergent parts of the loop depend on the regularization scale μ_n, while their sum is evidently scale-independent, *cf.* Eqs. (4.115) to (4.117). Therefore the $T^{J\pm}$-matrix should not depend on the scale either, since from Eqs. (4.94) and (4.117) we have

$$T^{J\pm} = \left[V^{J\pm\,-1} - \mathcal{G}_{\text{fin}}(\mu) - \mathcal{G}_\infty(\mu)\right]^{-1}, \tag{4.121}$$

where μ denotes the set or renormalization scales μ_n. In this regard however we note that the scattering equation (4.121) contains the divergence $\mathcal{G}_\infty$ and in this form is not suitable for explicit calculations. To formulate the scattering equation in terms of finite quantities, we follow the argument from Ref. [80] and decompose the potential as

$$V = V_{\text{fin}} + V_\infty \tag{4.122}$$

for which we demand that

$$T^{J\pm} = \left[V_{\text{fin}}^{J\pm\,-1}(\mu) - \mathcal{G}_{\text{fin}}(\mu)\right]^{-1}. \tag{4.123}$$

Using this method, it is in principle possible to cancel the divergent part $\mathcal{G}_\infty$ by the appropriate term V_∞ in the potential, such that the $T^{J\pm}$-matrix is derived from finite quantities and is still scale-independent. In practice though a residual scale dependence remains, reflecting the influence of higher-order processes which cannot be included in an explicit potential. This issue shall be discussed in more detail later in Chapter 5.

4.3.4 Decomposition of the scattering equation

In this section we return to the decomposition (4.111) and investigate its implications for the Bethe-Salpeter equation, specifically in the form given in (4.123), *i.e.* after re-absorbing the divergent part of the loop inside the potential. For this purpose we look for the solutions of Eq. (4.123) which similarly to the potential can be separated as

$$\Big[T\Big]^{J\pm} = \Big[T^{\rm P} + T^{\rm NP}\Big]^{J\pm} \tag{4.124}$$

into a pole and a non-pole part. In addition, to ensure that the $T^{J\pm}$-matrix satisfies the scattering equation even in the absence of explicit resonant fields, the background contribution $T^{\rm NP}$ should be a solution of

$$\Big[T^{\rm NP}\Big]^{J\pm} = \Big[V^{\rm NP}_{\rm fin} + V^{\rm NP}_{\rm fin}\mathcal{G}_{\rm fin}T^{\rm NP}\Big]^{J\pm}. \tag{4.125}$$

For the sake of clarity, we now omit angular momentum and parity superscripts and also the subscripts in V and $\mathcal{G}$ denoting that these are finite quantities. Nevertheless, it should kept in mind that here we deal with matrices in the $|JM_J,\lambda\pm\rangle$ basis and that both the potential and the loop are from now on scale dependent. Furthermore, we shall here use a concise matrix notation in which the resonant part of the potential reads:

$$V^{\rm P} = \gamma\cdot S_0\cdot\gamma^\dagger, \tag{4.126}$$

cf. Eq. (4.112), where S_0 is a diagonal matrix defined by its elements

$$[S_0]_{R'R} := \frac{1}{s - M_{0R}^2 + i\epsilon}\delta_{R'R}. \tag{4.127}$$

The derivation of a transition matrix $T^{J\pm}$ satisfying both the scattering equation and the conditions (4.124) and (4.125) is a standard procedure which will not be elaborated here. A more comprehensive derivation can be found in Section 2.6 of Ref. [75] and we shall merely sketch the method used there. The first step is to replace (4.124) and (4.125) into the scattering equation (4.123), so that after some basic algebra the latter is formulated as

$$\begin{aligned}\Big[I - V^{\rm NP}\mathcal{G}\Big]\,T^{\rm P} = V^{\rm P}\,\Big[I + \mathcal{G}T^{\rm NP}\Big] \\ + V^{\rm P}\,\Big[I + \mathcal{G}T^{\rm NP}\Big]\,\mathcal{G}\,\Big[I + T^{\rm NP}\mathcal{G}\Big]^{-1}\,T^{\rm P}.\end{aligned} \tag{4.128}$$

Then, we exploit the formal solution of (4.125) to eliminate $V^{\rm NP}$ from the left-hand side of Eq. (4.128) and thereby rewrite this equation as

$$T' = V' + V'\mathcal{G}T', \tag{4.129}$$

where we also introduced the auxiliary quantities

$$T' = \Big[I + T^{\rm NP}\mathcal{G}\Big]^{-1}\,T^{\rm P} \qquad \text{and} \qquad V' = V^{\rm P}\,\Big[I + \mathcal{G}T^{\rm NP}\Big]. \tag{4.130}$$

At this point, we note that Eqs. (4.129) and (4.130) may be solved for T^{P} if V' and T' are known. Therefore, to obtain these quantities, we now employ the explicit form (4.126) of V^{P} to calculate V' and then use the result to solve Eq. (4.129) for T'. Proceeding this way and also defining:

- **dressed vertex functions**

$$\Gamma := \gamma + T^{\mathrm{NP}}\mathcal{G}\gamma \overset{(4.125)}{=} \left[I - V^{\mathrm{NP}}\mathcal{G}\right]^{-1}\gamma \tag{4.131}$$

and

$$\tilde{\Gamma} := \gamma^\dagger + \gamma^\dagger\mathcal{G}T^{\mathrm{NP}} \overset{(4.125)}{=} \gamma^\dagger\left[I - \mathcal{G}V^{\mathrm{NP}}\right]^{-1}, \tag{4.132}$$

- **self-energy** contributions

$$\begin{aligned}\Sigma := \tilde{\Gamma}\mathcal{G}\gamma &\overset{(4.132)}{=} \gamma^\dagger\left[I + \mathcal{G}T^{\mathrm{NP}}\right]\mathcal{G}\gamma \\ &\equiv \gamma^\dagger\mathcal{G}\left[I + T^{\mathrm{NP}}\mathcal{G}\right]\gamma \overset{(4.131)}{=} \gamma^\dagger\mathcal{G}\Gamma\end{aligned} \tag{4.133}$$

- and **dressed resonance propagators**

$$S_D := \left[S_0^{-1} - \Sigma\right]^{-1}, \tag{4.134}$$

we finally arrive at the following expression for the resonant amplitude:

$$T^{\mathrm{P}} = \Gamma \cdot S_D \cdot \tilde{\Gamma}. \tag{4.135}$$

For convenience, we depict the results above as graphs in Fig. 4.3. Note that these graphs do not correspond to Feynman diagrams, as we solve the scattering equation in on-shell approximation. Nevertheless, a similar representation would be valid for the full Bethe-Salpeter equation (4.74) as well, since it may also be expressed in a matrix form, separated into pole and non-pole parts and thus formally decomposed as explained in this section. As shown in Fig. 4.3, provided the background potential V^{NP} and the bare vertex functions γ from a theoretical model are known, all quantities related to resonant contributions can be evaluated from these, in a calculation which follows the same order in which the graphs appear in the figure.

Finally, we should mention that such a treatment of the scattering equation is not only useful to study the influence of background contributions for baryon properties. It also provides a manner to clearly see both mechanisms through which a baryon resonance might be produced: Either the state is explicitly included in the underlying potential by means of bare vertex functions, or it is dynamically generated by unitary non-resonant interactions. Indeed, the non-pole part T^{NP} of the transition matrix as defined in (4.125) is itself unitary and, therefore, might also contain poles corresponding to the so-called dynamically generated resonances.

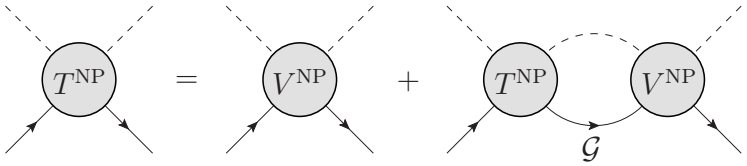

(a) Background amplitudes.

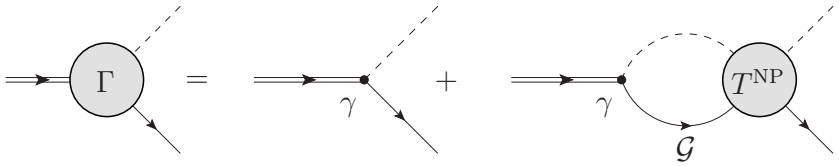

(b) Dressed resonance annihilation.

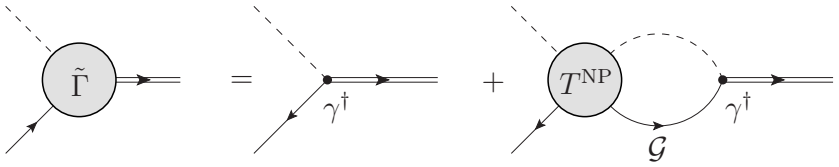

(c) Dressed resonance creation.

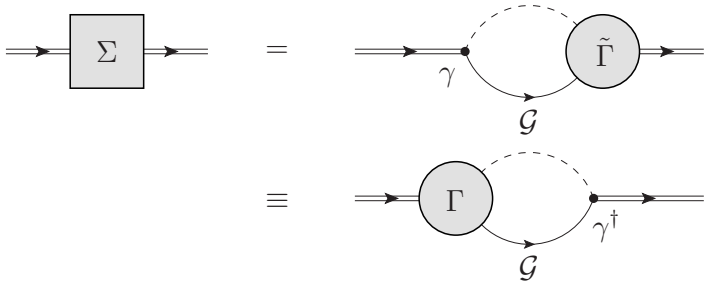

(d) Resonance self-energy.

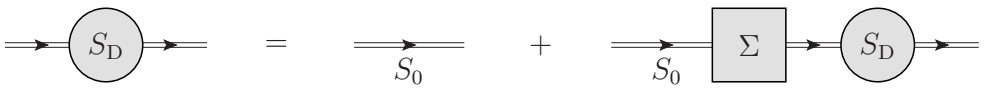

(e) Dressed Propagator.

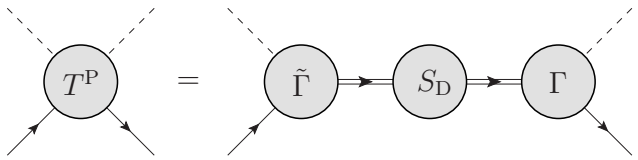

(f) Resonant amplitude.

Figure 4.3. Decomposition of the on-shell Bethe-Salpeter equation.

4.4 Masses and widths of baryon resonances

Using the results of Section 4.3.4, we can finally explain how the masses and strong decay widths of baryon resonances can be evaluated from transition amplitudes and vertex functions. More importantly, we are now able to discuss the interpretation of such properties as defined in the relativistic quark model, and finally explain how we here include final state interactions in strong decays. To this end, it is instructive to first analyse the case where (I) the center-of-mass energy is close to the physical mass of a specific resonance, so that it is sufficient to consider the contribution of a single bare state to the partial-wave $T^{J\pm}$, and (II) non-resonant contributions to the underlying potential can be neglected. In this instance the resonant part of $T^{J\pm}$ reduces to

$$\left[T^{\rm P}\right]^{J\pm}_{\lambda'\lambda}(\omega) = \frac{\gamma^{J\pm}_{\lambda'}(\omega)\gamma^{J\pm\dagger}_{\lambda}(\omega)}{s - M^2(\omega,\mu) - i\omega\Gamma(\omega)}, \tag{4.136}$$

with

$$M^2(\omega,\mu) := M_0^2 + \sum_{\lambda_n} {\rm Re}\left[\mathcal{G}\right]_n(\omega,\mu_n)\left|\gamma^{J\pm}_{\lambda_n}(\omega)\right|^2 \tag{4.137}$$

and

$$\Gamma(\omega) := \sum_{\lambda_n} \frac{|\mathbf{p}_n|}{8\pi\omega^2}\left|\gamma^{J\pm}_{\lambda_n}(\omega)\right|^2, \tag{4.138}$$

where we evaluated Eqs. (4.131) to (4.135) for $V^{\rm NP} = 0$ and a single baryon state with bare mass M_0, and also employed Eqs. (4.118) and (4.70) to decompose $\mathcal{G}$ into its real and imaginary parts and write the latter explicitly.

The resonant amplitude (4.136) resembles the well-known Breit-Wigner formula, and for $M \approx \omega \equiv \sqrt{s}$ it justifies the use of Eq. (3.23) to evaluate strong decay widths in the absence of rescattering effects, as it was done in Chapter 3. Now returning to the general case where $V^{\rm NP} \neq 0$ and bare states contributing to a single partial-wave may interfere, in analogy to (4.138) we define the **corrected decay widths** according to the formula:

$$\Gamma_{\rm corr}(\mu) := \sum_{\lambda_n} \frac{|\mathbf{p}_n|}{8\pi M^2}\left|\Gamma^{J\pm}_{\lambda_n}(\omega = M,\mu)\right|^2. \tag{4.139}$$

A few remarks regarding the important expression (4.139) and its application in the following chapters are in order. First of all, this definition implies that to obtain the corrected decay widths one basically has to determine the matrix elements of

$$\Gamma(\omega = M,\mu) = \Big[I - V^{\rm NP}(\omega = M,\mu)\,\mathcal{G}(\omega = M,\mu)\Big]^{-1}\gamma(\omega = M), \tag{4.140}$$

cf. Eq. (4.131), whose ingredients are bare vertices and the non-resonant part of the potential. As stated before, in this work we use the bare vertices from the relativistic quark model (as calculated in Chapter 3), while the background potential is derived from effective meson-baryon interactions (to be detailed in Chapter 5). On the other hand, to solve the matrix equation (4.140) one evidently needs the relative signs of the bare vertex functions as well.

As explained in Section 3.3, however, in the framework of the relativistic quark model it is not possible to determine the sign of γ-matrix elements, but only the magnitude of these amplitudes. In order to circumvent this problem here we proceed as follows: Besides background contributions we also include resonant terms in our model for meson-baryon interactions. In this way, from an adjustment of the resulting transition amplitudes to experimental data, we expect to determine the relative signs of the several γ-matrix elements.

Having established the method to account for rescattering in strong decays, we now turn to the interpretation of the baryon masses as calculated in the relativistic quark model. For this purpose, we recall from Chapter 2 that the baryon masses defined in that approach correspond to poles of the six-point Green's function in the *real* energy variable of the three-quark system, *cf.* Eq. (2.73). As such, these mass parameters are then equivalent to bare masses M_0 and, according to the result (4.137), to Breit-Wigner masses only in the limit where (I) non-resonant contributions to baryon properties can be neglected, and (II) the real part of the loop vanishes, *i.e.* the resonant amplitude is calculated in the so-called K-matrix approximation.

Accordingly, one should in principle apply the formalism of Section 4.3 not only to correct the decay widths but also to dress the baryon masses from the quark model. In the present thesis however, we will not investigate this matter for the following reason: As the parameters of the quark model are fitted to Breit-Wigner masses directly, it would require a readjustment of model parameters and a further correction of baryon masses in an iterative process, which is beyond the scope of this work. Instead, we here focus exclusively on including final state interactions in the strong decays via Eq. (4.139). Nevertheless, considering that the quark model does provide a reasonable description of experimental Breit-Wigner masses of low-lying N and Δ resonances (*cf.* Table 2.3), we employ those values calculated in Chapter 2 as the mass parameters M appearing in Eq. (4.139).

4.5 Summary

In this chapter we reviewed the most important points concerning the description of meson-baryon interactions in scattering theory. By applying basic physical principles such as Poincaré invariance and unitarity, we obtained a general expression for the corresponding partial-wave amplitudes $T^{J\pm}$. These amplitudes were then decomposed into background and resonant contributions, allowing for a clear understanding of how non-resonant terms contribute to the masses and the strong decay widths of baryon resonances. By investigating these issues, we finally established a method to include final state interactions in strong baryon decays: Together with Eq. (4.139) the result (4.140) gives us the calculational prescription. Firstly we need an effective model for meson-baryon interactions, in order to parametrize the non-resonant part of the potential and obtain the relative signs of bare resonance vertices. This model will be implemented in the next Chapter 5. After this, we then use the absolute value of bare vertex functions as calculated in the quark model, to finally account for final state interactions in strong baryon decays. The results of such a procedure will be discussed in Chapter 6.

Chapter 5

A coupled-channel model for πN scattering

5.1 Introduction

After describing strong properties of baryons resonances in a relativistic constituent quark model and discussing how these are related to the quantities from a hadronic approach, we now wish to elaborate on the last ingredient necessary to include final state interactions in strong baryon decays, *i.e.* a dynamical model for meson-baryon interactions. As explained in Section 4.4, this model has to include both background and resonant contributions, in order to both parameterize rescattering effects in strong decays and determine the sign of bare vertex functions. In addition, recalling that in Chapter 2 baryons were considered to be on-shell states, the framework implemented here should be an on-shell approach as well.

Among several models available in the literature the approach developed by the Jülich group [21, 40–46] is particularly suitable for this application, basically for two reasons: Firstly, the σ- and ρ-meson exchanges in elastic πN scattering are described by correlated $\pi\pi$ exchanges in the spin $J = 0, 1$ channels instead of the usual meson-exchange picture, providing realistic and well-constrained background amplitudes this way. Moreover, besides bare resonances of spin 1/2 and 3/2 in the effective Lagrangian this model includes phenomenological couplings for higher spins up to 9/2, allowing for a systematical extension of our approach in the future. As it stands, however, the Jülich model cannot be directly employed here, as it provides transition amplitudes which are in general constructed off-shell (see aforementioned references). Therefore, in the present chapter we perform an on-shell reduction of their approach.

Originally designed to describe elastic πN scattering [41, 42] the Jülich model had been extended over the years through inclusion of the inelastic ηN, σN, $\pi\Delta$ and ρN channels [21, 43]. Later improvements in the treatment of correlated $\pi\pi$ exchanges and in the underlying Lagrangian [44, 45] led to a better agreement with the partial-wave πN amplitudes resulting from the analysis of the GWU/SAID group [14]. Nowadays, after inclusion of strangeness production and couplings to high-spin baryons [40, 46] the Jülich model contains most of the decay channels coupling to non-strange baryons and describes πN amplitudes for center-of-mass energies even beyond 2000 MeV.

In this first study of rescattering effects, however, it is not necessary to consider energies up to these values. As stated before, here we only include couplings to the πN and ηN channels and also to the effective $\pi\Delta$ channel, which parameterizes a part of the three-body state $\pi\pi N$ and provides inelasticity in both isospin states $I = \frac{1}{2}$ and $\frac{3}{2}$ of the πN system. Accordingly, here we utilize a version of the Jülich model which already uses its final effective Lagrangian, but is still the closest possible to our approach in terms of the coupled-channel basis. This is the version published in Ref. [45], which besides the states considered here includes couplings to ρN and σN as well.

As we shall see in this chapter, considering only the states πN, $\pi\Delta$ and ηN in an on-shell coupled-channel approach leads to an adequate description of πN partial-waves for energies up to $\omega \approx 1700$ MeV, allowing for the study of rescattering effects in strong decays of most of the low-lying states listed in Tables 2.3 and 3.1. Exceptions are the $N(1720)$ and the $\Delta(1700)$ states which couple too strongly to the ρN channel, as well as any resonance coupling to the P_{11} πN-wave. In fact, due to the contribution of the Roper resonance $N(1440)$ to this wave, inelasticity is present at much lower energies than the threshold energies of the inelastic channels included in the model, which prevents a reasonable description of the amplitude.

This chapter is organized as follows: In Section 5.2 we explain the construction of the underlying potential entering in the on-shell scattering equations of Chapter 4 (see diagrams of Fig. 4.3) based on the Lagrangian of the Jülich model. In addition, we show in more detail why P_{11} resonances cannot be addressed in our framework. After describing the potential for both background and resonant interactions, we then discuss in Section 5.3 the unitarization method and the treatment of the renormalization scale dependence entering in both the potential and the scalar loop integrals (see *e.g.* the scattering equation (4.123)). As we shall see, in our model it is unfortunately not possible to treat the scale dependence in both these quantities simultaneously, because here we utilize an on-shell framework. For this reason, we first set the renormalization scales to a suitable mass parameter (of order of hadronic masses) and only then treat the scale dependence of the potential by means of cutoff-dependent form factors.

The model constructed in Section 5.2 and the unitarization of the corresponding transition amplitudes lead to a set of parameters, consisting of coupling constants, cutoff masses and bare resonance masses and couplings, which has to be determined from a fit to experimental data. In Section 5.4 we detail our procedure to adjust these parameters. In short, the coupling constants related to background contributions are set to the values from the Jülich model (specifically from its version of Ref. [45]) while the remaining parameters are adjusted in such a way to describe the solutions of the GWU/SAID partial-wave analysis [14]. As pointed out in Refs. [12, 75], this particular analysis can be considered model independent, in contrast to those from the MAID [15] or Bonn/Gatchina [13] groups which use model-dependent parameterizations. The resulting partial-wave amplitudes are finally presented in Section 5.4.

5.2 Construction of the potential

According to the formalism presented in Section 4.3.2, the hadronic potential employed in this work consists of tree-level diagrams which can be classified into background or resonant contributions. The first include pole graphs related to the exchange of a single baryon in the intermediate state, whereas the second consist of hadron exchanges in the t- and u-channels. In this section, we show which specific diagrams are included in both background and resonant parts of the potential and explain the derivation of the corresponding amplitudes.

5.2.1 Background contributions

For reactions involving the coupled-channels πN, $\pi\Delta$ and ηN the Jülich model of Ref. [45] includes the background contributions depicted in of Fig. 5.1. As we can see in the figure, transitions between $\pi\Delta$ and ηN as well as σ-exchange in $\pi\Delta \to \pi\Delta$ and f_0-exchange in $\eta N \to \eta N$ are disregarded in the framework. In our on-shell model for meson-baryon interactions, in principle we want to employ the same set of diagrams to construct the non-resonant potential. As we shall see in this section, this will be possible for all the diagrams shown in Fig. 5.1 except however for the contribution of N-exchange to $\pi\Delta \to \pi\Delta$.

Due to Lorentz invariance and parity conservation the amplitudes related to the graphs of Fig. 5.1 admit the following parameterizations:

- For the reactions $\pi N \to \pi N$, $\pi N \to \eta N$ and $\eta N \to \eta N$

$$V^{\mathrm{NP}}_{\lambda'\lambda}\left(p',p\right) = \bar{u}_{\lambda'}\left(p'\right)\left[A\left(s,t,u\right)\mathbb{1}_4 + B\left(s,t,u\right)\frac{\not{k}+\not{k}'}{2}\right]u_{\lambda}\left(p\right)(IF), \tag{5.1}$$

- for $\pi N \to \pi\Delta$

$$V^{\mathrm{NP}}_{\lambda'\lambda}\left(p',p\right) = \bar{u}^{\mu}_{\lambda'}\left(p'\right)\gamma^5\left[A_{\mu}\left(s,t,u\right)\mathbb{1}_4 + B_{\mu}\left(s,t,u\right)\frac{\not{k}+\not{k}'}{2}\right]u_{\lambda}\left(p\right)(IF), \tag{5.2}$$

- and finally for $\pi\Delta \to \pi\Delta$

$$V^{\mathrm{NP}}_{\lambda'\lambda}\left(p',p\right) = \bar{u}^{\mu}_{\lambda'}\left(p'\right)\left[A_{\mu\nu}\left(s,t,u\right)\mathbb{1}_4 + B_{\mu\nu}\left(s,t,u\right)\frac{\not{k}+\not{k}'}{2}\right]u^{\nu}_{\lambda}\left(p\right)(IF), \tag{5.3}$$

where we use the four-momentum variables and helicity labels previously defined in Section 4.2. In the equations above, u_λ and u^μ_λ represent Dirac and Rarita-Schwinger spinors (explicit forms are given in Appendix A), whereas A and B denote Lorentz invariant functions which in general depend on the Mandelstam variables s, t and u. Moreover, to each amplitude there is an isospin factor (IF) associated, resulting from the fact that isospin symmetry is considered to be exact in this work. The isospin factors for the diagrams of Fig. 5.1 are calculated in Appendix C.

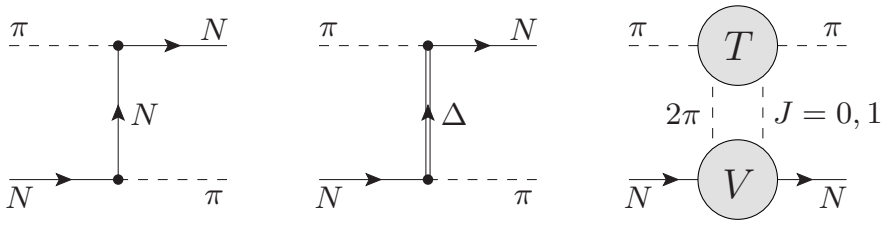

(a) Contributions to elastic πN-scattering.

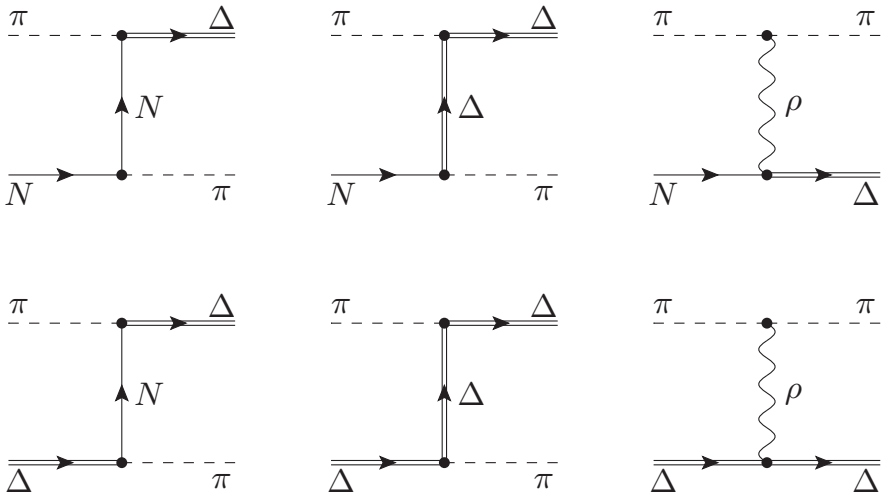

(b) Coupling to the $\pi\Delta$-channel.

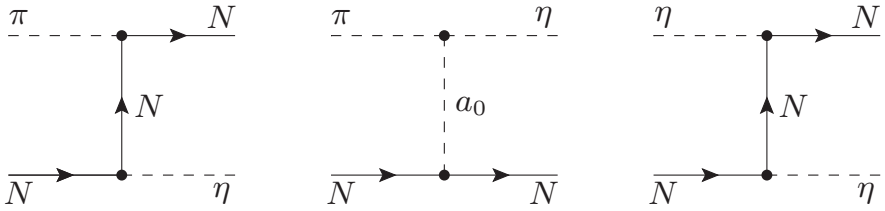

(c) Coupling to the ηN-channel.

Figure 5.1. Background contributions to the potential. Although considered in the Jülich model of Ref. [45], the contribution of N-exchange to $\pi\Delta \to \pi\Delta$ cannot be included in our on-shell approach. See text for explanation.

Table 5.1. Effective Lagrangians for background contributions.

Vertex	$\mathcal{L}_{\rm int}$
$NN\pi$	$-\frac{f_{NN\pi}}{m_\pi}\bar{N}\gamma^5\gamma^\mu\vec{\tau}\partial_\mu\vec{\pi}N$
$NN\eta$	$-\frac{f_{NN\eta}}{m_\pi}\bar{N}\gamma^5\gamma^\mu\partial_\mu\eta N$
NNa_0	$g_{NNa_0}m_\pi\bar{N}\vec{\tau}N\vec{a_0}$
$N\Delta\pi$	$\frac{f_{N\Delta\pi}}{m_\pi}\bar{\Delta}^\mu\vec{S}^\dagger\partial_\mu\vec{\pi}N+\text{H.c.}$
$N\Delta\rho$	$-i\frac{f_{N\Delta\rho}}{m_\rho}\bar{\Delta}^\mu\gamma^5\gamma^\nu\vec{S}^\dagger\left(\partial_\mu\vec{\rho}_\nu-\partial_\nu\vec{\rho}_\mu\right)N+\text{H.c.}$
$\Delta\Delta\pi$	$\frac{f_{\Delta\Delta\pi}}{m_\pi}\bar{\Delta}_\mu\gamma^5\gamma^\nu\vec{T}\partial_\nu\vec{\pi}\Delta^\mu$
$\Delta\Delta\rho$	$-g_{\Delta\Delta\rho}\bar{\Delta}_\lambda\left[\gamma^\mu-\frac{\kappa_{\Delta\Delta\rho}}{2M_\Delta}\sigma^{\mu\nu}\partial_\nu\right]\vec{\rho}_\mu\vec{T}\Delta^\lambda$
$\pi\pi\rho$	$-g_{\pi\pi\rho}\left(\vec{\pi}\times\partial_\mu\vec{\pi}\right)\vec{\rho}^{\,\mu}$
$\pi\eta a_0$	$g_{\pi\eta a_0}m_\pi\eta\vec{\pi}\vec{a_0}$

Except for correlated $\pi\pi$ exchange in elastic πN scattering (on the right in Fig. 5.1a) all the diagrams in Fig. 5.1 are evaluated using standard Feynman rules, derived from the effective Lagrangian of the Jülich model in its version of Ref. [45]. The relevant interaction terms are listed in Table 5.1 for convenience. After evaluating the graphs, partial-wave amplitudes of definite parity $\pi=(-)^{J\pm\frac{1}{2}}$ are then obtained according to the formula:

$$\left[V^{\rm NP}\right]^{J\pm}_{\lambda'\lambda}(\omega)=\frac{1}{2}\int_{-1}^{1}\mathrm{d}(\cos\bar{\theta})\Big[d^J_{\lambda\lambda'}(\bar{\theta})\left[V^{\rm NP}\right]_{\lambda'\lambda}(\omega,\bar{\theta}) \pm\eta\, d^J_{-\lambda\lambda'}(\bar{\theta})\left[V^{\rm NP}\right]_{\lambda'-\lambda}(\omega,\bar{\theta})\Big], \tag{5.4}$$

cf. Eq. (4.63), where $\omega=\sqrt{s}$ is the total energy, $\bar{\theta}$ denotes the scattering angle in the center-of-mass frame and $\eta=\eta_1\eta_2(-1)^{j_1+j_2+\frac{1}{2}}$.

In the following we proceed with further details about the correlated $\pi\pi$-exchange potential since it is derived in a distinct way. The amplitudes related to all other diagrams are presented in Appendix B. After this, we then inspect which of the contributions in Fig. 5.1 can be included in an on-shell approach as well. In fact, as one may already infer from Eq. (5.4), it will be possible to include only those diagrams whose invariant amplitudes $V^{\rm NP}_{\lambda'\lambda}(\omega,\bar{\theta})$ have no poles in the variable $z=\cos\bar{\theta}$ in the physical region above the threshold energy.

Correlated $\pi\pi$-exchange in πN scattering

In contrast to all other t-channel contributions to the potential, meson exchanges in elastic πN scattering are described in the Jülich model by correlated $\pi\pi$ exchanges in the spin $J = 0, 1$ channels. Such a description was introduced in Ref. [41] to avoid the ambiguities arising from usual σ- and ρ-meson parameterizations: In fact, a few πN models compared in that work [81–84] differ even in the sign of the σ-exchange potential, whereas the use of $\pi\pi$ exchange in a dispersion theoretical approach allows one to constrain the σ and ρ contributions from experimental data. This is evidently a desirable feature of the model, especially concerning its application in the description of final state interactions in baryon decays.

The derivation of the correlated $\pi\pi$-exchange potential (denoted by V in Fig. 5.1a) basically consists in writing dispersion relations for $\bar{N}N \to \pi\pi$ amplitudes, which are then projected on spin $J = 0, 1$ and analytically continued to the physical region of the $\pi N \to \pi N$ process. While constructing the dispersion relations, one also introduces suitable subtractions in such a way to fulfill low-energy theorems for πN scattering [85]. The procedure is explained in detail *e.g.* in Chapter 3 of Ref. [75], and leads to the invariant amplitudes

$$A^t_\sigma(t) = A_0 - 16(t - 2m_\pi^2) \times \int_{4m_\pi^2}^{\infty} \mathrm{d}\, t' \frac{\mathrm{Im}\left[f^0_+(t')\right]}{(t' - t)(t' - 4M_N^2)(t' - 2m_\pi^2)} \tag{5.5}$$

and

$$B^t_\sigma = 0 \tag{5.6}$$

in the σ-channel, where

$$A_0 = -\frac{4\pi f^0_+(2m_\pi^2)}{\frac{1}{2}m_\pi^2 - M_N^2} \tag{5.7}$$

is a constant which is treated as free parameter, and for the ρ-channel[1]

$$A^t_\rho(s,t) = i6(2s + t - 2M_N^2 - 2m_\pi^2) \times \int_{4m_\pi^2}^{\infty} \mathrm{d}\, t' \frac{\mathrm{Im}\left[\sqrt{2}\, M_N f^1_-(t') - 2f^1_+(t')\right]}{(t' - t)(t' - 4M_N^2)} \tag{5.8}$$

and

$$B^t_\rho(t) = i6\sqrt{2} \int_{4m_\pi^2}^{\infty} \mathrm{d}\, t' \frac{\mathrm{Im}\left[f^1_-(t')\right]}{t' - t}. \tag{5.9}$$

In the equations above, $f^J_\pm$ are partial-wave $N\bar{N} \to \pi\pi$ amplitudes free of kinematic singularities [86], introduced in the derivation to allow for the analytical continuation from the $N\bar{N} \to \pi\pi$ to the $\pi N \to \pi N$ reaction channel.

[1] The ρ-channel amplitudes differ from those of Ref. [75] by a factor i resulting from a different definition of isospin factors.

To evaluate the integrals in Eq. (5.5) to (5.9) we now need the imaginary parts of f_+^0 and $f_\pm^1$ given as functions of the Mandelstam variable t for $t \geq 4m_\pi^2$. In contrast to the Jülich model where these are derived from a dynamical model for $\pi\pi$ scattering [42], we choose a simpler approach and utilize parameterizations of experimental data as input. In this regard, empirical information about $N\bar{N} \to \pi\pi$ amplitudes for $t \geq 4m_\pi^2$ was obtained by Höhler and Pietarinen [87] from analytical continuation of both $\pi\pi$ and πN data. The pseudo-empirical amplitudes resulting from their analysis are shown in the graphs of Fig. 5.2.

As we can see in the figure, the imaginary part of f_+^0 is a rather broad function of the variable t, as one could expect from the large decay width the σ-meson: $\Gamma_\sigma = 400 - 700$ MeV [2]. In this case, we simply parameterize the data by fitting a polynomial

$$\mathrm{Im}[f_0^+(t)] \stackrel{!}{=} \sum_{k=0}^{m} a_k t^k. \tag{5.10}$$

The best fit was found for a polynomial of order $m = 5$ with coefficients

$$\begin{aligned} a_0 &= +0.57\,(19)\ \mathrm{GeV} & \qquad a_3 &= -1010\,(42)\ \mathrm{GeV}^{-5} \\ a_1 &= -22\,(3)\ \mathrm{GeV}^{-1} & \qquad a_4 &= +1050\,(49)\ \mathrm{GeV}^{-7} \\ a_2 &= +367\,(17)\ \mathrm{GeV}^{-3} & \qquad a_5 &= -398\,(22)\ \mathrm{GeV}^{-9}, \end{aligned} \tag{5.11}$$

merely listed here for reproducibility. The imaginary parts of $f_\pm^1$ on the other hand clearly suggest a Breit-Wigner parameterization of these amplitudes. We thus fit the imaginary part of a Breit-Wigner amplitude to the data in the $J = 1$ channel, *i.e.*

$$\mathrm{Im}[f_1^\pm(t)] \stackrel{!}{=} \alpha_\pm \frac{M_\pm^2 \Gamma_\pm^2}{M_\pm^2 \Gamma_\pm^2 + (t - M_\pm^2)^2}, \tag{5.12}$$

and thereby obtain the parameters

$$\begin{aligned} \alpha_+ &= 15.9\,(7)\ \mathrm{GeV}^{-1} & \qquad \alpha_- &= 86.1\,(8)\ \mathrm{GeV}^{-2} \\ M_+ &= 758.8\,(3)\ \mathrm{MeV} & \qquad M_- &= 753.7\,(7)\ \mathrm{MeV} \\ \Gamma_+ &= 149.0\,(11)\ \mathrm{MeV} & \qquad \Gamma_- &= 144\,(2)\ \mathrm{MeV}, \end{aligned} \tag{5.13}$$

which are in a fair agreement with the experimental (Breit-Wigner) mass and width parameters of the ρ meson: $m_\rho = 775.26\,(25)$ MeV and $\Gamma_\rho = 149.1\,(8)$ MeV [2].

The resulting parameterizations for both $J = 0, 1$ channels are depicted in Fig. 5.2 in comparison to the pseudo-empirical data from Ref. [87]. Before using these results to finally evaluate the integrals in Eq. (5.5) to (5.9), we note that these run over the variable t' until infinity and therefore have to be truncated in a numerical evaluation to a finite value $t' = t_c$. Fortunately the truncation is possible, due to the suppression factors $1/t'$ and $1/t'^2$ appearing in the integrand. Here, since we employ the pseudo-empirical data up to $40m_\pi^2$ as input to obtain the parameterizations for $\mathrm{Im}[f_+^0]$ and $\mathrm{Im}[f_\pm^1]$, the integrals are evaluated in the range from $t' = 4m_\pi^2$ to $t' = t_c = 40m_\pi^2$.

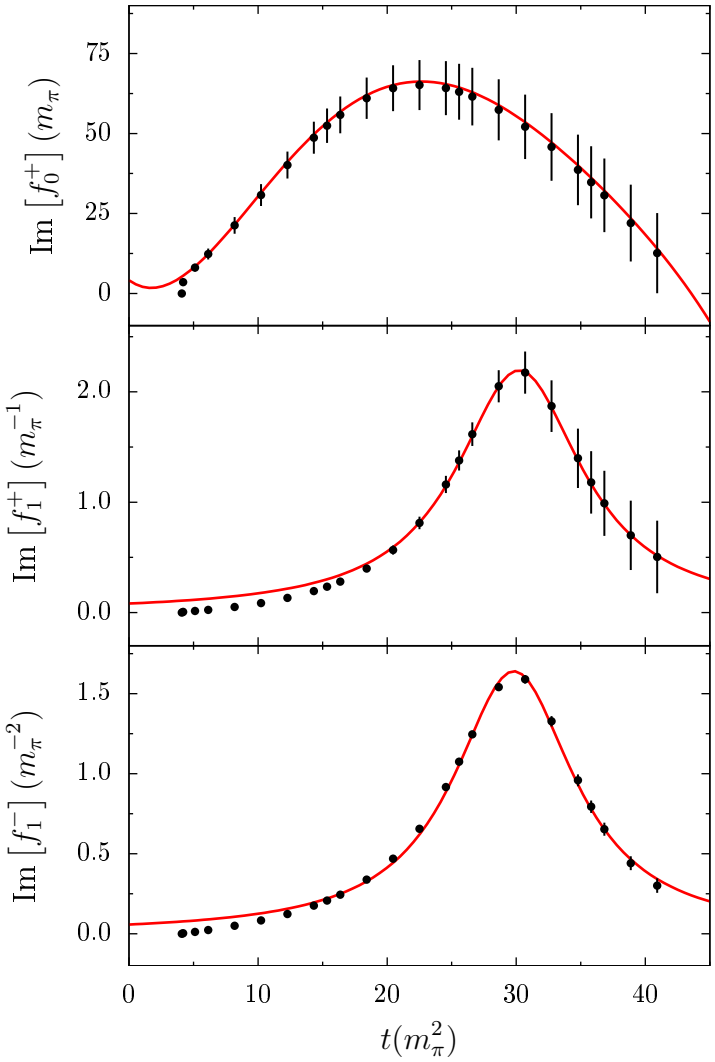

Figure 5.2. Partial-wave $\bar{N}N \to \pi\pi$ amplitudes in the $J = 0, 1$ channels. The pseudo-empirical data are from Ref. [87].

Logarithmic singularities in the partial-wave potential

After summarizing the construction of the background potential, we shall investigate which of the diagrams in Fig. 5.1 can be included in an on-shell framework. For this purpose we will show that any t- or u-channel amplitude may be considered as long as it has no poles in the physical region above the threshold energy of the corresponding process: In this instance, one easily solves the integrals in Eq. (5.4) and obtains the corresponding contribution to the partial-wave potential. If this is not the case, however, the integrals lead to logarithmic singularities in the potential which cannot be handled numerically in an on-shell approach.

To show this we consider t- and u-channel amplitudes simultaneously and denote the mass of the exchanged particle by m_x with $x = t, u$. For the masses of the initial and final states we use the same notation as in Eq. (4.1). Due to the propagator of the exchanged particle, the invariant amplitude related to a x-channel contribution has a pole at $x = m_x^2$ or, equivalently, at

$$\cos\bar{\theta} = z_0^x(\omega) = \begin{cases} \dfrac{2\omega_p\omega_{p'} - (M^2 + M'^2 - m_x^2)}{2|\mathbf{p}||\mathbf{p}'|} & \text{for } x = t \text{ and} \\ \dfrac{2\omega_p\omega_{p'} + (m^2 + m'^2 - m_x^2) - s}{2|\mathbf{p}||\mathbf{p}'|} & \text{for } x = u, \end{cases} \tag{5.14}$$

where we used Eqs. (4.31) and (4.32) to express the Mandelstam variables t and u in terms of $\cos\bar{\theta}$, $|\mathbf{p}|$ and $|\mathbf{p}'|$ and finally the energies ω_p and $\omega_{p'}$. Recall from Eqs. (4.10) and (4.11) that both ω_p and $|\mathbf{p}|$ (as well as the corresponding primed quantities) are functions of the total energy $\omega = \sqrt{s}$.

As we can see from Eqs. (5.4) and (5.14), the (on-shell) partial-wave potential can be easily evaluated as long as

$$|z_0^x(\omega)| > 1 \tag{5.15}$$

for any value of ω above threshold. Otherwise, the integrals in Eq. (5.4) have to be calculated using the formula

$$\int_{-1}^{1} \mathrm{d}\cos\bar{\theta}\, \frac{f(\omega,\bar{\theta})}{\cos\bar{\theta} - z_0^x \pm i\epsilon} = P\int_{-1}^{1} \mathrm{d}\cos\bar{\theta}\, \frac{f(\omega,\bar{\theta})}{\cos\bar{\theta} - z_0^x} \mp i\pi f(\omega,\bar{\theta}_0^x) \tag{5.16}$$

where $\bar{\theta}_0^x = \arccos z_0^x$. After integration the pole turns into logarithmic singularities at $z_0^x = \pm 1$, because for these values the pole position coincides with the limits of the principal value integral in Eq. (5.16). Such singularities are rather difficult to handle numerically since for t- and u-channel contributions the pole position depends on the energy of the process, *cf.* Eq. (5.14).

In the framework of the Jülich model this problem is treated using the method of contour rotation, as explained *e.g.* in Chapter 4 of Ref. [75]. This procedure consists in analytically continuing the singular contributions to the non-resonant potential to a region in the complex $|\mathbf{q}|$-plane where these are regular functions (q is the off-shell momentum of the exchanged particle). Following this method, the integrals appearing in off-shell scattering equations can then be evaluated by deforming the integration contour in the $|\mathbf{q}|$-plane, allowing one to obtain finite transition amplitudes despite the singularities in the underlying potential.

Such a procedure obviously cannot be applied in an on-shell framework, since the (algebraic) scattering equations of Section 4.3.4 can only be solved if the partial-wave potential is finite itself. Accordingly, we now have to inspect for which of the diagrams in Fig. 5.1 the condition (5.15) holds true. For this purpose, we plot in Fig. 5.3 the value of $|z_0^x|$ for all those contributions as a function of the total energy variable ω. The curves were evaluated using the physical masses provided by the Particle Data Group [2]. Concerning $\pi\pi$-exchanges in elastic πN-scattering, one should note that the integrands in Eqs. (5.5) to (5.9) when considered in the range from $4m_\pi^2$ to $t_c = 40m_\pi^2$ may have poles at $t = t'$. We therefore plot $|z_0^x|$ for correlated $\pi\pi$-exchanges using $m_x^2 = t'$ with t' considered within that range.

From Fig. 5.3 it turns out that among all contributions the only singular term comes from N-exchange in $\pi\Delta \to \pi\Delta$ scattering. In the present model we choose to neglect this contribution since it is the single term which violates the condition (5.15). Our procedure shall be justified later in Section 5.4, where we show that a reasonable description of experimental partial-wave $\pi N \to \pi N$ amplitudes can still be achieved nonetheless. We should mention, however, that further singular terms may arise with the inclusion of couplings to meson-baryon channels with higher thresholds.

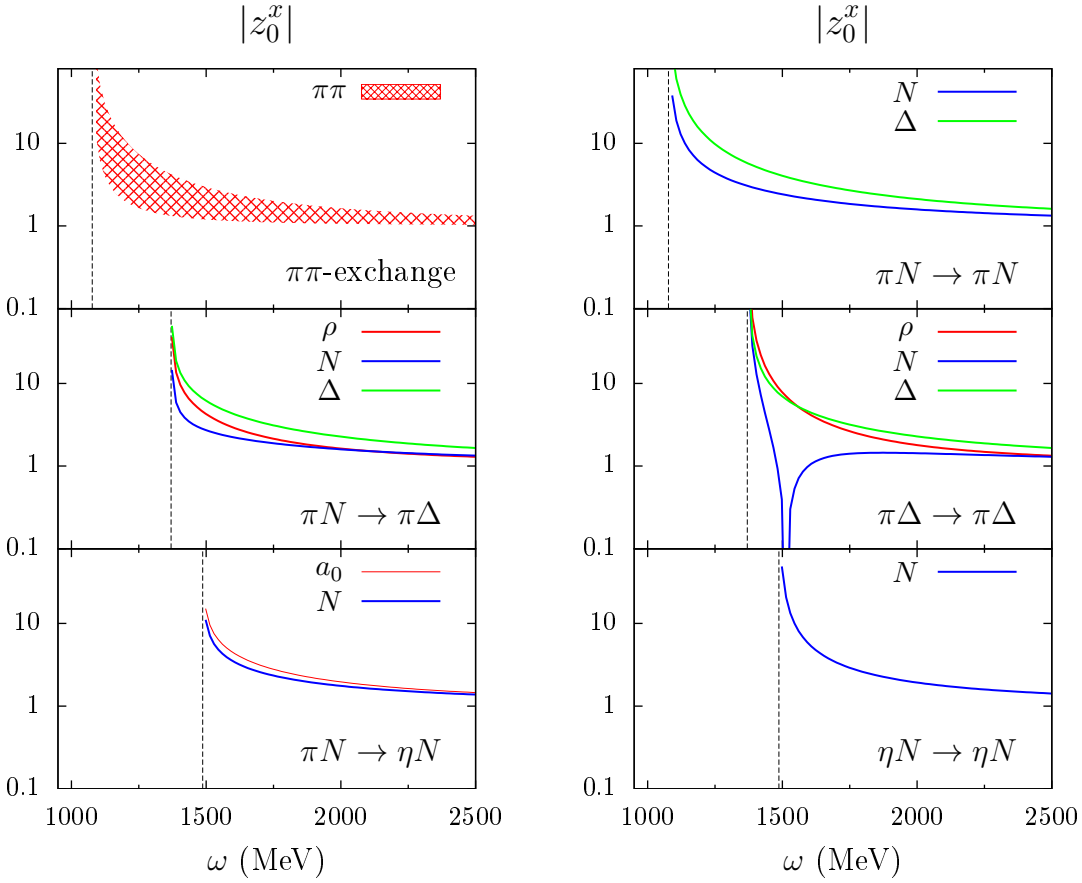

Figure 5.3. $|z_0^x(\omega)|$ (*cf.* Eq. (5.14)) for the contributions depicted in Fig. 5.1. Dashed lines indicate the threshold energy of the corresponding reaction channel.

5.2.2 Resonant contributions

As explained in Section 4.3.4, we will determine the relative signs of the bare vertex functions considered in Chapter 3 by including resonant terms in the meson-baryon potential, and then fitting the resulting unitary amplitudes to data. The purpose of doing this is to account for rescattering effects in the strong decays of low-lying N and Δ baryons, if possible for all the states listed in Tables 2.3 and 3.1. Accordingly, we shall now investigate which of those states may be included in the present framework, in which only couplings to πN, $\pi\Delta$ and ηN are taken into consideration.

For further discussion we show in Fig. 5.4 the threshold energies of strong decay channels with total strangeness $S = 0$, involving hadron ground-states only, for energy $\omega \lesssim 1720$ MeV. The values were obtained from the experimental Breit-Wigner masses given by the Particle Data Group [2]. It should be noted that some of the channels depicted in the figure, *i.e.* $\pi\Delta$, σN and ρN are not two-body channels in a strict sense, but effective parameterizations of the three-body channel $\pi\pi N$. As such, their influence extends to somewhat lower energies than the nominal thresholds indicated in the figure. This is particularly important for the effective σN channel, corresponding to $\pi\pi N$ with two pions in the scalar-isoscalar state $(\pi\pi)^{I=0}_{S\text{-wave}}$, due to the broad $\pi\pi$ mass distribution in the scalar channel (*cf.* Fig. 5.2). Here we used $m_\sigma = 500$ MeV for the mass of the σ meson.

Thus, considering the values presented in the figure, we should be able to include non-strange baryons with masses $M_R \lesssim 1700$ MeV, *i.e.* still below the ρN threshold, which do not couple too strongly to σN, to ρN itself or to the strangeness production channels $K\Lambda$ and $K\Sigma$. To find out which resonances fulfill these conditions we list the experimental Breit-Wigner widths and branching ratios of the lowest N and Δ baryons in Table 5.2 (the data are from Ref. [2]). In agreement with the data, we will not include the states $N(1720)$ and $\Delta(1700)$ since for these the experimental branching ratios into ρN are quite large. Strangeness production, on the other hand, seems to be a minor effect in strong decays of low-lying states. Concerning decays into σN, the only state coupling substantially to this channel is the $N(1710)$ which, in particular, contributes to the P_{11} partial-wave in πN scattering. In this regard, however, there is a more important issue preventing the inclusion of any P_{11} resonance as we shall see below.

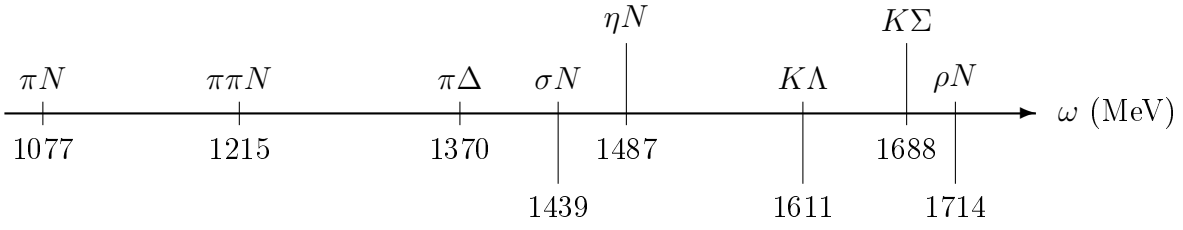

Figure 5.4. Experimental threshold energies of hadronic decay channels with total strangeness $S = 0$.

Table 5.2. Breit-Wigner widths (Γ) and branching ratios of low-lying N and Δ resonances. The data is from the Particle Data Group [2]. The states are classified by spin J, parity π and the corresponding partial-wave in πN scattering. A long dash (—-) indicates that no coupling to the channel has been observed and a blank space that the Particle Data Group gives no estimates based on the available data.

$L_{2I\,2J}$	J^π	State	Γ (MeV)	Branching ratios (%)						
				πN	$\pi\Delta$	σN	ηN	$K\Lambda$	$K\Sigma$	ρN
S_{11}	$\frac{1}{2}^-$	$N(1535)$	125 – 175	35 – 55	< 1	(2 ± 1)	(42 ± 10)	—	—	< 4
		$N(1650)$	120 – 180	50 – 90	0 – 25	< 4	5 – 15	3 – 11		4 – 12
P_{11}	$\frac{1}{2}^+$	$N(1440)$	200 – 450	55 – 75	20 – 30	10 – 20	(0.0 ± 1.0)	—	—	< 8
		$N(1710)$	50 – 250	5 – 20	15 – 40	10 – 40	10 – 30	5 – 25		5 – 25
P_{13}	$\frac{3}{2}^+$	$N(1720)$	150 – 400	8 – 14	60 – 90, P-wave		3 – 5	1 – 15		70 – 85
D_{13}	$\frac{3}{2}^-$	$N(1520)$	100 – 125	55 – 65	15 – 25	< 8	(0.23 ± 0.04)	—	—	15 – 25
		$N(1700)$	100 – 250	(12 ± 5)	10 – 90, S-wave < 20, D-wave		(0.0 ± 1.0)	< 3		< 35
D_{15}	$\frac{5}{2}^-$	$N(1675)$	130 – 165	35 – 45	50 – 60	(7 ± 3)	(0.0 ± 1.0)	< 1		$< 1 - 3$
F_{15}	$\frac{5}{2}^+$	$N(1680)$	120 – 140	65 – 70	5 – 15	(11 ± 5)	(0.0 ± 1.0)			3 – 15
S_{31}	$\frac{1}{2}^-$	$\Delta(1620)$	130 – 150	20 – 30	30 – 60	isospin violation			—	7 – 25
P_{33}	$\frac{3}{2}^+$	$\Delta(1232)$	114 – 120	100	—				—	—
		$\Delta(1600)$	220 – 420	10 – 15	40 – 70					< 25
D_{33}	$\frac{3}{2}^-$	$\Delta(1700)$	200 – 400	10 – 20	30 – 60					30 – 55

The P_{11} partial-wave in $\pi N \to \pi N$ scattering

Resonances appearing in the P_{11} wave of the πN system cannot be considered in the present model. To clarify the matter, let us introduce an alternative representation for (unitary) partial-wave $\pi N \to \pi N$ amplitudes based on the unitarity condition (4.72). It is well known that the solutions of (4.72) in the $\pi N \to \pi N$ channel can be written as (see *e.g.* the textbook [66]):

$$T^{J\pm}_{\pi N \leftarrow \pi N} = \frac{8\pi\omega}{|\mathbf{p}|}\left[\frac{\eta_{J\pm}e^{2i\delta_{J\pm}(\omega)}-1}{2i}\right] \tag{5.17}$$

where $\delta_{J\pm}$ is the phase shift and $\eta_{J\pm}$ the inelasticity parameter. The latter satisfies

$$|\eta_{J\pm}(\omega)| \leq 1 \qquad \text{and} \qquad |\eta_{J\pm}(\omega)| = 1 \text{ for } \omega < \omega_{\text{thr}} \tag{5.18}$$

where ω_{thr} denotes the threshold energy of the lowest inelastic channel coupling to the πN system. Experimentally the value of ω_{thr} might be as low as the threshold of the three-body channel $\pi\pi N$ (*cf.* Fig. 5.4), depending on the partial-wave amplitude under consideration. In a theoretical model on the other hand, it obviously depends on which channels are included in the framework.

Particularly in the current framework, we could not expect to describe $\pi N \to \pi N$ partial-waves for which $|\eta_{J\pm}| < 1$ below the $\pi\Delta$ threshold, *i.e.* for $\omega \lesssim 1370$ MeV as we use an on-shell approach. Unfortunately, this is the case of the P_{11} partial-wave: Due to the contribution of the Roper $N(1440)$ resonance, whose mass is remarkably low, inelasticity is present in this wave already closely above the $\pi\pi N$ threshold (see Fig. 5.5). In the (off-shell) framework of the Jülich model the Roper resonance is dynamically generated by non-resonant contributions only, among which the transition $\pi N \to \sigma N$ primarily leads to the correct behavior of the amplitude [21]. Here though, even if we included couplings to the σN channel, we would not be able to account for the width of the σ meson and provide inelasticity close to the $\pi\pi N$ threshold this way. For these reasons we will exclude P_{11} resonances from our analysis.

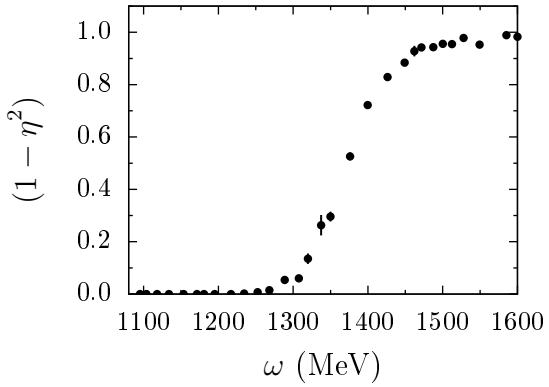

Figure 5.5. Inelasticity for the P_{11} wave in $\pi N \to \pi N$ scattering. The data are from the analysis of the GWU/SAID [14] group.

Calculation of the pole diagrams

Summarizing the former discussion, in our description of meson-baryon scattering we include bare resonant fields for the following states:

$$\begin{array}{ll} N[\frac{1}{2}^-](1535, 1650) & \\ N[\frac{3}{2}^-](1520, 1700) & \Delta[\frac{1}{2}^-](1620) \\ N[\frac{5}{2}^-](1675) \quad \text{and} & \Delta[\frac{3}{2}^+](1232, 1600), \\ N[\frac{5}{2}^+](1680) & \end{array} \tag{5.19}$$

where we use the notation $B[J^\pi](M)$ introduced in Section 2.5. The corresponding s-channel contributions, resulting from couplings to πN, $\pi\Delta$ and ηN, are depicted in the graphs of Fig. 5.6. There, it should be noted that we also include the N-pole graph in $\pi N \to \pi N$ scattering (on the right in Fig. 5.6a). Although this diagram affects the P_{11} wave only, which we exclude from our analysis, it will be considered in order to obtain at least the correct low-energy behavior of the amplitude in this wave.

As explained in Section 4.3.2, s-channel amplitudes are separable in the momenta of the scattering particles and thus completely determined by bare vertex functions. In the framework of the Jülich model these are evaluated using two distinct methods depending on the spin of the resonance: For baryons of spin $J = \frac{1}{2}$ and $\frac{3}{2}$ one applies standard Feynman rules (derived from the Lagrangian of Ref. [45]) to decay diagrams such as the graph in Fig. 5.7. The resulting bare vertices $\gamma_{\lambda\mu_R}$ can then be transformed to the $|JM_J, \lambda\pm\rangle$ basis according to

$$\gamma_\lambda^{J\pm}(\omega) = \sqrt{\frac{2J+1}{2}} \int_{-1}^{1} \mathrm{d}(\cos\bar{\theta})\, d^J_{\mu_R\lambda}(\bar{\theta})\, \gamma_{\lambda\mu_R}(\omega, \bar{\theta})(IF), \tag{5.20}$$

cf. Eq. (4.114), where μ_R and λ denote the helicity of the decaying resonance and the final meson-baryon state, respectively. Here, (IF) are isospin factors which evidently appear in resonant contributions too. For higher-spin resonances, on the other hand, one introduces phenomenological couplings

$$\gamma^{J\pm} = \left[\frac{|\mathbf{p}|}{M_{B^*}}\right]^n \gamma^{\frac{3}{2}\pm} \quad \text{with} \qquad n = \left(\frac{2J+1}{2}\right) - 2 \tag{5.21}$$

based on kinematics and parity considerations [12, 40]. Here, recall that in our notation the superscript $J\pm$ indicates that the corresponding *amplitude* has parity $\pi = (-)^{J\pm\frac{1}{2}}$, which should not be confused with the notation $B[J^\pi]$ for resonant states.

In our on-shell reduction we shall apply this method using the same underlying Lagrangian and phenomenological couplings. The relevant interaction terms are collected in Table 5.3, including the couplings to $N^*(P_{13})$ states; according to Eq. (5.21), the latter enter in the couplings to $N^*(D_{15})$. The resulting bare vertices $\gamma^{J\pm}$ are given in Appendix B and the isospin factors in Appendix C. As a final remark, the N-pole diagram will be treated in the same way as the other resonant contributions, except for the difference that the bare parameters cannot be considered as free because the (dressed) coupling $f_{N\pi\pi}$ and nucleon mass M_N are well-known physical quantities. We return to this topic later in Section 5.4.1, where we explain the method to adjust the model parameters.

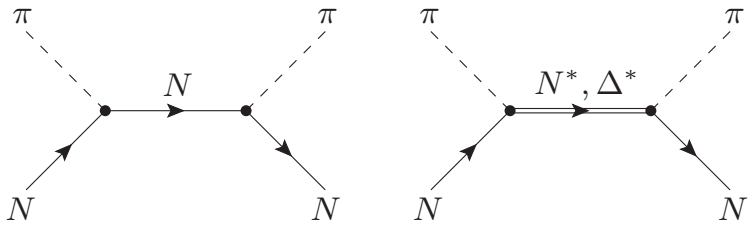

(a) Contributions to elastic πN-scattering.

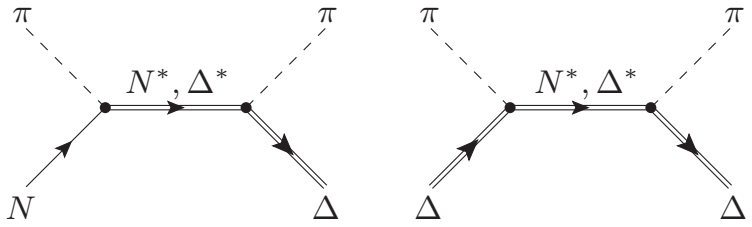

(b) Coupling to the $\pi\Delta$-channel.

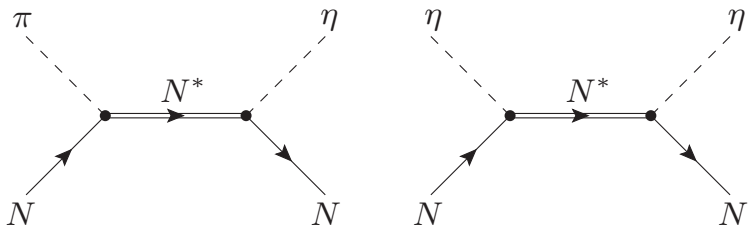

(c) Coupling to the ηN-channel.

Figure 5.6. Resonant contributions to the potential. The resonant states N^* and Δ^* included in the model are listed in (5.19).

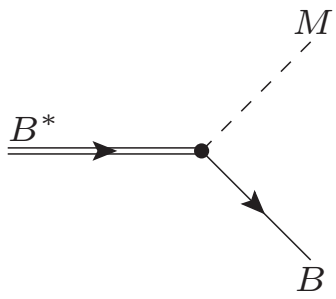

Figure 5.7. Decay of a baryon resonance $B^* = N^*$ or Δ^* into a meson-baryon state $MB \in \{\pi N, \pi\Delta, \eta N\}$ possibly coupling to the resonance.

Table 5.3. Effective Lagrangians for resonant contributions.

Vertex	$\mathcal{L}_{\text{int}}$
$N^*(S_{11})N\pi$	$\frac{f_{N^*N\pi}}{m_\pi}\bar{N}^*\gamma^\mu\vec{\tau}\partial_\mu\vec{\pi}N + \text{H.c.}$
$N^*(S_{11})N\eta$	$\frac{f_{N^*N\eta}}{m_\pi}\bar{N}^*\gamma^\mu\partial_\mu\eta N + \text{H.c.}$
$N^*(S_{11})\Delta\pi$	$\frac{f_{N^*\Delta\pi}}{m_\pi}\bar{N}^*\gamma^5\vec{S}\partial_\mu\vec{\pi}\Delta^\mu + \text{H.c.}$
$NN\pi$	(see Table 5.1)
$N^*(P_{13})N\pi$	$\frac{f_{N^*N\pi}}{m_\pi}\left(\bar{N}^*\right)^\mu\vec{\tau}\partial_\mu\vec{\pi}N + \text{H.c.}$
$N^*(P_{13})N\eta$	$\frac{f_{N^*N\eta}}{m_\pi}\left(\bar{N}^*\right)^\mu\partial_\mu\eta N + \text{H.c.}$
$N^*(P_{13})\Delta\pi$	$\frac{f_{N^*\Delta\pi}}{m_\pi}\left(\bar{N}^*\right)^\mu\gamma^5\gamma^\nu\vec{S}\partial_\nu\vec{\pi}\Delta^\mu + \text{H.c.}$
$N^*(D_{13})N\pi$	$\frac{f_{N^*N\pi}}{m_\pi^2}\bar{N}\gamma^5\gamma^\nu\vec{\tau}\partial_\nu\partial_\mu\vec{\pi}\,(N^*)^\mu + \text{H.c.}$
$N^*(D_{13})N\eta$	$\frac{f_{N^*N\eta}}{m_\pi^2}\bar{N}\gamma^5\gamma^\nu\partial_\nu\partial_\mu\eta\,(N^*)^\mu + \text{H.c.}$
$N^*(D_{13})\Delta\pi$	$i\frac{f_{N^*\Delta\pi}}{m_\pi}\left(\bar{N}^*\right)_\nu\vec{S}\gamma^\mu\partial_\mu\vec{\pi}\Delta^\nu + \text{H.c.}$
$\Delta^*(S_{31})N\pi$	$\frac{f_{\Delta^*N\pi}}{m_\pi}\bar{\Delta}^*\gamma^\mu\vec{S}^\dagger\partial_\mu\vec{\pi}N + \text{H.c.}$
$\Delta^*(S_{31})\Delta\pi$	$\frac{f_{\Delta^*\Delta\pi}}{m_\pi}\bar{\Delta}^*\gamma^5\vec{T}\partial_\mu\vec{\pi}\Delta^\mu + \text{H.c.}$
$\Delta^*(P_{33})N\pi$ $\Delta^*(P_{33})\Delta\pi$	analogous to $N\Delta\pi$ and $\Delta\Delta\pi$ (see Table 5.1)

5.3 Unitarization and scale dependence

After constructing the partial-wave potential we are now able to solve the on-shell scattering equations of Section 4.3.4, or equivalently to unitarize the full potential according to

$$T^{J\pm}(\omega) = \left[V_{\rm fin}^{J\pm\,-1}(\omega,\mu) - \left[\mathcal{G}_{\rm fin}\right](\omega,\mu)\right]^{-1} \tag{5.22}$$

(*cf.* Eq. (4.123)). In this equation, $\mathcal{G}_{\rm fin}$ is the diagonal matrix in channel space whose matrix elements are given by the finite contributions (4.115) to the meson-baryon loop integrals (4.91). In this context, μ denotes the set of renormalization scales μ_n resulting from the solution of these integrals for the meson-baryon channels n ($n = \pi N$, $\pi\Delta$ and ηN in our model). Finally, the divergent contributions to the loops were reabsorbed in the potential $V_{\rm fin}$ (*cf.* Eqs. (4.121) to (4.123)) which therefore depends on μ.

That said, we recall from Section 4.3.3 that the scale dependence was introduced in $V_{\rm fin}$ in such a way to formally obtain a scale-independent $T^{J\pm}$-matrix from (5.22). This would be the case if it was possible to evaluate Eq. (5.22) from the underlying interactions order-by-order in perturbation theory. However, in any explicit model for hadronic scattering, the potential has to be truncated to a finite set of contributions and therefore such a cancellation cannot be exact. As a result, a residual scale dependence in the $T^{J\pm}$-matrix should be expected, reflecting the influence of higher-order diagrams not included in the potential.

In the present model where we include lowest-order diagrams only, the potential does not even depend on the scale. A common method to introduce scale dependence in a tree-level potential V is by inserting form factors in the corresponding matrix elements, *i.e.*

$$\left[V_{\rm fin}\right]^{J\pm}_{\lambda'\lambda}(\omega,\mu) \equiv F(\omega,\Lambda)\left[V\right]^{J\pm}_{\lambda'\lambda}(\omega), \tag{5.23}$$

which depend on cutoff mass parameters Λ. Here we shall use the same form factors as in Ref. [45], which depend on the type of contribution as presented below:

- For the pole graphs the form factors are given by

$$F(p',p) = \left(\frac{\Lambda^4 + M_R^4}{\Lambda^4 + (\omega_{p'} + \omega_{k'})^4}\right)^{n'} \left(\frac{\Lambda^4 + M_R^4}{\Lambda^4 + (\omega_p + \omega_k)^4}\right)^{n} \tag{5.24}$$

  and are normalized at the position of the resonance. We choose $n, n' = 1$ when the particles couple to the resonance in S or P waves and $n, n' = 2$ when they couple in D or F waves.

- For t- and u-channel diagrams we employ conventional monopole ($n = 1$) and dipole ($n = 2$) form factors at each vertex, *i.e.*

$$F(q) = \left(\frac{\Lambda^2 - m_x^2}{\Lambda^2 + |\mathbf{q}|^2}\right)^{n} \tag{5.25}$$

  where m_x and $\mathbf{q}$ denote the mass and the three-momentum of the exchanged particle, respectively. A dipole type is used whenever ρ or Δ are present at the vertex and a monopole type is used otherwise.

- One exception to the previous case is the N-exchange in $\pi N \to \pi N$, for which the monopole form factor is modified to

$$F(q) = \frac{\Lambda^2 - M_N^2}{\Lambda^2 - ((M_N^2 - m_\pi^2)/M_N)^2 + |\mathbf{q}|^2}. \tag{5.26}$$

  This choice ensures that the N-pole and N-exchange contributions to $\pi N \to \pi N$ cancel each other at the Cheng-Dashen point as required by low-energy theorems for πN scattering [85].

- Another exception is the correlated $\pi\pi$-exchange potential, which is multiplied by the form factor

$$F(p', p) = \frac{\Lambda^2}{\Lambda^2 + |\mathbf{p}'|^2} \frac{\Lambda^2}{\Lambda^2 + |\mathbf{p}|^2}. \tag{5.27}$$

The cutoff masses Λ are treated as free parameters in the model and will be adjusted to data for $\pi N \to \pi N$ partial-wave amplitudes. These have values of a typical hadronic scale (of the order of 1 GeV) and are understood as a parameterization of the unknown high-momentum physics disregarded in lowest-order interactions at low energies.

Now, apart from the potential the finite parts of the loop integrals in Eq. (5.22) also depend on the renormalization scales μ_n. Although the scale dependence in both these quantities should be in principle treated simultaneously, this is not possible in the our framework because Eq. (5.22) is not an integral but an algebraic, on-shell approximated scattering equation. On the other hand, it would not be consistent to treat both the scales and the cutoffs as independent free parameters, since these are correlated in some way we cannot investigate here. Therefore we here proceed as follows: Firstly all the regularization scales are fixed to some mass parameter of the order of hadronic masses, say

$$\mu_n \stackrel{!}{=} \mu_0 \sim 1 \text{ GeV} \qquad \text{with} \qquad n = \pi N, \pi\Delta, \eta N, \tag{5.28}$$

using the same value of μ_0 for all possible $\pi N \to \pi N$ partial-waves, and only then the cutoff masses from the form factors are adjusted to experimental data. In this respect, small changes in the scale μ_0 should correspond to slight variations in the cutoffs so the result remains approximately the same regardless a particular choice for μ_0.

5.4 Partial-wave πN amplitudes

In this section we finally present the results of our model for partial-wave $\pi N \to \pi N$ amplitudes in the energy range from πN threshold up to $\omega = 1700$ MeV. To obtain the model parameters we specifically adjust the *normalized* amplitudes

$$\mathcal{T}^{J\pm} := \frac{|\mathbf{p}|}{8\pi\omega} T^{J\pm}_{\lambda'\lambda} \qquad \text{with} \qquad \lambda = \lambda' = (\pi N)_{+1/2} \tag{5.29}$$

to data, where $T^{J\pm}_{\lambda'\lambda}$ are the partial-wave amplitudes of parity $\pi = (-)^{J\pm\frac{1}{2}}$ defined in the helicity basis $|JM_J, \lambda\pm\rangle$, *cf.* Eqs. (4.53) to (4.56). Concerning definition (5.29), we recall from Section 4.2.3 that due to parity invariance it is sufficient to consider positive-helicity states only.

Table 5.4. Equivalence between πN partial-wave amplitudes given in the $L_{2I\,2J}$ representation and in the helicity basis.

Spin	Parity	$L_{2I\,2J}$	$\mathcal{T}^{J\pm}$
$\frac{1}{2}$	-	S_{11}, S_{31}	$\mathcal{T}^{\frac{1}{2}+}$
$\frac{1}{2}$	+	P_{11}, P_{31}	$\mathcal{T}^{\frac{1}{2}-}$
$\frac{3}{2}$	+	P_{13}, P_{33}	$\mathcal{T}^{\frac{3}{2}+}$
$\frac{3}{2}$	-	D_{13}, D_{33}	$\mathcal{T}^{\frac{3}{2}-}$
$\frac{5}{2}$	-	D_{15}, D_{35}	$\mathcal{T}^{\frac{5}{2}+}$
$\frac{5}{2}$	+	F_{15}, F_{35}	$\mathcal{T}^{\frac{5}{2}-}$

Experimental information about the πN amplitudes is provided by partial-wave analyses of meson scattering and production data, see for instance Refs. [13–16]. Following the Jülich model we utilize the GWU/SAID solutions [14] as input to determine the parameters. Before proceeding with the fit, we should mention that the GWU/SAID solutions are given for partial-wave amplitudes in the usual $L_{2I\,2J}$ representation (where L is the orbital angular momentum of the πN system) and not for helicity amplitudes $\mathcal{T}^{J\pm}$ as evaluated here. Nonetheless, a one-to-one relation exists between both representations because in the former the amplitudes are uniquely determined by the total angular momentum J and parity $\pi = (-1)^{L+1}$. It is thus unnecessary to perform a change of basis before adjusting our amplitudes to the GWU/SAID data. For convenience, we show the correspondence between the amplitudes in Table 5.4 as written in both bases up to angular momentum $J = 5/2$.

5.4.1 Parameters and fitting strategy

The potential constructed in Section 5.2 and the subsequent unitarization procedure lead to a set of parameters which we categorize as follows:

(I) The hadron masses from the propagators in t- and u-channel exchanges and the effective coupling constants from the non-resonant Lagrangian of Table 5.1,

(II) the subtraction constant A_0 from correlated $\pi\pi$ exchanges in the $J = 0$ channel (defined in Eq. (5.7) but treated here as a free parameter as in Ref. [45]),

(III) a set of cutoff masses and the renormalization scale μ_0 from unitarization of the non-resonant contributions,

(IV) the bare masses and couplings from the resonant Lagrangian of Table 5.3 and cutoff masses related to pole contributions.

The parameters will be fixed following the same order they appear in the categories above. We chose to start with the parameters related to non-resonant contributions, *i.e.* those collected in (I) to (III), because in contrast to bare resonance parameters the former affect all partial-waves in πN scattering. Note that once the background is fixed by experimental data it is much simpler to fit each resonant amplitude to the single partial-wave it contributes to, which motivates the method applied here.

Regarding the set included in (I), the hadron masses appearing in t- and u-channel amplitudes are fixed to the physical values provided by the Particle Data Group [2], more specifically to averages over the masses of the possible charge (or isospin) states of each particle. The effective coupling constants from the non-resonant Lagrangian, in turn, are all set to the values of the Jülich model of Ref. [45] and references therein. From background contributions the only parameters considered as free in our model are those included in (II) and (III), *i.e.* the subtraction constant A_0, the regularization scale μ_0 and finally the cutoff masses related to t- and u-channel amplitudes. These are here adjusted by hand, in such a way to provide a reasonable description of the background in all partial-waves simultaneously.

The constant A_0 influences predominantly the S_{11} and S_{31} waves in πN scattering (specially the low-energy region close to the πN threshold) and is therefore adjusted to these both S waves. Concerning the regularization scale μ_0, the background in all partial-waves can be reasonably described as long as its value is around the physical mass of the ρ meson ($m_\rho \approx 770$ MeV [2]). For values of μ_0 below 600 MeV or above 900 MeV, on the other hand, the low-energy behavior of the S_{31} wave is no longer in agreement with the data. For this reason we choose the value $\mu_0 = 700$ MeV.

At this point we shall adjust the cutoff parameters from t- and u-channel hadron exchanges. In this procedure, considering independent cutoff values for each vertex in the graphs of Fig. 5.1 would be in principle possible (*cf.* Ref. [45]), however at the expense of a large set of free parameters. It turns out though that a quite small set of cutoff parameters influence our results considerably, namely the cutoff masses from the correlated $\pi\pi$-exchange and N-exchange potentials in elastic πN scattering. Apart from these, a fine tunning of cutoff parameters could improve the description of the data in detail, but with a minor influence in the overall behavior of the amplitudes. Here, since our purpose is to obtain a simple description of the rescattering matrix in strong decays, to reduce the number of parameters we employ the same cutoff value for diagrams related to the exchange of the same particle (*e.g.* $\Lambda = \Lambda^u_\Delta$ for all Δ-exchange diagrams an so on). The only exception is the cutoff related to N exchange in $\pi N \to \pi N$, which is set separately as in this case the form factor is also given by a different expression (*cf.* Eqs. (5.25) and (5.26)).

The final background parameters are given in Table 5.5, as well as the reference from which we take either the parameter value or the experimental data as applicable. The coupling constants f and g from the non-resonant Lagrangian are there expressed as $\tilde{f} = f^2/(4\pi)$ and $\tilde{g} = g^2/(4\pi)$, merely to utilize the same notation as in Ref. [45]. Regarding the cutoff masses shown in the table, one should note that in most cases we restricted ourselves to values from 1100 MeV up to 1500 MeV, *i.e.* values in line with typical hadron scales as previously discussed in Section 5.3. For Δ exchange however we utilize a somewhat higher cutoff of 1700 MeV.

The last step now is to adjust those parameters collected in (IV) consisting of bare resonance masses and couplings as well as cutoff masses related to pole diagrams. As mentioned before, in contrast to the background (whose parameters were adjusted by hand) each resonant amplitude contributes to a single partial-wave only and therefore the fitting procedure in this case can be easily performed numerically. The resulting parameters for resonant contributions are presented in Table 5.6 and details on the numerical fit are given below.

Table 5.5. Model parameters for background contributions.

Parameter		Value	Ref.
Masses (MeV)	m_π	138	Experimental values from PDG [2]
	m_η	548	
	m_ρ	769	
	m_{a_0}	983	
	M_N	939	
	M_Δ	1232	
Couplings $\left(\tilde{f} = \frac{f^2}{4\pi}\right)$	$\tilde{f}_{NN\pi}$	0.0778	Jülich model of Ref. [45]
	$\tilde{f}_{NN\eta}$	0.00934	
	$\tilde{f}_{N\Delta\pi}$	0.36	
	$\tilde{f}_{N\Delta\rho}$	20.45	
	$\tilde{f}_{\Delta\Delta\pi}$	0.252	
	$\tilde{g}_{\Delta\Delta\rho}$	4.69	
	$\tilde{g}_{\pi\pi\rho}$	2.9	
	$\sqrt{\tilde{g}_{NNa_0}\tilde{g}_{\pi\eta a_0}}$	8.0	
	$\kappa_{\Delta\Delta\rho}$	6.1	
Sub. constant (MeV^{-1})	A_0	0.006	Adjusted to the solutions from the GWU/SAID analysis [14]
Cutoffs (MeV)	$\Lambda^t_{\pi\pi}$ $(J=0)$	1100	
	$\Lambda^t_{\pi\pi}$ $(J=1)$	1350	
	Λ^u_N $(\text{in } \pi N \to \pi N)$	1100	
	Λ^u_N $(\text{in other processes})$	1400	
	Λ^u_Δ	1700	
	Λ^t_ρ	1350	
	$\Lambda^t_{a_0}$	1300	
Reg. scale (MeV)	μ_0	700	

Table 5.6. Model parameters for resonant contributions. The states are classified by spin J, parity π and the corresponding partial-wave in πN scattering.

$L_{2I\,2J}$	J^π	State	Bare mass (MeV)	f_{MBB^*}			Cutoff (MeV)
				πN	$\pi\Delta$	ηN	
S_{11}	$\frac{1}{2}^-$	$N(1535)$	1596	0.094	−2.817	0.485	1800
		$N(1650)$	1668	0.270	6.101	0.171	1800
D_{13}	$\frac{3}{2}^-$	$N(1520)$	1516	0.090	−0.684	0.084	2200
		$N(1700)$	1834	0.021	−0.583	0.090	2200
D_{15}	$\frac{5}{2}^-$	$N(1675)$	1668	0.674	−2.215	0.517	2200
F_{15}	$\frac{5}{2}^+$	$N(1680)$	1676	0.176	−1.533	0.051	2000
S_{31}	$\frac{1}{2}^-$	$\Delta(1620)$	1586	0.209	−5.509	isospin violation	1800
P_{33}	$\frac{3}{2}^+$	$\Delta(1232)$	1265	1.879	—		1500
		$\Delta(1600)$	1622	−0.350	1.106		1800

While fitting resonant amplitudes the cutoff masses were allowed to vary between 1800 and 2200 MeV. The only exception is the cutoff related to the Δ-pole diagram, which had to be lowered to 1500 MeV so that we could describe the P_{33} partial-wave. In comparison to the cutoff masses used for background contributions (see Table 5.5), here we use higher cutoffs because the form factor (5.24) for pole diagrams falls off rapidly even for such large values [75]. In addition, the cutoff parameters given in Table 5.6 are in line with the general value of 2000 MeV utilized in the Jülich model for all resonant terms [40, 45].

By default we adopt positive bare coupling constants and use negative couplings when required by experimental data only. Using the GWU/SAID solutions for partial-wave $\pi N \to \pi N$ amplitudes allows one to uniquely determine the sign (and also obtain the strength) of the couplings to the πN and $\pi\Delta$ channels. At this point, we should mention that it is possible to find an unique solution as long as the resonance does not couple too strongly to ρN. This is in fact the reason why we excluded the $N(1720)$ and $\Delta(1700)$ states from our analysis: Although it is possible to roughly describe the data in the corresponding P_{13} and D_{33} waves, we could not find a single solution which definitely leads to the best results.

Now concerning the couplings to the ηN channel, most of the resonances listed in (5.19) couple very weakly to this state (*cf.* also Table 5.2). As a result the description of the $\pi N \to \pi N$ amplitudes should not depend too much on the corresponding bare couplings, and we indeed obtain different fits which are equally good regardless the sign of these constants. As expected the only exceptions are the S_{11} resonances, whose decay widths into ηN are relatively large. Here, to introduce an additional constraint, we employ the solutions from the Bonn/Gatchina partial-wave analysis for the reaction $\pi N \to \eta N$ [13, 88]. It is important to emphasize that we do not perform a numerical fit to their results, but only use their data to determine the sign of the couplings to the ηN channel. Please note that obtaining the signs of bare vertex functions is actually the reason why we include resonant contributions in our πN model.

Finally, before we proceed with the results of the model some remarks about the calculation of the N-pole diagram are in order. As mentioned before, this contribution can be evaluated in the same fashion as the other resonant terms, but here the bare mass and coupling constant cannot be treated as free parameters. In the Jülich model the bare parameters for this contribution are fixed in such a way to obtain the physical values of $f_{NN\pi}$ and M_N after unitarization [40, 45]. Here, since P_{11} resonances are excluded from our analysis anyway, we simply set the bare parameters to their physical values from the beginning and then adjust the corresponding cutoff mass Λ_N^s to describe the low-energy behavior of the amplitude in this wave. The best value found in this procedure was

$$\Lambda_N^s = 1550 \text{ MeV}. \tag{5.30}$$

5.4.2 Results for background amplitudes

Our results for background contributions to partial-wave $\pi N \to \pi N$ amplitudes in the isospin channels $I = \frac{1}{2}$ and $\frac{3}{2}$ are presented in Figs. 5.8 and 5.9, respectively. In these graphs we also compare our amplitudes to the GWU/SAID solutions and to the non-resonant amplitudes from the Jülich model of Ref. [45][2]. According to these results, despite the on-shell approximation, the exclusion of the N-exchange diagram in the $\pi\Delta \to \pi\Delta$ potential and finally the reduced coupled-channel basis (in contrast to that model we disregard couplings to σN and ρN), a reasonable agreement between both models was achieved for most partial-waves up to $J = \frac{5}{2}$ within the energy range under consideration. As expected the only exception is the P_{11} partial-wave, because in the Jülich model the Roper resonance $N(1440)$ is dynamically generated by non-resonant interactions involving the coupling to an (off-shell) σN state [21]. Considering all other partial-waves, the two models differ for higher energies only and not in the overall behavior of the amplitudes.

Regarding the P_{11} amplitude as shown in Fig. 5.8 the contribution of the N-pole diagram was already included in the result, without which it would not be possible to describe the low-energy behavior of the real part of the amplitude. In this partial-wave one observes a large attraction for energies close to the position of the Roper $N(1440)$, which results from the correlated $\pi\pi$-exchange potential in the $J = 1$ channel [75]. In fact, this contribution almost provides sufficient strength for the dynamical generation of the resonance, but it is only from the coupling to the σN channel that the correct resonant behavior appears in the P_{11} wave [21].

In conclusion, given the reasonable agreement between our results and those from the Jülich model, we consider our on-shell reduction to be a good parameterization for rescattering effects in strong decays of N and Δ baryons, excluding decays of P_{11} resonances. From the behavior of the P_{13} and D_{33} amplitudes we see that the $N(1720)$ and $\Delta(1700)$ states, respectively contributing to these partial waves, could be included in our model as well. However, since here we are interested not only in describing the partial waves but also in obtaining the sign of the bare vertex functions as precisely as possible, including these two states (which couple too strongly to the ρN channel) would not be meaningful in this context.

[2] In this reference the partial-waves are given in terms of phase shifts $\delta_{J\pm}$ and inelasticities $\eta_{J\pm}$, see definitions in Section 5.2.2.

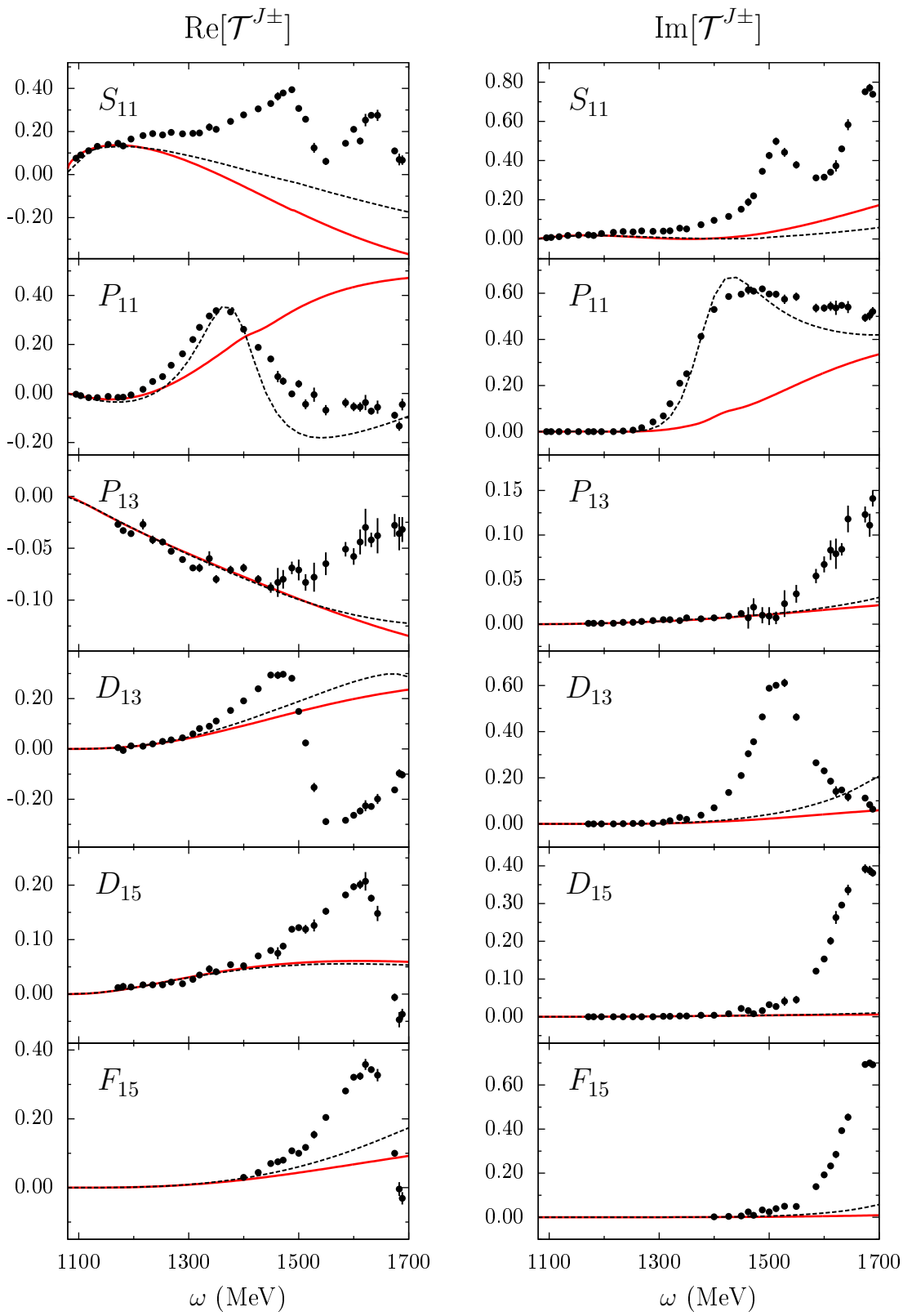

Figure 5.8. Background contributions to partial-wave $\pi N \to \pi N$ amplitudes of isospin $I = 1/2$. Full red lines indicate the results of our model and black dashed lines the results of the Jülich model of Ref. [45]. The data points are the solutions of the GWU/SAID partial-wave analysis for the full amplitude [14].

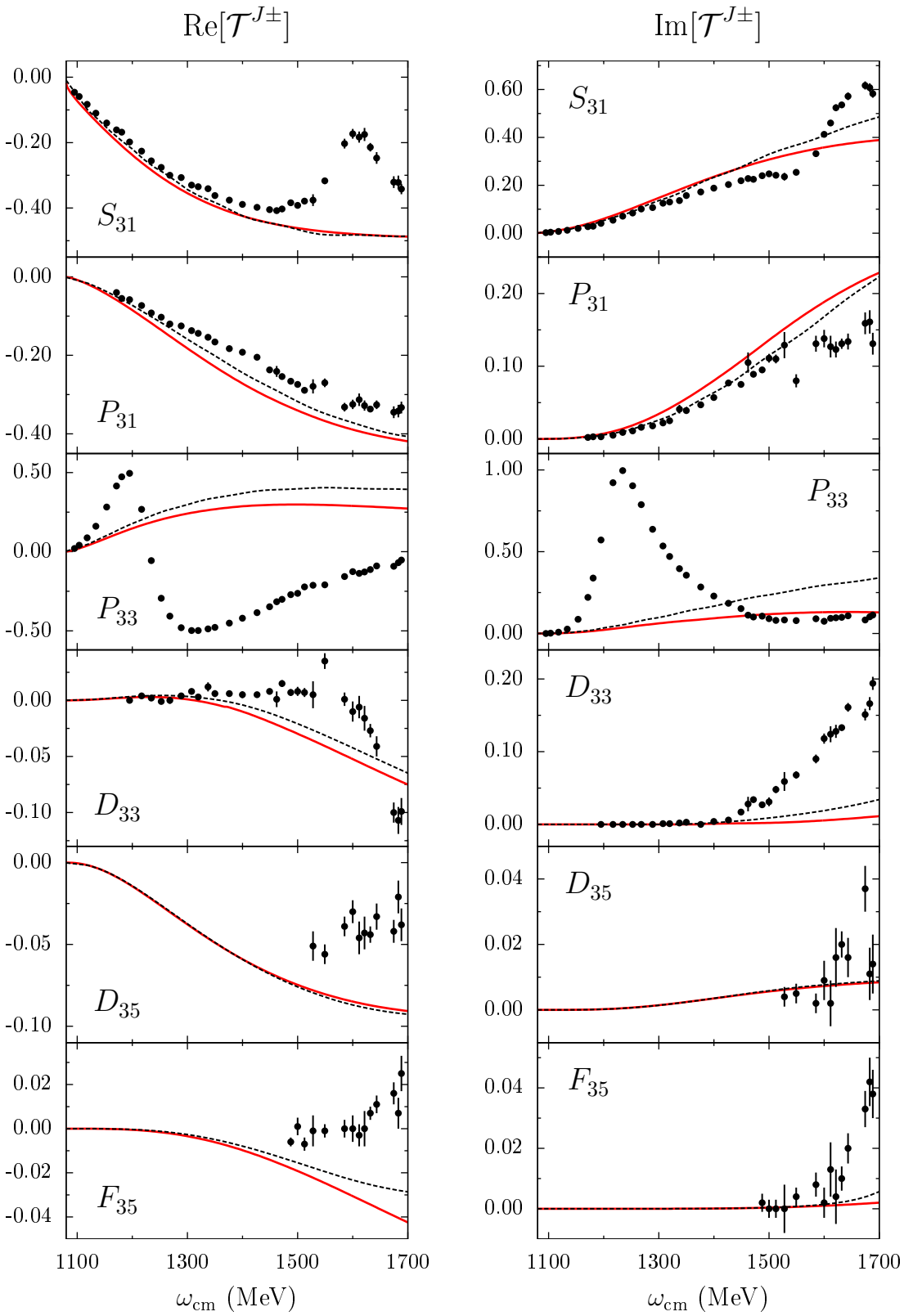

Figure 5.9. Background contributions to partial-wave $\pi N \to \pi N$ amplitudes of isospin $I = 3/2$. The notation is the same as in Fig. 5.8.

5.4.3 Results for the full model

Finally, our results for the full partial-wave $\pi N \to \pi N$ amplitudes given in comparison to the data points from the GWU/SAID analysis are presented in Figs. 5.10 and 5.11, for isospin $I = \frac{1}{2}$ and $\frac{3}{2}$ respectively. As one can see in these graphs, we could achieve a very good description of the data in all partial-waves for which we included resonant contributions, in particular for the D_{13}, D_{15} and F_{15} waves in the N sector and the P_{33} wave in the Δ sector. For the S_{31} wave the model slightly differs from the data, but the overall description of the amplitude is still very good. For the corresponding S_{11} wave in the N sector, on the other hand, the difference between model and data is somewhat larger in the energy region of the second resonance $N(1650)$. This effect can be traced back to the calculated background amplitude in this wave, for which (apart from the P_{11} wave) we found the largest discrepancy between our approach and the amplitudes from the Jülich model (*cf.* Fig. 5.8 and 5.9).

As mentioned before, we utilize the solutions of the Bonn/Gatchina partial-wave analysis to constraint the signs of the bare couplings to the ηN channel. According to Ref. [88] the Bonn/Gatchina analysis leads to two different classes of solutions, called BG2011-01 and BG2011-02, which basically differ in the number and properties of some positive-parity N resonances at masses above 1900 MeV. Within each class a number of different solutions is also found in their analysis, which for the $\pi N \to \eta N$ reaction channel lead to the boundaries depicted in Fig. 5.12. In our model, we adjust the sign of the bare ηN couplings to qualitatively describe the boundaries related to BG2011-01 solutions (the resulting amplitudes are also presented in Fig. 5.12) for the reasons we explain below. We emphasize that the results are here considered to be qualitatively good if the signs of the corresponding amplitudes agree with those from the Bonn/Gatchina solutions.

On the one hand, the magnitude of the ηN couplings to the $N(1520)$ and $N(1720)$ states could be adjusted to roughly describe both classes of solutions for the D_{13} wave, provided these coupling constants are positive. For the F_{15} wave, on the other hand, we are able to describe both classes of solutions for the real but not for the imaginary part of the amplitude, whose negative sign close to the ηN threshold and subsequent change of sign at higher energies, occurring in both solutions, cannot be accounted for in our model. In this case we thus choose a positive coupling to the $N(1680)$ state, in order to at least describe the real part of this amplitude. Finally, in contrast to the partial waves discussed above, just the BG2011-01 solutions for the D_{15} wave can be depicted in our model, using for this a positive coupling to the $N(1675)$ resonance. This is the reason why we choose this class of solutions to determine the couplings to all partial waves or, more specifically, to first adjust the ηN couplings to data, fix the signs as explained above and then use the magnitude as input parameter for the fit to the $\pi N \to \pi N$ partial-waves from the GWU/SAID analysis.

Although the agreement with the $\pi N \to \eta N$ data is just qualitative the method above does constraint the signs of the bare ηN couplings to D_{13}, D_{15} and F_{15} states, which would not be possible from a fit to $\pi N \to \pi N$ amplitudes alone. We recall that the procedure is not necessary for S_{11} resonances as these substantially decay into the ηN channel (see Table 5.2). In this sense, the description of the S_{11} wave in $\pi N \to \eta N$ scattering as shown in Fig. 5.12 consists of a pure prediction of the model.

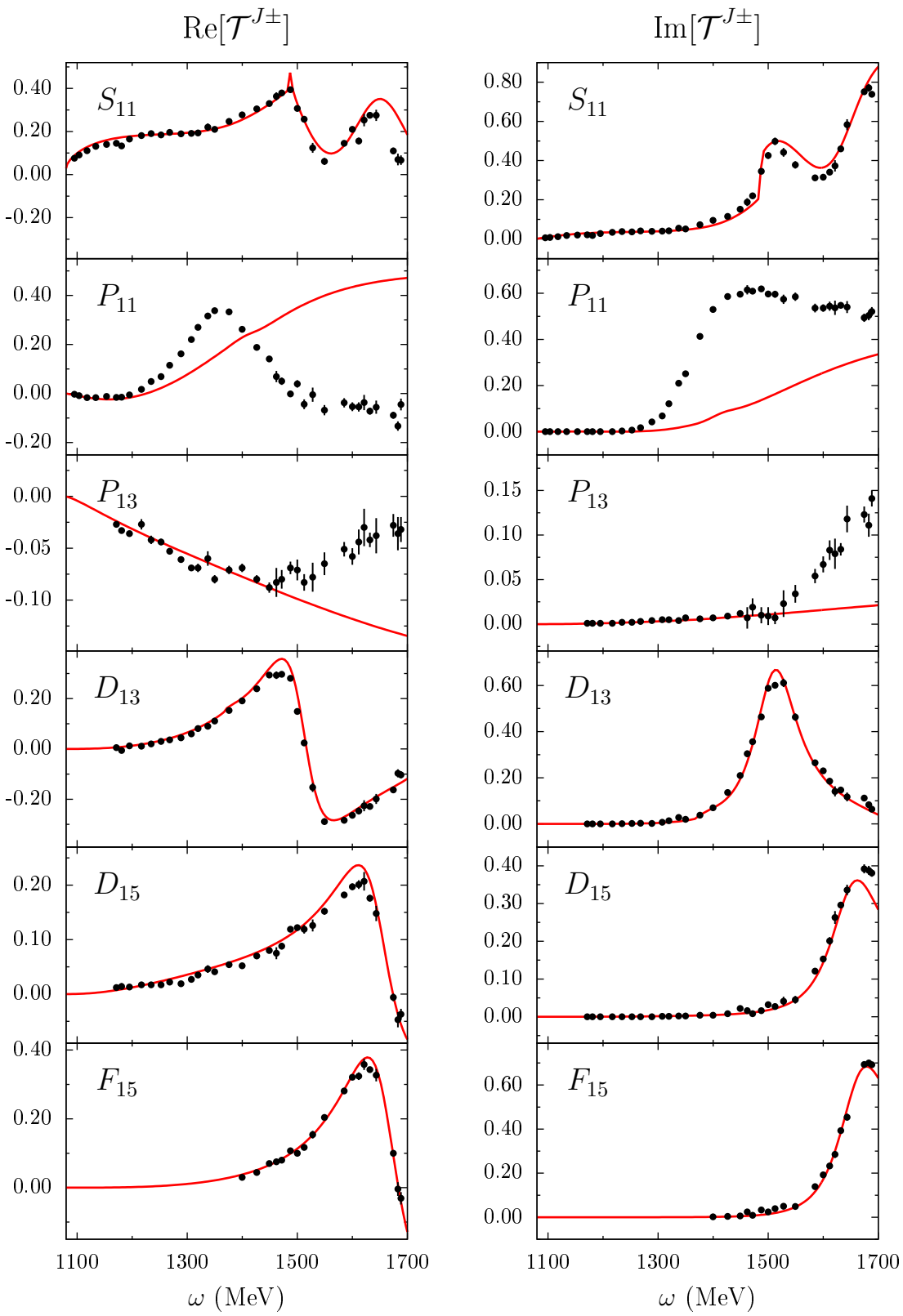

Figure 5.10. Full model results for partial-wave $\pi N \to \pi N$ amplitudes of isospin $I = 1/2$. The data points are the same as in Fig. 5.8.

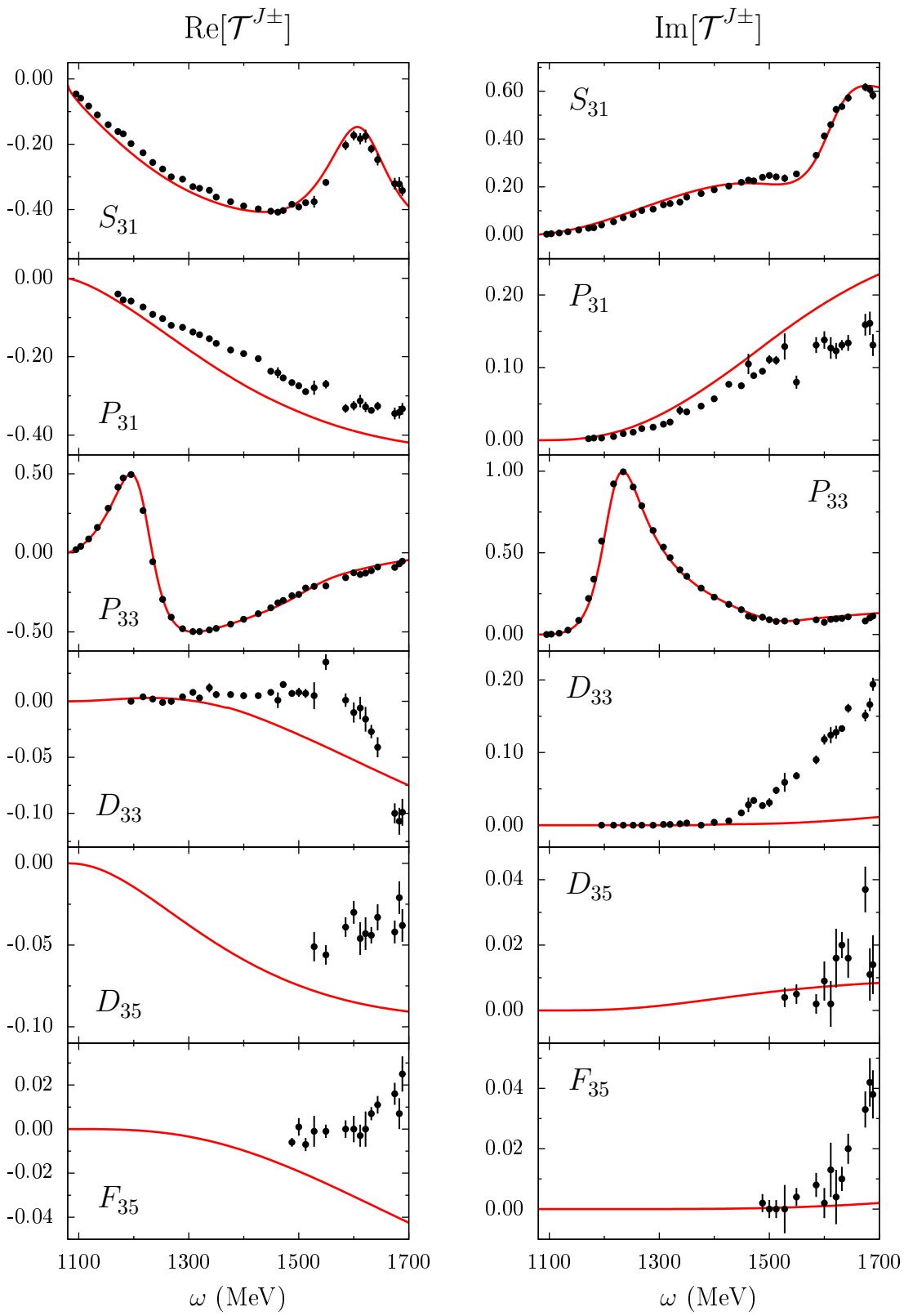

Figure 5.11. Full model results for partial-wave $\pi N \to \pi N$ amplitudes of isospin $I = 3/2$. The data points are the same as in Fig. 5.8.

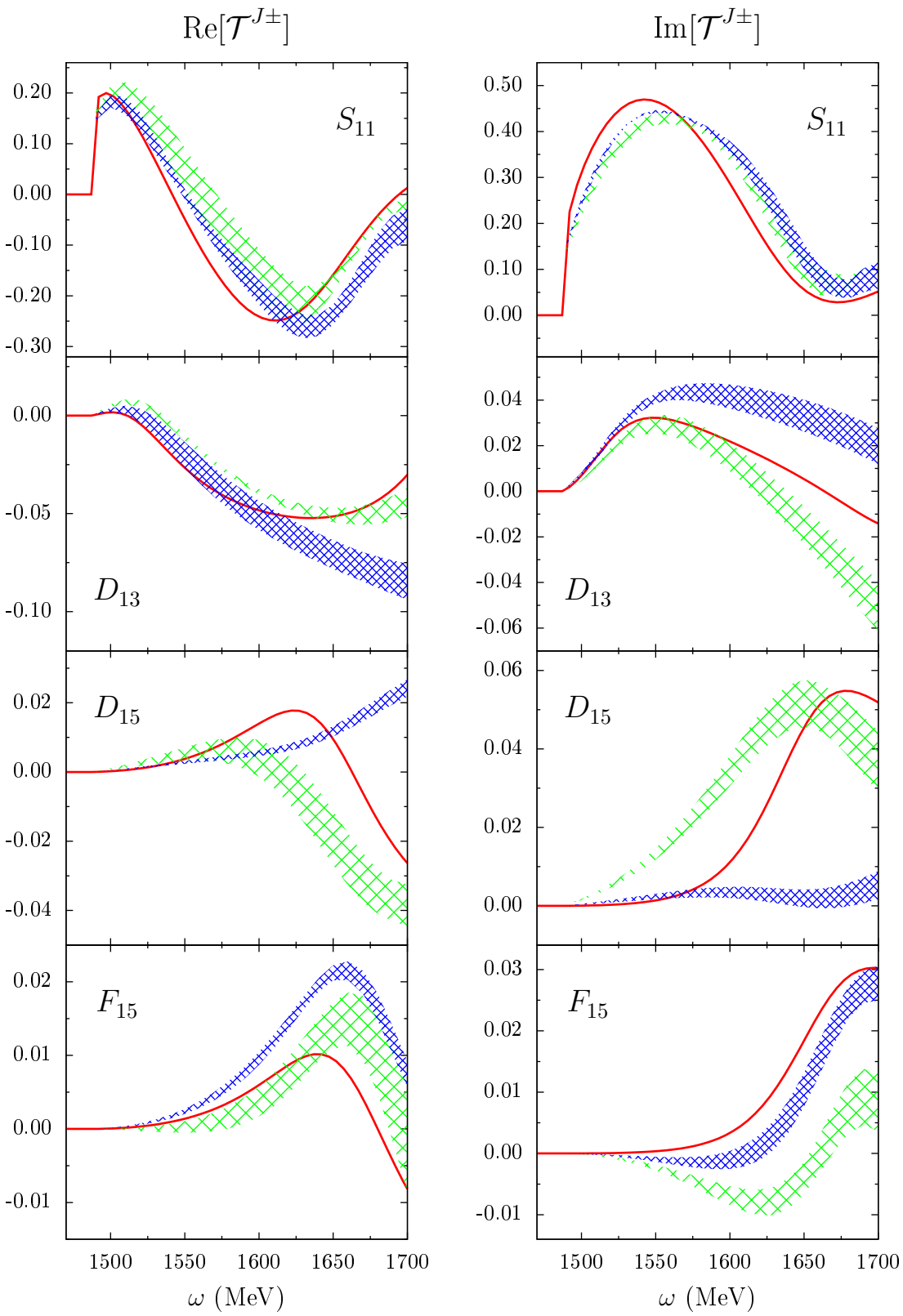

Figure 5.12. Full model results for partial-wave $\pi N \to \eta N$ amplitudes which couple to isospin $I = 1/2$ only. The boundaries are from the solutions BG2011-01 (green) and BG2011-02 (blue) of the Bonn/Gatchina partial-wave analysis [88].

5.5 Summary

In this chapter we implemented a coupled-channel model for meson-baryon scattering, including the πN, ηN and $\pi\Delta$ channels. The model was based on an on-shell reduction of the Jülich model in the version of Ref. [45], which besides the channels above also includes σN and ρN. Despite the on-shell approximation and the exclusion of the σN and ρN channels, our results for background $\pi N \to \pi N$ amplitudes turned out to be quite similar to those of Ref. [45], within the energy range from πN threshold up to $\omega \approx 1700$ MeV and for most partial waves with total angular momentum $J \leq \frac{5}{2}$.

The only exception is unfortunately the P_{11} partial-wave. Due to the contribution of the very low Roper resonance $N(1440)$ to this wave, inelasticity is present already at energies closely above the $\pi\pi N$ threshold. Whereas in the Jülich model this effect is parameterized by non-resonant interactions involving an (off-shell) σN state, which eventually leads to the dynamical generation of the Roper resonance, our formulation lacks a mechanism to account for inelasticity at such low energies. Consequently we are not able to describe the non-resonant amplitude in this wave, which represents the major drawback of the present on-shell approach.

Our purpose was to provide a suitable parameterization for final state interactions in the strong decays of low-lying N and Δ baryons (as described in the quark model of Chapters 2 and 3) as well as to determine the sign of the bare couplings to the channels included here (which cannot be done directly from the quark model). Given the reasonable description of non-resonant $\pi N \to \pi N$ amplitudes, we could achieve a very good agreement with experimental data in all partial waves for which we included resonant contributions, namely the S_{11}, D_{13}, D_{15} and F_{15} waves in the N sector and the S_{31} and P_{33} waves in the Δ sector. Accordingly we are now able to investigate rescattering effects in the strong decays of all low-lying N and Δ baryons which couple to the πN system in these partial waves.

Chapter 6

Final state interactions in strong baryon decays

6.1 Introduction

At this point, we finally use the model of Chapter 5 to include final state rescattering in the strong decays depicted in Chapter 3. The calculational procedure was detailed in Section 4.4 and consists of evaluating baryon dressed vertices Γ_{λ_n} from

$$\Gamma^{J\pm}(\omega = M, \mu) = \Big[I - (V^{\rm NP})^{J\pm}(\omega = M, \mu)\, \mathcal{G}(\omega = M, \mu) \Big]^{-1} \gamma^{J\pm}(\omega = M), \tag{6.1}$$

in terms of which the corrected decay widths are then given by

$$\Gamma_{\rm corr}(\mu) := \sum_{\lambda_n} \frac{|\mathbf{p}_n|}{8\pi M^2} \left| \Gamma^{J\pm}_{\lambda_n}(\omega = M, \mu_n) \right|^2 . \tag{6.2}$$

For the decays into a specific helicity-channel state λ_n, we define (corrected) partial decay widths by

$$\left[\Gamma_{\rm corr}\right]_{\lambda_n}(\mu) := \frac{|\mathbf{p}_n|}{8\pi M^2} \left| \Gamma^{J\pm}_{\lambda_n}(\omega = M, \mu) \right|^2 , \tag{6.3}$$

such that

$$\Gamma_{\rm corr}(\mu) = \sum_{\lambda_n} \left[\Gamma_{\rm corr}\right]_{\lambda_n}(\mu). \tag{6.4}$$

Here, $\mathbf{p_n}$ is the relative momentum between the final (asymptotic) meson and baryon states, $V^{\rm NP}$ is the non-resonant meson-baryon potential constructed in Section 5.2.1 and γ are the bare vertex functions calculated from Eq. (3.20) in the relativistic quark model. The baryon masses M at which these equations are evaluated are also taken from the latter framework, *cf.* Chapter 2. As discussed before, the relative signs of the various γ-matrix elements cannot be directly determined from Eq. (3.20) and are thus fixed to those obtained from the meson-baryon model by fitting resonant amplitudes to data. Finally, μ denotes the set of renormalization scales of the scalar loop integrals $\mathcal{G}_n$, which were all fixed to the same value $\mu_n \stackrel{!}{=} \mu_0 = 700$ MeV in such a way to describe non-resonant contributions to several $\pi N \to \pi N$ waves simultaneously.

The results of the procedure above for the decays of low-lying N and Δ baryons (*i.e.* those listed in Table 5.6 only) into πN, $\pi\Delta$ and ηN are presented in Section 6.2. According to Eq. (6.3) the corrected widths were obtained from

$$[\Gamma_{\rm corr}]_{\pi N}(\mu) := \frac{|\mathbf{p}_{\pi N}|}{8\pi M^2}\left|\Gamma^{J\pm}_{\pi N_{+1/2}}(\omega = M,\mu)\right|^2 \tag{6.5}$$

and similarly for ηN, while for decays into $\pi\Delta$ we employed

$$[\Gamma_{\rm corr}]_{\pi\Delta}(\mu) := \frac{|\mathbf{p}_{\pi\Delta}|}{8\pi M^2}\left(\left|\Gamma^{J\pm}_{\pi\Delta_{+1/2}}(\omega = M,\mu)\right|^2 + \left|\Gamma^{J\pm}_{\pi\Delta_{+3/2}}(\omega = M,\mu)\right|^2\right) \tag{6.6}$$

since both helicity $\pi\Delta_{+1/2}$ and $\pi\Delta_{+3/2}$ states contribute to the latter. Unfortunately, it turns out that the method does not improve the description of strong decay widths at all: After inclusion of rescattering effects, the values are roughly the same for the decays into πN and ηN and considerably smaller than before for most of the decays into $\pi\Delta$. In view of the good description for non-resonant $\pi N \to \pi N$ amplitudes as achieved in Chapter 5 (see Figs. 5.8 and 5.9), such results suggest that the problem lies in the quark-model description of strong baryon decays.

As a matter of fact, it has been argued (see resonances review of the Particle Data Group in [2]) that unitarity imposes different constraints over transition amplitudes and dressed vertex functions: Whereas the imaginary part of a partial-wave T-matrix is proportional to its square (*cf.* Eq. (4.72)), the unitarity relation for a dressed vertex Γ is linear:

$$i\left[(\Gamma^{J\pm}) - (\Gamma^{J\pm})^*\right] = \rho\left[(T^{\rm NP})^{J\pm}\right]^\dagger \Gamma^{J\pm} \tag{6.7}$$

where ρ is the phase-space matrix defined in (4.70). Consequently, decay widths as calculated here are model dependent – as it could be inferred from the μ-dependence in definition (6.1) –, which becomes an issue especially in our approach where bare vertex functions are evaluated in one model and the rescattering matrix in another. In fact, it is well-known that masses and decay widths of resonances are more properly defined in terms of the poles $\sqrt{s_R} = M_R - i\Gamma_R/2$ appearing in the unphysical sheets of an analytic transition matrix, while partial decay widths are evaluated from the corresponding residua at these poles [46].

In principle, it would be possible to determine the poles of the transition matrix from the relativistic quark model by deriving the meson-baryon potential (or at least its resonant part) directly in that framework; the method is sketched in Appendix D. After unitarization, the approach would allow one to define baryon properties from the poles and residua of the resulting transition matrix instead of the phenomenological definitions for baryon masses (see Chapter 2) and corrected decay widths utilized here, even if the non-resonant potential was still taken from the model of Chapter 5. Such a self-consistent calculation, in which contributions to baryon masses and decay widths are considered simultaneously, could lead to different results for the corrected decay widths. It is however unclear if such a method could be implemented numerically, since in the quark model the evaluation of bare vertices at a single energy value is already a very computer-demanding task. Moreover, regardless the method we define the corrected decay widths, the present results strongly indicate that the quark-model

couplings of baryon excitations to strong decay channels are much too small and should be improved before any further investigation on the issue.

In this context, a possible modification in the relativistic quark model was already pointed out in Chapter 2: As shown by Lucha and Schöberl in Ref. [55], there for the case of mesons only, the reduction of the Bethe-Salpeter to the Salpeter equation as performed in Section 2.2.4 is also possible with full quark propagators as long as these are considered to be instantaneous in the hadron rest frame, in the same fashion as the underlying quark interactions. We recall that in our quark model we parameterized the full propagators by their usual free forms with poles at constituent quark masses. Such a modification would introduce more freedom in the framework without changing the underlying instanton-based interactions, perhaps allowing for a better description of strong decay couplings this way. In Section 6.3 we shall shortly comment about this possibility and its effects in the description of strong decays.

6.2 Results and discussion

Before proceeding with the results, let us first inspect to which extent the πN, $\pi\Delta$ and ηN threshold energies as calculated in the quark model differ from the corresponding experimental values. The former are obtained from the ground-state masses given in Table 2.3 and Eq. (2.128) and the latter from the empirical masses provided by the Particle Data Group [2]. For convenience, all these values are collected in Table 6.1, from which we see that the difference between theoretical and experimental thresholds is rather small and never larger then 40 MeV.

Next, we investigate if such differences would considerably affect the non-resonant potential we employ to parameterize rescattering in baryon decays. For this purpose we evaluate the background $\pi N \to \pi N$ amplitudes using two distinct parameter sets: Firstly with the parameters of Table 5.5 and then with the N, Δ, π and η masses set to the corresponding quark-model values. It turns out that in both cases the amplitudes are almost the same, with the most noticeable difference being for the S_{11} partial-wave (shown in Fig. 6.1 as an example). Hence, to evaluate the non-resonant potential V^{NP} and then the corrected decay widths using Eqs. (6.1), (6.5) and (6.6), we simply set the ground-state N, Δ, π and η masses to the values from the quark model.

Finally, the results of the calculation are presented in Table 6.2, in comparison to the widths without final state interactions and also to the experimental values from the review of the Particle Data Group [2]. Recall from Section 3.3 that we call empirical data the product between branching ratios and total Breit-Wigner widths as estimated in their review, considered within the corresponding experimental uncertainties. As we can see from these results, the decay widths into πN and ηN remain basically unchanged after inclusion of rescattering effects; the only significant correction was obtained for the width of the $\Delta(1232)$ resonance which decays into πN only. On the other hand, the corrected widths for the decays into $\pi\Delta$ turn out to be much smaller than before for most of the states considered in this work, specially for the decay of the $N(1700)$ resonance. This latter example shows that final state interactions might lead to very large corrections in strong decays of baryons (at least concerning decays into $\pi\Delta$) although the effect is the opposite of what we initially expected.

Table 6.1. Quark-model thresholds for the πN, $\pi\Delta$ and ηN channels compared to the experimental values [2] (PDG). Baryon (meson) masses and thresholds are denoted by M (m) and $\omega_{\rm thr}$, respectively. All the values are given in MeV.

Channel	PDG			Quark Model			$\lvert\omega_{\rm thr}^{\rm Q.M.} - \omega_{\rm thr}^{\rm PDG}\rvert$
	M	m	$\omega_{\rm thr}$	M	m	$\omega_{\rm thr}$	
πN	939	138	1077	945	139	1084	7
$\pi\Delta$	1232	138	1370	1262	139	1401	31
ηN	939	548	1487	945	503	1448	39

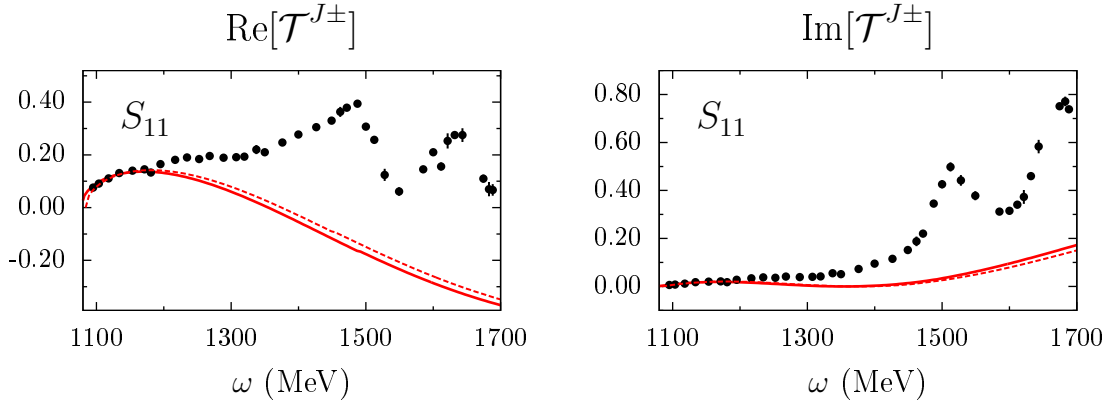

Figure 6.1. Background contributions to the S_{11} $\pi N \to \pi N$ wave as calculated in the model of Chapter 5, using the empirical threshold energies (dashed lines) and those from the quark model (full lines). The data are the same as in Fig. 5.8.

Table 6.2. Strong decay widths of low-lying N and Δ baryons into πN, $\pi\Delta$ and ηN. The quark-model predictions with and without rescattering effects ($\Gamma_{\rm corr}$ and Γ_0, respectively) are compared to the estimates from the Particle Data Group [2] (PDG). A long dash (—) indicates that the decay is kinematically forbidden.

$L_{2I\,2J}$	J^π	Label	$\Gamma_{\pi N}$ (MeV)			$\Gamma_{\pi\Delta}$ (MeV)			$\Gamma_{\eta N}$ (MeV)		
			Γ_0	$\Gamma_{\rm corr}$	PDG	Γ_0	$\Gamma_{\rm corr}$	PDG	Γ_0	$\Gamma_{\rm corr}$	PDG
S_{11}	$\frac{1}{2}^-$	$N(1535)$	32	31	44 – 97	0	1	0 – 2	—	—	40 – 91
		$N(1650)$	3	3	60 – 162	5	0	0 – 45	0	0	6 – 27
D_{13}	$\frac{3}{2}^-$	$N(1520)$	35	36	55 – 81	58	34	15 – 31	0	0	0
		$N(1700)$	0	0	7 – 43	104	3	10 – 225, S-wave < 50, D-wave	1	1	0 – 3
D_{15}	$\frac{5}{2}^-$	$N(1675)$	3	3	46 – 74	35	30	65 – 99	6	6	0 – 2
F_{15}	$\frac{5}{2}^+$	$N(1680)$	35	34	78 – 98	5	4	6 – 21	3	3	0 – 1
S_{31}	$\frac{1}{2}^-$	$\Delta(1620)$	4	3	26 – 45	73	19	39 – 90	isospin violation		
P_{33}	$\frac{3}{2}^+$	$\Delta(1232)$	63	75	114 – 120	—	—	—			
		$\Delta(1600)$	15	13	22 – 105	3	4	88 – 294			

6.3 Further developments

Since the outcome of our investigations shows no improvement in the quark-model description of strong decays, we now wish to discuss a possible modification in that framework which might lead to better results. For this purpose, let us return to the derivations in Chapters 2 and 3 and recall that, firstly in the calculation of hadron spectra, (I) the underlying quark interactions were assumed to be instantaneous in the hadron rest frame and (II) full quark propagators were parameterized by their usual free forms

$$S_F^i(p_i) \stackrel{!}{=} \frac{i}{\not{p}_i - m_i + i\epsilon} = i\left[\frac{\Lambda_i^+(\mathbf{p}_i)}{p_i^0 - \omega_i(\mathbf{p}_i) + i\epsilon} + \frac{\Lambda_i^-(\mathbf{p}_i)}{p_i^0 + \omega_i(\mathbf{p}_i) - i\epsilon}\right]\gamma^0 \tag{6.8}$$

(*cf.* Eq. (2.84)) with poles at constituent quarks m_i. Concerning strong baryon decays, (III) the bare vertex functions were evaluated in lowest-order (quark-loops) only, due to the impossibility of implementing higher-order terms from the underlying instanton interactions numerically (see Appendix B of Ref. [39]). In this respect, however, we recall that instanton interactions are highly selective in flavor space and, among the processes considered in this thesis, affects decays into ηN only. Therefore, including higher-order terms in the expansion of the strong decay kernel would not change the results for decays into πN and $\pi\Delta$.

Whereas approximations (I) and (III) consist of truncating the infinite series in the corresponding interaction kernels, as usual in phenomenological descriptions of hadron properties, approximation (II) is in conceptual inconsistency with the picture of quarks being confined in hadronic states. As pointed out in Ref. [55], in quantum field theory quark propagators (*i.e.* two-point Green's functions) are connected to other Green's functions describing quark interactions via Dyson-Schwinger equations. Accordingly, the propagators and interaction kernels in the Bethe-Salpeter equation could not in principle be chosen independently of each other, as it was done in Chapter 2.

On the other hand, we recall that the free-quark approximation was employed in the framework to allow for analytic integration over relative energy variables and also introduce some projection properties, which ultimately enable the formulation of the Bethe-Salpeter equation as an equivalent eigenvalue problem (*cf.* Sections 2.2.4 and 2.3.4 for the procedure in the case of quark-antiquark and three-quark bound states, respectively). In this regard, however, Lucha and Schöberl demonstrated [55] (there for quark-antiquark states only) that this derivation is also possible with full quark propagators, as long as these – in consonance with approximation (I) – are assumed to be instantaneous in the hadron rest frame. Their argument lies on the fact that exact quark propagators

$$S_F^i(p_i) = \frac{iZ_i(p_i^2)}{\not{p}_i - M_i(p_i^2) + i\epsilon} \tag{6.9}$$

may be recast in a form which is similar to (6.8) by neglecting the p_i^0-dependence of the two Lorentz-scalar functions $Z_i(p_i^2)$ and $M_i(p_i^2)$ in the hadron rest frame, *i.e.*

$$\begin{matrix} Z_i(p_i^2) \stackrel{!}{=} Z_i(\mathbf{p}_i^2) \\ M_i(p_i^2) \stackrel{!}{=} M_i(\mathbf{p}_i^2) \end{matrix} \quad \text{for} \quad \bar{P} =: \begin{pmatrix} M \\ \mathbf{0} \end{pmatrix} \tag{6.10}$$

where $\bar{P}$ denotes the total four-momentum of the hadron. In this instance, one may define new projection operators

$$\tilde{\Lambda}_i^{\pm}(\mathbf{p}_i) := \frac{\tilde{\omega}_i(\mathbf{p}_i) I \pm \tilde{H}_i(\mathbf{p}_i)}{2\tilde{\omega}_i(\mathbf{p}_i)} \tag{6.11}$$

in terms of single-quark energies

$$\tilde{\omega}_i(\mathbf{p}_i) := \sqrt{|\mathbf{p}_i|^2 + M_i^2(\mathbf{p}_i^2)} \tag{6.12}$$

and generalized Dirac Hamiltonians

$$\tilde{H}_i(\mathbf{p}_i) := \gamma^0 \left(\gamma \cdot \mathbf{p}_i + M_i(\mathbf{p_i})\right) \tag{6.13}$$

– see Eqs. (2.39) to (2.41) for the corresponding definitions in the free-quark case –, such that the exact propagator can finally be expressed in the form of

$$S_F^i(p_i) = i Z_i(\mathbf{p}_i^2) \left[\frac{\tilde{\Lambda}_i^+(\mathbf{p}_i)}{p_i^0 - \tilde{\omega}_i(\mathbf{p}_i) + i\epsilon} + \frac{\tilde{\Lambda}_i^-(\mathbf{p}_i)}{p_i^0 + \tilde{\omega}_i(\mathbf{p}_i) - i\epsilon} \right] \gamma^0, \tag{6.14}$$

which features similar pole structure and projection properties as Eq. (6.8). Thus, the reduction from the Bethe-Salpeter to the Salpeter equation with (instantaneous) full propagators proceeds in the same way as in Chapter 2, and for quark-antiquark bound states one ends up with [55]

$$\begin{aligned} \Phi(\mathbf{p}) = &- \frac{Z_1(\mathbf{p}_1^2) Z_2(\mathbf{p}_2^2)}{M - \omega_1 - \omega_2} \tilde{\Lambda}_1^+(\mathbf{p}) \gamma^0 \left[\int \frac{\mathrm{d}^3 p'}{(2\pi)^3} V^{(2)}(\mathbf{p}, \mathbf{p}') \Phi(\mathbf{p}') \right] \gamma^0 \tilde{\Lambda}_2^-(-\mathbf{p}) \\ &+ \frac{Z_1(\mathbf{p}_1^2) Z_2(\mathbf{p}_2^2)}{M + \omega_1 + \omega_2} \tilde{\Lambda}_1^-(\mathbf{p}) \gamma^0 \left[\int \frac{\mathrm{d}^3 p'}{(2\pi)^3} V^{(2)}(\mathbf{p}, \mathbf{p}') \Phi(\mathbf{p}') \right] \gamma^0 \tilde{\Lambda}_2^+(-\mathbf{p}) \end{aligned} \tag{6.15}$$

for the Salpeter amplitudes Φ, where $p = (p_1 - p_2)/2$. The derivation for three-quark states was not performed in Ref. [55] but should be possible within the same method.

Based on the former discussion, we finally inspect the consequences of using full propagators for the description of strong baryon decays. To this end we recall that strong decay widths were calculated in Chapter 3 from the vertex functions

$$\begin{aligned} \gamma_{\bar{P}\bar{K}\leftarrow\bar{Q}} \approx 3 \int &\frac{\mathrm{d}^4 p_\xi}{(2\pi)^4} \frac{\mathrm{d}^4 p_\eta}{(2\pi)^4} \bar{\Gamma}_{\bar{P}} \left(p_\xi, p_\eta + \tfrac{2}{3}\bar{K}\right) \\ &\times S_F^1 \left(\tfrac{1}{3} M_R + p_\xi + \tfrac{1}{2} p_\eta\right) \otimes S_F^2 \left(\tfrac{1}{3} M_R - p_\xi + \tfrac{1}{2} p_\eta\right) \\ &\otimes S_F^{\bar{q}} \left(\tfrac{1}{3} M_R + p_\eta - \bar{K}\right) \bar{\Gamma}_{\bar{K}} \left(\tfrac{1}{3} M_R - p_\eta - \tfrac{1}{2}\bar{K}\right) \\ &\otimes S_F^q \left(\tfrac{1}{3} M_R - p_\eta\right) \Gamma_{M_R}(p_\xi, p_\eta), \end{aligned} \tag{6.16}$$

cf. Eqs. (3.20) and (3.22), in which the amputated Bethe-Salpeter amplitudes Γ are determined from Salpeter amplitudes according to Eqs. (3.16) and (3.18). From the expression above, it is clear that extending the formalism in the way explained in this section would lead to different results for strong decay widths, as in this case both propagators and amputated amplitudes (via Salpeter amplitudes) would depend on the functions $Z_i(\mathbf{p}_i^2)$ and $M_i(\mathbf{p}_i^2)$.

To close the discussion, we emphasize that using full propagators in the relativistic quark model not only opens the possibility for a better description of strong decays: It also improves the framework conceptually since both quark propagators and interaction kernels would be treated in the same instantaneous approximation. Another interesting point to be mentioned is that, as discussed in Section 2.5, the light-flavored meson and baryon spectra could not be described within the same set of constituent quark-mass parameters yet. We remind the reader that the constituent masses in the model for mesons have been readjusted to those from the model for baryons, in order to enable the calculation of bare vertex functions as in Eq. (6.16). In this respect, extending the framework as suggested here allows for the investigation of this latter issue as well.

6.4 Summary

In this chapter we concluded our investigation of rescattering effects in strong decays of baryon resonances as depicted in the quark model. Unfortunately, the results show no improvement in the theoretical decay widths: In the only case where final state interactions lead to sizable corrections, *i.e.* decays into the $\pi\Delta$ channel, the widths turn out to be even smaller than before. In view of these results we closed the chapter with a suggestion for a possible extension of the framework, based on the reduction of the Bethe-Salpeter to the Salpeter equation with full quark propagators, which in line with the underlying quark interactions are assumed to be the instantaneous in the hadron rest frame. Such a modification would improve the model conceptually and, in addition, might lead to a better description of strong baryon decays.

Chapter 7

Summary and outlook

The aim of this work was to investigate the effect of final state interactions in strong two-body decays of baryons, specifically in the way these are described in Ref. [39], *i.e.* on the basis of the relativistic constituent quark model of Refs. [23–30]. For this purpose we limited the scope of our study to strong decays of low-lying N and Δ resonances (with masses $M \lesssim 1700$ MeV) into the πN, $\pi\Delta$ and ηN channels, which should form a sufficiently large basis to estimate the effect of (coupled-channel) rescattering.

In Chapter 2 we reviewed the quark-model framework, in which meson and baryon resonances are described by the solutions of the corresponding fermion-antifermion and three-fermion Bethe-Salpeter equations, taken in instantaneous approximation and with effective free-quark propagators. Based on the general structure of the empirical light-flavored hadron spectrum, the interaction kernels were there parameterized by a confinement potential supplemented by a residual spin- and flavor-dependent force motivated by instanton effects. The results for N and Δ resonances and for π and η mesons were presented in this chapter, showing that the model accounts for the gross features observed in the non-strange baryon spectra, *e.g.* Regge trajectories $M^2 \propto J$ and mass splittings between octet and decuplet states, and also for the $\pi - \eta$ splitting in the pseudoscalar meson sector. In particular the masses of the low-lying N and Δ states (whose decays were investigated in this thesis) are properly described, with a deviation between theoretical and experimental values of at most 110 MeV.

As any constituent quark model, in the high-energy sector of the baryon spectrum the model above leads to theoretical states whose experimental counterparts have not been observed, the so-called missing resonances. In this context, the investigation of strong decays is mandatory, as baryon resonances are detected in meson-production experiments and thus only observed if they couple to the measured decay channels. The description of strong two-body decays of baryons within the approach, achieved by means of the Mandelstam formalism [47] in lowest-order of perturbation theory, was explained in Chapter 3. There we showed that, in contrast to the good results for hadronic spectra, the theoretical decay widths are generally too small and only in qualitative agreement with experimental data. Whereas these results offer a natural solution to the missing resonance problem (*e.g.* missing N and Δ resonances simply decouple from πN), also the decay widths of well-established, low-lying states were found to be too small in comparison to the data.

Since the strong decay widths were just evaluated in lowest-order of perturbation theory, the purpose of this work was to find out if such an outcome results from the absence of rescattering effects, which are neglected in this approximation. Such an investigation requires the study of meson-baryon scattering equations, as carried out in Chapter 4, in order to connect strong decay amplitudes to the meson-baryon rescattering matrix. After solving the scattering equation in on-shell approximation and decomposing the result into resonant and non-resonant (or background) contributions, we could establish the method to include final state interactions: The procedure corresponds to dressing the decay amplitudes (or bare vertices) obtained in the quark model and subsequent re-evaluation of the decay widths from the resulting dressed vertices.

For the procedure above a suitable parameterization of non-resonant meson-baryon amplitudes was necessary, and therefore in Chapter 5 we implemented a model for coupled-channel πN, $\pi\Delta$ and ηN scattering. The approach was based on an on-shell reduction of the Jülich model [21, 40–46] which, among the several dynamical models available in the literature, is very suitable for describing final state interactions as it provides well-constrained non-resonant amplitudes. In that chapter we demonstrated that despite the on-shell approximation the resulting amplitudes are very similar to those from Jülich model, within the energy range from πN threshold up to 1700 MeV and partial waves with total angular momentum $J \leq \frac{5}{2}$. One exception was however the P_{11} wave, which due to the contribution of the Roper resonance $N(1440)$ cannot be described in our on-shell framework. This could be expected since in the Jülich model the Roper resonance is dynamically generated by non-resonant interactions involving an (off-shell) σN state [21], whereas in our approach such a mechanism is absent.

Using the formalism of Chapter 4 and the amplitudes from Chapter 5 we were able to account for rescattering effects in the decays of most of the N and Δ resonances with masses up to 1700 MeV. For the reasons mentioned above, the states coupling to πN in P_{11} wave were excluded from our analysis. The results for the corrected decay widths (*i.e.* after including final state interactions) were presented in Chapter 6 and can be summarized as follows: Whereas rescattering effects are practically irrelevant for the decays into πN and ηN, these lead to large corrections for the decays into $\pi\Delta$, however in the opposite direction of what we expected. In the latter case, the corrected decay widths turned out to be much smaller than before. According to this outcome, including final state interactions does not lead to any better results for strong decay widths in the way these are described in the relativistic quark model.

On the one hand, one may argue that our method to include final state interactions is too phenomenological, since masses and decay widths of resonances are properly defined from the poles of an unitary, analytical transition matrix and corresponding residua. Indeed, we pointed out in Chapter 6 that in this method the corrected decay widths are model dependent, which becomes an issue specially in our framework where bare vertices are obtained from one model and the rescattering matrix from another. Whereas a self-consistent calculation of baryon properties from the poles of the transition matrix might lead to substantial corrections to the strong decay widths, the present results allow us to estimate the effect of final state interactions and thereby infer that the strong decay amplitudes in the quark model are in fact too small.

In this regard, a possible modification in the model was suggested in Chapter 6. We recall that in the approach the full quark propagators were parameterized by their usual free forms, with poles at constituent quark masses, which allowed us to obtain a solvable bound-state equation to describe hadrons in terms of constituent quarks. However, such an approximation is in principle inconsistent with the picture of quarks being bound in hadronic states. In addition, it was shown in Ref. [55] (there for the case of mesons) that the use of full quark propagators would also lead to a solvable bound-state equation in case that the propagators are also taken in the instantaneous approximation, in line with the quark interactions used in the approach. Concerning the description of strong decays, we showed that the formalism with full propagators would in fact lead to different results for the strong decay widths and, therefore, should be investigated in the future.

Appendix A

Conventions and normalization

We summarize below the conventions and normalization used in this thesis. For this purpose we denote

- four-vectors by italic letters p,
- three-vectors by bold letters $\mathbf{p}$ and
- unit vectors by $\hat{p}$.

Following the Jacob and Wick convention [64], $\hat{p}$ is defined by the rotation matrix

$$R(\Omega_p) = R_z(\phi_p)R_y(\theta_p)R_z(-\phi_p) \in SO(3)$$

such that $\hat{p} = R(\Omega_p)\hat{e}_z$. Here, $\Omega = (\theta_p, \phi_p)$ indicates the direction of $\mathbf{p}$, $\hat{e}_z$ denotes the unit vector in the z-direction and $R_i(\alpha)$ represents a rotation through angle α about the i-axis.

To present the explicit forms of Dirac and Rarita-Schwinger spinors, polarization vectors and finally Feynman propagators, we consider single-particle states of mass m, helicity λ and four-momentum p. In case that such a state is on the mass-shell, *i.e.*

$$p = \begin{pmatrix} \omega_p \\ \mathbf{p} \end{pmatrix} \qquad \text{with} \qquad \omega_p = \sqrt{m^2 + \mathbf{p}^2}, \tag{A.1}$$

it can be represented by the simultaneous eigenstates of four-momentum and helicity. In this work these are denoted by $|p, \lambda\rangle$ and covariantly normalized according to

$$\langle p', \lambda' | p\,, \lambda \rangle = (2\pi)^3 2\omega_p \delta^{(3)}(\mathbf{p}' - \mathbf{p})\delta_{\lambda'\lambda}. \tag{A.2}$$

Metric tensor

Scalar products $p \cdot k := g_{\mu\nu}p^\mu k^\nu$ in Minkowski space are defined in relation to the metric tensor

$$g_{\mu\nu} = \begin{pmatrix} 1 & 0 & 0 & 0 \\ 0 & -1 & 0 & 0 \\ 0 & 0 & -1 & 0 \\ 0 & 0 & 0 & -1 \end{pmatrix}. \tag{A.3}$$

Pauli and Dirac matrices

The Pauli spin matrices $\boldsymbol{\sigma} = (\sigma_1, \sigma_2, \sigma_3)$ are given by

$$\sigma_1 = \begin{pmatrix} 0 & 1 \\ 1 & 0 \end{pmatrix}, \quad \sigma_2 = \begin{pmatrix} 0 & -i \\ i & 0 \end{pmatrix} \quad \text{and} \quad \sigma_3 = \begin{pmatrix} 1 & 0 \\ 0 & -1 \end{pmatrix} \tag{A.4}$$

and fulfill the relations

$$[\sigma_i, \sigma_j] = 2i\epsilon_{ijk}\sigma_k \quad \text{and} \quad \{\sigma_i, \sigma_j\} = 2\delta_{ij}\mathbb{1}_2, \tag{A.5}$$

where ϵ_{ijk} is the Levi-Civita symbol and $\mathbb{1}_n$ represents the $n \times n$ identity matrix. The Dirac matrices $\gamma^\mu = (\gamma^0, \boldsymbol{\gamma})$ are defined by the anticommutator

$$\{\gamma^\mu, \gamma^\nu\} = 2g^{\mu\nu}\mathbb{1}_4 \tag{A.6}$$

and in the standard Dirac representation are given by

$$\gamma^0 = \begin{pmatrix} \mathbb{1}_2 & 0 \\ 0 & -\mathbb{1}_2 \end{pmatrix} \quad \text{and} \quad \boldsymbol{\gamma} = \begin{pmatrix} 0 & \boldsymbol{\sigma} \\ -\boldsymbol{\sigma} & 0 \end{pmatrix}. \tag{A.7}$$

Further important combinations of the Dirac matrices are

$$\gamma^5 = i\gamma^0\gamma^1\gamma^2\gamma^3 = \begin{pmatrix} 0 & \mathbb{1}_2 \\ \mathbb{1}_2 & 0 \end{pmatrix} \tag{A.8}$$

and the commutator

$$\sigma^{\mu\nu} = \frac{i}{2}\left[\gamma^\mu, \gamma^\nu\right]. \tag{A.9}$$

Spinors and polarization vectors

- The spin-1/2 Dirac spinors are solutions of the Dirac equation

$$(\not{p} - m)\, u_\lambda(p) = 0, \tag{A.10}$$

and according to Eq. (A.2) are normalized by

$$u^\dagger_{\lambda'}(p) u_\lambda(p) = 2\omega_p \delta_{\lambda'\lambda}. \tag{A.11}$$

The latter equation might also be written as

$$\bar{u}_{\lambda'}(p) u_\lambda(p) = 2m\delta_{\lambda'\lambda} \tag{A.12}$$

by using the definition $\bar{u} := u^\dagger\gamma^0$. In agreement with (A.10) and (A.11) the Dirac spinors can be written as

$$u_\lambda(p) = \sqrt{\omega_p + m} \begin{pmatrix} \mathbb{1}_2 \\ \frac{\boldsymbol{\sigma}\cdot\mathbf{p}}{\omega_p + m} \end{pmatrix} \chi_\lambda \tag{A.13}$$

where χ_λ represent Pauli spinors.

- The spin-1/2 Pauli spinors appearing in Eq. (A.13) take the form

$$\chi_{+1/2}(\Omega_p) = \begin{pmatrix} \cos(\theta_p/2)\, e^{-i(\phi_p/2)} \\ \sin(\theta_p/2)\, e^{+i(\phi_p/2)} \end{pmatrix} \qquad \text{if} \qquad \lambda = +1/2 \tag{A.14}$$

and

$$\chi_{-1/2}(\Omega_p) = \begin{pmatrix} -\sin(\theta_p/2)\, e^{-i(\phi_p/2)} \\ \cos(\theta_p/2)\, e^{+i(\phi_p/2)} \end{pmatrix} \qquad \text{if} \qquad \lambda = -1/2. \tag{A.15}$$

Moreover, they represent eigenstates of the helicity operator, *i.e.*

$$\frac{\boldsymbol{\sigma}\cdot\mathbf{p}}{2|\mathbf{p}|}\chi_\lambda = \lambda\chi_\lambda, \tag{A.16}$$

which are normalized according to

$$\chi^\dagger_{\lambda'}\chi_\lambda = \delta_{\lambda'\lambda}. \tag{A.17}$$

- The spin-1 polarization four-vectors ϵ_λ are defined by

$$\epsilon^\mu_{\pm1}(p) = \frac{1}{\sqrt{2}} \begin{pmatrix} 0 \\ \mp\cos\theta_p\cos\phi_p + i\sin\phi_p \\ \mp\cos\theta_p\sin\phi_p - i\cos\phi_p \\ \pm\sin\theta_p \end{pmatrix} \qquad \text{for} \qquad \lambda = \pm1 \tag{A.18}$$

and

$$\epsilon^\mu_0(p) = \frac{1}{m} \begin{pmatrix} |\mathbf{p}| \\ \omega_p\sin\theta_p\cos\phi_p \\ \omega_p\sin\theta_p\sin\phi_p \\ \omega_p\cos\theta_p \end{pmatrix} \qquad \text{for} \qquad \lambda = 0. \tag{A.19}$$

In addition, they fulfill the normalization

$$\epsilon^\dagger_\mu\epsilon^\mu = -1 \tag{A.20}$$

for each $\lambda \in \{0, -1, 1\}$.

- The spin-3/2 Rarita-Schwinger spinors result from the coupling of Dirac spinors and polarization vectors, *i.e.*

$$u^\mu_\lambda(p) = \sum_{\lambda_1,\lambda_2} \langle 1\lambda_1, \frac{1}{2}\lambda_2 | \frac{3}{2}\lambda\rangle \epsilon^\mu_{\lambda_1}(p) u_{\lambda_2}(p), \tag{A.21}$$

where the matrix elements denote the usual Clebsch-Gordan coefficients. These spinors fulfill the Rarita-Schwinger equations

$$\begin{aligned} (\not{p} - m)\, u^\mu_\lambda(p) &= 0 \\ p\cdot u_\lambda(p) &= 0 \\ \gamma\cdot u_\lambda(p) &= 0 \end{aligned} \tag{A.22}$$

and also the normalization

$$\bar{u}_{\lambda'}(p) \cdot u_{\lambda}(p) = -2m\delta_{\lambda'\lambda}, \tag{A.23}$$

which follows from Eq. (A.12), (A.17) and (A.20).

Feynman propagators

The propagation of a spin-s particle is described by

- the scalar propagator

$$\Delta(p) = \frac{i}{p^2 - m^2 + i\epsilon} \quad \text{if} \quad s = 0, \tag{A.24}$$

- the Dirac propagator

$$S(p) = i\,\frac{\not{p} + m}{p^2 - m^2 + i\epsilon} \quad \text{if} \quad s = 1/2, \tag{A.25}$$

- the vector propagator

$$\Delta^{\mu\nu}(p) = \Delta(p)\left[-g^{\mu\nu} + \frac{p^\mu p^\nu}{m^2}\right] \quad \text{if} \quad s = 1, \tag{A.26}$$

- and finally the Rarita-Schwinger propagator

$$S^{\mu\nu}(p) = S(p)\left[-g^{\mu\nu} + \frac{\gamma^\mu\gamma^\nu}{3} + \frac{2p^\mu p^\nu}{3m^2} - \frac{p^\mu\gamma^\nu - p^\nu\gamma^\mu}{3m}\right] \quad \text{if} \quad s = 3/2. \tag{A.27}$$

Appendix B

The effective meson-baryon potential

We give below the transition amplitudes related to the diagrams of Figs. 5.1 and 5.6. Recall from Chapter 5 that each amplitude has to be multiplied by the corresponding form factor (see Section 5.3) and isospin factor (see Appendix C).

B.1 Background contributions

Given the parametrizations (5.1) to (5.3) of the non-resonant amplitudes, we list the Lorentz invariant functions A and B for the diagrams of Fig. 5.1. Except for the case of correlated $\pi\pi$ exchange these are derived from the Lagrangian of Table 5.1.

Elastic πN-scattering, Fig. 5.1a

- N-exchange:

$$A_N^u = \frac{f_{NN\pi}^2}{m_\pi^2} 2M_N, \qquad B_N^u = \frac{f_{NN\pi}^2}{m_\pi^2}\left(1 + \frac{4M_N^2}{u - M_N^2}\right). \tag{B.1}$$

- Δ-exchange:

$$A_\Delta^u = \frac{f_{NN\pi}^2}{m_\pi^2} \frac{a_\Delta(u,t)}{6M_\Delta^2(u - M_\Delta^2)}, \qquad B_\Delta^u = -\frac{f_{NN\pi}^2}{m_\pi^2} \frac{b_\Delta(u,t)}{6M_\Delta^2(u - M_\Delta^2)}, \tag{B.2}$$

where

$$\begin{aligned} a_\Delta(u,t) = {} & M_\Delta^2(M_\Delta + M_N)(6m_\pi^2 - 3t - 2u + 2M_N^2) \\ & - 2m_\pi^2 M_\Delta(u - M_N^2 + m_\pi^2) - M_N(u - M_N^2 + m_\pi^2)^2 \end{aligned}$$

and

$$\begin{aligned} b_\Delta(u,t) = {} & 4M_\Delta^3 M_N + M_\Delta^2(4m_\pi^2 - 3t + 4M_N^2) \\ & - 2M_\Delta M_N(u - M_N^2 + m_\pi^2) - (u - M_N^2 + m_\pi^2)^2. \end{aligned}$$

The invariant amplitudes corresponding to correlated $\pi\pi$ exchange in the σ and ρ channels are given in Eq. (5.5) to (5.9).

Coupling to $\pi\Delta$, Fig. 5.1b

- N-exchange in $\pi N \to \pi\Delta$:

$$\begin{aligned}(A_N^u)_\mu &= \frac{f_{N\Delta\pi} f_{NN\pi}}{m_\pi^2} \frac{u + M_N M_\Delta}{u - M_N^2} k_\mu, \\ (B_N^u)_\mu &= \frac{f_{N\Delta\pi} f_{NN\pi}}{m_\pi^2} \frac{2M_N}{u - M_N^2} k_\mu.\end{aligned} \tag{B.3}$$

- Δ-exchange in $\pi N \to \pi\Delta$:

$$\begin{aligned}(A_\Delta^u)_\mu &= -\frac{f_{\Delta\Delta\pi} f_{N\Delta\pi}}{m_\pi^2} \left[\frac{a_1(u) k'_\mu + a_2(u) k_\mu}{6M_\Delta^2(u - M_\Delta^2)}\right], \\ (B_\Delta^u)_\mu &= \frac{f_{\Delta\Delta\pi} f_{N\Delta\pi}}{m_\pi^2} \left[\frac{b_1(u) k'_\mu + b_2(u) k_\mu}{6M_\Delta^2(u - M_\Delta^2)}\right],\end{aligned} \tag{B.4}$$

where

$$a_1(u) = 6M_\Delta^2(u + M_\Delta M_N),$$

$$\begin{aligned}a_2(u) = {} & 3M_\Delta^4 + 5M_\Delta^3 M_N + M_\Delta^2 \left(2M_N^2 - 4m_\pi^2 - u\right) \\ & + M_\Delta M_N \left(2M_N^2 - 2m_\pi^2 - 3u\right) \\ & + 2u \left(M_N^2 - m_\pi^2 - u\right),\end{aligned}$$

$$b_1(u) = 12M_\Delta^3$$

and

$$b_2(u) = -6M_\Delta^3 - 4M_\Delta^2 M_N + 2M_\Delta \left(2M_N^2 - 2m_\pi^2 - u\right).$$

- ρ-exchange in $\pi N \to \pi\Delta$:

$$\begin{aligned}\left(A_\rho^t\right)_\mu &= i \frac{f_{N\Delta\rho} f_{\rho\pi\pi}}{m_\rho} \frac{M_N + M_\Delta}{t - m_\rho^2} \left(k + k'\right)_\mu, \\ \left(B_\rho^t\right)_\mu &= i \frac{f_{N\Delta\rho} f_{\rho\pi\pi}}{m_\rho} \frac{2}{t - m_\rho^2} \left(k - k'\right)_\mu.\end{aligned} \tag{B.5}$$

Although considered in the Jülich model of Ref. [45], N-exchange in $\pi\Delta \to \pi\Delta$ cannot be included in our approach (see Section 5.2.1).

- Δ-exchange in $\pi\Delta \to \pi\Delta$:

$$\begin{aligned}(A_\Delta^u)_{\mu\nu} &= -\frac{f_{\Delta\Delta\pi}^2}{m_\pi^2} \frac{6M_\Delta^3(u - M_\Delta^2) g_{\mu\nu} - 2M_\Delta(3M_\Delta^2 + u) k_\mu k'_\nu}{3M_\Delta^2(u - M_\Delta^2)}, \\ (B_\Delta^u)_{\mu\nu} &= -\frac{f_{\Delta\Delta\pi}^2}{m_\pi^2} \frac{3M_\Delta^2(3M_\Delta^2 + u) g_{\mu\nu} - 2(3M_\Delta^2 + u) k_\mu k'_\nu}{3M_\Delta^2(u - M_\Delta^2)}.\end{aligned} \tag{B.6}$$

- ρ-exchange in $\pi\Delta \to \pi\Delta$:

$$\begin{aligned}(A_t^\rho)_{\mu\nu} &= i\,\frac{g_{\Delta\Delta\rho}g_{\pi\pi\rho}\kappa_{\Delta\Delta\rho}}{2M_\Delta}\,\frac{u-s}{t-m_\rho^2}\,g_{\mu\nu},\\ (B_t^\rho)_{\mu\nu} &= i\,g_{\Delta\Delta\rho}g_{\pi\pi\rho}(1+\kappa_{\Delta\Delta\rho})\,\frac{2}{t-m_\rho^2}\,g_{\mu\nu}\end{aligned} \tag{B.7}$$

Coupling to ηN, Fig. 5.1c

- N-exchange in $\pi N \to \eta N$:

$$A_N^u = \frac{f_{NN\eta}f_{NN\pi}}{m_\pi^2}2M_N, \qquad B_N^u = \frac{f_{NN\eta}f_{NN\pi}}{m_\pi^2}\left(1+\frac{4M_N^2}{u-M_N^2}\right). \tag{B.8}$$

- a_0-exchange in $\pi N \to \eta N$:

$$A_{a_0}^t = -\frac{g_{NNa_0}g_{\pi\eta a_0}m_\pi}{t-m_{a_0}^2} \tag{B.9}$$

  and $B_{a_0}^t = 0$ in the scalar channel.

- N-exchange in $\pi N \to \eta N$:

$$A_N^u = \frac{f_{NN\eta}^2}{m_\pi^2}2M_N, \qquad B_N^u = \frac{f_{NN\pi}^2}{m_\pi^2}\left(1+\frac{4M_N^2}{u-M_N^2}\right). \tag{B.10}$$

B.2 Resonant contributions

As explained in Section 4.3.2 resonant amplitudes are fully determined by bare vertex functions. In the following we give the bare vertices entering in the calculation of the graphs depicted in Fig. 5.6 which are derived from the Lagrangian of Table 5.3 and transformed to the basis of the helicity and parity eigenstates $|JM_J,\lambda\pm\rangle$ according to Eq. (4.114). Since bare vertex functions are equal (up to isospin factors) for two diagrams which differ only in the isospin quantum numbers of the particles, we give just one expression for both cases and denote the bare coupling constants by f without subscripts. As a last remark about our notation, we recall from Chapter 4 that the superscript $J\pm$ indicates that the corresponding amplitude has parity $\pi = (-)^{J\pm\frac{1}{2}}$.

Coupling to πN (ηN), $\lambda = 1/2$

- S_{11} (S_{31}):

$$\gamma_\lambda^{\frac{1}{2}+} = \frac{if}{m_\pi}(\omega - M_N)\sqrt{2\omega}\,\sqrt{E_N+M_N}\,\delta_{\lambda\frac{1}{2}}, \tag{B.11}$$

- P_{11} (P_{31}):

$$\gamma_\lambda^{\frac{1}{2}-} = \frac{if}{m_\pi}\,(\omega + M_N)\,\sqrt{2\omega}\,\sqrt{E_N-M_N}\,\delta_{\lambda\frac{1}{2}}, \tag{B.12}$$

- $\underline{P_{13}\ (P_{33})}$:

$$\gamma_\lambda^{\frac{3}{2}+} = \sqrt{\frac{1}{3}}\,\frac{if}{m_\pi}\,\sqrt{2\omega}\,\sqrt{E_N + M_N}\,|\mathbf{p}|\,\delta_{\lambda\frac{1}{2}}, \tag{B.13}$$

- $\underline{D_{13}\ (D_{33})}$:

$$\gamma_\lambda^{\frac{3}{2}-} = \sqrt{\frac{1}{3}}\,\frac{f}{m_\pi^2}\,(\omega + M_N)\,\sqrt{2\omega}\,\sqrt{E_N - M_N}\,|\mathbf{p}|\,\delta_{\lambda\frac{1}{2}}, \tag{B.14}$$

where E_N and $\mathbf{p}$ are the on-shell energy and the three-momentum of the N belonging to the πN (ηN) state, respectively.

Coupling to $\pi\Delta$, $\lambda = 1/2$ or $3/2$

- $\underline{S_{11}\ (S_{31})}$:

$$\gamma_\lambda^{\frac{1}{2}+} = \sqrt{\frac{2}{3}}\left(-\frac{if}{m_\pi}\right)\,\frac{\omega}{M_\Delta}\,\sqrt{2\omega}\,\sqrt{E_\Delta - M_\Delta}\,|\mathbf{p}|\,\delta_{\lambda\frac{1}{2}}, \tag{B.15}$$

- $\underline{P_{11}\ (P_{31})}$:

$$\gamma_\lambda^{\frac{1}{2}-} = \sqrt{\frac{2}{3}}\left(-\frac{if}{m_\pi}\right)\,\frac{\omega}{M_\Delta}\,\sqrt{2\omega}\,\sqrt{E_\Delta + M_\Delta}\,|\mathbf{p}|\,\delta_{\lambda\frac{1}{2}}, \tag{B.16}$$

- $\underline{P_{13}\ (P_{33})}$:

$$\gamma_\lambda^{\frac{3}{2}+} = \sqrt{\frac{1}{2}}\,\frac{if}{m_\pi}\,(\omega + M_\Delta)\,\sqrt{2\omega}\,\sqrt{E_\Delta - M_\Delta}\left[\left(\frac{2E_\Delta - M_\Delta}{3M_\Delta}\right)\delta_{\lambda\frac{1}{2}} + \delta_{\lambda\frac{3}{2}}\right], \tag{B.17}$$

- $\underline{D_{13}\ (D_{33})}$:

$$\gamma_\lambda^{\frac{3}{2}-} = \sqrt{\frac{1}{2}}\left(-\frac{f}{m_\pi}\right)\,(\omega - M_\Delta)\,\sqrt{2\omega}\,\sqrt{E_\Delta + M_\Delta}\left[\left(\frac{2E_\Delta + M_\Delta}{3M_\Delta}\right)\delta_{\lambda\frac{1}{2}} + \delta_{\lambda\frac{3}{2}}\right], \tag{B.18}$$

where E_Δ and $\mathbf{p}$ are the on-shell energy and the three-momentum of the Δ belonging to the $\pi\Delta$ state, respectively.

Finally, we recall that the bare vertex functions related to couplings to higher spin resonances are given by the phenomenological couplings of Eq. (5.21).

Appendix C

Isospin factors

Since isospin symmetry is considered to be exact in this thesis, the contributions to the meson-baryon potential constructed in Chapter 5 have to be multiplied by isospin factors. Accordingly, in this appendix we detail the calculation of the isospin factors related to the diagrams depicted in Figs. 5.1[1] and 5.6. For this purpose we consider isospin states given in the spherical basis, *i.e.*

$$\begin{array}{l} \chi_{+\frac{1}{2}} = |\frac{1}{2}\ +\frac{1}{2}\rangle \\ \chi_{-\frac{1}{2}} = |\frac{1}{2}\ -\frac{1}{2}\rangle \end{array}, \qquad \begin{array}{l} \phi_{+1} = |1\ +1\rangle \\ \phi_{0}\ \ = |1\,0\rangle \\ \phi_{-1} = |1\ -1\rangle \end{array} \qquad \text{and} \qquad \begin{array}{l} \Delta_{+\frac{3}{2}} = |\frac{3}{2}\ +\frac{3}{2}\rangle \\ \Delta_{+\frac{1}{2}} = |\frac{1}{2}\ +\frac{1}{2}\rangle \\ \Delta_{-\frac{1}{2}} = |\frac{1}{2}\ -\frac{1}{2}\rangle \\ \Delta_{-\frac{3}{2}} = |\frac{3}{2}\ -\frac{3}{2}\rangle \end{array} \tag{C.1}$$

for particles with isospin $I = \frac{1}{2}$, 1 and $\frac{3}{2}$, respectively.

The isospin amplitudes associated to the graphs of Figs. 5.1 and 5.6 are obtained from the structures appearing in the underlying Lagrangian (see Tables 5.1 and 5.3) and the summation over the possible isospin states of the corresponding exchanged particles. For instance in the case of N exchange in $\pi N \to \pi N$ scattering, by applying the $NN\pi$ Lagrangian at each vertex we obtain

$$\langle \tfrac{1}{2}\beta, 1b|T(I)|\tfrac{1}{2}\alpha, 1a\rangle = \sum_{\mu} \left[\chi^{\dagger}_{\beta}\vec{\tau}\vec{\phi}_{a}\chi_{\mu}\right]\left[\chi^{\dagger}_{\mu}\vec{\tau}\vec{\phi}^{*}_{b}\chi_{\alpha}\right] \tag{C.2}$$

where α (β) and a (b) denote the isospin states of the N and the π in the initial (final) configuration. For the isospin amplitude for $\pi\pi$ exchange in $\pi N \to \pi N$ scattering in the $J = 0(1)$ channel, we use Lagrangians describing the $NN\sigma(\rho)$ and $\pi\pi\sigma(\rho)$ vertices. In the Jülich model these are given by [40, 45]

$$\begin{array}{rcl} \mathcal{L}_{NN\sigma} &=& -g_{NN\sigma}\bar{N}N\sigma, \\ \mathcal{L}_{\pi\pi\sigma} &=& \frac{g_{\pi\pi\sigma}}{2m_{\pi}}(\partial_{\mu}\vec{\pi})(\partial^{\mu}\vec{\pi})\sigma, \\ \mathcal{L}_{NN\rho} &=& -g_{NN\rho}\bar{N}\left[\gamma^{\mu} - \frac{\kappa_{NN\rho}}{2M_{N}}\sigma^{\mu\nu}\partial_{\nu}\right]\vec{\tau}\vec{\rho}_{\mu}N \end{array} \tag{C.3}$$

and $\mathcal{L}_{\pi\pi\rho}$ as given in Table 5.1.

[1] Except for N exchange in $\pi N \to \pi N$ which is not included in the model.

In the course of the calculation some typical isospin structures appear, which in the spherical basis can be evaluated using the formulae [75]:

$$\begin{aligned}
\vec{\phi}_a\vec{\phi}_b &= (-)^a\delta_{a,-b} \\
\vec{\phi}_a\times\vec{\phi}_b &= \textstyle\sum_{c=0,\pm1} i\sqrt{2}\langle 1a,1b|1c\rangle\vec{\phi}_c \\
\chi^\dagger_\alpha\chi_\beta &= \delta_{\alpha\beta} \\
\chi^\dagger_\alpha\vec{\tau}\vec{\phi}_c\chi_\beta &= \sqrt{3}\langle\tfrac{1}{2}\beta,1c|\tfrac{1}{2}\alpha\rangle \\
\Delta^\dagger_\alpha\vec{S}^\dagger\vec{\phi}_c\chi_\beta &= \langle\tfrac{1}{2}\beta,1c|\tfrac{3}{2}\alpha\rangle \\
\Delta^\dagger_\alpha\vec{T}\vec{\phi}_c\Delta_\beta &= \sqrt{\tfrac{5}{3}}\langle\tfrac{3}{2}\beta,1c|\tfrac{3}{2}\alpha\rangle.
\end{aligned} \tag{C.4}$$

Here, the matrix elements on the right-hand sides denote Clebsch-Gordan coefficients and τ, S and T represent the isospin transition operators for $1/2\to1/2$, $1/2\to3/2$ and $3/2\to3/2$, respectively.

Finally, once the amplitude for each graph is obtained, the corresponding isospin factors are given by the matrix element of $T(I)$ between initial and final meson-baryon states $|IM\rangle$ with fixed total isospin [75]:

$$\begin{aligned}
IF(I) &:= \langle IM|T(I)|IM\rangle \\
&= \sum_{\beta,b}\sum_{\alpha,a}\langle IM|\tfrac{1}{2}\beta,1b\rangle\langle\tfrac{1}{2}\beta,1b|T(I)|\tfrac{1}{2}\alpha,1a\rangle\langle\tfrac{1}{2}\alpha,1a|IM\rangle,
\end{aligned} \tag{C.5}$$

where we employ the same notation as in Eq. (C.2). Using this expression, one obtains the same result regardless of the choice of the quantum number M. Moreover, it should be noted that in the Clebsch-Gordan coefficients in (C.5) the baryon isospin quantum numbers appear before those related to mesons, in consonance with definition (4.16) for meson-baryon helicity states.

The resulting isospin factors for background and resonant diagrams are collected in Tables C.1 and C.2, respectively. Since the isospin factors for resonant contributions factorize, in Table C.2 we present the factors related to each one of the vertex functions appearing in the pole diagrams. In this case the factor for a full resonant amplitude is then given by the product of the factors at each vertex.

Table C.1. Isospin factors for background contributions.

Reaction channel	Diagram	IF(1/2)	IF(3/2)
$\pi N \to \pi N$	N exchange	-1	2
	Δ exchange	$\frac{4}{3}$	$\frac{1}{3}$
	$\pi\pi$ exchange $(J=0)$	1	1
	$\pi\pi$ exchange $(J=1)$	$2i$	$-i$
$\pi N \to \pi\Delta$	N exchange	$-\sqrt{\frac{8}{3}}$	$\sqrt{\frac{5}{3}}$
	Δ exchange	$-\frac{5}{3}\sqrt{\frac{2}{3}}$	$-\frac{2}{3}\sqrt{\frac{5}{3}}$
	ρ exchange	$i\sqrt{\frac{2}{3}}$	$i\sqrt{\frac{5}{3}}$
$\pi\Delta \to \pi\Delta$	Δ exchange	$-\frac{10}{9}$	$\frac{11}{9}$
	ρ exchange	$\frac{5i}{3}$	$\frac{2i}{3}$
$\pi N \to \eta N$	N exchange	$\sqrt{3}$	isospin violation
	a_0 exchange	$\sqrt{3}$	
$\eta N \to \eta N$	N exchange	1	
	f_0 exchange	1	

Table C.2. Isospin factors for resonant contributions (at each vertex).

Decay channel	IF(1/2)	IF(3/2)
πN	$\sqrt{3}$	1
$\pi\Delta$	$-\sqrt{2}$	$\sqrt{\frac{5}{3}}$
ηN	1	isospin violation

Appendix D

Pole diagrams in the quark model

As pointed out in Chapter 6, deriving the resonant part of a meson-baryon potential in the framework of the relativistic quark model would allow one to redefine baryon properties directly from the poles and residua of an unitary transition matrix. In this appendix we sketch this derivation which is analogous to the Mandelstam formalism presented in Chapter 3.

We start by considering that meson-baryon scattering in a constituent quark model may be depicted as a five-body interaction involving four quarks and one antiquark which, at large times before and after the reaction, appear confined in asymptotic meson ($q\bar{q}$) and baryon (qqq) states. Such a process in quantum field theory is a contribution to the ten-point Green's function, which is defined by (*cf.* Eq. (3.10))

$$\begin{aligned} G^{(10)}(x_1', x_2', x_3', y_1', y_2'; x_1, x_2, x_3, y_1, y_2) := \\ -\langle\Omega|T\,\Psi^{1'}(x_1')\Psi^{2'}(x_2')\Psi^{3'}(x_3')\Psi^{q'}(y_1')\bar{\Psi}^{\bar{q}'}(y_2') \\ \times \Psi^{\bar{q}}(y_2)\bar{\Psi}^{q}(y_1)\bar{\Psi}^{1}(x_1)\bar{\Psi}^{2}(x_2)\bar{\Psi}^{3}(x_3)|\Omega\rangle \end{aligned} \tag{D.1}$$

in the Heisenberg picture. In the equation above, we employed the same notation as in Chapters 2 and 3, thus Ψ and $\bar{\Psi}$ are quark field operators, T is the time-ordering operator and $|\Omega\rangle$ is the physical vacuum state. Moreover, the superscripts $i = 1, 2, 3$ ($i' = 1', 2', 3'$) and $j = q, \bar{q}$ ($j = q', \bar{q}'$) label the constituent quarks in the initial (final) baryon and meson, respectively.

Since the initial and final meson-baryon states are asymptotic, we shall choose the time-dependence

$$x_1'^0, x_2'^0, x_3'^0, y_1'^0, y_2'^0 \to +\infty \qquad \text{and} \qquad x_1^0, x_2^0, x_3^0, y_1^0, y_2^0 \to -\infty \tag{D.2}$$

for the ten-point Green's function (D.1), so that it can be written as

$$\begin{aligned} G^{(10)}(x_1', x_2', x_3', y_1', y_2'; x_1, x_2, x_3, y_1, y_2) := \\ -\langle\Omega|\left(T\Psi^{1'}(x_1')\Psi^{2'}(x_2')\Psi^{3'}(x_3')\Psi^{q'}(y_1')\bar{\Psi}^{\bar{q}'}(y_2')\right) \\ \times \left(T\Psi^{\bar{q}}(y_2)\bar{\Psi}^{q}(y_1)\bar{\Psi}^{1}(x_1)\bar{\Psi}^{2}(x_2)\bar{\Psi}^{3}(x_3)\right)|\Omega\rangle. \end{aligned} \tag{D.3}$$

The contribution from meson-baryon scattering is then isolated by inserting complete

sets

$$\int \frac{\mathrm{d}^3\,\bar{P}}{(2\pi)^3 2\omega_{\bar{P}}} \int \frac{\mathrm{d}^3\,\bar{K}}{(2\pi)^3 2\omega_{\bar{K}}} |\bar{P}\bar{K}\rangle\langle\bar{P}\bar{K}| = 1 \tag{D.4}$$

of two-particle momentum eigenstates $|\bar{P}\bar{K}\rangle := |\bar{P}\rangle \otimes |\bar{K}\rangle$ between the time-ordered products in (D.3). Following this procedure we arrive at

$$\begin{aligned} G^{(10)}(x_1', x_2', x_3', y_1', y_2'; x_1, x_2, x_3, y_1, y_2) = \\ - \int \frac{\mathrm{d}^3\,\bar{P}'}{(2\pi)^3 2\omega_{\bar{P}'}} \frac{\mathrm{d}^3\,\bar{K}'}{(2\pi)^3 2\omega_{\bar{K}'}} \frac{\mathrm{d}^3\,\bar{P}}{(2\pi)^3 2\omega_{\bar{P}}} \frac{\mathrm{d}^3\,\bar{K}}{(2\pi)^3 2\omega_{\bar{K}}} \\ \times \left[\chi_{\bar{P}'}(x_1', x_2', x_3') \otimes \chi_{\bar{K}'}(y_1', y_2')\right] \langle \bar{P}'\bar{K}'|\bar{P}\bar{K}\rangle \\ \times \left[\bar{\chi}_{\bar{P}}(x_1, x_2, x_3) \otimes \bar{\chi}_{\bar{K}}(y_1, y_2)\right], \end{aligned} \tag{D.5}$$

where we also used Eqs. (2.16), (2.17), (2.69) and (2.70) to identify the Bethe-Salpeter amplitudes χ and $\bar{\chi}$. Here, $\langle \bar{P}'\bar{K}'|\bar{P}\bar{K}\rangle$ is the scattering matrix element between the initial and final meson-baryon states as defined in the Heisenberg picture.

Now, by assuming that the scattering occurs via s-channel resonance exchange we decompose the ten-point Green's function in terms of an integral interaction kernel $K^{(4)}$ as follows (*cf.* Fig. D.1):

$$\begin{aligned} G^{(10)}(x_1', x_2', x_3', y_1', y_2'; x_1, x_2, x_3, y_1, y_2) =: \\ \int \mathrm{d}^4 x_1''' \mathrm{d}^4 x_2''' \mathrm{d}^4 x_3''' \mathrm{d}^4 y_1''' \mathrm{d}^4 y_2''' \mathrm{d}^4 z_1''' \mathrm{d}^4 z_2''' \mathrm{d}^4 z_3''' \\ \times \int \mathrm{d}^4 x_1'' \mathrm{d}^4 x_2'' \mathrm{d}^4 x_3'' \mathrm{d}^4 y_1'' \mathrm{d}^4 y_2'' \mathrm{d}^4 z_1'' \mathrm{d}^4 z_2'' \mathrm{d}^4 z_3'' \\ \times G^{(6)}(x_1', x_2', x_3'; x_1''', x_2''', x_3''') \otimes G^{(4)}(y_1', y_2'; y_1''', y_2''') \\ \times K^{(4)}(x_1''', x_2''', x_3''', y_1''', y_2'''; z_1''', z_2''', z_3''') \\ \times G^{(6)}(z_1''', z_2''', z_3'''; z_1'', z_2'', z_3'') \\ \times K^{(4)\dagger}(z_1'', z_2'', z_3''; y_1'', y_2'', x_1'', x_2'', x_3'') \\ \times G^{(6)}(x_1'', x_2'', x_3''; x_1, x_2, x_3) \otimes G^{(4)}(y_1'', y_2''; y_1, y_2), \end{aligned} \tag{D.6}$$

where $G^{(4)}$ and $G^{(6)}$ are the four- and six-point Green's functions defined in Eqs. (2.1) and (2.47), respectively. Then, by considering the time-dependence (D.2) for all the Green's functions in (D.6) and inserting complete sets (D.4) of momentum eigenstates

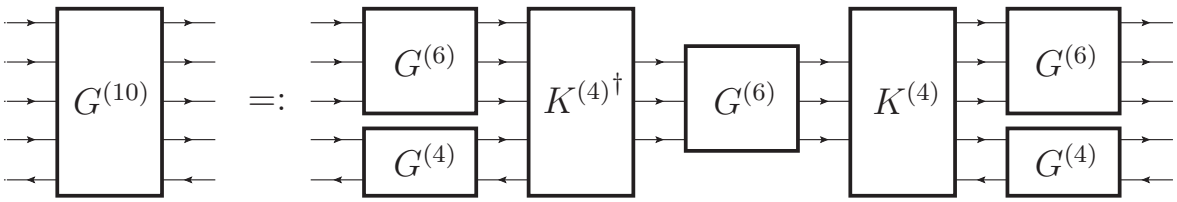

Figure D.1. The contribution of s-channel resonance exchange to the ten-point Green's function $G^{(10)}$.

into the result, we end up with

$$
\begin{aligned}
G^{(10)}&(x_1',x_2',x_3',y_1',y_2';x_1,x_2,x_3,y_1,y_2) =: \\
&\int \mathrm{d}^4x_1'''\mathrm{d}^4x_2'''\mathrm{d}^4x_3'''\mathrm{d}^4y_1'''\mathrm{d}^4y_2'''\mathrm{d}^4z_1'''\mathrm{d}^4z_2'''\mathrm{d}^4z_3''' \\
&\quad\times\int \mathrm{d}^4x_1''\mathrm{d}^4x_2''\mathrm{d}^4x_3''\mathrm{d}^4y_1''\mathrm{d}^4y_2''\mathrm{d}^4z_1''\mathrm{d}^4z_2''\mathrm{d}^4z_3'' \\
&\qquad\times\left(-\int\frac{\mathrm{d}^3\bar{P}'}{(2\pi)^3 2\omega_{\bar{P}'}}\chi_{\bar{P}'}(x_1',x_2',x_3')\otimes\bar{\chi}_{\bar{P}'}(x_1''',x_2''',x_3''')\right) \\
&\qquad\times\left(-\int\frac{\mathrm{d}^3\bar{K}'}{(2\pi)^3 2\omega_{\bar{K}'}}\chi_{\bar{K}'}(y_1',y_2')\otimes\bar{\chi}_{\bar{K}'}(y_1''',y_2''')\right) \\
&\qquad\times K^{(4)}(x_1''',x_2''',x_3''',y_1''',y_2''';z_1''',z_2''',z_3''') \\
&\qquad\times G^{(6)}(z_1''',z_2''',z_3''';z_1'',z_2'',z_3'') \\
&\qquad\times {K^{(4)}}^{\dagger}(z_1'',z_2'',z_3'';x_1'',x_2'',x_3'',y_1'',y_2'') \\
&\qquad\times\left(-\int\frac{\mathrm{d}^3\bar{P}}{(2\pi)^3 2\omega_{\bar{P}}}\chi_{\bar{P}}(x_1'',x_2'',x_3'')\otimes\bar{\chi}_{\bar{P}}(x_1,x_2,x_3)\right) \\
&\qquad\times\left(-\int\frac{\mathrm{d}^3\bar{K}}{(2\pi)^3 2\omega_{\bar{K}}}\chi_{\bar{K}}(y_1'',y_2'')\otimes\bar{\chi}_{\bar{K}}(y_1,y_2)\right),
\end{aligned}
\tag{D.7}
$$

which in comparison to (D.5) gives

$$
\begin{aligned}
S_{\bar{P}'\bar{K}'\leftarrow\bar{P}\bar{K}} &:= \langle\bar{P}'\bar{K}'|\bar{P}\bar{K}\rangle \\
&= -\int \mathrm{d}^4x_1'\mathrm{d}^4x_2'\mathrm{d}^4x_3'\mathrm{d}^4y_1'\mathrm{d}^4y_2'\mathrm{d}^4z_1'\mathrm{d}^4z_2'\mathrm{d}^4z_3' \\
&\qquad\times\int \mathrm{d}^4x_1\mathrm{d}^4x_2\mathrm{d}^4x_3\mathrm{d}^4y_1\mathrm{d}^4y_2\mathrm{d}^4z_1\mathrm{d}^4z_2\mathrm{d}^4z_3 \\
&\qquad\quad\times\left[\bar{\chi}_{\bar{P}'}(x_1',x_2',x_3')\otimes\bar{\chi}_{\bar{K}'}(y_1',y_2')\right] \\
&\qquad\quad\times K^{(4)}(x_1',x_2',x_3',y_1',y_2';z_1',z_2',z_3') \\
&\qquad\quad\times G^{(6)}(z_1',z_2',z_3'z_1,z_2,z_3) \\
&\qquad\quad\times {K^{(4)}}^{\dagger}(z_1,z_2,z_3;x_1,x_2,x_3,y_1,y_2); \\
&\qquad\quad\times\left[\chi_{\bar{P}}(x_1,x_2,x_3)\otimes\chi_{\bar{K}}(y_1,y_2)\right].
\end{aligned}
\tag{D.8}
$$

To simplify the integrals above, we now approximate the interaction kernel by its lowest-order quark-loop contributions (*cf.* Eq. (3.14))

$$
\begin{aligned}
K_0^{(4)}&(x_1,x_2,x_3,y_1,y_2,z_1,z_2,z_3) \\
&= {S_F^1}^{-1}(x_1,z_1)\otimes{S_F^2}^{-1}(x_2,z_2)\otimes{S_F^{\bar{q}}}^{-1}(x_3,y_2)\otimes{S_F^q}^{-1}(y_1,z_3) \\
&+ {S_F^2}^{-1}(x_2,z_2)\otimes{S_F^3}^{-1}(x_3,z_3)\otimes{S_F^{\bar{q}}}^{-1}(x_1,y_2)\otimes{S_F^q}^{-1}(y_1,z_1) \\
&+ {S_F^3}^{-1}(x_3,z_3)\otimes{S_F^1}^{-1}(x_1,z_1)\otimes{S_F^{\bar{q}}}^{-1}(x_2,y_2)\otimes{S_F^q}^{-1}(y_1,z_2),
\end{aligned}
\tag{D.9}
$$

where S_F denote quark propagators, in line with the formalism of Chapter 3. Recall from that chapter that higher-order terms from the underlying instanton interactions

affect decays into ηN only and were not numerically evaluated yet. After inserting Eq. (D.9) into (D.8), the integrals in the latter can then be performed by using the Jacobi coordinates and Fourier-transforms from Chapter 2. This is a straightforward procedure which leads to

$$\begin{aligned} S_{\bar{P}'\bar{K}'\leftarrow\bar{P}\bar{K}} = & -3^2(2\pi)^4\delta^{(4)}(\bar{P}'+\bar{K}'-\bar{P}-\bar{K}) \\ & \times\int\frac{\mathrm{d}^4\,q'_\xi}{(2\pi)^4}\frac{\mathrm{d}^4\,q'_\eta}{(2\pi)^4}\frac{\mathrm{d}^4\,q_\xi}{(2\pi)^4}\frac{\mathrm{d}^4\,q_\eta}{(2\pi)^4} \\ & \times\bar{\chi}_{\bar{P}'}\left(q'_\xi,q'_\eta+\tfrac{2}{3}\bar{K}'\right)S_F^{1'^{-1}}\left(\tfrac{1}{3}Q+q'_\xi+\tfrac{1}{2}q'_\eta\right) \\ & \otimes S_F^{2'^{-1}}\left(\tfrac{1}{3}Q-q'_\xi+\tfrac{1}{2}q'_\eta\right)\otimes S_F^{\bar{q}'^{-1}}\left(\tfrac{1}{3}Q-q'_\eta-\bar{K}'\right) \\ & \times\bar{\chi}_{\bar{K}'}\left(\tfrac{1}{3}Q-q'_\eta+\tfrac{1}{2}\bar{K}'\right)S_F^{q'^{-1}}\left(\tfrac{1}{3}Q-q'_\eta\right) \\ & \times G_Q^{(6)}(q'_\xi,q'_\eta,q_\xi,q_\eta) \\ & \times S_F^{1^{-1}}\left(\tfrac{1}{3}Q+q_\xi+\tfrac{1}{2}q_\eta\right)S_F^{2^{-1}}\left(\tfrac{1}{3}Q-q_\xi+\tfrac{1}{2}q_\eta\right) \\ & \times S_F^{q^{-1}}\left(\tfrac{1}{3}Q-q_\eta\right)\chi_{\bar{K}}\left(\tfrac{1}{3}Q-q_\eta+\tfrac{1}{2}\bar{K}\right) \\ & \times S_F^{\bar{q}^{-1}}\left(\tfrac{1}{3}Q-q_\eta-\bar{K}\right)\chi_{\bar{P}}\left(q_\xi,q_\eta+\tfrac{2}{3}\bar{K}\right), \end{aligned} \tag{D.10}$$

where we defined $Q := \bar{P}+\bar{K} = \bar{P}'+\bar{K}'$, and thus $\omega := \sqrt{s} \equiv \sqrt{Q^2}$ gives the total energy of the system. The remaining six-point Green's function in (D.10) corresponds to the resonance propagator, which in the quark model is given by

$$G_Q^{(6)}(q'_\xi,q'_\eta,q_\xi,q_\eta) \approx \frac{-i}{2\omega_{\bar{Q}}}\frac{\zeta_{\bar{Q}}(q'_\xi,q'_\eta,Q^0-\omega_{\bar{Q}})\otimes\bar{\zeta}_{\bar{Q}}(q_\xi,q_\eta,Q^0-\omega_{\bar{Q}})}{Q^0-\omega_{\bar{Q}}+i\epsilon} \tag{D.11}$$

as detailed in Section 2.3.2. Here, ζ and $\bar{\zeta}$ represent the generalized Bethe-Salpeter amplitudes (2.74) and (2.75). which fulfill the conditions $\zeta_{\bar{P}}(p_\xi,p_\eta,0)=\chi_{\bar{P}}(p_\xi,p_\eta)$ and $\bar{\zeta}_{\bar{P}}(p_\xi,p_\eta,0)=\bar{\chi}_{\bar{P}}(p_\xi,p_\eta)$, and $\omega_{\bar{Q}}=\sqrt{M^2+\mathbf{Q}^2}$ where M is the resonance bare mass.

As we included no trivial contributions in the interaction kernel, the (tree-level) scattering and transition matrices are here related by

$$S = i(2\pi)^4\delta^{(4)}(\bar{P}'+\bar{K}'-\bar{P}-\bar{K})V. \tag{D.12}$$

Hence, by replacing Eq. (D.11) into (D.10) and employing relation (D.12), we finally arrive at the expression for resonant contributions to the meson-baryon potential as depicted in the quark model:

$$V^{\mathrm{P}}_{\bar{P}'\bar{K}'\leftarrow\bar{P}\bar{K}} = \frac{\gamma_{\bar{P}'\bar{K}'\leftarrow Q}\;\gamma^\dagger{}_{Q\leftarrow\bar{P}\bar{K}}}{s-M^2+i\epsilon}, \tag{D.13}$$

where we used the relation

$$\frac{1}{2\omega_{\bar{Q}}}\;\frac{1}{Q^0-\omega_{\bar{Q}}+i\epsilon} = \frac{1}{2\omega_{\bar{Q}}}\;\frac{Q^0+\omega_{\bar{Q}}}{(Q^0)^2-\omega_{\bar{Q}}^2+i\epsilon} \approx \frac{1}{\omega^2-M^2+i\epsilon} \tag{D.14}$$

to obtain the denominator of a relativistic Feynman propagator and also defined the (energy-dependent) bare vertex functions

$$\begin{aligned}\gamma_{\bar{P}\bar{K}\leftarrow Q} := 3 \int \frac{d^4q_\xi}{(2\pi)^4}\frac{d^4q_\eta}{(2\pi)^4}\bar{\chi}_{\bar{P}}\left(q_\xi, q_\eta + \tfrac{2}{3}\bar{K}\right) \\ \times \left[{S_F^1}^{-1}\left(\tfrac{1}{3}Q + q_\xi + \tfrac{1}{2}q_\eta\right) \otimes {S_F^2}^{-1}\left(\tfrac{1}{3}Q - q_\xi + \tfrac{1}{2}q_\eta\right)\right] \\ \otimes \left[{S_F^{\bar{q}}}^{-1}\left(\tfrac{1}{3}Q - q_\eta - \bar{K}\right)\bar{\chi}_{\bar{K}}\left(\tfrac{1}{3}Q - q_\eta + \tfrac{1}{2}\bar{K}\right){S_F^q}^{-1}\left(\tfrac{1}{3}Q - q_\eta\right)\right] \\ \times \zeta_{\bar{Q}}(q_\xi, q_\eta, Q^0 - \omega_{\bar{Q}}),\end{aligned} \tag{D.15}$$

which considered in the limit $Q^0 \to M$ and thus $\zeta \to \chi$ correspond to those calculated in Chapter 3, *cf.* Eq. (3.15).

In case that the bare vertex functions above can be evaluated, one may apply the formulae of Section 4.3.4 to write the resonant part of the meson-baryon transition matrix in terms of quark-model quantities. Due to the energy dependence in (D.15) (with $Q^0 = \omega$ in the center-of-mass frame) the procedure would allow one to search for the poles of the transition matrix, even if the non-resonant contributions to the potential were still taken from the model of Chapter 5. Investigating this possibility though is beyond the scope of the present work: The idea was simply to show that defining baryon masses and decay widths in terms of poles of a resonant transition matrix is in principle possible in the relativistic quark model.

Bibliography

[1] H. L. Anderson, E. Fermi, E. A. Long, and D. E. Nagle, Phys. Rev. **85**, 936 (1952).

[2] Particle Data Group Collaboration, J. Beringer *et al.*, Phys. Rev. **D86**, 010001 (2012), Updates available at http://pdg.lbl.gov/.

[3] D. J. Gross and F. Wilczek, Phys. Rev. Lett. **30**, 1343 (1973).

[4] H. D. Politzer, Phys. Rev. Lett. **30**, 1346 (1973).

[5] K. G. Wilson, Phys. Rev. **D10**, 2445 (1974).

[6] S. Dürr *et al.*, Science **322**, 1224 (2008), hep-lat/0906.3599.

[7] R. G. Edwards, J. J. Dudek, D. G. Richards, and S. J. Wallace, Phys. Rev. **D84**, 074508 (2011), hep-ph/1104.5152.

[8] M. Göckeler *et al.*, Phys. Rev. **D86**, 094513 (2012), hep-lat/1206.4141.

[9] V. Bernard, D. Hoja, U. Meißner, and A. Rusetsky, JHEP **1209**, 023 (2012), hep-lat/1205.4642.

[10] K. Polejaeva and A. Rusetsky, Eur. Phys. J. **A48**, 67 (2012), hep-lat/1203.1241.

[11] Hadron Spectrum Collaboration, J. Bulava *et al.*, Phys. Rev. **D82**, 014507 (2010), hep-lat/1004.5072.

[12] D. Rönchen, Unified Analysis of Kaon-Hyperon and Pion-Nucleon Reactions in a Coupled-Channel Approach, Diplomarbeit, Universität Bonn, 2010.

[13] A. V. Anisovich *et al.*, Eur. Phys. J. **A48**, 15 (2012), hep-ph/1112.4937. Updates available at http://pwa.hiskp.uni-bonn.de/.

[14] R. A. Arndt, W. J. Briscoe, I. I. Strakovsky, and R. L. Workman, Phys. Rev. **C74**, 045205 (2006), nucl-th/0605082. Updates available at http://gwdac.phys.gwu.edu/.

[15] D. Drechsel, S. S. Kamalov, and L. Tiator, Eur. Phys. J. **A34**, 69 (2007), nucl-th/0710.0306. Updates available at http://www.kph.uni-mainz.de/MAID/.

[16] V. Shklyar, H. Lenske, and U. Mosel, Phys. Rev. **C87**, 015201 (2013), nucl-th/1206.5414.

[17] E. Klempt and J.-M. Richard, Rev. Mod. Phys. **82**, 1095 (2010), hep-ph/0901.2055.

[18] U.-G. Meißner and J. A. Oller, Nucl. Phys. **A673**, 311 (2000), nucl-th/9912026.

[19] J. A. Oller and U.-G. Meißner, Phys. Lett. **B500**, 263 (2001), hep-ph/0011146.

[20] P. C. Bruns, M. Mai, and U.-G. Meißner, Phys. Lett. **B697**, 254 (2011), nucl-th/1012.2233.

[21] O. Krehl, C. Hanhart, S. Krewald, and J. Speth, Phys. Rev. **C62**, 025207 (2000), nucl-th/9911080.

[22] S. Capstick and W. Roberts, Prog. Part. Nucl. Phys. **45**, S241 (2000), nucl-th/0008028.

[23] J. Resag, C. R. Münz, B. C. Metsch, and H. R. Petry, Nucl. Phys. **A578**, 397 (1994), nucl-th/9307026.

[24] C. R. Münz, J. Resag, B. C. Metsch, and H. R. Petry, Nucl. Phys. **A578**, 418 (1994), nucl-th/9307027.

[25] E. Klempt, B. C. Metsch, C. Münz, and H. R. Petry, Phys. Lett. **B361**, 160 (1995), hep-ph/9507449.

[26] M. Koll, R. Ricken, D. Merten, B. C. Metsch, and H. R. Petry, Eur. Phys. J. **A9**, 73 (2000), hep-ph/0008220.

[27] R. Ricken, M. Koll, D. Merten, B. C. Metsch, and H. R. Petry, Eur. Phys. J. **A9**, 221 (2000), hep-ph/0008221.

[28] U. Löring, K. Kretzschmar, B. C. Metsch, and H. R. Petry, Eur. Phys. J. **A10**, 309 (2001), hep-ph/0103287.

[29] U. Löring, B. C. Metsch, and H. R. Petry, Eur. Phys. J. **A10**, 395 (2001), hep-ph/0103289.

[30] U. Löring, B. C. Metsch, and H. R. Petry, Eur. Phys. J. **A10**, 447 (2001), hep-ph/0103290.

[31] U. Löring and B. Metsch, Parity doublets from a relativistic quark model, in *Proceedings of the Workshop on the Physics of Excited Nucleons – NSTAR 2001*, pp. 221–224, 2001, hep-ph/0110412.

[32] D. Merten, U. Löring, K. Kretzschmar, B. Metsch, and H. R. Petry, Eur. Phys. J. **A14**, 477 (2002), hep-ph/0204024.

[33] D. Merten, U. Löring, B. Metsch, and H. Petry, Eur. Phys. J. **A18**, 193 (2003).

[34] T. Van Cauteren *et al.*, Eur. Phys. J. **A20**, 283 (2004), nucl-th/0310058.

[35] T. Van Cauteren, J. Ryckebusch, B. Metsch, and H.-R. Petry, Eur. Phys. J. **A26**, 339 (2005), nucl-th/0509047.

[36] S. Migura, D. Merten, B. Metsch, and H.-R. Petry, Eur. Phys. J. **A28**, 55 (2006), hep-ph/0602152.

[37] B. Metsch, U. Löring, D. Merten, and H. Petry, Eur. Phys. J. **A18**, 189 (2003).

[38] B. Metsch, Eur. Phys. J. **A35**, 275 (2008).

[39] S. Migura, *Weak and Strong Baryon Decays in a Constituent Quark Model*, Dissertation, Universität Bonn, 2006.

[40] D. Rönchen *et al.*, Eur. Phys. J. **A49**, 44 (2013), nucl-th/1211.6998.

[41] C. Schütz, J. Durso, K. Holinde, and J. Speth, Phys. Rev. **C49**, 2671 (1994).

[42] C. Schütz, K. Holinde, J. Speth, B. C. Pearce, and J. W. Durso, Phys. Rev. **C51**, 1374 (1995), nucl-th/9411022.

[43] C. Schütz, J. Haidenbauer, and J. Speth, Phys. Rev. **C57**, 1464 (1998).

[44] O. Krehl, C. Hanhart, S. Krewald, and J. Speth, Phys. Rev. **C60**, 055206 (1999), nucl-th/9906090.

[45] A. M. Gasparyan, J. Haidenbauer, C. Hanhart, and J. Speth, Phys. Rev. **C68**, 045207 (2003), nucl-th/0307072.

[46] M. Döring *et al.*, Nucl. Phys. **A851**, 58 (2011), nucl-th/1009.3781.

[47] S. Mandelstam, Proc. Roy. Soc. Lond. **A233**, 248 (1955).

[48] E. E. Salpeter and H. A. Bethe, Phys. Rev. **84**, 1232 (1951).

[49] E. E. Salpeter, Phys. Rev. **87**, 328 (1952).

[50] A. L. Fetter and J. D. Walecka, *Quantum Theory of Many-Particle Systems,* Dover Books on Physics (Dover Publications, 2003).

[51] M. Gell-Mann and F. Low, Phys. Rev. **84**, 350 (1951).

[52] C. R. Münz, *Meson Decays and Form Factors in a Relativistic Quark Model*, Dissertation, Universität Bonn, 1994.

[53] M. Koll, *Electroweak Processes with Light Mesons in a Relativistic Quark Model*, Dissertation, Universität Bonn, 2001.

[54] C. Itzykson and J. B. Zuber, *Quantum Field Theory,* Dover Books on Physics (Dover Publications, 2012).

[55] W. Lucha and F. F. Schöberl, J. Phys. **G31**, 1133 (2005), hep-th/0507281.

[56] J. Resag, *Analysis of the Instantaneous Bethe-Salpeter Equation and its Applications for Quark-Antiquark States*, Dissertation, Universität Bonn, 1994.

[57] K. Kretzschmar, *Electroweak Form Factors in a Covariant Quark Model of Baryons*, Dissertation, Universität Bonn, 2001.

[58] U. Löring, *A Covariant Quark Model of Baryons with Instanton-Induced Forces*, Dissertation, Universität Bonn, 2001.

[59] G. 't Hooft, Phys. Rev. **D14**, 3432 (1976), Erratum-*ibid*: **D18** 2199 (1978).

[60] C. Ritter, Instantoninduzierte Zerfälle Skalarer und Pseudoskalarer Mesonen, Diplomarbeit, Universität Bonn, 2010.

[61] M. Ronniger and B. C. Metsch, Eur. Phys. J. **A47**, 162 (2011), hep-ph/1111.3835.

[62] D. Merten, *Hadron Form Factors and Decays*, Dissertation, Universität Bonn, 2002.

[63] M. E. Peskin and D. V. Schroeder, *An Introduction to Quantum Field Theory,* Advanced book classics (Addison-Wesley Pub. Co., 1995).

[64] M. Jacob and G. C. Wick, Annals Phys. **7**, 404 (1959).

[65] M. Döring, C. Hanhart, F. Huang, S. Krewald, and U. G. Meißner, Phys. Lett. **B681**, 26 (2009), nucl-th/0903.1781.

[66] A. D. Martin and T. D. Spearman, *Elementary Particle Theory* (North-Holland Pub. Co., 1970).

[67] G. Penner, *Vector Meson Production and Nucleon Resonance Analysis in a Coupled-Channel Approach*, Dissertation, Universität Gießen, 2002.

[68] D. A. Varshalovich, A. N. Moskalev, and V. K. Khersonskiĭ, *Quantum Theory of Angular Momentum* (World Scientific Pub. Co., Inc., 1988).

[69] A. Dobado and J. R. Peláez, Phys. Rev. **D56**, 3057 (1997), hep-ph/9604416.

[70] E. Oset and A. Ramos, Nucl. Phys. **A635**, 99 (1998), nucl-th/9711022.

[71] J. Nieves and E. Ruiz Arriola, Phys. Rev. **D64**, 116008 (2001), hep-ph/0104307.

[72] L. P. S. Singh, Phys. Rev. **D23**, 2236 (1981).

[73] J. A. Oller and E. Oset, Nucl. Phys. **A620**, 438 (1997), hep-ph/9702314.

[74] L. Roca, V. K. Magas, E. Oset, and S. Sarkar, AIP Conference Proceedings **814**, 266 (2006).

[75] A. Gasparyan, *Study of Pion-Nucleon Scattering up to 1.9 GeV Through a Coupled-Channel Meson-Nucleon Model*, Dissertation, Universität Bonn, 2002.

[76] A. D. Lahiff and I. R. Afnan, Phys. Rev. **C60**, 024608 (1999), nucl-th/9903058.

[77] A. Matsuyama, T. Sato, and T.-S. H. Lee, Phys. Rept. **439**, 193 (2007), nucl-th/0608051.

[78] W. Pauli and F. Villars, Rev. Mod. Phys. **21**, 434 (1949).

[79] G. 't Hooft and M. Veltman, Nucl. Phys. **B44**, 189 (1972).

[80] M. Mai, *From Meson-baryon Scattering to Meson Photoproduction*, Dissertation, Universität Bonn, 2012.

[81] B. C. Pearce and B. K. Jennings, Nucl. Phys. **A528**, 655 (1991).

[82] C. Lee, S. N. Yang, and T.-S. H. Lee, J. Phys. **G17**, L131 (1991).

[83] F. Gross and Y. Surya, Phys. Rev. **C47**, 703 (1993).

[84] P. F. A. Goudsmit, H. J. Leisi, and E. Matsinos, Phys. Lett. **B299**, 6 (1993).

[85] T. P. Cheng and R. Dashen, Phys. Rev. Lett. **26**, 594 (1971).

[86] W. R. Frazer and J. R. Fulco, Phys. Rev. **117**, 1603 (1960).

[87] G. Höhler, F. Kaiser, R. Koch, and E. Pietarinen, *Handbook of Pion-Nucleon Scattering,* Physics Data 12-1 (Fachinformationzentrum Karlsruhe, 1979).

[88] A. V. Anisovich *et al.*, Eur. Phys. J. **A48**, 88 (2012), nucl-th/1205.2255.

Acknowledgments

Foremost, I would like to thank my advisor Priv.-Doz. Dr. Bernard Metsch for giving me the opportunity to work on this interesting subject. Due to the application of two different models I was able to gain valuable scientific experience in hadron physics. I also wish to thank him for his helpful suggestions for the project and the careful reading of this thesis.

I am grateful to Dr. Michael Döring from whom I learned much about the Jülich model and hadron physics in general. I wish to thank Dr. Michael Ronniger for his assistance with the numerical codes used in the quark model calculations. For the help with computing issues, several discussions about physics and a very nice working atmosphere I would like to thank all the colleagues of my research group.

The accomplishment of this work was possible thanks to the financial support from DAAD (Deutscher Akademischer Austauschdienst).

Finally, I would like to say thanks to my family: my husband Sebastian Zang for his support and assistance during the years of my PhD studies, my mother-in-law Brigitte Zang for her help in the end phase of this project and *aos meus pais, Pedro e Iracy, por sempre apoiarem o meu interesse em física e por sua ajuda e encorajamento durante todo este processo.*